Targeting the PI3K/AKT Pathway using Pan-AKT Degraders

HARVARD UNIVERSITY
Graduate School of Arts and Sciences

DISSERTATION ACCEPTANCE CERTIFICATE

The undersigned, appointed by the

Division of Medical Sciences

in the subject of Biological and Biomedical Sciences

have examined a dissertation entitled

Targeting the PI3K/AKT Pathway using Pan-AKT Degraders

presented by Emily Colleen Erickson

candidate for the degree of Doctor of Philosophy and hereby certify that it is worthy of acceptance.

Signature: _____

Typed Name: Dr. Kevin Haigis

Signature: Taru Muranen (Feb 22, 2022 13:49 EST) _____

Typed Name: Dr. Taru Muranen

Signature: Philip Cole (Feb 22, 2022 13:35 EST) _____

Typed Name: Dr. Philip Cole

Signature: Benjamin Turk _____

Typed Name: Dr. Benjamin Turk

Date: February 16, 2022

Targeting the PI3K/AKT Pathway using Pan-AKT Degraders

A dissertation presented
by
Emily Colleen Erickson

to
The Division of Medical Sciences

in partial fulfillment of the requirements
for the degree of
Doctor of Philosophy
in the subject of
Biological and Biomedical Sciences

Harvard University
Cambridge, Massachusetts
February 2022

Dissertation Advisor: Dr. Alex Toker Emily Colleen Erickson

Targeting the PI3K/AKT Pathway using Pan-AKT Degraders

Abstract

The serine/threonine protein kinase AKT, a downstream effector of phosphoinositide 3-kinase (PI3K), is a critical regulator of numerous cellular processes including proliferation, survival, metabolism, and apoptosis. Genetic aberrations in PI3K pathway components are prevalent across cancer types, resulting in AKT hyperactivation. Thus, AKT represents a rational and appealing therapeutic target. The AKT family of kinases is comprised of three highly homologous isoforms, AKT1, AKT2, and AKT3. Several ATP-competitive, allosteric, and covalent pan-AKT inhibitors have been developed, but thus far have displayed limited therapeutic benefit in clinical trials, due to lack of efficacy at tolerable concentrations and development of resistance. To effectively target hyperactive AKT signaling for cancer treatment, new modalities are needed that address these challenges.

Recently, targeted protein degradation has been developed as an alternative strategy to inhibition. This thesis reports the development and extensive characterization of two heterobifunctional degraders that selectively deplete AKT1, AKT2, and AKT3 *in vitro* and *in vivo*. These compounds, INY-03-041 and INY-05-040, comprise the catalytic AKT inhibitor GDC-0068 (ipatasertib) chemically conjugated to ligands for Cereblon or Von Hippel Lindau (VHL) ubiquitin ligases. Both degraders demonstrated improved selectivity and potency compared to GDC-0068. AKT degradation was rapid and unexpectedly long-lasting, even after compound washout, and maintained suppression of downstream signaling. AKT degraders demonstrated more potent anti-proliferative effects than catalytic AKT inhibition in cancer cells *in vitro* and induced degradation of AKT *in vivo*.

AKT degraders were further used to investigate AKT biology with the goal of delineating non-kinase dependent roles of AKT. Using a multi-omics approach to examine the metabolic and transcriptional consequences of AKT degradation versus inhibition, we identified and validated activation of stress kinase signaling as a cellular response specific to AKT degradation. Degrader-specific induction of stress kinases was validated by immunoblotting, and inhibition of the stress kinase JNK rescued AKT degrader-specific cell death. Together, these data support the use of AKT degraders as novel tools to decode the pleiotropic mechanisms that govern AKT signaling in human cancer, and as potential cancer therapeutics.

Table of Contents

TITLE PAGE ..... *i*

COPYRIGHT ..... *ii*

ABSTRACT ..... *iii*

TABLE OF CONTENTS ..... *v*

TABLE OF FIGURES ..... *vii*

ACKNOWLEDGEMENTS ..... *ix*

CHAPTER 1 ..... *1*

1.1 Overview **2**

1.2 Cellular signaling through the PI3K/AKT pathway **2**

1.2.1 PI3K/AKT signaling in metabolism 15

1.3 PI3K/AKT pathway dysregulation in cancer **18**

1.3.1 Targeting the PI3K/AKT pathway in cancer 24

1.3.2 PI3K pathway biomarkers for tumor risk and response 32

1.4 Targeted protein degradation as an alternative to pharmacological inhibition **39**

1.4.1 Targeting proteins for proteasomal degradation using PROTACs 43

1.4.2 Advantages and limitations of targeted protein degradation 46

CHAPTER 2 ..... *49*

2.1 Abstract **50**

2.2 Introduction **50**

2.3 Results **52**

2.3.1 Design and development of the pan-AKT degrader INY-03-041 52

2.3.2 INY-03-041 is a potent and highly selective pan-AKT degrader 55

2.3.3 INY-03-041 exhibits enhanced anti-proliferative effects compared to GDC-0068 59

2.3.4 INY-03-041 suppresses downstream signaling more potently than GDC-0068 63

2.4 Discussion **68**

2.5 Materials and Methods **70**

2.6 Acknowledgements **82**

CHAPTER 3 ..... *83*

3.1 Abstract **84**

3.2 Introduction **85**

3.3 Results **87**

3.3.1 Biochemical and cellular characterization of pan-AKT degrader INY-05-040 87

3.3.2 Multi-omics profiling of the effects of INY-05-040-mediated AKT degradation 94

3.3.3 COSMOS network analysis 100

3.3.4 COSMOS validation of degrader-specific stress kinase signaling 103
3.4 Discussion **109**
3.5 Materials and Methods **113**
CHAPTER 4 ..... ***126***
4.1 Summary of Thesis **127**
4.2 Discussion **129**
4.2.1 Advantages and Challenges of Targeting AKT using PROTACs 129
4.2.2 PROTACs as tool compounds to study AKT function 134
4.3 Future Directions **142**
4.4 Summary **146**
Appendix 1 ..... ***147***
Appendix 2 ..... ***157***
BIBLIOGRAPHY ***166***

Table of Figures

CHAPTER 1

Figure 1-1: Overview of PI3K/AKT signaling pathway 4
Figure 1-2. Mechanisms of AKT regulation 8
Figure 1-3. Signaling downstream of PI3K effector AKT....11
Figure 1-4. Genetic alteration frequency across PI3K pathway components....19
Figure 1-5. Frequent genetic alterations in PI3K pathway in cancer 20
Figure 1-6. Selected inhibitors targeting the PI3K pathway....25
Table 1-1: Table of selected AKT inhibitors in clinical trials 28
Table 1-2: Biomarkers of response and resistance to PI3K pathway inhibition 36
Figure 1-7: PROTAC-induced targeted protein degradation....44

CHAPTER 2

Figure 2-1. Design and development of INY-03-041....53
Table 2-1. Biochemical IC50s 54
Figure 2-2. INY-03-041 induces potent degradation of AKT isoforms dependent on CRBN, neddylation, and the proteasome. 56
Figure 2-3. INY-03-041 requires CRBN binding to induce highly selective AKT degradation. 57
Figure 2-4. INY-03-041 induces enhanced anti-proliferative effects compared to GDC-006860
Table 2-2. Hormone receptor and mutational status of PIK3CA and PTEN in cancer cell line panel....61
Table 2-3. GR values indicate anti-proliferative advantage of INY-03-041. 62
Figure 2-5. INY-03-041 induces degradation of AKT isoforms in T47D cells. 64
Figure 2-6. INY-03-041 exhibits more potent and durable downstream signaling effects than GDC-0068 65
Figure 2-7. INY-03-041 induces potent downregulation of AKT signaling in MOLT4, IGROV1 and PC3 cells. 66
Figure 2-8. INY-03-041 requires longer time points than GDC-0068 to display inhibition of downstream AKT signaling....67

CHAPTER 3

Figure 3-1. Design and characterization of INY-05-040. 88
Figure 3-2. INY-05-040 biochemical selectivity and proteomics....89
Figure 3-3. INY-05-040 degradation is dependent on neddylation and the proteasome and more potent than parental inhibitor GDC-0068....91
Figure 3-4. INY-05-040 degradation kinetics: dose curve and time course 92
Figure 3-5. INY-05-040 single treatment and washout 93
Figure 3-6. Anti-proliferative effects of AKT degradation or inhibition 95
Figure 3-7. Degrader-specific induction of cell death in BT474 cells....96
Figure 3-8. Metabolic profiling reveals increases in nucleoside species after INY-05-040 but not GDC-0068 treatment....97
Figure 3-9. RNA-seq differential expression analysis 99
Figure 3-10. Gene set enrichment analysis of RNA-seq analysis 101
Figure 3-11. Graphical summary of COSMOS platform 102
Figure 3-12. COSMOS networks....104
Figure 3-13. Top degrader and inhibitor degree nodes 105
Figure 3-14. COSMOS validation of induction of stress kinase signaling 107

Figure 3-15. JNK inhibition rescues cell death of BT474 cells 108

CHAPTER 4

Figure 4-1. Model of JNK activation after degradation of AKT 140
Figure 4-2. Model of AKT degrader-dependent increase in nucleoside levels.....141

Acknowledgements

It is difficult to adequately express my gratitude for the support and guidance I have received from Alex Toker, who has been instrumental in both my scientific and personal development. It's hard to imagine anyone more genuinely dedicated to their lab than Alex, both to the science and to the people. His ability to cultivate relationships and ideas has set an example that I hope to emulate in my own life. Alex's honest feedback and frequent reassurance have built my confidence to pursue new ideas with courage. Through Alex, I have been fortunate to find a trusted mentor and friend, Ralitsa Madsen. Ralitsa has taught me what it means to be generous with your time and talent, and how to be a good friend.

Beyond supporting my individual growth and development as a scientist, Alex has fostered a dynamic of camaraderie and collaboration in his lab, making the Toker lab truly feel like my scientific home. Special thanks to former and current Toker Lab members including Renee, Emily, Hui, Laura, Christian, Sam, Adrija, Ali, Grace, Gil, Josefina, and Tash for making the Toker Lab a place I genuinely look forward to going to every morning. You showed me how to embrace my creativity, and how to recognize and lean into my strengths. This environment has taught me both what it takes to be a good mentor, and how to receive feedback and criticism gracefully. Though I cannot individually thank everyone here, I am undoubtedly a more mature scientist and better person thanks your examples.

I am grateful for many productive collaborations throughout my time in Alex's lab. First and foremost, I would like to thank our collaborators Nathanael Gray and Inchul You for their essential contributions to my project. I would also like to thank my dissertation advisory committee members Kevin Haigis, Joan Brugge, and Stephen Elledge for their guidance, support, and feedback throughout my PhD. I would not be here today without many past mentors, including Karen Plaut, Theresa Casey, Christine Watson, Gil Smith, Andrew Limper, Michael Zanis, and Joe Ruhl, who I wish to thank for igniting my love for science, and for continued support over the years.

Finally, I must thank my friends and family for supporting me through this journey. I am incredibly fortunate to have a strong support network. Although it is impossible to thank everyone individually here, I am so grateful to my friends, near and far, for making my time outside the lab both interesting and fulfilling. A special thanks to my current and former roommates who have been there for me through thick and thin. I am so grateful to my parents, especially my mom, for fostering my love of learning and for the support to pursue a career that I find meaningful. Lastly, my sister and brother have always been my closest friends, and I am grateful that our shared pursuit of graduate school has brought us even closer.

What if

What if 1 plus 1 makes 3.
And all you know is Wrong
would anybody care?

What if up is Down.
And down is uP,
no matter your stare?

What if Earth stops turning.
Or never did because
there is no Sun out there?

What if what you see.
Is never what there is
the Truth no longer bare?

What if “what if” isn't.
And life you have, to live it
But would you even dare?

— Ralitsa Madsen

CHAPTER 1

INTRODUCTION

This chapter incorporates a manuscript that has been published in *Cancer Research*.

Erickson, E. C. & Toker, A. Can Improved Use of Biomarkers Alter the Fate of PI3K Pathway Inhibitors in the Clinic? Cancer Res. 1–5 (2021) doi:10.1158/0008-5472.CAN-21-2035.

1.1 Overview

The orchestration of diverse physiological processes in response to extracellular stimuli is essential for the maintenance of cellular homeostasis. The phosphoinositide-3-kinase (PI3K) pathway is an evolutionarily conserved mechanism for responding to external cues to promote cell growth, survival, metabolism, proliferation, and migration[1]. In order to direct responses across multiple facets of cellular physiology, the PI3K signaling network coordinates a complex set of effectors, including the major target of PI3K, the protein kinase AKT[2]. Because of their roles in promoting growth, survival, and biosynthesis, genes in the PI3K/AKT signaling pathway are among the most frequently altered across human cancers[3,4]. The frequency of PI3K/AKT pathway activation across cancer types, along with the presence of actionable targets in the pathway, has made PI3K/AKT signaling components a major focus for drug development in cancer therapy.

1.2 Cellular signaling through the PI3K/AKT pathway

The PI3K/AKT signaling network integrates a broad range of signals from growth factors, cytokines, and hormones to regulate a diverse set of cellular processes, including metabolism, proliferation, migration, and secretion[1,5]. This orchestration of multiple distinct fundamental processes is necessary to support the complex regulation of metabolic demands that accompany cell growth and division[5]. The PI3K family is divided into three classes (I-III) based on sequence homology and substrate specificity[6,7]. Class I PI3Ks are the most well-studied due to their contribution to oncogenesis[6]. These highly conserved heterodimeric lipid kinase complexes act in response to pro-growth signals from growth factors, hormones, and cytokines[5].

Activation of the class I PI3K pathway (henceforth “PI3K pathway”) can occur through several mechanisms, most commonly though activation of PI3Ks by receptor tyrosine kinases (RTKs), small GTPases, and heterotrimeric G proteins[5,8]. In mammals, activation of the PI3K pathway by different RTKs is linked to specific phenotypic responses: the PDGF receptor

(PDGFR) and epidermal growth factor receptor (EGFR) promote proliferation and migration, insulin-like growth factor receptor (IGFR) drives growth and survival, and insulin receptor (INSR) promotes metabolic homeostasis[5]. Growth factor binding induces conformational changes and often dimerization of RTKs that result in their autophosphorylation and activation, thereby activating downstream signaling cascade[5].

Mammals express four isoforms of class I PI3K catalytic subunits: p110α, p110β, p110δ, and p110γ, encoded by *PIK3CA, PIK3CB, PIK3CD,* and *PIK3CG*[2,5]. The p110α and p110β isoforms are ubiquitously expressed, whereas p110δ and p110γ are predominantly expressed in immune cells[5]. Class IA PI3K catalytic isoforms (p110α, β, and δ) associate with regulatory subunits (p85α/p55α/p50α, p85β, and p55γ) which bind to phosphotyrosine residues on receptor tyrosine kinases or adaptor proteins via SH2 domains (**Figure 1-1**)[5,9,10]. The class IB PI3K isoform p110γ associates with the regulatory subunits p101 and p87 to mediate binding to heterotrimeric G proteins β and γ after G protein coupled receptor activation[5]. Molecular contacts between the helical, kinase and C2 domains of the catalytic subunits contact the regulatory SH2 and iSH2 domain to maintain the enzymatic activity low under basal conditions[5,7]. Relief of inhibition by the regulatory subunit occurs when the SH2 domains bind to phosphotyrosine residues on RTKs, releasing inhibitory contacts on the catalytic subunit and positioning the dimer near the plasma membrane where it can phosphorylate PtdIns-4,5-P_2 (PI45P2)[5,7].

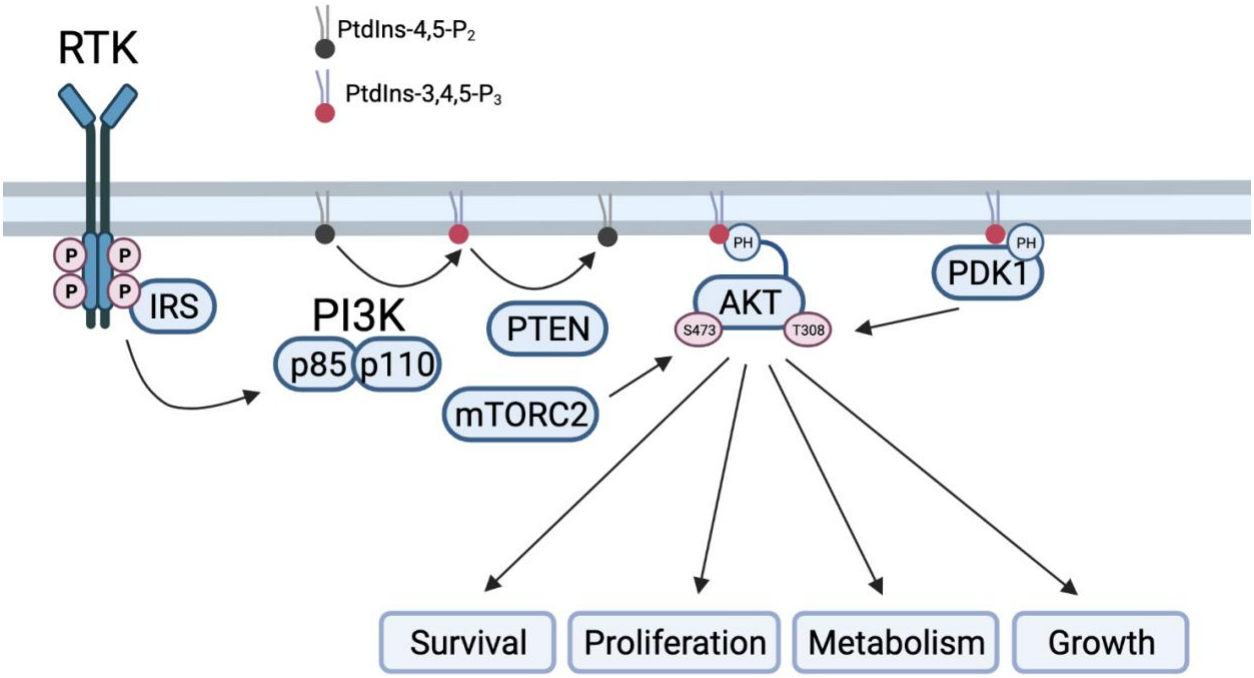

Figure 2-1: Overview of PI3K/AKT signaling pathway. Stimulation of RTKs activates Class I PI3K through direct binding or through interaction with scaffolding adaptors such as IRS1. PI3K phosphorylates membrane phospholipid PI-4,5-P_2 to generate PI-3,4,5-P_3. This reaction can be reversed by the PTEN lipid phosphatase to attenuate PI3K pathway signaling. AKT is recruited to the plasma membrane through PH domain interactions with PI-3,4,5-P_3 resulting in activating phosphorylation on Thr308 and Ser473 residues by PDK1 and mTORC2, respectively. AKT phosphorylates a host of downstream substrates involved in diverse cellular processes. Adapted from Manning and Toker, *Cell.* 2017.

Growth factor stimulation activates class I PI3K to catalyze the phosphorylation of the 3'-hydroxyl group on the head group of the inositol lipid PI45P2 to generate PtdIns-3,4,5-P_3 (PIP3)[5]. PIP3 is a lipid second messenger that promotes signaling through the PI3K pathway upon specific recruitment of cytosolic signaling proteins to the plasma membrane (**Figure 1-1**)[1,5,7]. PI3K signaling is rapidly terminated upon dephosphorylation of PIP3 by lipid phosphatases such as phosphatase and tensin homolog (PTEN), which negatively regulates PI3K signaling by catalyzing the removal of the 3'-phosphate from PIP3 to generate PI45P2 (**Figure 1-1**)[1,5]. PIP3 can also be depleted after sequential dephosphorylation by SH2-domain containing inositol phosphatases (SHIP1/2) to generate PI34P2, followed by inositol polyphosphate 4-phosphatases A and B (INPP4A/B) which dephosphorylate PI34P2 to generate PtdIns-3-P (PI3P)[1,11,12].

Phosphoinositides represent only a small fraction of the total plasma membrane lipid pool, with PI45P2 and PIP3 comprising less than 1% of membrane phospholipids[13]. Furthermore, only a small fraction of proteins able to bind phosphoinositides can interact with 3-phosphoinositides specifically[8]. Further, even subtle changes in the abundance of PIP3 have major effects on downstream signaling due to signal amplification through the PI3K/AKT/mTOR kinase cascade that frequently occurs in cancer.

Effectors of PI3K signaling

Production of PIP3 by Class I PI3K results in the recruitment of specific signaling effectors with a pleckstrin homology (PH) domain that binds specifically to the membrane phospholipids PIP3 and/or PI34P2[14]. The most well-studied effectors belong to the AGC family of serine/threonine kinases, including AKT[5]. However, multiple downstream signaling pathways can be activated upon PI3K activation, including the TEC family tyrosine kinases, guanine nucleotide exchange factors (GEFs), and GTPase-activating proteins (GAPs).

Non-AKT effectors

The serum and glucocorticoid-regulated kinase (SGK) family of protein kinases, consisting of three highly homologous isoforms, SGK1, SGK2, and SGK3, are critical mediators of PI3K signaling downstream of PDK1 and mTORC2. Instead of PH domains, SGK3 possesses a phox homology (PX) domains that binds to PI3P, primarily produced at endosomes by the class III PI3K hVps34[15,16]. SGKs can also be activated at the plasma membrane after sequential dephosphorylation of PIP3 to PI3P by lipid phosphatases SHIP1/2 and INPP4A/B[17,18]. PDK1 and mTORC2 promote the activation of SGKs by phosphorylating their activation loop and hydrophobic motif[16]. Because SGK and AKT share some substrates, activation of SGK signaling has been identified as a mechanism of resistance to PI3K and AKT inhibitors. For example, SGK1 can activate mTORC1 through phosphorylation and inhibition of TSC2, and inhibit the transcription factor FOXO3, countering the effects of AKT inhibition[19].

RAC proteins (RAC1, RAC2, and RAC3) are a subfamily of RHO small GTPases that act downstream of PI3K and play important roles in actin cytoskeleton remodeling[20]. RAC proteins alternate between inactive GDP-bound and active GTP-bound states. PI3K activates RAC by stimulating PIP3-dependent RAC guanine-nucleotide exchange factors (GEFs) Phosphatidylinositol-3,4,5-Trisphosphate Dependent Rac Exchange Factor 1 and 2 (PREX1 and PREX2), Vav guanine nucleotide exchange factor 1 (VAV1), SOS Ras/Rac Guanine Nucleotide Exchange Factor 1 (SOS1), and Switching B Cell Complex Subunit SWAP70 (SWAP-70), to promote activation of RAC[16]. Activated RAC-GTP binds to and activates target proteins, such as p21-activated kinase (PAK) and Wiskott-Aldrich syndrome protein (WASP) family protein (WAVE), to promote actin cytoskeleton reorganization[16]. RAC-mediated cytoskeleton remodeling has been implicated in the migration and invasion of multiple cancer types[20–22]. RAC signaling has also been reported to stimulate glycolysis independently of AKT through the release of aldolase A from its inhibitory actin cytoskeleton bound state[23].

PI3K signaling can also promote membrane localization and activation of non-receptor tyrosine kinases (NRTKs) in the TEC family, including the SRC proto-oncogene (SRC) tyrosine kinase expressed in hepatocellular carcinoma (TEC), bone marrow tyrosine kinase gene on chromosome X (BMX), Bruton's tyrosine kinase (BTK), interleukin-2-inducible T-cell kinase (ITK), and tyrosine kinase TXK[16]. This family of tyrosine kinases, with the exception of TXK, contain an N-terminal PH domain, resulting in their accumulation at the plasma membrane in response to the generation of PIP3[24]. SRC and TEC family NRTKs mediate signaling downstream of the T cell receptor (TCR), B cell receptor (BCR), toll-like receptors (TLRs), and integrins in immune cells[25]. BTK is a TEC family member involved in B-cell lymphoma. PI3K recruits BTK to the plasma membrane via its PH domain, where it is activated through phosphorylation by LYN and SYK kinases. Through its SH2 domain, BTK participates in a signaling complex composed of B cell linker (BLNK), PLCγ, and the RHO family GEF VAV1[16]. BTK phosphorylation and activation of PLCγ promotes calcium mobilization, which ultimately results in Ras activation as well as the activation of NF-κB and NFAT transcriptional programs[16].

AKT as an effector of PI3K signaling

The AKT family of AGC serine/threonine kinases (AKT1, AKT2, and AKT3) are canonical effectors of receptor-mediated PI3K activation whose activation can promote survival, proliferation, growth, and metabolic changes[1,5,26]. AKT isoforms are encoded by paralogous genes with a high degree of sequence similarity[1,26–30]. Although AKT isoforms share most downstream targets, tissue- and cell-specific functions of AKT isoforms have also been identified.

The domain structure of the AKT isoforms is highly conserved, comprising an N-terminal pleckstrin homology (PH) domain, a linker domain, an AGC kinase conserved catalytic domain, and a C-terminal regulatory domain, also known as the hydrophobic motif (**Figure 1-2**)[1,26–31].

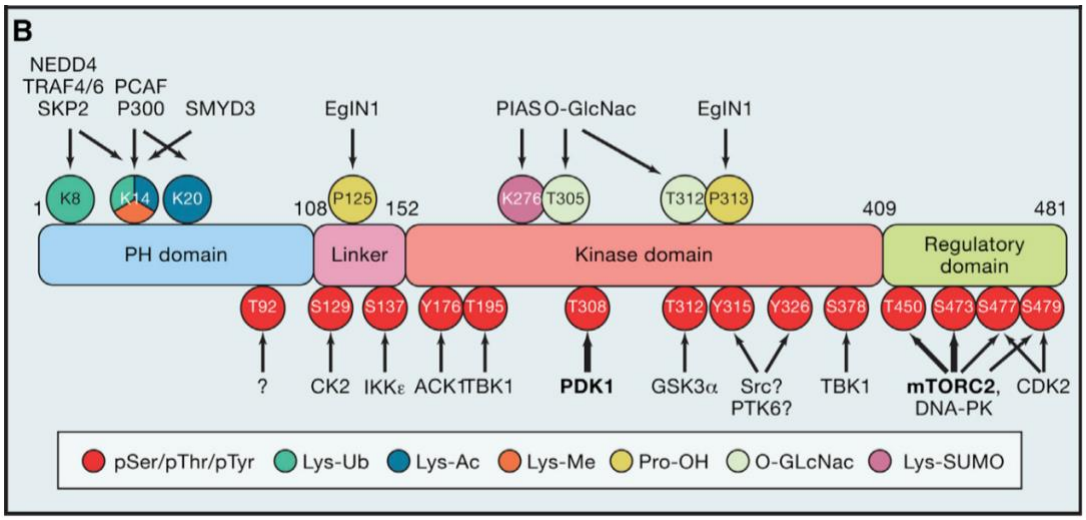

Figure 1-2. Mechanisms of AKT regulation. Linear structure of AKT1 with posttranslational modifications, including phosphorylation, acetylation, ubiquitylation, methylation, hydroxylation, glycosylation, and SUMOylation. Roles of specific enzymes in adding modifications are indicated by arrows; "?" denotes modifier protein is unidentified. Adapted from Manning and Toker. Cell. 2017.

AKT is recruited to membranes by the high affinity interaction of its PH domain with PIP3 and PI34P2.

At the plasma membrane, AKT is activated by phosphorylation on two regulatory motifs that are required for full activation of kinase activity: the activation loop in the catalytic domain, and the hydrophobic motif near the C-terminus (**Figure 1-2**)[31]. The binding of the PH domain of AKT to plasma membrane phosphoinositides induces a conformational change (the "PH-out" conformation) that allows PDK1 to access and phosphorylate Thr308/Thr309/Thr305 of the activation loop in the catalytic domain of AKT1/2/3 respectively, which results in its partial activation[1]. In the "PH-in" inactive conformation, the PH domain autoinhibits AKT through interactions with the kinase domain[1]. Full activation of AKT requires phosphorylation by mTORC2 on an additional regulatory residue on the hydrophobic motif: Ser473/Ser474/Ser472 on AKT1/2/3 (**Figures 1-1** and **1-2**)[31]. Beyond phosphorylating AKT, mTORC2 phosphorylates other kinases with sites analogous to AKT's hydrophobic motif, including SGKs and protein kinase C (PKC)[5]. This hydrophobic motif phosphorylation site on AKT can alternatively be phosphorylated by DNA-dependent protein kinase (DNA-PK) in response to DNA damage[1]. Recently, it was proposed that mTORC2 phosphorylation of the TOR interaction motif (TIM) on AKT enables autophosphorylation of the hydrophobic motif[32].

In addition to these two crucial regulatory phosphorylation sites, several additional post-translational modifications have been discovered to regulate AKT activity and localization and some proposed to mediate substrate specificity (**Figure 1-2**)[1]. AKT is constitutively phosphorylated on its turn-motif at Thr450, a co-translational event that is required for proper protein folding[1,31]. Ser477 and Thr479 can also be phosphorylated by the CyclinA-CDK2 complex in a cell cycle-dependent manner to enhance the activity of AKT in the S and G2 phases of the cell cycle[1,33]. Regulation by other post-translational modifications has also been reported, including acetylation, glycosylation, and hydroxylation. Acetylation of K14 in the PH domain has been proposed to facilitate AKT membrane recruitment through PIP3 binding[34].

Additionally, glycosylation of Thr305 and Thr312 in the catalytic core have been reported, as well as hydroxylation of proline residues, including Pro125 and Pro313, to promote interaction of AKT with pVHL[1,35,36]. AKT can also be ubiquitylated on several lysine residues by CHIP, BRCA1, TTC3, and MULAN ubiquitin ligases to promote K48-linked ubiquitination and subsequent proteasomal degradation of AKT[1,37]. In contrast to K48-linked ubiquitination, AKT can be targeted for K63-linked ubiquitination by TRAF6, Skp2, and NEDD4-1 E3 ligases to enhance membrane localization. AKT can also be modified by SUMOylation at various lysine residues by PIAS, including Lys276, which is reported to be involved in AKT activation[1,38].

After activation, AKT phosphorylates a host of protein substrates in diverse subcellular locations (**Figure 1-3**). These substrates are phosphorylated on serine (Ser) and threonine (Thr) residues and contain the minimal AKT consensus recognition motif R-X-R-X-X-S/T-B (where X is any amino acid and B represents a preference for bulky hydrophobic residues)[1,26].

Opposing models have been proposed for the requirement of membrane engagement in AKT activity. Ebner *et al.* recently proposed a membrane-restricted model of AKT activation, in which PIP3 binding is required to allosterically activate AKT and promote substrate binding, limiting AKT activity to cellular membranes containing PIP3 or PI34P2 lipid products[39]. In this model, dissociation of AKT from PIP3 is rate-limiting for AKT dephosphorylation, which would increase substrate specificity and selection[39]. Additionally, Ebner *et al.* reported that the E17K PH-domain activating mutation of AKT, which uncouples kinase activation from PIP3 binding, resulted in active cytosolic AKT, providing a mechanistic explanation for its oncogenic potential[39]. However, localization of validated AKT substrates to subcellular compartments other than the plasma membrane, including the nucleus and endomembranes, has led to acceptance that AKT can remain active and phosphorylate substrates irrespective of PIP3 binding. In opposition to the membrane-restricted model of AKT activation, C-terminal phosphorylation of AKT by mTORC2 displaces the PH domain from the kinase domain and relieves autoinhibition[40].

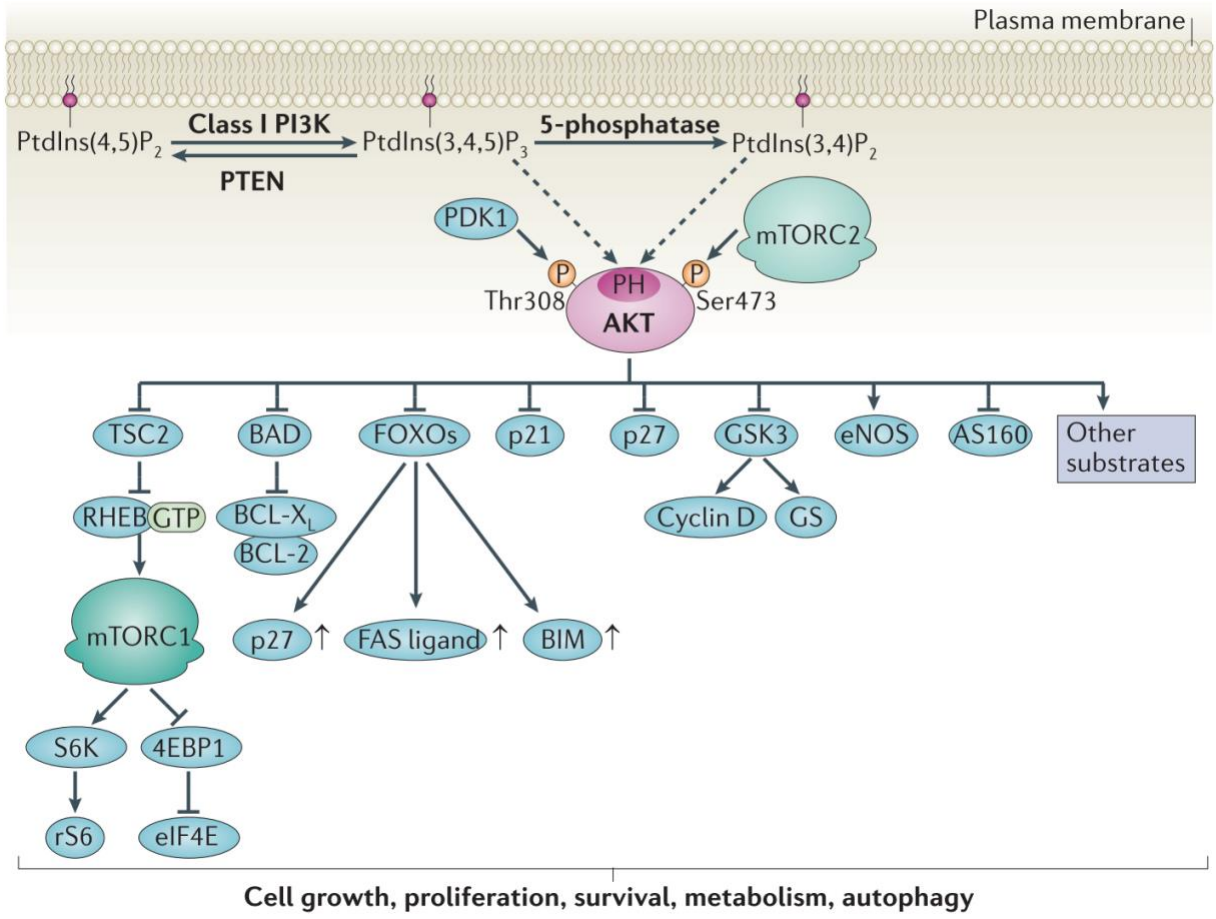

Figure 1-3. Signaling downstream of PI3K effector AKT. Upon full activation of AKT after regulatory phosphorylation by PDK1 and mTORC2 at canonical regulatory phosphorylation sites Thr308 and Ser473, respectively, AKT phosphorylates several downstream substrates, including a subset of major targets listed here involved in cell growth, proliferation, survival, metabolism, and autophagy. 4EBP1, eIF4E-binding protein 1; AS160, AKT substrate of 160 kDa; BAD, BCL-2 antagonist of cell death; BIM, BCL-2-interacting mediator of cell death; eIF4E, eukaryotic translation-initiation factor 4E; eNOS, epithelial nitric oxide synthase; FOXO, forkhead box O; GS, glycogen synthase; GSK3, GS kinase 3; GTP, guanosine triphosphate; PTEN, phosphatase and tensin homologue; RHEB, RAS homologue enriched in brain; rS6, ribosomal S6 protein; S6K, S6 kinase; TSC, tuberous sclerosis 2. Adapted from Vanhaesebroeck, B. *et al. Nat. Rev. Mol. Cell Bio.* 2012.

This suggests that intermolecular interactions between the C-terminal tail and PH domain, rather than PH engagement of PIP3, relieve PH domain-mediated autoinhibition of AKT. However, there is consensus that PIP3 is important for the membrane recruitment of AKT, where it is subsequently phosphorylated by its major regulators PDK1 and mTORC2 for full activation.

AKT isoforms

Despite their homology, AKT isoforms regulate distinct and sometimes opposing cellular functions. Context-specific factors such as tissue expression and subcellular localization may in part explain the functional specificity of AKT isoforms[27,30]. AKT1 is ubiquitously expressed, AKT2 is expressed in insulin-responsive tissues such as liver, skeletal muscle, and fat, and AKT3 is expressed less widely, predominantly in the brain[41–44]. Mouse studies examining individual AKT isoform knockouts suggest non-redundant functions and tissue-specific roles. AKT1 has been implicated in survival, as AKT1 knockout mice are smaller than their wild-type littermates and exhibit perinatal lethality[41]. AKT2 knockout mice develop insulin resistance[45], and AKT3 knockout mice exhibit neurological defects and small brain size[46,47]. Reported differences in the subcellular localization of AKT isoforms may contribute to differential substrate access[48]. For example, studies using fluorescent reporters and total internal reflection fluorescence microscopy (TIRF) have shown preferential accumulation of AKT2 at the plasma membrane of adipocytes relative to AKT1[49]. This difference in subcellular localization may also explain AKT2-specific regulation of GLUT4 and the contribution of AKT2 to glucose metabolism[50].

Intrinsic molecular differences are also hypothesized to contribute to the distinct functions of AKT isoforms. Although the kinase and PH domains are highly conserved, the linker domains of AKT isoforms are more divergent than other domains and have been implicated in isoform-specific interactions. AKT1-specfic phosphorylation of microfilamental protein PALLADIN is dependent on the presence of the linker domain of AKT1[51]. Differences in sequence or structural homology between domains of AKT isoforms may also contribute to

independent post-translational modifications, which may preferentially activate individual AKT isoforms or promote localization to different subcellular compartments. One example of sequence-specific differences between AKT isoforms is the regulation of Cys124 on the linker region of AKT2, which has been identified as a unique redox-sensitive regulatory site and implicated in glucose uptake in response to PDGF stimulation[52,53].

Although the majority of AKT substrates are shared between all isoforms, isoform-specific substrates have been identified[54], which may underlie the unique contribution of these isoforms to distinct characteristics. For example; PALLADIN[51], SKP2[55,56], and p21[57,58] have been described as AKT1-specific substrates; AS160[59], HDM2[60], Myosin5a[61], and Ankrd2/ARRP[62] have been identified as AKT2-specific substrates; and TBX3[63] has been proposed to be an AKT3-specific substrate. Cell culture studies have further dissected non-redundant and even opposing functions of AKT isoforms in normal physiology and cancer, particularly migration and metastasis[64–67]. AKT1 and AKT2 have been found to play opposing roles in metastasis: while AKT1 suppresses breast cancer cell migration and invasion, AKT2 enhances these phenotypes[51,68]. Despite a deep understanding of AKT signaling as it contributes to several cellular phenotypes, our understanding of the specific role of AKT isoforms in normal physiology and cancer remains underdeveloped. The lack of isoform-specific inhibitors remains a limitation to understanding the individual contribution of AKT isoforms to pathway activation and pathological conditions.

Downstream effectors of AKT

AKT coordinates organismal growth and metabolism primarily through the regulation of the mechanistic target of rapamycin (mTOR) serine/threonine kinase to promote a number of biosynthetic processes[69]. The complex mTORC1, defined by core components mTOR, Raptor, and mLST8, promotes a variety of anabolic processes and suppresses catabolic processes[70]. mTORC1 also associates with inhibitory subunits PRAS40 and DEPTOR[69]. Its negative

regulator, tuberous sclerosis complex 2 (TSC2), functions together with TSC1 and TBC1DC to form the TSC complex which acts as a GAP for the RHEB GTPase, an essential activator of mTORC1[1]. AKT-mediated phosphorylation and inhibition of TSC2 indirectly activates mTORC1 to promote biosynthetic processes (**Figure 1-3**). The activity of mTORC1 can be regulated by mitogenic signaling through the PI3K and RAS pathways, but also requires input from nutrient-sensing pathways[69,71].

Growing cells require increased production of proteins, lipids, and nucleotides to meet biosynthetic demands. mTORC1 promotes these anabolic processes, and suppresses catabolic processes like autophagy[69]. Regulation of p70S6 kinase 1 (S6K1) and eukaryotic initiation factor-4E (eIF4E)-binding protein (4EBP) by mTORC1 promotes the initiation of mRNA translation and 5'-cap-dependent mRNA translation[69]. Nucleotide synthesis and ribosome biogenesis are promoted by mTORC1 through an increase in ATF4-dependent MTHFD2 expression[72]. mTORC1 regulates a number of transcription factors that can be independently controlled by cellular stress, including ATF4, TFEB, SREBP, HIF1α, and PGC1α[69]. mTORC1 promotes cellular growth by suppressing catabolic processes such as autophagy, through the negative regulation of ULK1, an activator of autophagy, and through inhibiting TFEB, a transcription factor that promotes expression of lysosomal biogenesis and autophagy machinery genes[69].

S6K1 is another AKT-dependent mediator of metabolic reprogramming which activates a host of biosynthetic pathways including glycolysis, protein, lipid, and nucleotide metabolism[70]. Cells contain regulatory feedback loops to control these processes, such that upon inhibition of mTORC1 and S6K1, cells reactivate signaling through PI3K, ERK, and AKT[69,73]. Loss of phosphorylation of S6K1 on Thr389 is a highly sensitive readout of mTORC1 inhibition by rapamycin[5]. Another substrate of mTORC1 that regulates proliferation and survival of cells are the 4EBPs. The phosphorylation of 4E-BPs by mTORC1 prevents their binding to eIF4E, freeing eIF4E to associate with eIF4G and eIF4A for assembly of the cap-binding translation initiation

complex[5]. Cell cycle and survival factor-related mRNA transcripts are particularly dependent on cap-dependent translation. Interestingly, the inhibition of 4E-BP phosphorylation is achieved to a greater extent by mTORC1 and mTORC2 inhibitors than by rapamycin[5].

1.2.1 PI3K/AKT signaling in metabolism

Glucose metabolism

Systemically, the effects of PI3K pathway activation on glucose metabolism in muscle and fat cells can be attributed to increased translocation of glucose transporter GLUT4 to the membrane after insulin stimulation, thereby increasing glucose uptake into cells to clear plasma glucose after food intake[74,75]. In tissues other than muscle and fat, the transcription and translation of glucose transporter GLUT1 is necessary for IGF1-dependent response to glucose uptake[5]. Glycolytic flux can be driven in a PI3K-dependent, AKT-independent manner through RAC-dependent release of aldolase A from a low activity actin-bound state[75].

PI3K signaling regulates the expression of GLUT1 through indirect regulation of the transcription factors that drive expression of genes involved in glucose metabolism, including hypoxia-inducible factor 1α (HIF1α) and MYC[5]. HIF1α is stabilized under hypoxic conditions, and its expression can be increased by mTORC1 activation downstream of AKT signaling[75]. Stabilization of HIF1α induces the expression of nearly all enzymes of glycolysis as well as glucose transporter GLUT1[76]. Likewise, MYC induces the expression of many glycolytic enzymes and glucose transporters, and its abundance is increased downstream of PI3K pathway signaling through transcriptional, translational, and post-translational mechanisms[75]. AKT can also stabilize MYC levels through inhibition of GSK3 (**Figure 1-3**), which targets MYC for proteasomal degradation[75]. Negative regulation of glycolytic enzymes and MYC transcription by the FOXO transcription factors can be relieved by AKT phosphorylation of FOXO (**Figure 1-3**)[75].

AKT itself can regulate glucose metabolism via diverse mechanisms. Phosphorylation of thioredoxin-interacting protein (TXNIP), an adaptor protein, by AKT can reduce the endocytosis of GLUT1 and GLUT4 glucose transporters resulting in increased plasma membrane localization[77]. AKT can also phosphorylate and inhibit TBC1D4 (also known as AS160, as in **Figure 1-3**), a GAP for RAB GTPases that promote GLUT4 trafficking, though this mechanism appears to be specific to GLUT4[75]. AKT phosphorylates and promotes the activity of hexokinase 2 (HK2) and 6-phosphofructo-2-kinase/fructose-2,6-bisphosphate (PFKFB2), which functions to convert fructose-6-phosphate to fructose 2,6-bisphosphate, whose elevated levels allosterically activate PFK1 and enhance glycolytic flux[78]. AKT-driven glycolysis also generates metabolic intermediates that act as substrates for additional biosynthetic processes, including the generation of nucleotides, proteins, and lipids required for cell growth[75].

Anabolic metabolism

Regulation of anabolic processes is critical for proliferating cells to keep pace with the biosynthetic demands of the cell. PI3K and AKT drive anabolic processes including protein and nucleotide synthesis and the transcription of pentose phosphate pathway and glycolysis genes through the activation of S6K1/2 and inhibition of 4EBP by mTORC1[71]. Activation of mTORC1 also promotes lipid synthesis through regulation of sterol regulatory element binding protein (SREBP) family transcription factors[79,80].

The majority of cells rely on fatty acid and lipoprotein supplies through uptake from the bloodstream. However, cancer cells often generate lipids *de novo* to support increased proliferation rates and membrane generation. AKT stimulates *de novo* lipid synthesis through phosphorylation of ATP citrate lyase (ACLY), increasing the production of cytosolic acetyl-CoA that can be used to generate sterols and fatty acids and promote histone acetylation[75]. Activation of SREBP transcription factors downstream of PI3K signaling also promotes *de novo* lipid synthesis. SREBPs require processing via trafficking to the Golgi for proteolytic cleavage

for full activation. The N-terminal active portion of SREBP translocates to the nucleus and binds to sterol response elements of lipogenic genes[75]. SREBP processing and nuclear translocation is mTORC1-dependent. Further, inhibition of GSK3 by AKT phosphorylation can prevent the ubiquitin-mediated degradation of mature SREBP, thereby promoting its stability and activity[75].

Nucleotide metabolism requires inputs from several metabolic pathways, including the pentose phosphate pathway (PPP), serine, glycine, and aspartate synthesis, one-carbon metabolism, and glutamine uptake and metabolism[75]. Glucose uptake stimulated by PI3K pathway signaling fuels the PPP to produce ribose for nucleic acid synthesis[75]. AKT also drives nucleotide metabolism through regulation of MYC, which induces the expression of several purine and pyrimidine biosynthetic enzymes[81].

mTORC1 activation promotes nucleotide synthesis and in tandem drives the synthesis of ribosomal proteins to support rRNA synthesis, contributing to ribosome biogenesis[82]. Ribosomes are composed of approximately 55% rRNA by mass, and account for the majority of intracellular nucleotides[81]. The activation of ribosome biogenesis through RNA Pol I and III downstream of mTORC1 creates a great demand for nucleotide production, which can be met either by *de novo* synthesis or nucleotide salvage[81]. mTORC1 can promote *de novo* synthesis of pyrimidine and purine nucleotides through post-translational mechanisms, such as the S6K1-mediated phosphorylation of the enzyme carbamoyl-phosphate synthetase 2, aspartate transcarbamylase, and dihydroorotase (CAD) to increase its activity in driving the first three steps of pyrimidine biosynthesis[81]. Activation of mTORC1 can also promote purine synthesis through transcriptional regulation of enzymes in pathways that feed into purine synthesis, including the pentose phosphate pathway, serine and glycine synthesis, and the mitochondrial tetrahydrofolate pathway. The uncoupling of nucleotide synthesis from rRNA synthesis causes DNA replication stress[82].

AKT activation promotes protein synthesis downstream of mTORC1 through the regulation of two major effectors, p70S6 Kinase 1 (S6K1) and eIF4E Binding Protein (4EBP).

S6K1 promotes the initiation of mRNA translation through the phosphorylation of several substrates, including eIF4B, which positively regulates the 5'-cap binding eIF4F complex[69]. The negative regulation of eIF4B inhibitor PDCD4 by S6K1 also enhances the translation efficiency of spliced mRNAs[69]. Independent of its regulation of S6K1, mTORC1 phosphorylates and inhibits 4EBP to prevent its negative regulation of eIF4F complex assembly[69]. Dissociation of 4EBP from eIF4E allows 5'-cap-dependent mRNA translation to occur[69]. Increased ribosome biogenesis through the synthesis of both ribosomal proteins and rRNA translation is another major contribution of mTORC1 to increased protein synthesis over extended periods of times[81].

1.3 PI3K/AKT pathway dysregulation in cancer

The PI3K/AKT is one of the most frequently dysregulated pathways in cancer: aberrant PI3K pathway signaling can promote the survival, expansion, and dissemination of cancer cells[1,2,83]. The aberrant activation of the PI3K pathway can occur through several distinct mechanisms, including the amplification of receptor tyrosine kinases (RTKs), genetic mutation or amplification of signaling proteins (*PIK3CA, AKT*), and deletion or mutation of tumor suppressors (*PTEN, INPP4B*) (**Figure 1-4**)[83–85]. *PIK3CA* and *PTEN* are the second and third most highly mutated genes in human cancer[86]. PI3K pathway alterations are found across cancer types (**Figure 1-5**), and preclinical experiments support the potential of targeting the PI3K pathway therapeutically[87–90]. As a result, therapeutic approaches to targeting the PI3K pathway in cancer have been heavily investigated, which will be discussed in more detail below.

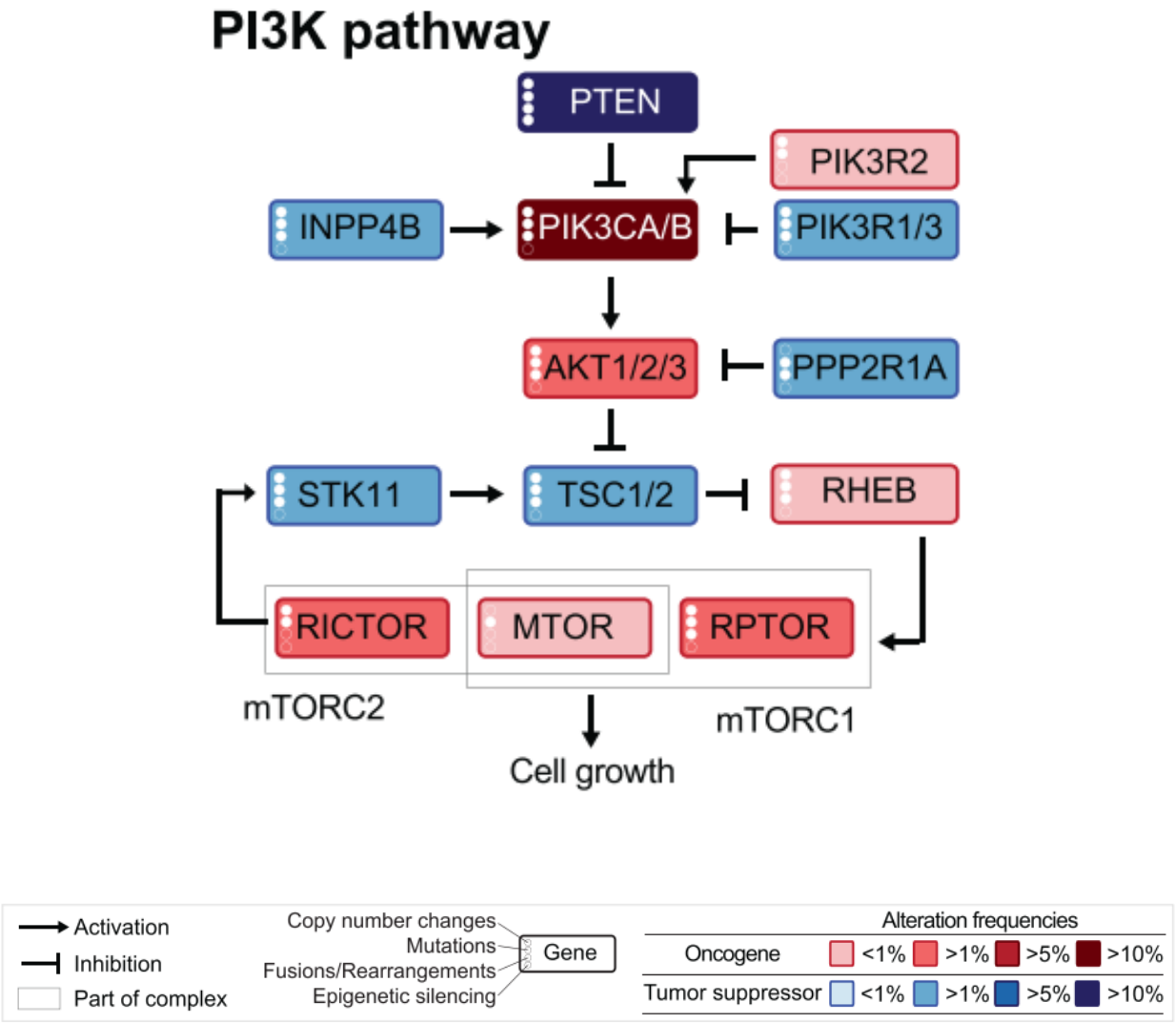

Figure 1-4. Genetic alteration frequency across PI3K pathway components. PI3K pathway signaling diagram colored by frequency of alteration of oncogene activation (red) and tumor suppressor inactivation (blue). Vertical dots indicate the type of somatic alteration contributing to each gene (copy number alterations, mutations, fusions, or epigenetic silencing). Adapted from Sanchez-Vega, F. *et al*. *Cell.* 2018.

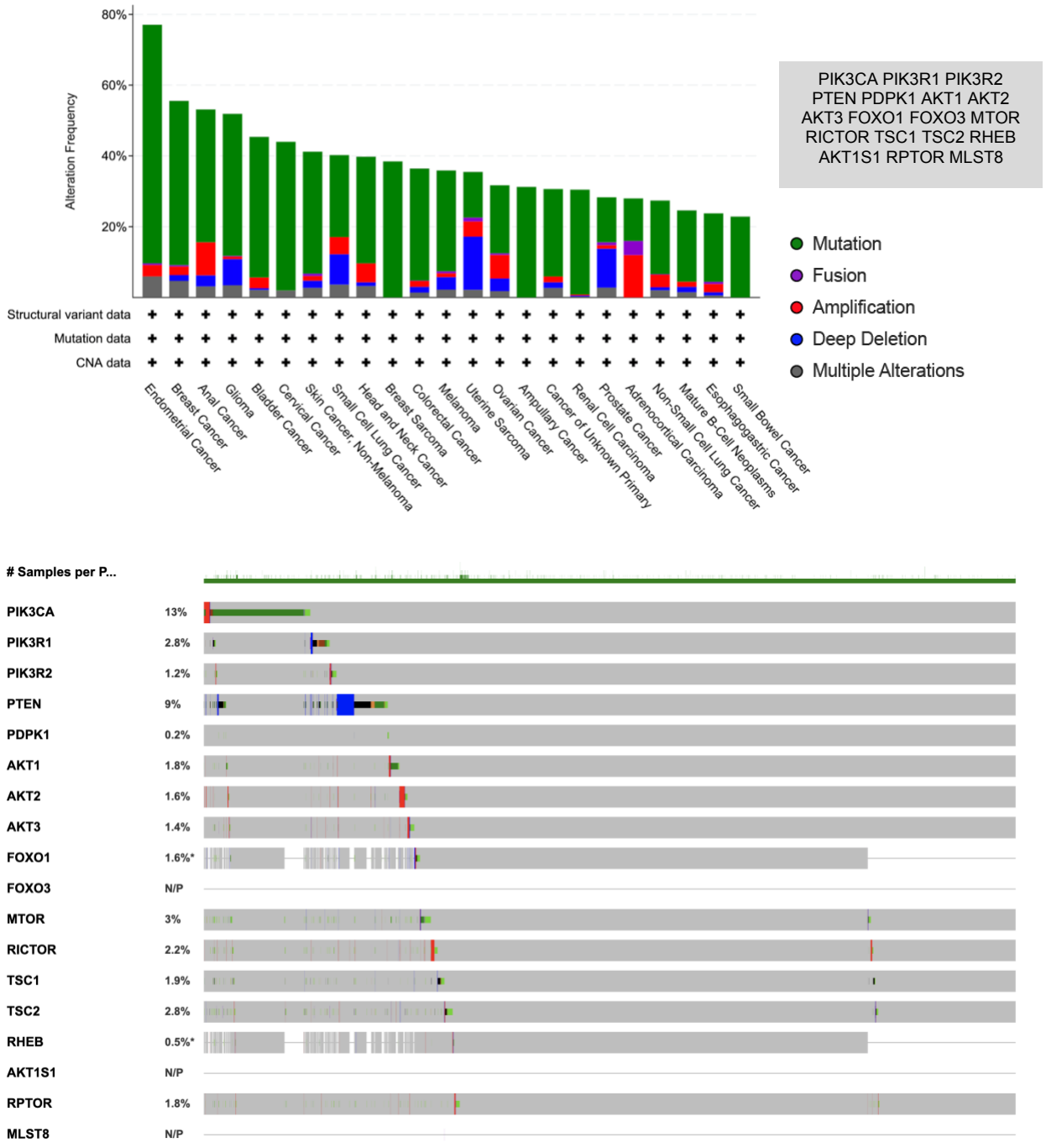

Figure 1-5. Frequent genetic alterations in PI3K pathway in cancer. (**A**) Alteration frequency of PI3K pathway components across cancer types. (**B**) Oncoprint summary of genomic alteration event frequency in PI3K pathway components across cancer types. Generated using cBioPortal. Queried pan-cancer study IMPACT MSKCC Nat Med 2017. Genes queried: PIK3CA PIK3R1 PIK3R2 PTEN PDPK1 AKT1 AKT2 AKT3 FOXO1 FOXO3 MTOR RICTOR TSC1 TSC2 RHEB AKT1S1 RPTOR MLST8. Min # cases = 10, Min % altered = 20%.

PI3K in cancer

PIP3 levels are often increased in cancer cells due to increased activation of RTKs or decreased PTEN activity. Activating mutations in *PIK3CA* itself, the gene encoding PI3Kα, have been identified in many human tumors, including frequent single amino acid kinase domain (H1047R) and helical domain (E542K and E545K) "hotspot" mutations[5]. The H1047R mutation bypasses the requirement for association with RAS for PI3K activity, and increases the interaction of the kinase domain with the membrane[91]. The E542K and E545K mutations disrupt the inhibitory interaction with the regulatory subunit N-SH2 domains. Interestingly, although mutations in regulatory subunits (especially those that disrupt the iSH2 domain of *PIK3R1)* occur in certain cancers*,* mutations in other Class I PI3Ks aside from *PIK3CA* are rare[5,92]. Mutations in *PIK3CA* have been identified across multiple cancer types, though they are especially frequent in estrogen receptor (ER) positive and human epidermal growth factor 2 (HER2) negative breast cancer. Mosaic *PIK3CA* mutations that occur during development have been associated with tissue overgrowth syndromes, as well as brain and venous malformations[93]. Oncogenic lesions in RTKs and RAS can promote signaling through the PI3K pathway independently of mutations in *PIK3CA*.

Functional loss of negative PI3K pathway regulators increases PIP3 levels, though these events are not mutually exclusive with *PIK3CA* or *RAS* mutations. Negative pathway regulators, including in lipid phosphatases *PTEN* or *INPP4B,* are subject to mutation, posttranslational modification, and deletion*.* Loss of the *PTEN* tumor suppressor increases PI3K pathway activation through increasing PIP3 levels, and heterozygous *PTEN* loss induces epithelial neoplasia in intestine, prostate, endometrium, and mammary gland[94]. Homozygous *PTEN* loss leads to prostate carcinoma formation[95,96]. INPP4B is a tumor suppressor whose protein is lost in 84% of aggressive basal-like breast carcinomas[97]. INPP4B directly dephosphorylates PI34P2; thus loss of INPP4B hyperactivates PI3K/AKT signaling[11] and renders tumor cells sensitive to AKT inhibition[12].

mTORC1 and PDK1 in cancer

Alterations in upstream regulators that increase mTOR activity, including oncogenic lesions promoting the activation of PI3K, RAS, AKT, activation or overexpression of RTKs, or the inactivation of PTEN, neurofibromin 1/2 (NF1/2), TSC1/2, are frequent across cancer types[98]. Overexpression of the *MTOR* gene is frequent across human cancers, including 8% of skin cancers, 7% of urinary tract cancers, and 6% of soft tissue cancers[99]. The incidence of mutations in mTOR itself varies greatly across cancer types[98–100]. Functionally characterization of cancer-associated mTOR mutations have revealed their oncogenic potential and ability to confer sensitization to mTOR inhibitors[98–100]. Dysregulation of PDK1 has also been implicated in cancer, both through its regulation of AKT and through the regulation of S6K1, SGK family, p90 ribosomal protein S6 kinase (p90RSK) and the PKC family[101]. Mutations in PDK1 are rare, suggesting that because PDK1 is constitutively active, further activation by genetic mutation is unlikely. However, overexpression and amplification of PDK1 are frequent in tumor samples, including the majority breast cancer samples[102].

AKT in cancer

Hyperactivation of AKT due to its aberrant activation, mutation, or overexpression, are frequent events across many cancer types[1,103]. AKT can be aberrantly activated by a variety of lesions in PI3K pathway components upstream of AKT, as discussed above. Activating mutations in AKT itself are rare but occur in 8% of breast cancers, 5% of colorectal cancers, and 2% of ovarian cancers[104]. The canonical PH-domain E17K activating mutation in AKT increases membrane localization in the absence of PIP_3[5]. This mutation has been identified in all three AKT isoforms and weakly activates downstream signaling and proliferation. AKT2 (E17K) is constitutively active and drives growth factor-independent signaling and proliferation more potently than AKT1 (E17K)[105]. However, AKT2 (E17K) mutations are rare; the majority of these

activating mutations are identified in AKT1, with a few AKT3 (E17K) mutations identified in melanoma samples and cell lines[106–108]. Additional mutations including AKT1 (E49K) PH domain mutations and AKT3 (G171R) kinase domain mutations have been reported in bladder cancer[103,109,110]. Other mutations that have been reported to increase AKT membrane localization and activation include L52R, C77F, and Q79K[111]. Overexpression and amplification of AKT isoforms also occurs frequently in a subset of cancer types, with varying frequency in different cancer settings[26,103,112]. Amplification of AKT1 is frequently observed in gastric, breast, and colon cancers, amplification of AKT2 has been reported in ovarian, breast, and pancreatic cancers; and amplification of AKT3 has been observed primarily in breast and prostate cancers[26,103,112–114].

Increasing evidence suggests a non-overlapping role for AKT isoforms in cancer. For example, loss of AKT2 reduced metastasis in colorectal cancer cell lines that was not rescued by expression of AKT1[115], and AKT3 expression is associated with hormone-independent breast cancers[116]. AKT1 has been identified as a driver of proliferation and survival of breast cancer cells, though it does not promote metastasis[117]. Upregulation of AKT3 has been identified as a mechanism of resistance of breast cancer cells treated with the AKT inhibitor MK-2206[118]. Knockdown of AKT3 was also shown to sensitize TNBC cells to pan-AKT inhibition with GSK690693[66].

1.3.1 Targeting the PI3K/AKT pathway in cancer

Due to the high frequency of mutations across cancer types and the abundance of actionable targets in the PI3K network, significant efforts have been dedicated to targeting this pathway (**Figure 1-6**). Numerous preclinical experiments and clinical trials have supported the value of targeting the PI3K pathway therapeutically. Drug development has focused on PI3K, mTOR, and AKT inhibitors, though to date only a few compounds have been FDA approved for the treatment of cancer[119]. However, the development of novel inhibitors that increase target selectivity, such as the PI3Kα-specific inhibitor alpelisib, have improved the efficacy and toxicity profiles compared to less selective agents[120]. Notably, the development of robust predictive and response biomarkers has been a challenge to the clinical development of PI3K inhibitors, limiting the appropriate selection of patient populations and the evaluation of drug efficacy[121].

Targeting PI3K in cancer

The majority of PI3K inhibitors evaluated in clinical trials to date are reversible catalytic inhibitors. Most PI3K inhibitors induce cytostatic rather than cytotoxic responses, reflecting the fundamental role of PI3K as a sensor of growth factors and nutrients and the nature of *PIK3CA* mutations as weak oncogenes[119,122,123]. The modest efficacy of most PI3K inhibitors may be due to off-target effects, insufficient inhibition, development of adaptive or acquired resistance, and lack of tolerability[85,122,123]. Isoform-selective PI3K inhibitors have improved tolerability compared to pan-PI3K inhibitors, but may lack efficacy due to compensation by other PI3K isoforms[124,125]. Hyperglycemia and hyperinsulinemia are additional challenges resulting from on-target PI3K inhibition due to the critical role of PI3Kα in regulating glucose homeostasis[126]. High circulating insulin upon PI3K inhibition is thought to contribute to resistance, including reactivation of the PI3K pathway or activation of parallel signaling pathways such as the MAPK pathway[126].

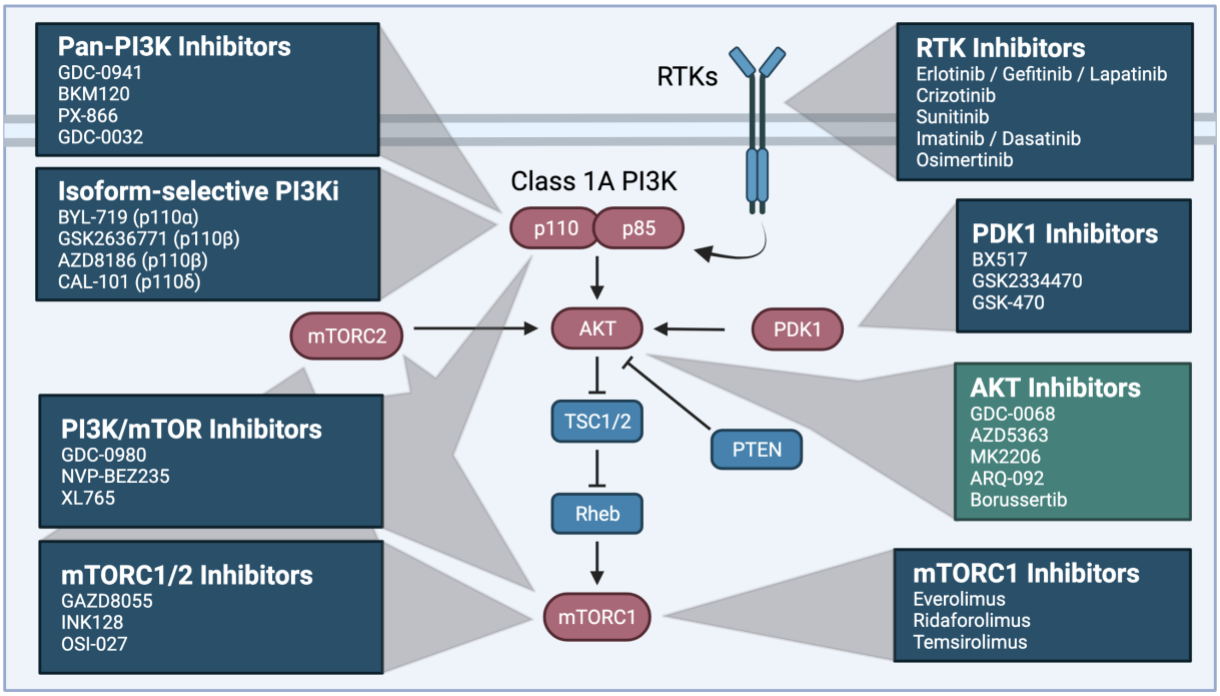

Figure 1-6. Selected inhibitors targeting the PI3K pathway. Diagram of the PI3K pathway featuring selected inhibitors that have been designed to target pathway nodes. Adapted from Slomovitz, B. *et al*. *Clin. Can. Res.* 2012.

Inhibition of PI3K can contribute to antitumor effects through non-cell-autonomous mechanisms and modulation of the microenvironment. For example, PI3Kα inhibition has been shown to modulate angiogenesis by curbing the production of proangiogenic growth factors such as VEGF[127,128]. Because PI3K signaling is an important contributor to immune cell function, inhibition of PI3K can also enhance immune-related inhibition of tumor growth. This led to the development and approval of PI3Kδ/PI3Kγ specific inhibitors for the treatment of hematological malignancies, though there is evidence that these immune effects could contribute to antitumor effects in solid tumors or increased efficacy in combination with immune therapies[122,129,130].

Pan-PI3K inhibitors have been developed to inhibit all four class I PI3K isoforms, although the degree of selectivity for each isoform varies by compound[119]. The broad selectivity of these compounds increases efficacy against a wider range of molecular alterations, but also increases their on-target and off-target toxicities[83]. This may account for their lack of success as clinical agents; only one pan-PI3K inhibitor, copanlisib, has been FDA approved[131]. Although the advancement of pan-PI3K inhibitors buparlisib (BKM120) and pictilisib (GDC-0941) were limited by serious toxicity concerns, results from clinical trials investigating these agents indicated that breast cancers with *PIK3CA* mutations may be sensitive to PI3K inhibition[119]. The p110β-sparing inhibitor taselisib (GDC-0032), evaluated in the SANDPIPER clinical trial in a population of participants enriched for *PIK3CA* mutations, demonstrated the potential benefit of selecting for *PIK3CA* mutations. However, the poor tolerability of taselisib, with side effects including hyperglycemia, rash, diarrhea, and fatigue, raised questions about the safety and efficacy of this inhibitor[123,132,133].

PTEN deficient cancer cells have been shown to be particularly dependent on p110β to sustain growth and proliferation, so clinical trials evaluating the efficacy of p110β-specific inhibitors, such as GSK2636771, have been initiated for the treatment of patients whose tumors exhibit PTEN loss[134–136]. Specific inhibitors for the p110δ and p110γ isoforms of PI3K have been generated and approved for leukemia and lymphoma: the p110δ-specific inhibitor duvelisib and

the p110δ and p110γ dual inhibitor idelalisib, which have demonstrated largely positive clinical responses[119]. The p110α-specific inhibitor alpelisib was recently approved in combination with estrogen receptor antagonist fulvestrant for the treatment of ER+/HER2- *PIK3CA*-mutant metastatic breast cancer after results from the phase III SOLAR-1 trial[137]. Despite intense efforts, alpelisib is the only PI3K pathway inhibitor that has been FDA-approved for the treatment of breast cancer, highlighting the need to develop novel strategies to target this pathway[119,138,139]. The development of more specific inhibitors in combination with patient stratification may further improve the therapeutic index of PI3K inhibitors.

Targeting AKT in cancer

Despite the relative infrequency of oncogenic mutations in AKT itself, dysregulation of this critical node of PI3K pathway signaling underlies numerous human diseases, especially cancer. AKT signaling is hyperactivated in over 50% of human tumors, making it one of the most frequent molecular perturbations in cancer. A number of upstream molecular perturbations can activate AKT, including RTK amplification, mutations in EGFR, HER2, PDK1 or PI3K, loss of tumor suppressors PTEN or INPP4B, or the oncogenic mutation of AKT isoforms, culminating in increased PI3K pathway signaling[140]. Preclinical and clinical evidence support the targeting of AKT, with data suggesting tumors with high phospho-AKT (Ser473 and Thr308) are the most addicted to AKT signaling regardless of whether the genetic lesion leading to activation of the pathway is in AKT itself or upstream[141].

Several AKT-targeting compounds have been synthesized and tested in clinical trials to date, including catalytic, allosteric, and covalent inhibitors (**Table 1-1**). The development of isoform-selective inhibitors has been challenging due to the homology of AKT isoforms; thus, most compounds under clinical development are pan-AKT targeting. To date, no AKT inhibitors have been FDA approved for the treatment of cancer.

Table 1-1: Table of selected AKT inhibitors in clinical trials.

Drug Name	Compound Name	Targets	Mechanism	Clinical Trial Phase
Ipatasertib	GDC-0068	AKT1, AKT2, AKT3	ATP-competitive	Phase III
Capivasertib	AZD5363	AKT1, AKT2, AKT3	ATP-competitive	Phase III
Uprosertib	GSK2141795	AKT1, AKT2, AKT3	ATP-competitive	Phase II
Afuresertib	GSK2110183	AKT1, AKT2, AKT3	ATP-competitive	Phase II
Miransertib	ARQ 092	AKT1, AKT2, AKT3	Allosteric	Phase I
--	MK-2206	AKT1, AKT2, AKT3	Allosteric	Phase II
	TAS-117	AKT1, AKT2, AKT3	Allosteric	Phase II
	Borussertib	AKT1, AKT2, AKT3	Covalent	N/A

Adapted from Martorana, F. *et al.* Frontiers in Pharmacology. 2021.

The druggability of the ATP-binding site has lent itself to the development of several ATP-competitive AKT inhibitors. However, the high degree of conservation of the ATP-binding pocket between related kinases, such as individual AKT isoforms, as well as across the more than 500 kinases in the human kinome, has led to challenges in the development of selective compounds[142]. The catalytic AKT inhibitors developed include GSK690693, GSK2141795 (uprosertib), GSK2110183 (afuresertib), among others[140]. These inhibitors bind to the PH-out conformation of AKT and increase the localization of AKT to the plasma membrane where it is phosphorylated by PDK1 and mTORC2. Of the ATP-competitive inhibitors, ipatasertib (GDC-0068) and capivasertib (AZD5363) have progressed the farthest in clinical trials and are currently under phase II and III clinical investigation in breast and prostate cancers. These two compounds have been tested in a variety of cancer types, and extensively in breast cancer, due to the high frequency of PI3K pathway mutations in this cancer type.

However, these inhibitors lack selectivity within the AGC kinase family, which may limit their tolerability. Recent phase III IPATunity130 trial data indicating lack of efficacy of GDC-0068 have shifted the focus to development of AZD5363 in phase III clinical trials[143]. FAKTION phase II clinical trial data demonstrated that addition of catalytic AKT inhibitor capivasertib (AZD5363) to fulvestrant improved progression-free survival in breast cancer patients who relapsed on aromatase inhibitors, but dose reductions were required to mitigate side effects[144]. The Phase II PAKT study also demonstrated improved progression-free and overall survival in patients with advanced TNBC, especially those with *PIK3CA*, *AKT1*, or *PTEN* mutations[145]. Reports of a kinase-independent pro-survival function of AKT may limit the efficacy of catalytic AKT inhibitors and supports the investigation of allosteric AKT inhibitors[146].

Unlike catalytic inhibitors, allosteric inhibitors lock AKT in a PH-in autoinhibitory conformation[147]. This conformational difference between catalytic and allosteric AKT inhibitors may differentiate inhibitors based on their ability to inhibit kinase-independent or conformation-specific functions. However, some allosteric AKT inhibitors are less functional against AKT

(E17K) compared to catalytic AKT inhibitors[110]. Although allosteric AKT inhibitors MK-2206, miransertib (ARQ 092), and ARQ 751 are highly selective for AKT, clinical efficacy has been hindered by dose limiting toxicities and requires further investigation[83,148,149]. The covalent allosteric AKT inhibitor borussertib has been reported to be efficacious against tumor cells *in vitro* and in patient-derived xenograft models of *KRAS*-mutant pancreatic and colon cancer but has not entered clinical trials[89,150]. Lack of selectivity, development of resistance, toxicity, and the persistence of kinase-independent functions have limited the success of AKT inhibitors in clinical trials.

Targeting mTOR and PDK1 in cancer

mTOR inhibitors were the first compounds targeting the PI3K pathway to advance to the clinic[151,152]. The mTORC1 and mTORC2 signaling complexes both support growth and proliferation through the regulation of metabolic homeostasis and growth, or through their activation of protein kinases like AKT. Because of the high incidence of mTORC1 activation across cancers, there has been wide interest in developing inhibitors, including allosteric inhibitors, rapamycin analogs, and catalytic mTOR kinase domain inhibitors, which inhibit both mTORC1 and mTORC2[153]. These compounds are generally well-tolerated, though their efficacy has been modest in clinical settings, especially as monotherapies, indicating mTORC1 inhibition is not sufficient to induce tumor regression[83,153]. Dual mTOR and pan-PI3K inhibitors have been evaluated, though none of these drugs have been clinically approved[154]. Despite its central role in PI3K signaling, efforts to identify PDK1 inhibitors have been overshadowed by the energy dedicated to targeting other pathway members, including PI3K and AKT. However, several PDK1 inhibitors have been reported and evaluated in preclinical studies[155,156].

Mechanisms of resistance to PI3K pathway inhibitors

Feedback loops that regulate pathway activation are common features of signaling networks. Unfortunately, the physiological systems in place to regulate pathway activation often counteract the effects of pathway inhibitors. The rapid induction of resistance through non-genetic mechanisms such as adaptive resistance is a frequent feature of PI3K pathway inhibition. PI3K/AKT/mTOR inhibitors can increase expression of upstream growth factor receptors, thereby increasing PI3K pathway activity and RAS signaling, among other survival pathways[157]. This rebound in signaling is driven by increased transcription of FOXO target genes including the RTKs HER3, EGFR, and INSR[158–160]. The upregulation of multiple RTKs as a mechanism of resistance presents a challenging problem to address clinically. Similarly, negative pathway feedback involving S6K1-mediated destabilization of IRS-1 is lost upon PI3K/mTORC1 inhibition, leading to hyperactivation of AKT[161].

Resistance to PI3K pathway inhibitors can also be acquired through non-genetic means. *PIK3CA*-mutant breast cancer cells can acquire resistance to the PI3Kα inhibitor alpelisib through upregulation of mTORC1 activity[162]. Activation of PDK1 and SGK family kinases have also been identified as mechanisms of resistance to PI3K inhibitors in breast cancer cells that can increase downstream AKT and mTORC1 activity[19]. Like AKT, SGK1 is recruited to the plasma membrane and activated by mTORC2 and PDK1 phosphorylation and can also activate mTORC1 through inhibitory phosphorylation of its negative regulator, TSC2. SGK3 overexpression has also been demonstrated as a mechanism of resistance to PI3K inhibitors in breast cancer cells to increase signaling output downstream of PDK1[18]. Likewise, upregulation of PIM1, a serine/threonine kinase that shares common phosphorylation targets with AKT and SGK, has also been implicated in resistance to PI3K inhibitors in breast cancer[163].

Crosstalk between pathways parallel to PI3K signaling, such as the RAS effectors extracellular signal-regulated kinase (ERK) and ribosomal protein S6 kinase (RSK), can promote mTORC1 activity through regulation of TSC2 at residues that are distinct from AKT

regulatory sites. mTORC1 activity can also be modulated by glycogen synthase kinase 3 (GSK3) by phosphorylation of Ser859 on Raptor, leading to mTORC1 activation[164]. Alternatively, GSK3 phosphorylation of TSC2 after AMP-activated protein kinase (AMPK)-mediated phosphorylation of TSC2 inhibits mTORC1 activity[165]. RAS and PI3K pathway signaling converge on MYC stabilization; therefore, MYC amplification or activation downstream of RAS represents a driver of resistance to PI3K pathway inhibitors[166].

1.3.2 PI3K pathway biomarkers for tumor risk and response

Despite the frequency of PI3K pathway mutations in solid tumors, establishing predictive biomarkers for cancer risk and treatment outcomes based on pathway mutational status has been a challenge. Preclinical data indicate that *PIK3CA* and *AKT* are relatively weak oncogenic drivers that produce variable degrees of tumor cell addiction to PI3K/AKT signaling[123]. Furthermore, hotspot mutations such as *PIK3CA* E545K or H1047R may differentially potentiate cancer growth, especially on distinct mutational backgrounds.

It is still largely unclear whether tumors with distinct *PIK3CA* mutations respond differentially to different PI3K inhibitors. Recent studies have shown that double *PIK3CA* mutations in cis, which occur in up to 15% of breast cancer patients, increase PI3K activity and consequently sensitivity to PI3K alpha-selective inhibitors[139]. The complexities of pathway regulation and feedback mechanisms pose a challenge when determining if response is correlated to mutational status, singly or as a result of multiple coexisting mutations. Additionally, certain pathway alterations occur at low frequency (i.e., *PTEN* and *AKT* mutations), and thus their incorporation into predictive models, especially retrospective analyses, is compromised due to low statistical power.

Despite initial contradictory preclinical and clinical evidence, the sensitivity of *PIK3CA*-mutant tumors to PI3K inhibitors was confirmed by the SANDPIPER and SOLAR-1 trials, the latter leading to approval of alpelisib[167]. *PIK3CA* mutations in tissue or liquid biopsies have since

been approved by the FDA as predictive biomarkers for the use of alpelisib[168]. However, *PIK3CA* mutation had no predictive value for response to the pan-PI3K inhibitor pictilisib (OPPORTUNE) or alpelisib (NEO-ORB) in the neoadjuvant setting, which retrospectively assessed the contribution of *PIK3CA* mutations[168]. This disconnect in predictive value of *PIK3CA* mutation status may be explained by the low tolerability of pan-PI3K inhibitors compared to isoform-selective PI3K inhibitors, or the prospective vs retrospective assessment of *PIK3CA* mutations as criteria for patient inclusion. Most of the analyses conducted to date, with the exception of the SANDPIPER and SOLAR-1 trials, which used PIK3CA mutational status in their inclusion criteria, have been retrospective, exploratory, and based on a relatively small number of patients[167]. Another possibility is that anti-tumor efficacy of these inhibitors is only revealed in combination settings, for example with endocrine therapy in estrogen receptor-positive tumors.

PI3K pathway mutational status is already used with some success for predicting combination therapy efficacy. Since PI3K pathway inhibitors display limited efficacy as monotherapies, preclinical modeling with adequate biomarker information may optimize selection for combination therapies, such as endocrine therapies, chemotherapy, and molecular targeted agents such as CDK4/6 inhibitors, mTOR inhibitors, and HER2 inhibitors[123,168,169]. As immunotherapy becomes a potential avenue of treatment for patients with breast cancer, it will become important to assess the role of the tumor microenvironment in predicting response to treatments, especially given recent data showing that PI3K inhibitors act on the stroma to contribute to antitumor effects[123].

The evidence presented above emphasizes the critical importance of proper patient selection and argues for the expansion of predictive biomarker studies for future clinical trials. Mutational analysis will likely help refine patient selection and determine whether different PI3K mutations predict improved response to specific inhibitors. Mutational analysis of intertumoral heterogeneity, including predicted markers of resistance to PI3K pathway inhibitors (KRAS,

TP53), may also inform patient selection[123]. Alternative methods for predicting response to PI3K pathway inhibitors, for example through assessment of early metabolic response by 18FDG-PET/CT imaging, may also efficiently predict response to PI3K inhibitors[168,170,171].

Biomarkers of response to PI3K pathway inhibition

Inhibition of the PI3K pathway produces well-characterized signaling and metabolic changes that can be monitored as surrogate measures for pathway inhibition (**Table 1-2**). Measurement of phosphoprotein biomarkers, such as AKT (pThr308, pSer473), PRAS40 (pThr246), 4EBP1 (pSer65, pThr70), and RPS6 (pSer240, pSer244), have been used to evaluate the degree of pathway inhibition and confirm target engagement in early phase clinical trials[172]. Although more direct and quantitative measurements of PI3K inhibition have been developed, such as cellular and tissue measurement of PIP3, these techniques have yet to reach the clinic[173].

Measurements of phosphoprotein biomarkers are often imperfect at gauging target engagement or predicting efficacy of inhibitors in patients, and this has proven to be a particular challenge for PI3K and AKT inhibitors. Inconsistency in sample handling, especially in multicenter clinical trials, may prevent accurate assessment of phosphoproteins downstream of PI3K/AKT. Additionally, the cells sampled to measure response, such as skin or hair follicle biopsies, often have a different compound exposure level than the tumor, leading to inaccurate assessment of exposure or efficacy. Many downstream targets that are used as biomarkers, such as phosphorylation of RPS6 (pSer 240, pSer244) and 4EBP1 (pSer65, pThr70), can be regulated by alternative pathways and thus mask successful target engagement. The disadvantage of this approach is the imperfect ability to predict efficacy, as robust responses can be associated with incomplete inhibition of protein phosphorylation. Lastly, discrepancies between robust preclinical efficacy validated by downstream signaling markers and the

corresponding modest inhibition observed in clinical trials highlights the challenge of using signaling markers at predicting efficacy PI3K inhibitors.

Table 1-2: Biomarkers of response and resistance to PI3K pathway inhibition.

Type	Biomarker	Function	Advantages	Disadvantages
Predictive	*PIK3CA* mutations	Predict sensitivity to PI3K pathway inhibitors	Predict sensitivity to alpelisib	Pathway feedback and tumor heterogeneity complicate use of prediction of genotype as marker of response. Lack of standardized assays (i.e. biopsy), driver mutations, and predictive value of coexisting mutations related to resistance.
	PTEN loss	Predict sensitivity to PI3K pathway inhibitors		
	^{18}FDG-PET/CT imaging	Predict early metabolic response to PI3K pathway inhibitors		Not yet utilized in clinical trials, predictive value unclear
PI3K Pathway Signaling	AKT (pThr308, pSer473), PRAS40 (pThr246), 4EBP1 (pSer65, pThr70), and RPS6 (pSer240, pSer244)	Demonstrate target engagement and pathway modulation		Targets may be regulated by alternative pathways, cells sampled (skin/hair follicle biopsies) may not accurately reflect exposure or efficacy in tumor
Metabolic Response	Plasma glucose	Surrogate measure of pathway modulation	Minimally invasive	Inferior to insulin and C-peptide, as plasma glucose is subject to compensatory insulin and C-peptide release
	Insulin	Surrogate measure of pathway modulation	Minimally invasive	Relationship between dose and response not yet clear
	C-peptide	Surrogate measure of pathway modulation	Minimally invasive	Relationship between dose and response not yet clear
Functional Imaging	^{18}F-FDG-PET	Surrogate measure of pathway modulation	Minimally invasive, highly quantitative, assessment of on-and off-target toxicities	Relationship between dose and response not yet clear
	^{18}F-FLT-PET	Surrogate measure of pathway modulation, proliferation	Minimally invasive, highly quantitative	Not yet utilized in clinical trials for PI3K pathway inhibitors
	Magnetic resonance spectroscopy	Surrogate measure of response	Minimally invasive	Not yet utilized in clinical trials for PI3K pathway inhibitors
	Diffusion-weighted and dynamic contrast enhanced MRI	Surrogate measure of response	Minimally invasive	Not yet utilized in clinical trials for PI3K pathway inhibitors
Circulating	Circulating tumor cells (CTCs)	Surrogate marker of target engagement	Minimally invasive, monitor response over time	Cells in blood exposed to plasma drug concentrations, not concentrations achieved in solid tumors
	Cell-free DNA (cfDNA)	Surrogate marker of target engagement	Minimally invasive	Low plasma DNA levels may prevent detection of mutations and clonal evolution
	Circulating markers of cell death	Surrogate marker for cell death	Minimally invasive	High variability between patients

Alternative means of measuring target engagement are through circulating tumor cells (CTC), cell-free circulating tumor DNA (ctDNA), and circulating markers of apoptosis. These minimally invasive methods detect cancer cells originating from solid tumors, fragments of DNA, or markers of cell death circulating in peripheral blood. A major advantage of circulating biomarkers is their ability to rapidly demonstrate target engagement or tumor shrinkage, and their potential to follow response to inhibitors in real time. Phosphoprotein biomarkers for pathway modulation can be assessed in CTCs, though a clear correlation between these markers and clinical response has not yet been established for PI3K pathway inhibition. One major limitation of circulating biomarkers it that drug concentrations in plasma blood may be significantly different from concentrations to which tumors are exposed.

Due to the pivotal role the PI3K pathway plays in cellular metabolism, several biomarkers to measure metabolic changes in response to PI3K pathway inhibition have been developed. Inhibition of PI3K or AKT prevents AKT-mediated plasma membrane translocation of the glucose transporter GLUT4, dampening cells' ability to uptake glucose. To compensate, the body releases insulin from the pancreas to check glucose levels. Consequently, measurement of plasma glucose, insulin, and C-peptide levels have been adopted as surrogate markers of target engagement. However, a robust understanding of the relationship between these markers and pathway inhibition remains under evaluation[172].

In addition to these plasma biomarkers, several non-invasive functional imaging technologies have emerged as novel approaches to measure both on- and off-target effects and could also be used to inform optimum dosing schedules to reduce toxicities. Metabolic imaging techniques such as positron emission tomography (PET) with 2-deoxy-2-[fluorine-18]fluoro- D-glucose ([18F]-FDG-PET) or 3-deoxy-3-[18F]-fluorothymidine ([18F]-FLT-PET), magnetic resonance spectroscopy including measurement of hyperpolarized of [1-^{13}C]pyruvate metabolism, and diffusion weighted or dynamic contrast enhanced magnetic resonance imaging are means of measuring the metabolic effects of PI3K pathway modulation[171,174]. Noninvasive

imaging techniques offer the advantage of not requiring sample biopsy or acquisition of tumor tissue. These highly quantitative measurements also allow for assessment of both tumor-specific and systemic metabolic effects and the assessment of both on- and off-target toxicities. Quantitative measurements are important for assessing time- and dose-dependent inhibition of downstream signaling to confirm target engagement, since the magnitude and duration of pathway inhibition is often used to predict efficacy[172]. However, there is a clear need for biomarker studies to robustly associate these biomarkers to clinical response. Many of these new technologies have not yet been applied in PI3K clinical trials.

Outlook and future applications of biomarkers for PI3K pathway inhibition

The use of any single biomarker is unlikely to optimally assess clinical response to PI3K pathway inhibition. Instead, the use of a composite biomarker that monitors signaling, metabolic, and immunologic effects may allow for a more detailed evaluation of drug efficacy in patients. Expanding the use of biomarkers throughout the duration of a clinical trial may also inform our understanding of disease progression and development of resistance. Similarly, collecting biomarker data at multiple timepoints, instead of solely at trial endpoint, will allow monitoring of treatment efficacy and disease progression. This strategy may be able to predict emergence of therapeutic resistance. This also emphasizes the need to prospectively, rather than retrospectively, assess patient mutation status[175]. For example, the predictive value of *PIK3CA* mutations was only discovered with prospective mutational analysis in the SOLAR-1 and SANDPIPER trials, indicating that retrospective studies are not sufficient to identify clinical benefit for specific subpopulations of patients[168].

Lastly, there is a clear need for a management strategy for clinical biomarker data. A major barrier to the development of predictive and prognostic biomarkers is the lack of a centralized set of clinical and biomarker data. In the era of big data and personalized patient care, the expansion of biomarker utility will depend on platforms to collect, manage, and share

clinical data. Increasingly detailed biomarker data from genetic sequencing, flow cytometry, metabolic assays, and omics analyses have become less expensive and complex to acquire. The vast amounts of data that clinical trials generate to characterize disease progression and provide evidence of drug efficacy may serve as a resource to inform future trials as well as preclinical studies. Although the collection of these data has become increasingly common, their diverse sources and formats have led to challenges integrating and centralizing information. The development of broadly accessible platforms to strategically manage molecular profiling data and clinical features represents a critical need in cancer management.

Although *PIK3CA* is one of the most frequently altered genes in cancer, the complexity of this signaling network has made it difficult to develop therapeutic agents that successfully target these aberrations and are tolerated in patients[139]. The recent success of the PI3K alpha-specific inhibitor alpelisib in combination with fulvestrant in advanced ER+ breast cancer demonstrates that life-extending therapies are within developmental capacity if the context is correctly understood. Success can be enhanced by improved translation of preclinical models, pre-selection of patients who will respond to therapies, refined monitoring of patient response, and prediction of resistance. Efforts to collect and share clinical data, understand the translatability of *in vitro* and *in vivo* models, and explore additional biomarkers of prediction and response may promote the success of PI3K pathway-targeting agents in the clinic.

1.4 Targeted protein degradation as an alternative to pharmacological inhibition

Several strategies have been developed to target proteins of interest in cancer including biological drugs, such as antibodies, recombinant proteins, or nucleic acids produced from cells, and chemically synthesized small molecules. Cell-permeable small molecules target intracellular proteins to interfere with their function. However, for small molecules to exert their effect, they require tight binding in an active site or pocket such that binding will either block the function of the protein or change the conformation of the target. Approximately 75% of the human proteome

lacks targetable active sites, making over three quarters of human proteins "undruggable" by this classic definition[176]. Furthermore, for proteins that have multiple functions or participate in formation of protein complexes, inhibiting one function may only affect a subset of roles of the protein of interest.

Most inhibitors rely on occupancy-based pharmacological inhibition, and thus require maintenance of high concentrations to achieve the therapeutic effect. However, this is hampered by off-target effects caused by high concentrations of non-specific ligands. Inhibitors may also induce compensatory upregulation of the target pathway or induce mutational changes that contribute to acquired resistance. Event-driven strategies, such as RNA interference or CRISPR-Cas9, use drug binding to induce depletion of the protein of interest and are therefore not dependent on occupancy. These also have the benefit that they do not require an active site. However, genetic strategies are relatively unstable *in vivo* and have low bioavailability.

An alternate strategy is targeted protein degradation. The idea of using protein degradation in cancer therapy has been explored previously using technologies such as selective estrogen receptor degraders (SERDs), and through lysosomal or proteasomal degradation of RTKs upon antibody therapeutic binding[177,178]. Fulvestrant, an estrogen receptor antagonist, has been FDA approved since 2002 for hormone receptor positive breast cancer.

The idea of rationally designing molecules to induce proteasomal degradation of a protein of interest is more recent. A 1999 patent first described the idea of protein degradation, but the idea of artificially targeting a protein for ubiquitination and proteasomal degradation was first raised in the literature in 2001 by Sakamoto *et al.*, who reported a methionine aminopeptidase-2 (MetAP-2) degrader. This chimeric degrader was based on a small molecule ovalicin, tethered to a $SCF^{\beta\text{-}TRCP}$ binding phospho-peptide, and was tested in *Xenopus* egg extracts[179].

Targeted protein degradation expounds on the concept of targeted therapies, namely small molecules or antibodies that recognize specific molecular targets with the goal of

modulating their activity. However, because antibodies are not cell-permeable, their use is largely restricted to cell-surface proteins. Small molecule inhibitors are cell-permeable, allowing their functionality to extend to intracellular targets, however their use has mainly been limited to targeting proteins with enzymatic activities, or targetable active site pockets. Recently, a number of technologies have been developed to induce degradation of specific protein targets, collectively termed targeted protein degradation. These technologies can be broadly categorized into three approaches: genetic degradation tags, protein conjugates, and small molecule-induced degradation[180].

Genetic fusion of degradation tags precisely controls the abundance of a target protein. A number of degradation tags exist, including auxin inducible degron (AID), destabilizing domain of $FKBP12^{L106P}$, dTAG, IKZF3 peptide degron, HaloTag, and small molecule assisted shutoff (SMASh)[180]. These strategies employ the genetic modification of protein of interest with a degradation tag ranging in size from 3-34 kDa using CRISPR-Cas9 knock-in[180]. Degradation of the resulting fusion protein can be induced upon addition of a compound that specifically binds the genetically encoded tag on the protein of interest. This strategy is advantageous due to the extreme precision over which protein abundance can be controlled without significant synthetic chemistry efforts. However, it also requires genome editing and cell line engineering, and the addition of a bulky tag may affect target protein localization, activity, and ability to interact with binding partners or substrates. Efforts to ensure tagged proteins still functionally replicate endogenous proteins are a necessary accompaniment to this protein degradation strategy.

Protein conjugates, such as Trim-Away, lysosome targeting chimeras (LYTACs), and peptide-directed lysosomal degradation can also be used to induce targeted protein degradation. Trim-Away exploits the tight binding of the ubiquitin ligase TRIM21 to antibody Fc domains to recruit a complex of antibody with the protein of interest, resulting in degradation of the entire complex including TRIM21 and antibodies[181]. This approach has limitations, including the inability of antibodies to cross cell membranes, and the possible degradation of non-target

proteins in complex with the protein of interest. LYTACs consist of an antibody fused to a glycopeptide ligand for cation-independent mannose-6-phosphate receptor (CI-M6PR)[180]. These conjugates bind the protein of interest via the conjugated antibody, are internalized and targeted to the lysosome through M6PR receptor internalization and degraded via the lysosome pathway. Lastly, peptide-directed lysosomal degradation uses a fusion peptide comprised of a cell membrane penetrating domain (CPMD) fused to a protein-binding domain to target the protein of interest, followed by a chaperone-mediated autophagy-targeting motif[180]. Lysosomal targeting methods are limited by their long times required for degradation in comparison to strategies that target proteins to the ubiquitin proteasome system, and by their potential for degrading interacting partners of the protein of interest[180].

Small molecule protein degraders rely on the hijacking of ubiquitin ligase activity by small molecules. This idea was first discovered in the plant hormone auxin in the 1990s, which recruits the Cul1-Rbx1-Skp1-Tir1 (SCF^{Tir1}) ubiquitin ligase, functioning as a “molecular glue” to induce the degradation of auxin-responsive transcriptional repressors[180]. The immunomodulatory drugs (IMiDs) thalidomide, pomalidomide, and lenalidomide, are another class of molecular glues that hijack the ubiquitin ligase $CRL4^{CRBN}$ to target the transcription factors IKZF1/3, ZFP91, ZNF692, SALL4, the kinase CSNK1A, and other proteins for proteasomal degradation[180]. These IMiD drugs are currently used in the clinic for the treatment of multiple myeloma, among other indications. Notably, though murine CRBN is capable of binding IMiDs, the Ile391 residue causes steric hindrance that prevents murine CRBN from recruiting neo-substrates for degradation[180]. A mouse model harboring the humanizing mutation $CRBN^{I391V}$ was recently developed and can be used as a tool to assess protein degradation in mouse models. Aryl-sufonamides are another class of small molecule degraders that bind the complex formed between ubiquitin ligase $CRL4^{DCAF15}$ and neo-substrate RBM39, a splicing factor, to stabilize the interface and induce degradation[180].

The discovery of ligands for E3 ubiquitin ligases fueled the development of Proteolysis Targeting Chimeras (PROTACs), bi-functional small molecules designed to induce proteasomal degradation of the protein of interest. PROTACs hijack the cellular ubiquitin proteasome protein degradation machinery to target proteins for degradation by covalent modification of surface lysine residues with the small protein ubiquitin (**Figure 1-7**). A number of proteins have been successfully targeted for induced degradation using PROTACs[180], including kinases[182–184], nuclear receptors[185–187], and epigenetic regulators[188,189].

1.4.1 Targeting proteins for proteasomal degradation using PROTACs

Posttranslational modification of proteins with ubiquitin is a highly conserved process whose resulting code can specify a number of different cellular outcomes[190]. These highly stable 76-residue ubiquitin proteins are post-translationally attached to target proteins through a cascade of three enzymes: an E1 activating enzyme, an E2 conjugating enzyme, and an E3 ligase[190]. The human genome encodes increasing numbers of the enzymes involved in this process: two E1s, 38 E2s, and reportedly over 600 E3s[191]. Ubiquitin is covalently attached to an E1 enzyme to form a thioester bond between the catalytic cystine of the E1 enzyme and the C-terminus of ubiquitin in an ATP-dependent manner. The E1 transfers the ubiquitin to the catalytic cysteine of an E2 enzyme, which is subsequently bound by an E3 ligase to facilitate the transfer of ubiquitin from thioesterified E2 enzyme to the substrate[192]. E3 ubiquitin ligases pair substrate and E2s, which determines the specificity of protein ubiquitination[192].

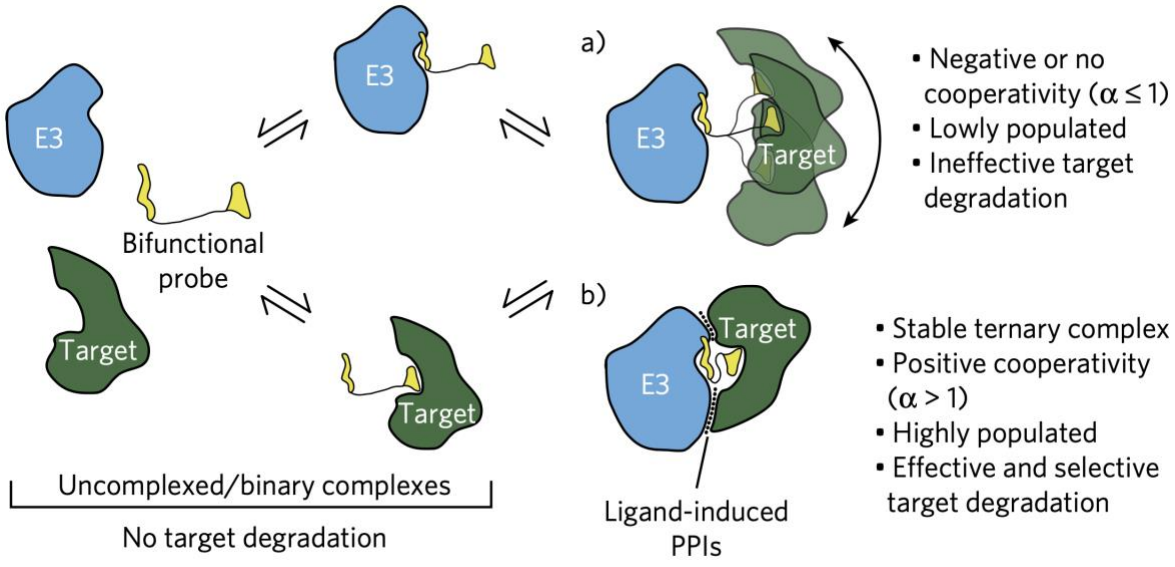

Figure 1-7: PROTAC-induced targeted protein degradation. Formation of a stable ternary complex with E3 ubiquitin ligase is required for selective degradation of target protein. Binding of bifunctional PROTAC independently to target or E3 does not result in productive degradation. Adapted from Gadd, M. *et al. Nat. Chem. Bio.* 2017. PPIs: protein-protein interactions.

Together, these enzymes catalyze the formation of the isopeptide bond attaching the C-terminus of ubiquitin to the lysine of the substrate protein, leading to monoubiquitylation. Substrate-attached ubiquitin can itself be ubiquitinated at one of eight attachment sites, either its seven lysine residues or the N-terminus, to create a polymeric lysine chain of homogenous residue modification or mixed linkages at succeeding positions along the chain[190]. Polyubiquitination of at least four ubiquitin moieties linked by the Lys48 residue marks the modified protein for degradation by the 26S proteasome: the ubiquitin chains are removed for recycling and the tagged protein is unfolded and degraded into constituent amino acids[192].

Protein degradation technology harnesses the ubiquitin ligase system to degrade specific target proteins. Specifically, ligands for E3 ubiquitin ligases can be chemically conjugated to a small molecule designed to target the protein of interest. Target engagement brings the protein of interest into close proximity with the E3 ubiquitin ligase and associated ubiquitination machinery, forming a ternary complex. The associated E2 transfers ubiquitin to surface lysine residues of the target protein, resulting in its ectopic ubiquitination and subsequent proteasomal degradation[193].

Relatively few E3 ubiquitin ligases have been used for degrader molecule design, mostly based on the availability of ligands to recruit them. The availability of small molecule ligands for Cereblon (CRBN) and Von Hippel-Lindau (VHL), as well as the fact that they are widely and well-expressed in different tissue types, has led to their frequent use in PROTAC design. CRBN is an E3 that is ubiquitously expressed across both normal and pathogenic tissues[194]. The IMiD thalidomide and its analogues pomalidomide and lenalidomide are commonly used to recruit the E3 ligase CRBN[194]. Several CRBN-based degraders have been published targeting a number of proteins, including BRD4[195], CDK9[196], BET[197], FLT-3[198], BTK[199], ALK[200], PCAF/GCN5[189], CK2[201], BCL6[202], MDM2[203], and HDAC6[188]. VHL, together with ElonginB, ElonginC, Cul2, and RBX2 forms the multi-subunit E3 ligase complex whose major substrate is hypoxia inducible factor-1α (HIF-1α)[194]. VHL ligands were developed based on the structure of the HIF-1α peptide structure,

and now these small molecule ligands represent a viable strategy to recruit VHL as an E3 ubiquitin ligase for PROTAC-mediated degradation of target proteins, including RIPK2[186], BRD4[204,205], c-ABL[206], EGFR[207], FLT-3[184], TRIM24[208], FAK[209], and p38α and p38δ[210].

In addition to VHL- and CRBN-recruiting elements, ligands targeting XIAP, cAIP, Keap1, RNF4, RNF114, and MDM2 have all been employed to recruit E3 ubiquitin ligases[211,212]. More than 600 E3 ubiquitin ligases have been identified, prompting the development of tissue-specific degraders based on E3 ubiquitin ligase expression[191,193]. Furthermore, the E3 ubiquitin ligase choice can affect tertiary complex formation, which may affect the kinetics and efficiency of target protein ubiquitination and degradation.

Recently, our group and others have reported the development of pan-AKT degrader compounds based on the catalytic AKT inhibitors GDC-0068, AZD5363, or GSK690693, and the E3 ligases VHL or CRBN[213–215]. Our group designed and developed INY-03-041, a pan-AKT degrader based on the catalytic AKT inhibitor GDC-0068 and the CRBN recruiting ligand lenalidomide, and demonstrated improved selectivity and potency over the parent catalytic AKT inhibitor GDC-0068. This AKT degrader also exhibited prolonged depletion of AKT and suppression of downstream signaling, even following compound washout[213]. Another AKT degrader, MS21, designed from AZD5363 and a ligand to recruit the E3 ligase VHL, was reported to suppress cell growth and PI3K pathway signaling for extended periods of time, and shown to destabilize Aurora kinase B[215]. Most recently, a structure activity relationship (SAR) paper was published characterizing AKT degraders with various linkers, AKT, and E3 binding moieties[214].

1.4.2 Advantages and limitations of targeted protein degradation

Targeted protein degradation offers several advantages over both small molecule inhibitors and genetic approaches to protein depletion. Advantages of degraders over genetic inhibition include their rapid mechanism of action, degrading target proteins in minutes to hours,

rather than days or weeks required for genetic manipulation[180]. Faster degradation kinetics prevent rewiring of cellular pathways that adapt to the loss of the target protein, which can complicate the collection and interpretation of phenotypic readouts. Small molecule PROTACs act catalytically to deplete target protein levels by an event-driven rather than occupancy-driven mechanism of action, which lowers the concentrations required to exert pharmacological effects[193,216]. Since it is recycled, one molecule of degrader can sequentially induce multiple rounds of ubiquitination and degradation of the target protein[217]. Although measuring functional engagement of endogenous E3 ligases in cells has been a challenge, degraders have the potential to act sub-stoichiometrically on E3 ubiquitin ligases which would prevent antagonizing the natural functions of the E3[216].

The design and development of degrader molecules has faced numerous challenges. Currently, the relationship between compound structure and activity is difficult to predict, including linker length and composition, and choice of ligands recruiting either the target protein or the E3. The lack of optimal predictions results in significant and iterative chemistry efforts towards compound design. Additionally, degrader molecules may degrade off-target proteins that were not affected by their parental inhibitors, or have undesirable on-target effects based on the E3 targeting ligand[211]. For example, CRBN-recruiting degraders target IKZF1 and IKZF3, known IMiD off-targets, for proteasomal degradation[218,219]. Lastly, because these molecules are larger than most traditional small molecules used in the clinic, they often have poor membrane permeability and are susceptible to efflux pumps[211,220,221].

1.5 Summary

The aberrant activation of the PI3K pathway, including dysregulation of the downstream effector AKT, is frequent across cancer types. Substantial efforts have been dedicated to targeting this pathway pharmacologically and in the clinic, although these efforts have been hampered by dose-limiting toxicities and the development of acquired or intrinsic resistance

mechanisms. Therefore, novel strategies to target this pathway are required to overcome the limitations of current therapies. Targeted protein degradation has recently emerged as a new therapeutic modality and a functional discovery tool. From a therapeutic standpoint, PROTACs have been reported to increase the selectivity of parental inhibitors and have demonstrated efficacy *in vivo*. Additionally, these tools permit the rapid degradation of cellular protein levels to allow for the assessment of acute cellular perturbations. This thesis reports the development and characterization of two pan-AKT degraders, INY-03-041 and INY-05-040, and investigates their functionalities both as therapeutic agents and as discovery tools in PI3K and AKT signaling.

CHAPTER 2

DISCOVERY OF AN AKT DEGRADER WITH PROLONGED INHIBITION OF DOWNSTREAM SIGNALING

This chapter represents a manuscript that has been published in *Cell Chemical Biology*

You, I.*, Erickson, E. C.*, Donovan, K. A., Eleuteri, N. A., Fischer, E. S., Gray, N. S., & Toker, A. (2020). Discovery of an AKT Degrader with Prolonged Inhibition of Downstream Signaling. *Cell Chemical Biology*, *27*(1), 66-73.e7.

Author Contributions

A.T. and N.S.G. conceived the study. I.Y. designed and synthesized the compounds. E.C.E. and I.Y. designed and conducted the biological profiling of the degraders. K.A.D. and N.A.E. performed the proteomics. I.Y and E.C.E wrote the manuscript, with guidance from E.S.F., N.S.G., and A.T. All authors gave feedback on the manuscript.

2.1 Abstract

The PI3K/AKT signaling pathway is a key regulator of many cellular processes including cell growth, proliferation, and metabolism. Aberrant activation of this pathway is one of the most frequent molecular perturbations in cancer, with over half of human tumors exhibiting AKT hyperactivation. Although several small molecule AKT inhibitors are under investigation in clinical trials, robust therapeutic responses have not been observed. An alternate strategy for targeting AKT is to directly reduce cellular protein levels via targeted protein degradation. We report the development of a pan-AKT degrader, INY-03-041, consisting of the ATP-competitive AKT inhibitor GDC-0068, chemically conjugated to lenalidomide, a recruiter of the E3 ubiquitin ligase substrate adaptor Cereblon (CRBN). INY-03-041 induced potent and selective degradation of all three AKT isoforms, and exhibited enhanced anti-proliferative effects compared to GDC-0068. Notably, INY-03-041 induced prolonged degradation of AKT and inhibition of downstream signaling for up to 96 hours, even after compound washout. Our results indicate that AKT degradation may confer sustained pharmacological effects compared with AKT inhibition and highlight the potential advantages of targeted AKT degradation.

2.2 Introduction

The serine/threonine kinase AKT is a central component of the phosphoinositide 3-kinase (PI3K) signaling pathway and is a key regulator of many cellular processes including cell growth, proliferation, survival, and metabolism[1,26]. The AKT protein kinase family is comprised of three highly homologous isoforms, AKT1, AKT2, and AKT3, that possess both redundant functions and isoform-specific activities[222]. Aberrant activation of this pathway due to

amplification or gain-of-function mutations in oncogenes (*PIK3CA,* receptor tyrosine kinases, *AKT1/2/3*), or inactivation of tumor suppressors (*PTEN, INPP4B, PHLPP*) disrupts normal pathway regulation resulting in malignant phenotypes associated with tumor initiation and progression[5,84,223–225]. As these lesions that drive tumorigenesis hyperactivate AKT, significant efforts have been dedicated to developing AKT-targeted therapies[226].

Several ATP-competitive, allosteric, and covalent AKT inhibitors have been developed. ATP-competitive inhibitors, such as ipatasertib (GDC-0068) or capivasertib (AZD5363), are under investigation in phase II and III clinical trials. However, these inhibitors lack selectivity within the AGC kinase family, which may limit their tolerability[227,228]. Interestingly, the polypharmacology of ATP-competitive inhibitors may actually enhance their efficacy[229]. Allosteric AKT inhibitors, such as MK-2206 or miransertib (ARQ 092), are highly selective for AKT, but lack clinical efficacy or require further investigation[230,231]. Covalent allosteric AKT inhibitors have been reported, but have not yet entered clinical trials[89,232]. Still, the development of acquired resistance to targeted therapy has been a major barrier to PI3K pathway inhibition[84,233–235].

An alternate strategy to pharmacologically inhibiting AKT activity is to reduce cellular AKT protein levels through targeted protein degradation. Heterobifunctional degrader molecules, or proteolysis targeting chimeras (PROTACs), consist of a moiety that recruits an E3 ubiquitin ligase, which is chemically linked to another moiety that binds engages a target protein[236]. Recruitment of an E3 ligase into close proximity with the target protein results in the ubiquitination and subsequent proteasomal degradation of the target protein[195]. Several advantages of protein degradation over inhibition have been reported. Protein degradation has been shown to enhance selectivity of multi-targeted kinase inhibitors (CDK9)[196], abrogate kinase-independent functions (FAK)[209], and overcome resistance mutations and compensatory upregulation of target proteins (BTK)[218]. In contrast to classical occupancy-dependent inhibition, degraders act catalytically to induce degradation of target proteins at sub-stoichiometric levels, often achieving robust protein depletion at low nanomolar concentrations[217]. Pharmacological

effects of degraders depend on target protein re-synthesis rate rather than sustained target occupancy, which may result in significantly prolonged biological effects in comparison to reversible inhibitors. However, no degraders have yet been reported to achieve such an extended duration of pharmacological action[237]. Given the long half-life of AKT[238], along with its importance in cancer initiation and progression, AKT is an attractive target for protein degradation.

We report the development of INY-03-041, a pan-AKT degrader that potently degrades all three AKT isoforms for an extended time period. We demonstrate that INY-03-041 exhibits more potent and prolonged suppression of downstream effectors, as well as enhanced anti-proliferative effects in cell-based assays compared to the parental catalytic inhibitor, GDC-0068. The prolonged duration of AKT inhibition along with the corresponding robust pharmacological effects highlights a potentially novel aspect of degrader pharmacology.

2.3 Results

2.3.1 Design and development of the pan-AKT degrader INY-03-041

We designed AKT-targeting heterobifunctional degrader compounds based on GDC-0068, the most advanced AKT inhibitor in clinical trials[227]. The co-crystal structure of GDC-0068 bound to AKT1 (PDB ID: 4EKL) revealed that the isopropylamine of GDC-0068 is solvent-exposed. The amine was chosen as a suitable attachment site for linkers without adversely affecting AKT affinity of GDC-0068 (**Figure 2-1A**). A ten-hydrocarbon linker was used to conjugate GDC-0068 with lenalidomide to generate INY-03-041 (**Figure 2-1B**).

To verify that conjugation of the linker and lenalidomide did not affect the ability of INY-03-041 to bind to AKT, INY-03-041 was tested in a commercially available fluorescence resonance energy transfer (FRET)-based assay (Invitrogen, Z'-Lyte) for AKT1, AKT2, and AKT3 inhibition (Table 2-1).

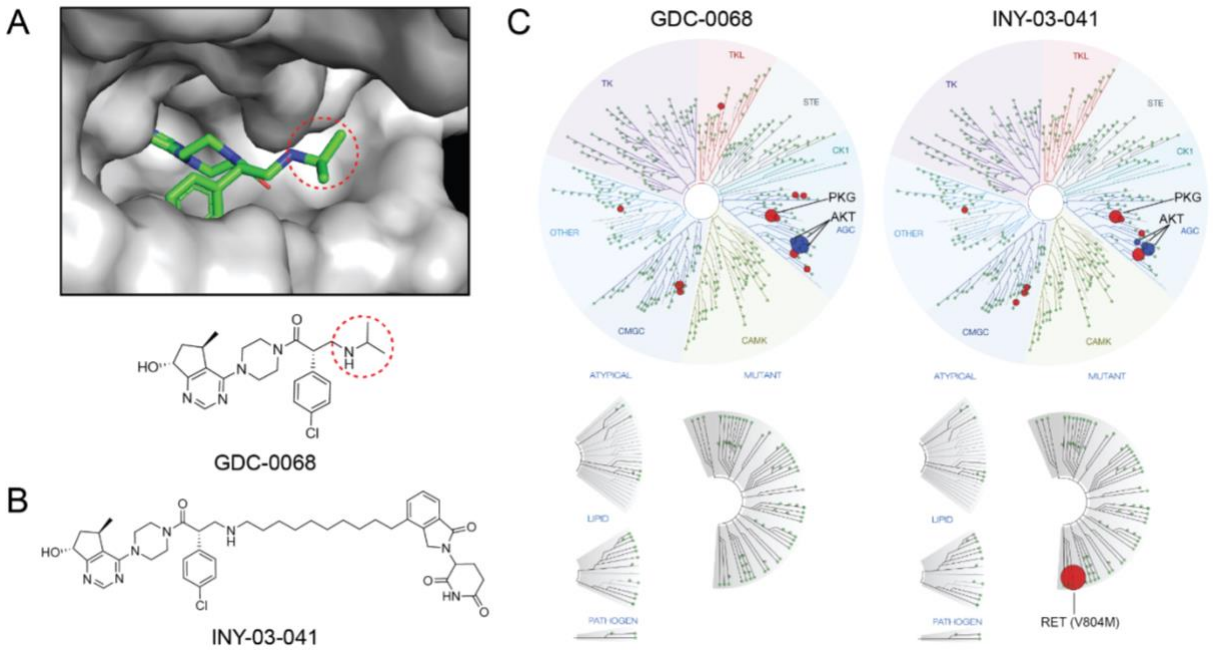

Figure 2-1. Design and development of INY-03-041. (**A**) Co-crystal structure of GDC-0068 (green) bound to AKT1 (gray, PDB: 4EKL) revealing solvent-exposed isopropylamine (circled) where linker was attached. (**B**) Chemical structure of INY-03-041. (**C**) TREE*spot* visualization of the biochemical kinome selectivity profile of GDC-0068 and INY-03-041 (1 μM). AKT isoforms are highlighted in blue, while all other inhibited kinases are highlighted in red (Table S1 in ref.[239]).

Table 2-1. Biochemical IC50s.

	Compound	
Kinase	**INY-03-041**	**INY-03-112**
	IC_{50} (nM)	**IC_{50} (nM)**
AKT1	1.96	1.5
AKT2	6.78	13.7
AKT3	3.51	4.45
PKG1	33.2	N/A
S6K1	37.3	N/A
PKN1	51.7	N/A
ßMSK2	3.31	N/A
Haspin	4020	N/A
RET (V804M)	>10000	N/A

Invitrogen LanthaScreen.

INY-03-041 had similar inhibitory activity against AKT1 (IC_{50} = 2.0 nM), AKT2 (IC_{50} = 6.8 nM), and AKT3 (IC_{50} = 3.5 nM) as GDC-0068 (IC_{50}s for AKT1, 2, and 3 = 5, 18, and 8 nM, respectively)[240], demonstrating that INY-03-041 retained comparable biochemical affinity to all three AKT isoforms as its parent inhibitor. In addition, we evaluated the biochemical selectivity of INY-03-041 against a panel of 468 kinases at 1 μM (KINOMEscan) and observed that INY-03-041 had a similar selectivity profile as GDC-0068 (**Figure 2-1C**). Although INY-03-041 scored as a strong binder of RET (V804M) in the KINOMEscan assay, this was confirmed to be a false positive, as its biochemical IC_{50} was determined to be >10000 nM (Invitrogen, LanthaScreen) (Table S1 in ref.[239]).

2.3.2 INY-03-041 is a potent and highly selective pan-AKT degrader

After verifying that INY-03-041 engaged AKT biochemically, we sought to characterize its degradation activity in cells. We first chose to evaluate the AKT degrader in the triple negative breast cancer cell line MDA-MB-468 due to its high expression of all three AKT isoforms. We found that INY-03-041 induced potent degradation of all three AKT isoforms in a dose-dependent manner after a 12-hour treatment, with maximal degradation observed between 100 to 250 nM (**Figure 2-2A**). At concentrations of 500 nM and greater, we observed diminished AKT degradation, consistent with the hook effect, in which independent engagement of AKT and CRBN by INY-03-041 prevents formation of a productive ternary complex[176]. Treatment of MDA-MB-468 cells with 250 nM of INY-03-041 over time revealed partial degradation of all AKT isoforms within 4 hours and progressive loss of AKT abundance out to 24 hours (**Figure 2-2B**).

To ensure that INY-03-041-induced AKT degradation was dependent on CRBN, we synthesized INY-03-112, a negative control compound with an N-methylated glutarimide that substantially weakens CRBN binding (**Figure 2-3A**)[241]. INY-03-112 did not induce potent degradation of any AKT isoform (**Figure 2-3B**), demonstrating that INY-03-041-induced AKT degradation was CRBN-dependent.

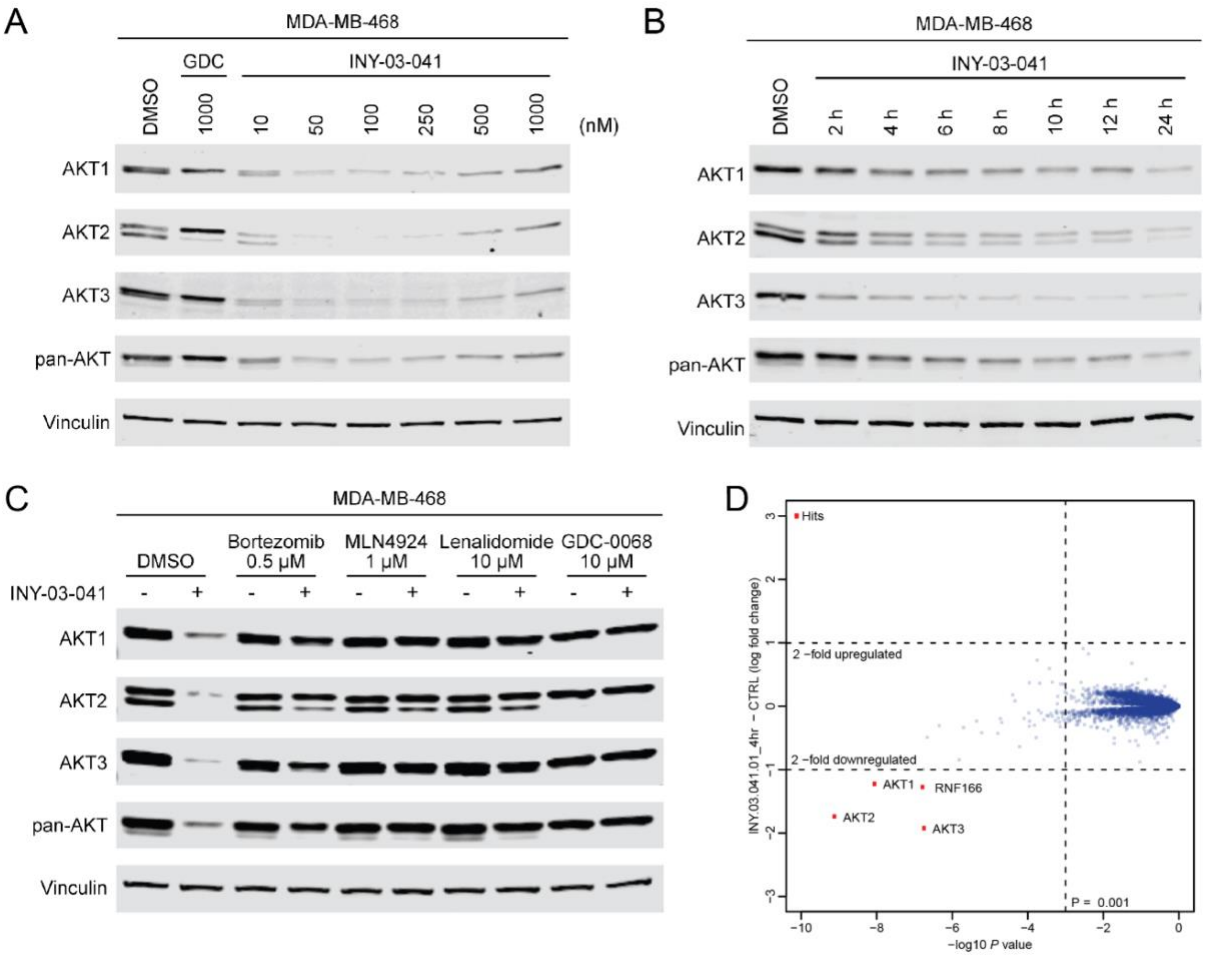

Figure 2-2. INY-03-041 induces potent degradation of AKT isoforms dependent on CRBN, neddylation, and the proteasome. (**A**) Immunoblots for AKT1, AKT2, AKT3, pan-AKT and Vinculin in MDA-MB-468 cells after 12-hour treatment with DMSO, GDC-0068 (GDC), or INY-03-041 at the concentrations indicated (n=4). (**B**) Immunoblots for AKT1, AKT2, AKT3, pan-AKT and Vinculin in MDA-MB-468 cells after treatment with INY-03-041 (250 nM) at indicated times or DMSO (24 h) (n=4). (**C**) Immunoblots for AKT1, AKT2, AKT3, pan-AKT and Vinculin after 12-hour co-treatment of MDA-MB-468 cells with DMSO, bortezomib (0.5 μM), MLN-4924 (1 μM), lenalidomide (Len, 10 μM), or GDC-0068 (GDC, 10 μM) and either INY-03-041 (250 nM) or DMSO (n=4). (**D**) Scatterplot depicts the change in relative protein abundance of INY-03-041 (250 nM, 4 hour) treated MOLT4 cells compared to DMSO vehicle control treated cells. Protein abundance measurements were made using TMT quantitative mass spectrometry and significant changes were assessed by moderated t-test as implemented in the limma package. The $\log_2$ fold change ($\log_2$ FC) is shown on the y-axis and negative $\log_{10}$ p value ($-\log_{10}$ p value) on the x-axis for three independent biological replicates of each treatment. See also Table S2 in ref[239].

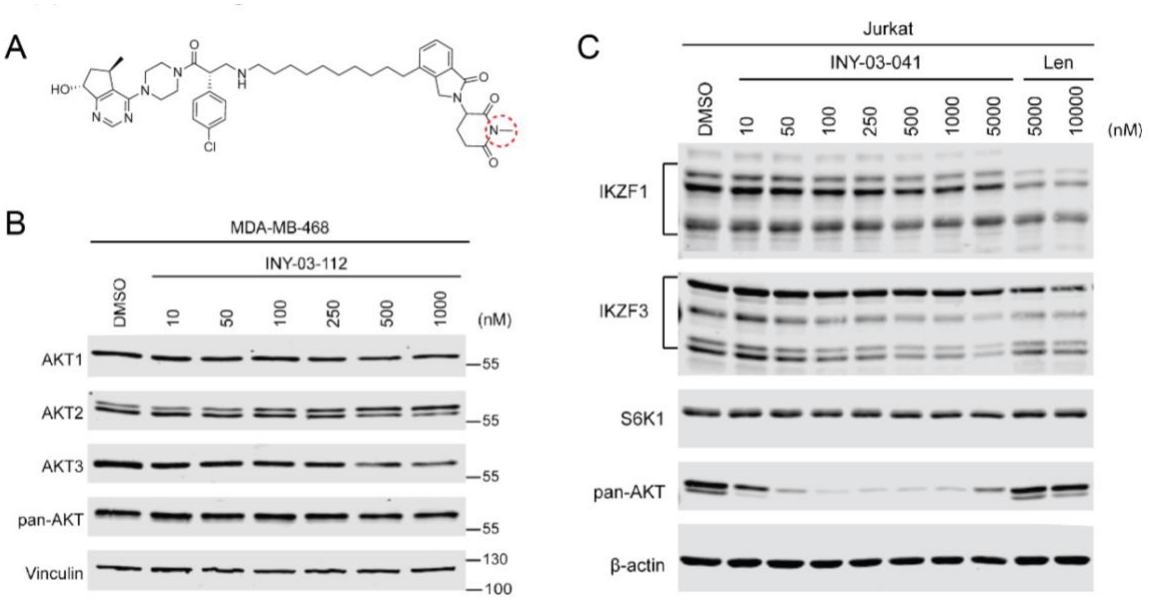

Figure 2-3. INY-03-041 requires CRBN binding to induce highly selective AKT degradation. (**A**) Chemical structure of negative control compound INY-03-112, with N-methylated glutarimide circled. (**B**) Immunoblots for AKT1, AKT2, AKT3, pan-AKT and Vinculin in MDA-MB-468 cells after 12-hour treatment with DMSO or INY- 03-112 at the concentrations indicated (n=2). (**C**) Immunoblots for IKZF1, IKZF3, S6K1, pan-AKT and β-actin in Jurkat cells after 24-hour treatment with DMSO, INY-03-041, or lenalidomide (Len) at the concentrations indicated (n=3).

Furthermore, co-treatment of INY-03-041 with bortezomib, a proteasome inhibitor, or MLN-4924, a NEDD8-activating enzyme inhibitor that prevents neddylation required for the function of cullin RING ligases such as $CRL4^{CRBN242}$, prevented AKT destabilization, indicating that degradation was dependent on the ubiquitin-proteasome system (**Figure 2-2C**). Finally, we co-treated INY-03-041 with excess quantities of either GDC-0068 or lenalidomide to compete for binding to AKT or CRBN, respectively, both of which prevented AKT degradation, demonstrating that engagement to both AKT and CRBN are required for INY-03-041-induced AKT degradation (**Figure 2-2C**).

To broadly assess degrader selectivity, MOLT4 cells, a cell line that is amenable to proteomics and expresses all three AKT isoforms, were treated with 250 nM of INY-03-041 for 4 hours and an unbiased, multiplexed mass spectrometry (MS)-based proteomic analysis was performed. This analysis identified significant downregulation of all three AKT isoforms, as well as RNF166, a ring-finger protein known to be downregulated by lenalidomide treatment (**Figure 2-2D**)[187]. Although INY-03-041 exhibited potent *in vitro* inhibition of S6K1 (IC_{50} = 37.3 nM) and PKG1 (IC_{50} = 33.2 nM), both of which are known off-targets of GDC-0068, no downregulation of either kinase was observed in the proteomics (Table S1 in ref.[239]). Further immunoblot analysis confirmed that INY-03-041 did not induce S6K1 degradation (**Figure 2-3C**). While the time-course (**Figure 2-2B**) indicates that stronger AKT degradation would be observed at longer time points, it is likely that the results would be confounded by subsequent transcriptional changes caused by AKT degradation.

As CRBN-targeting degraders often destabilize zinc finger proteins, and because we observed IMiD-induced downregulation of RNF166, we examined whether INY-03-041 affected protein abundance levels of Ikaros (IKZF1) and Aiolos (IKZF3), well-established targets of lenalidomide[219]. Immunoblot analysis revealed weak IKZF1 and IKZF3 degradation after 24 hours of drug treatment, albeit at relatively high concentrations of 500 nM or greater, indicating that INY-03-041 is primarily a selective degrader for AKT (**Figure 2-3C**).

2.3.3 INY-03-041 exhibits enhanced anti-proliferative effects compared to GDC-0068

As AKT has well-characterized functions in regulating cell proliferation, we next compared the anti-proliferative effects of AKT degradation and inhibition using growth rate inhibition (GR) to account for variation in division rates among cells, as this can confound other drug response metrics, such as IC_{50} values[243]. In a panel of cell lines with PI3K pathway mutations that have been reported to be sensitive (ZR-75-1, T47D, LNCaP, and MCF-7) and insensitive (MDA-MB-468 and HCC1937) to AKT inhibition (**Table 2-2**), we found that INY-03-041 was most potent in ZR-75-1 cells (GR_{50} = 16 nM), with a 14-fold increased potency compared to GDC-0068 (GR_{50} = 229 nM). The anti-proliferative effect of INY-03-041 was degradation-dependent, as INY-03-112 was significantly less potent (GR_{50} = 413 nM) than INY-03-041 and had a comparable GR_{50} value to GDC-0068 (**Figure 2-4A; Table 2-3**). Similar trends were seen in the other cell lines sensitive to AKT inhibition, with 8- to 14-fold lower GR_{50} values for INY-03-041 in comparison to GDC-0068 (**Figures 2-4A-D; Table 2-3**). In addition, lenalidomide, used as a control for RNF166, IKZF1, and IKZF3 degradation, did not have strong anti-proliferative effects, suggesting that the enhanced anti-proliferative effects were due to AKT degradation (**Figures 2-4A-D**).

While INY-03-041 displayed enhanced anti-proliferative effects compared to GDC-0068 in MDA-MB-468 and HCC1937 cells, there were no apparent differences in GR_{50} values between INY-03-041 and INY-03-112, its non-CRBN binding control (**Figures 2-4E and F; Table 2-3**). Thus, the anti-proliferative effects of INY-03-041 in these cell lines were likely due to off-target effects unrelated to AKT degradation that manifest at elevated concentrations of INY-03-041 and INY-03-112. This is consistent with previous studies reporting resistance of MDA-MB-468 and HCC1937 to AKT inhibition and indicates that AKT degradation has similar phenotypic effects as AKT inhibition in these cell lines. Overall, the data show that INY-03-041 suppresses proliferation more potently than GDC-0068 and highlight the potential therapeutic value of targeted AKT degradation.

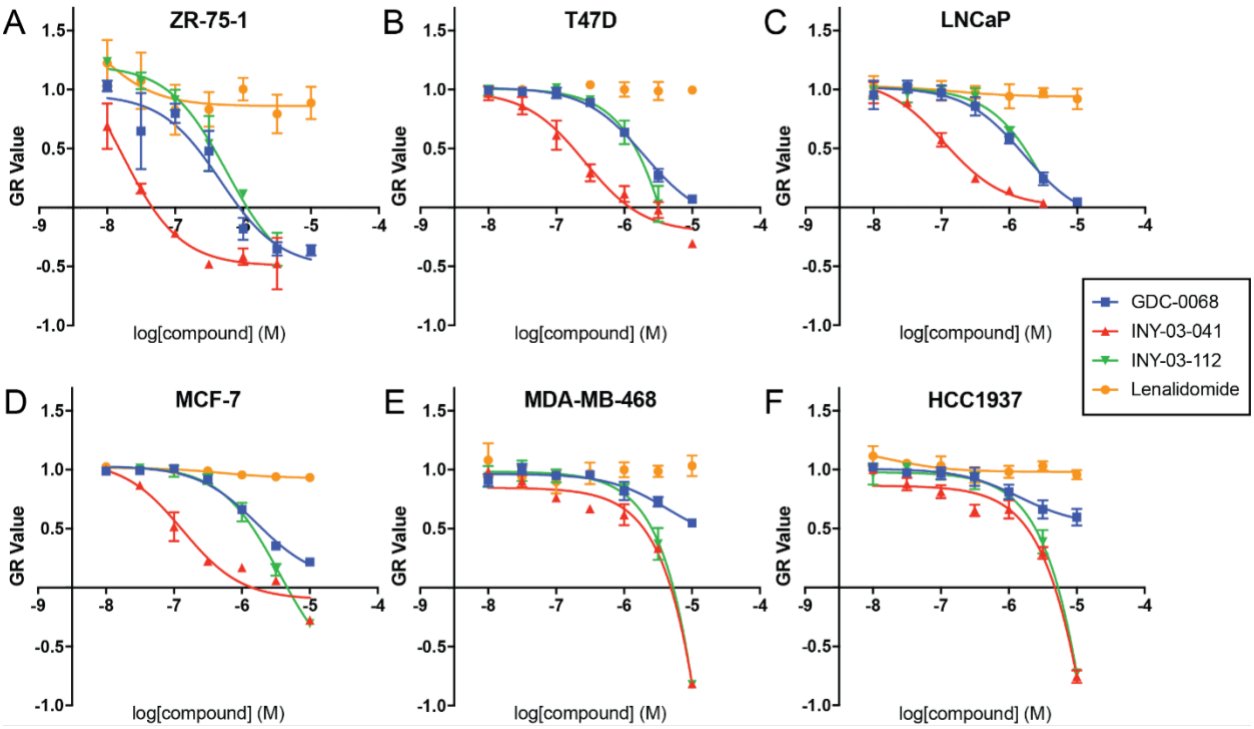

Figure 2-4. INY-03-041 induces enhanced anti-proliferative effects compared to GDC-0068. GR values across concentrations in (**A**) ZR-75-1, (**B**) T47D, (**C**) LNCaP, (**D**) MCF-7, (**E**) MDA-MB-468, and (**F**) HCC1937 cells after 72-hour treatment with GDC-0068 (blue), INY-03-041 (red), INY-03-112 (green), and lenalidomide (orange). Error bars represent standard deviation of three technical replicates.

Table 2-2. Hormone receptor and mutational status of PIK3CA and PTEN in cancer cell line panel.

Cell Line	Tissue	Cancer Subtype	PIK3CA	PTEN
ZR-75-1	Breast	Luminal A	wt	mut (L108R)
T47D	Breast	Luminal A	mut (H1047R)	wt
LNCaP	Prostate	Androgen-dependent	wt	del/mut
MCF-7	Breast	Luminal A	mut (E545K)	wt
MDA-MB-468	Breast	TNBC – Basal A	wt	del
HCC1937	Breast	TNBC – Basal A	wt	del

The tissue, cancer subtype and status of each gene (Meric-Bernstam *et al.*, 2012; Vlietstra *et al*., 1998) as wild-type (wt), mutated (mut) or deleted (del) is indicated. Triple negative breast cancer (TNBC).

Table 2-3. GR values indicate anti-proliferative advantage of INY-03-041.

GR_{50} (μM)				
Cell Line	**INY-03-041**	**INY-03-112**	**GDC-0068**	**Lenalidomide**
ZR-75-1	0.016	0.413	0.229	inf
T47D	0.178	1.34	1.53	inf
LNCaP	0.130	1.38	1.32	inf
MCF-7	0.148	1.49	1.72	inf
MDA-MB-468	1.69	2.70	12.9	inf
HCC1937	1.65	2.42	inf	inf

GR_{max}				
Cell Line	**INY-03-041**	**INY-03-112**	**GDC-0068**	**Lenalidomide**
ZR-75-1	-0.688	-0.517	-0.384	0.744
T47D	-0.321	-0.163	0.054	0.999
LNCaP	0.011	0.212	0.017	0.829
MCF-7	-0.305	-0.332	0.218	0.910
MDA-MB-468	-0.819	-0.832	0.518	0.940
HCC1937	-0.813	-0.726	0.538	0.905

GR_{AOC}				
Cell Line	**INY-03-041**	**INY-03-112**	**GDC-0068**	**Lenalidomide**
ZR-75-1	1.17	0.329	0.705	0.085
T47D	0.630	0.198	0.285	-0.010
LNCaP	0.549	0.186	0.330	0.042
MCF-7	0.627	0.320	0.243	0.021
MDA-MB-468	0.430	0.319	0.140	0.033
HCC1937	0.415	0.313	0.156	-0.008

GR values were calculated after 72-hour treatment with the compounds indicated over a range of concentrations. GR_{50} values represent compound potency, GR_{max} values measure the efficacy of the drug at high concentrations. GR_{AOC} captures changes in potency and efficacy and is calculated by integrating GR curve over a range of concentrations.

2.3.4 INY-03-041 suppresses downstream signaling more potently than GDC-0068

Given the enhanced anti-proliferative effects of INY-03-041 compared to GDC-0068, we sought to compare their effects on downstream AKT signaling. In T47D cells, which were highly sensitive to INY-03-041 in terms of anti-proliferation, we confirmed that INY-03-041 induced potent AKT degradation, with no detectable levels of all three AKT isoforms observed after a 24-hour treatment with 250 nM of INY-03-041 (**Figure 2-5**). Moreover, INY-03-041 treatment resulted in robust and dose-dependent inhibition of phosphorylated PRAS40 (pPRAS40) and GSK3β (pGSK3β), well-established direct substrates of AKT[244,245] as well as S6 (pS6), a downstream marker of AKT activity[246] (**Figure 2-6A**). While 250 nM INY-03-041 significantly reduced pPRAS40, pGSK3β, and pS6 levels, doses up to 1 μM of GDC-0068 were required to observe comparable effects (**Figure 2-6A**). To test whether these effects were generalizable across distinct cell lines, we also compared the effects of INY-03-041 and GDC-0068 in MDA-MB-468, MOLT4, IGROV1 and PC3 cells (**Figure 2-6A** and **Figures 2-7A-C**). Similar to that observed in T47D cells, INY-03-041 significantly reduced phosphorylation of PRAS40, GSK3β and S6 at 250 nM, while weaker responses were seen with equivalent doses of GDC-0068 (**Figure 2-6A** and **Figures 2-7A-C**). Thus, INY-03-041 suppresses downstream AKT signaling more potently than GDC-0068 in a variety of cancer cell lines.

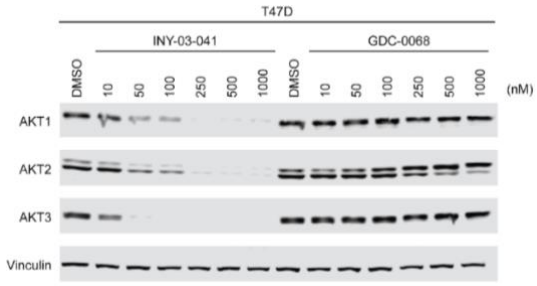

Figure 2-5. INY-03-041 induces degradation of AKT isoforms in T47D cells. Immunoblots of AKT1, AKT2, AKT3 and Vinculin after treating T47D cells for 24 hours with DMSO, INY-03-041, or GDC-0068 at the concentrations indicated (n=3).

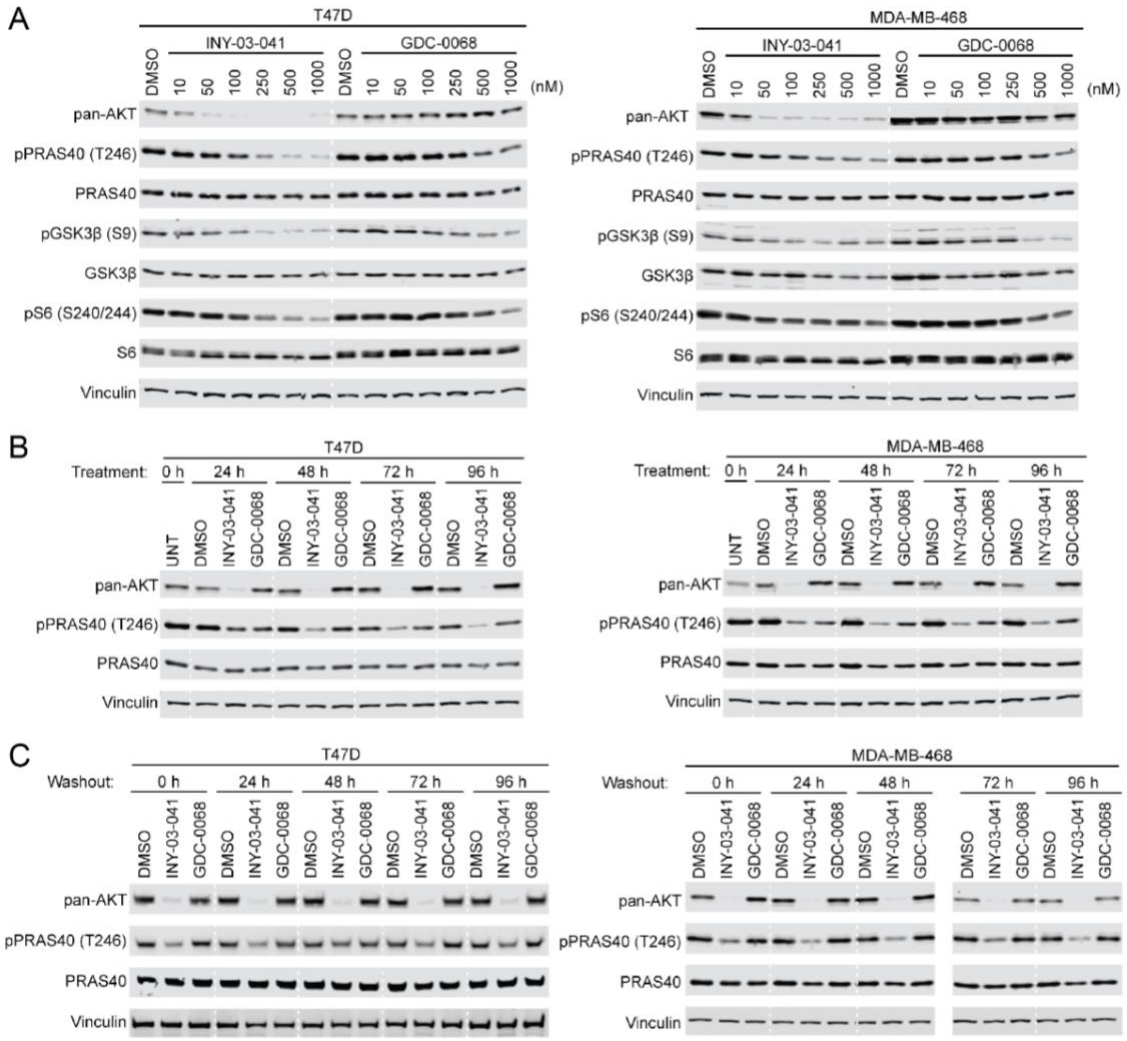

Figure 2-6. INY-03-041 exhibits more potent and durable downstream signaling effects than GDC-0068. (**A**) Immunoblots of pan-AKT, phospho-PRAS40 (T246), total PRAS40, phospho-GSK3β (S9), total GSK3β, phospho-S6 (S240/244), total S6 and Vinculin after treating T47D or MDA-MB-468 cells for 24 hours with DMSO, INY-03-041, or GDC-0068 at the concentrations indicated (n=3). (**B**) Immunoblots of pan-AKT, phospho-PRAS40 (T246), total PRAS40 and Vinculin after treatment of T47D or MDA-MB-468 cells with 250 nM of INY-03-041 or GDC-0068 at time points indicated (n=3). (**C**) Immunoblots of pan-AKT, phospho-PRAS40 (T246), total PRAS40 and Vinculin in T47D or MDA-MB-468 cells treated for 12 hours with INY-03-041 or GDC-0068 (250 nM), followed by washout for indicated times (n=4). Solid vertical white line indicates samples run on separate gels.

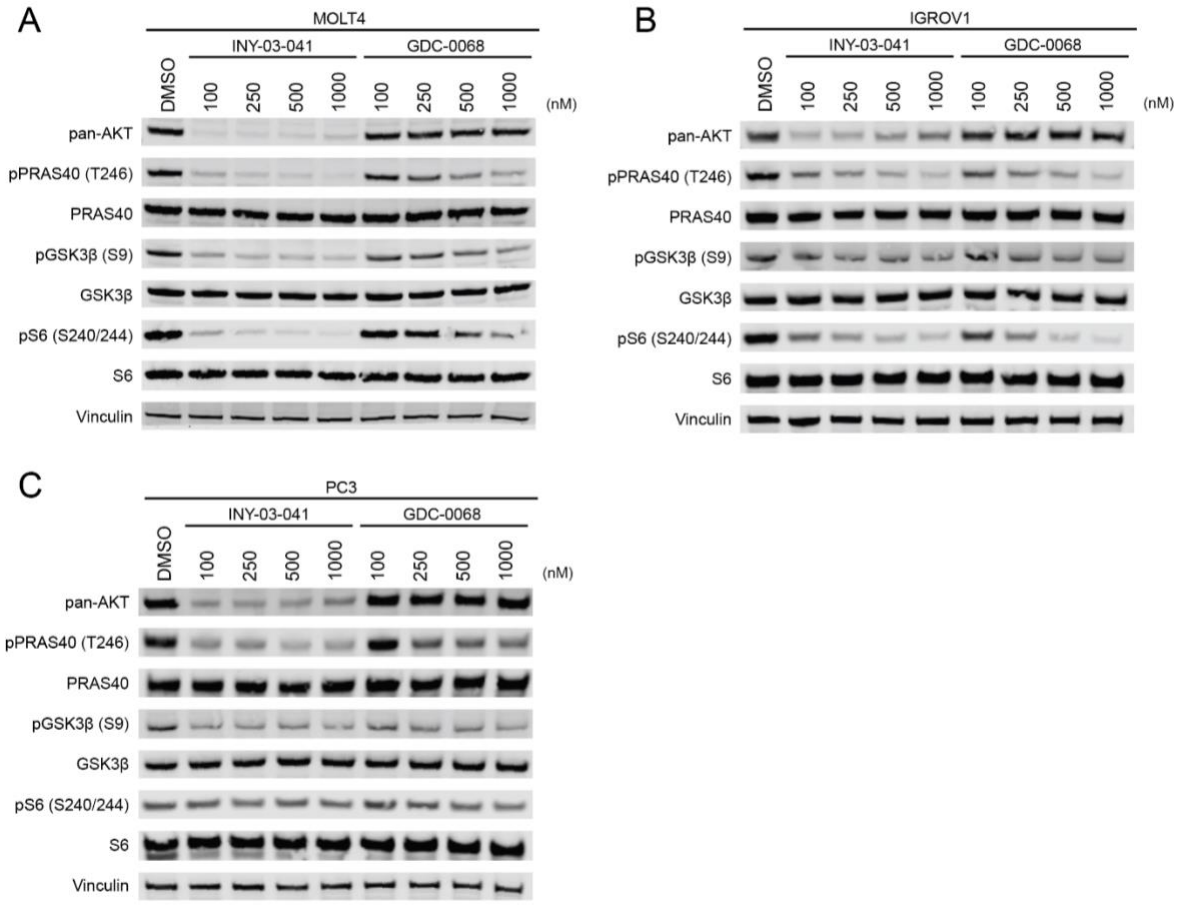

Figure 2-7. INY-03-041 induces potent downregulation of AKT signaling in MOLT4, IGROV1 and PC3 cells. Immunoblots of pan-AKT, phospho-PRAS40 (T246), total PRAS40, phospho-GSK3β (S9), total GSK3β, phospho-S6 (S240/244), total S6 and Vinculin in (**A**) MOLT4, (**B**) IGROV1 and (**C**) PC3 cells after treatment with DMSO, INY-03- 041, or GDC-0068 for 24 hours at concentrations indicated (n=2).

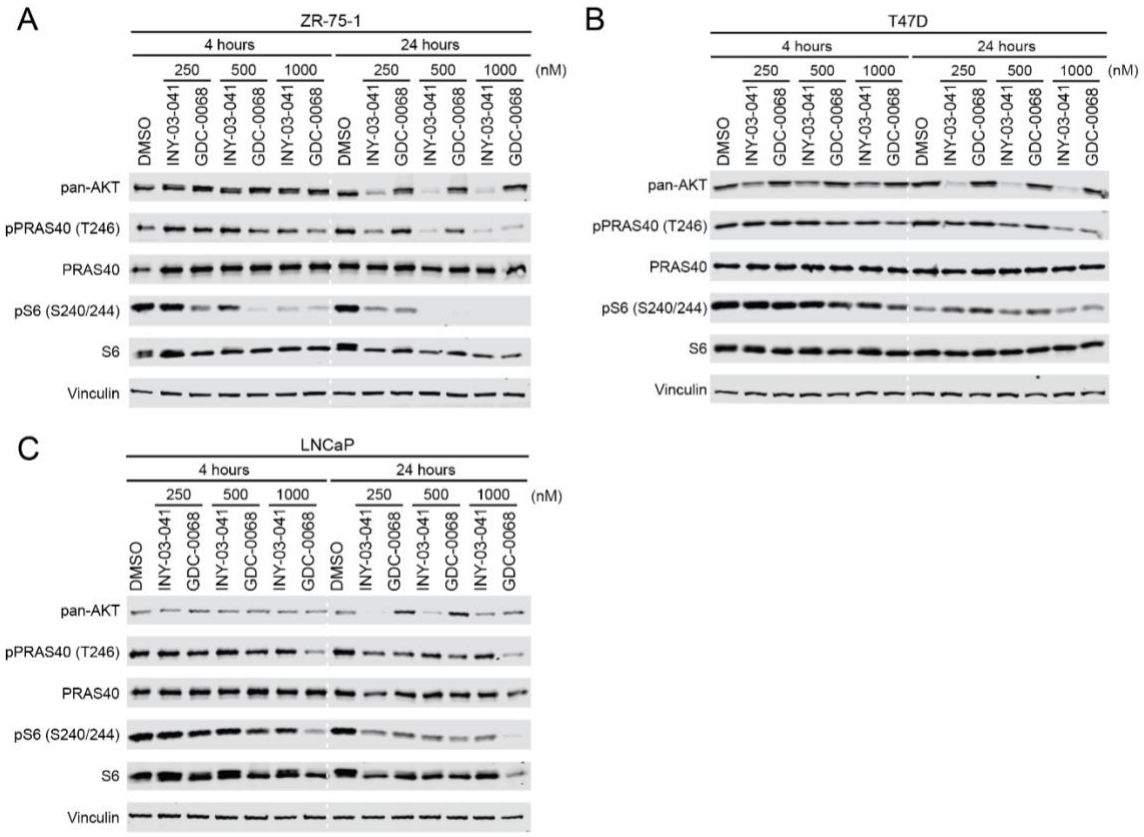

Figure 2-8. INY-03-041 requires longer time points than GDC-0068 to display inhibition of downstream AKT signaling. Immunoblots of pan-AKT, phospho-PRAS40 (T246), total PRAS40, phospho-S6 (S240/244), total S6 and Vinculin in (**A**) ZR-75-1, (**B**) T47D and (**C**) LNCaP cells after treatment with DMSO, INY-03-041, and GDC-0068 for 4 or 24 hours at indicated concentrations (n=2).

Notably, we also found that INY-03-041 promoted sustained destabilization of all three AKT isoforms for at least 96 hours after treatment with 250 nM of INY-03-041 in both T47D and MDA-MB-468 cells (**Figure 2-6B**). This durable AKT degradation resulted in sustained inhibition of downstream signaling, as pPRAS40 (T246) levels were also significantly reduced for up to 96 hours (**Figure 2-6B**). By contrast, treatment with an equivalent dose of GDC-0068 not only resulted in less pronounced inhibition of pPRAS40 (T246), but the duration of this effect was also shorter (**Figure 2-6B**).

To further characterize the mechanism underlying the extended duration of AKT degradation induced by INY-03-041, we performed compound washout experiments after 12 hours of treatment with either 250 nM of INY-03-041 or GDC-0068. We observed no detectable rebound of AKT levels for up to 96 hours after washout in INY-03-041 treated cells (**Figure 2-6C**), suggesting that the re-synthesis rate of AKT is slow. Consistently, INY-03-041 potently suppressed levels of pPRAS40 (T246) for up to 96 hours after washout, while washout in GDC-0068 treated cells resulted in rebound of pPRAS40 (T246), as would be expected of a reversible inhibitor (**Figure 2-6C**). Taken together, our data suggest that INY-03-041-mediated AKT degradation resulted in more potent and durable pharmacological effects than AKT inhibition.

2.4 Discussion

Heterobifunctional degraders have garnered attention recently due to potential advantages over traditional small molecule inhibitors, including their ability to target proteins deemed undruggable through the use of non-functional ligands[247,248] and to achieve selectivity with promiscuous ligand[249]. However, one advantage of degraders that has not been fully investigated is their potential to exert long-lasting pharmacological effects. Given that degraders deplete abundance of a targeted protein, short-term drug exposure may deliver sustained pharmacological effects, uncoupling pharmacodynamics from pharmacokinetics. This distinction

may be more apparent for proteins with slow re-synthesis rates, as longer periods of time may be required for protein levels to recover and re-establish physiological signaling.

Consistent with the long reported half-life for AKT[238], INY-03-041 destabilized all three AKT isoforms and diminished downstream signaling effects for up to 96 hours, even after compound washout. This durable and prolonged pharmacodynamic effect, which was significantly greater than that of the parent AKT inhibitor GDC-0068, may explain, at least in part, the more potent anti-proliferative effects of INY-03-041. To the best of our knowledge, this is the first example of a small molecule degrader that sustains knockdown and downstream signaling effects for such an extended period of time, and exemplifies a distinguishing feature of degrader pharmacology.

Although several ATP-competitive and allosteric AKT inhibitors have entered clinical trials, dose-limiting toxicities or lack of clinical efficacy have hindered their progress[250]. Moreover, AKT has been reported to have kinase-independent functions[146] that would reduce efficacy of small molecule inhibitors, and resistance to AKT inhibitors can arise in some contexts due to upregulation of AKT3[251]. As degraders have been reported to abrogate kinase-independent functions[209] and overcome inhibitor-induced compensatory upregulation of target proteins[252,253], targeted AKT degradation may be a promising alternative approach for therapeutic intervention in cancers with PI3K/AKT pathway alterations. Although our data indicate that AKT degraders can induce more potent and durable downstream effects than AKT inhibitors, further optimization, particularly of the pharmacokinetic properties of the large heterobifunctional degrader molecules will be necessary. In addition, reported on-target toxicities with AKT inhibitors[250] suggest that more potent degraders may have a narrow therapeutic window, further necessitating the need to investigate the therapeutic viability of targeted AKT degradation.

Our data also support the value of INY-03-041 as a chemical probe for studying the acute biological effects of pan-AKT depletion. Existing methods for inducing AKT1, AKT2 and

AKT3 depletion in cells have relied on CRISPR knockout or repression, doxycycline-inducible shRNAs, or transient transfection with siRNA, all of which require relatively long incubation periods[254,255]. This not only prevents assessment of acute biological changes resulting from loss of AKT, but also may allow reprogramming and compensation of cellular networks. By contrast, INY-03-041 induces rapid degradation of all three AKT isoforms, thereby permitting the investigation of the phenotypes of acute pan-AKT depletion. Therefore, INY-03-041 will be a useful chemical tool to explore AKT biology inaccessible with current strategies.

Significance

While many small molecule AKT inhibitors have been developed, here we demonstrate an alternative approach to targeting AKT by inducing its degradation, which resulted in distinct pharmacological effects. INY-03-041, a heterobifunctional degrader, promoted rapid and highly selective degradation of all three AKT isoforms and had more potent anti-proliferative effects than GDC-0068, the most clinically advanced AKT inhibitor. More importantly, INY-03-041-induced degradation of AKT and the ensuing suppression of downstream signaling were sustained for several days. Our work showcases the extended pharmacodynamic effects of degraders and presents INY-03-041 as a tool to study acute changes to the AKT signaling network after rapid AKT degradation.

2.5 Materials and Methods

Experimental Models

MOLT4, Jurkat, ZR-75-1, LNCaP, T47D, MCF-7, MDA-MB-468, and HCC1937 cells were cultured in RPMI media (Wisent Bioproducts) supplemented with 10% heat inactivated fetal bovine serum (Thermo Fisher Scientific) and 100U/mL Penicillin-Streptomycin (Gibco) at 37°C in the presence of 5% CO_2. IGROV1 and PC3 cells were cultured in DMEM media (Gibco)

supplemented with 10% heat inactivated fetal bovine serum (Thermo Fisher Scientific) and 100U/mL Penicillin-Streptomycin (Gibco) at 37°C in the presence of 5% CO_2.

Drug Treatment Experiments

Cells were plated at 250,000 cells per mL (MDA-MB-468, MOLT4, IGROV1, PC3, and Jurkat) or 200,000 cells per mL (T47D) in 2 mL per well of RPMI or DMEM media with 10% serum in 6-well treated tissue culture plates (Greiner, Cat # TCG-657160) or 60 mm treated tissue culture plates (Corning, Cat # 430166) and incubated overnight. The next day, cells were treated with the indicated compounds at the appropriate concentration and protein lysates were harvested at the times specified.

Immunoblotting

Cells were washed once in 1x PBS then lysed in RIPA buffer (150 mM Tris-HCl, 150 mM NaCl, 0.5% (w/v) sodium deoxycholate, 1% (v/v) NP-40, pH 7.5) containing 0.1% (w/v) sodium dodecyl sulfate, 1 mM sodium pyrophosphate, 20 mM sodium fluoride, 50 nM calyculin, and 0.5% (v/v) protease inhibitor cocktail (Sigma-Aldrich) for 15 minutes. Cell extracts were precleared by centrifugation at 14,000 rpm for 10 minutes at 4°C. The Bio-Rad DC protein assay was used to assess protein concentration, and sample concentration was normalized using SDS sample buffer. Lysates were resolved on acrylamide gels by SDS-polyacrylamide gel electrophoresis and electrophoretically transferred to nitrocellulose membrane (BioRad) at 100 volts for 90 minutes. Membranes were blocked in 5% (w/v) nonfat dry milk in tris-buffered saline (TBS) buffer for 1 hour then incubated with specific primary antibodies diluted in 5% (w/v) nonfat dry milk in TBS-T (TBS with 0.05% Tween-20) at 4°C overnight, shaking. The next day, membranes were washed with TBS-T then incubated for 1 hour at room temperature with fluorophore-conjugated secondary antibodies (LI-COR Biosciences). The membrane was

washed again with TBS-T then imaged with a LI-COR Odyssey CLx Imaging System (LI-COR Biosciences).

Growth Rate Assay and Analysis

Cell lines were plated at densities ranging from 500 to 2000 cells per well in a 384-well plate using a Matrix WellMate Reagent Dispenser (Thermo Fisher) and allowed 24 hours to adhere to plate prior to treatment. A D300 Digital Dispenser (Hewlett-Packard) was used to treat cells with dilution series of compounds as indicated. At the time of treatment and after 72 hours of treatment, cells were stained and fixed for subsequent analysis. Cells were stained with LIVE/DEAD Far Red Dead Cell Stain (LDR) (Thermo Fisher Scientific) at 1:2000 for 1 hour at 37°C. Cells were fixed for 30 minutes at room temperature in 4% formaldehyde (Sigma Aldrich) then permeabilized with 0.5% Triton X-100 in PBS. Cells were blocked for 1 hour using Odyssey Blocking Buffer (LI-COR Biosciences) and stained overnight at 4°C with 2 µg/ml Hoechst 33342 (Sigma Aldrich). An Operetta microscope was used to image fixed cells, and data was stored and analyzed using Columbus software (PerkinElmer). Nuclei were segmented by Hoechst signal using the Columbus system (Perkin Elmer). The average LDR and Hoechst intensities were determined within the nuclear area. Dead cells were classified by LDR signal. Experiments were performed in technical triplicate.

In Vitro Kinase Assays

Z'-LYTE assays were conducted for AKT1, AKT2, AKT3, PKG1, S6K1, PKN1, ßMSK2, and Haspin at Life Technologies in a 10-point dose response using Km ATP concentrations. LanthaScreen assays were conducted for RET (V804M) in a 10-point dose response at Life Technologies.

TMT LC-MS Sample Preparation

MOLT4 cells were treated with DMSO, 250 nM INY-03-041-01 for 4 hours in biological triplicates. Cells were harvested by centrifugation. Lysis buffer (8 M Urea, 50 mM NaCl, 50 mM 4-(2hydroxyethyl)-1-piperazineethanesulfonic acid (EPPS) pH 8.5, 1x Roche protease inhibitor and 1x Roche PhosphoStop was added to the cell pellets and cells were homogenized by 20 passes through a 21 gauge (1.25 in. long) needle to achieve a cell lysate with a protein concentration between 0.5-4 mg mL-1. The homogenized sample was clarified by centrifugation at 20,000 x g for 10 minutes at 4°C. A Bradford assay was used to determine the final protein concentration in the cell lysate. 200 µg protein for each sample were reduced and alkylated as previously described (An *et al*., 2017). Proteins were precipitated using methanol/chloroform. In brief, four volumes of methanol were added to the cell lysate, followed by one volume of chloroform, and finally three volumes of water. The mixture was vortexed and centrifuged at 14,000 x g for 5 minutes to separate the chloroform phase from the aqueous phase. The precipitated protein was washed with three volumes of methanol, centrifuged at 14,000 x g for 5 min, and the resulting washed precipitated protein was allowed to air dry. Precipitated protein was resuspended in 4 M Urea, 50 mM HEPES pH 7.4, followed by dilution to 1 M urea with the addition of 200 mM EPPS pH 8 for digestion with LysC (1:50; enzyme:protein) for 12 hours at RT. The LysC digestion was diluted to 0.5 M Urea, 200 mM EPPS pH 8 and then digested with trypsin (1:50; enzyme:protein) for 6 hours at 37°C. Tandem mass tag (TMT) reagents (Thermo Fisher Scientific) were dissolved in anhydrous acetonitrile (ACN) according to manufacturer's instructions. Anhydrous ACN was added to each peptide sample to a final concentration of 30% v/v, and labeling was induced with the addition of TMT reagent to each sample at a ratio of 1:4 peptide:TMT label. The 11-plex labeling reactions were performed for 1.5 hours at RT and the reaction quenched by the addition of 0.3% hydroxylamine for 15 minutes at RT. The sample channels were combined at a 1:1:1:1:1:1:1:1:1:1:1 ratio, desalted using C18 solid phase extraction cartridges (Waters) and analyzed by LC-MS for channel ratio comparison. Samples

were then combined using the adjusted volumes determined in the channel ratio analysis and dried down in a speed vacuum. The combined sample was then resuspended in 1% formic acid and acidified (pH 2-3) before being subjected to desalting with C18 SPE (Sep-Pak, Waters). Samples were then offline fractionated into 96 fractions by high pH reverse-phase HPLC (Agilent LC1260) through an aeris peptide xb-c18 column (phenomenex) with mobile phase A containing 5% acetonitrile and 10 mM NH4HCO3 in LC-MS grade H2O, and mobile phase B containing 90% acetonitrile and 10 mM NH4HCO3 in LC-MS grade H2O (both pH 8.0). The 96 resulting fractions were then pooled in a non-continuous manner into 24 fractions and every fraction was used for subsequent mass spectrometry analysis.

Data were collected using an Orbitrap Fusion Lumos mass spectrometer (Thermo Fisher Scientific, San Jose, CA, USA) coupled with a Proxeon EASY-nLC 1200 LC pump (Thermo Fisher Scientific). Peptides were separated on a 50 cm and 75 μm inner diameter Easyspray column (ES803a, Thermo Fisher Scientific). Peptides were separated using a 190 minute gradient of 6 – 27% acetonitrile in 1.0% formic acid with a flow rate of 300 nL/min. Each analysis used an MS3-based TMT method as described previously (McAlister *et al.*, 2014). The data were acquired using a mass range of m/z 340 – 1350, resolution 120,000, AGC target 5 x 105, maximum injection time 100 ms, dynamic exclusion of 120 seconds for the peptide measurements in the Orbitrap. Data dependent MS2 spectra were acquired in the ion trap with a normalized collision energy (NCE) set at 35%, AGC target set to 1.8 x 104 and a maximum injection time of 120 ms. MS3 scans were acquired in the Orbitrap with a HCD collision energy set to 55%, AGC target set to 2 x 105, maximum injection time of 150 ms, resolution at 50,000 and with a maximum synchronous precursor selection (SPS) precursors set to 10.

LC-MS Data analysis

Proteome Discoverer 2.2 (Thermo Fisher) was used for .RAW file processing and controlling peptide and protein level false discovery rates, assembling proteins from peptides,

and protein quantification from peptides. MS/MS spectra were searched against a Uniprot human database (September 2016) with both the forward and reverse sequences. Database search criteria are as follows: tryptic with two missed cleavages, a precursor mass tolerance of 10 ppm, fragment ion mass tolerance of 0.6 Da, static alkylation of cysteine (57.02146 Da), static TMT labeling of lysine residues and N-termini of peptides (229.16293 Da), variable phosphorylation of serine, threonine and tyrosine (79.966 Da), and variable oxidation of methionine (15.99491 Da). TMT reporter ion intensities were measured using a 0.003 Da window around the theoretical *m/z* for each reporter ion in the MS3 scan. Peptide spectral matches with poor quality MS3 spectra were excluded from quantitation (summed signal-to-noise across 10 channels < 200 and precursor isolation specificity < 0.5). Only proteins containing at least two unique peptides identified in the experiment were included in final quantitation.

Chemistry Synthetic Scheme

Scheme 1

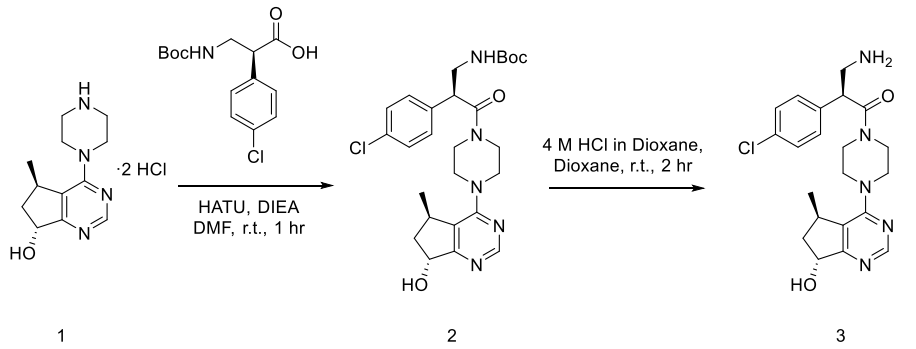

1 2 3

Scheme 2

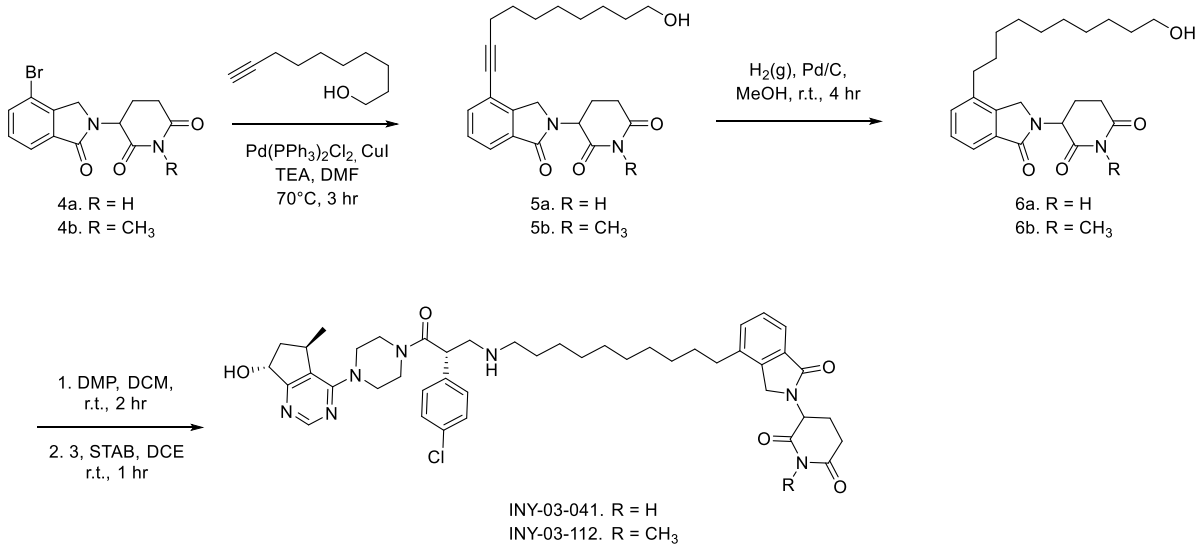

4a. R = H
4b. R = CH_3

5a. R = H
5b. R = CH_3

6a. R = H
6b. R = CH_3

INY-03-041. R = H
INY-03-112. R = CH_3

General Chemistry Methods

Reagents and solvents were purchased from commercial suppliers and were used without further purification unless otherwise noted. Reactions were monitored using a Waters Acquity UPLC/MS system (Waters PDA eλ Detector, QDa Detector, Sample manager - FL, Binary Solvent Manager) using Acquity UPLC BEH C18 column (2.1 x 50 mm, 1.7 µm particle size): solvent gradient = 85% A at 0 min, 1% A at 1.7 min; solvent A = 0.1% formic acid in Water; solvent B = 0.1% formic acid in Acetonitrile; flow rate: 0.6 mL/min. Products were purified by

flash column chromatography using CombiFlash®Rf with Teledyne Isco RediSep® normal-phase silica flash columns (4 g, 12 g, 24 g, 40 g or 80 g) and preparative HPLC using Waters SunFireTM Prep C18 column (19 x 100 mm, 5 μm particle size) using a gradient of 15-75% methanol in water containing 0.05% trifluoroacetic acid (TFA) over 48 min (60 min run time) at a flow of 40 mL/min. ^{1}H NMR spectra were recorded on 500 MHz Bruker Avance III spectrometer, and chemical shifts are reported in million (ppm, δ) downfield from tetramethylsilane (TMS). Coupling constants (J) are reported in Hz. Spin multiplicities are described as s (singlet), br (broad singlet), d (doublet), t (triplet), q (quartet) and m (multiplet). Purities of assayed compounds were in all cases greater than 95%, as determined by reverse-phase HPLC analysis.

Abbreviations Used

DCM: Dichloromethane

DIEA: N,N-Diisopropylethylamine

DMF: Dimethylformamide

TEA: Triethylamine

DMP: Dess–Martin periodinane

STAB: Sodium triacetoxyborohydride

DCE: 1,2-Dichloroethane

MeOH: Methanol

Chemical Synthesis of INY-03-041 and INY-03-112

Chemical Synthesis of 3

Tert-butyl((S)-2-(4-chlorophenyl)-3-(4-((5R,7R)-7-hydroxy-5-methyl-6,7-dihydro-5H-cyclopenta[d]pyrimidin-4-yl)piperazin-1-yl)-3-oxopropyl)carbamate (2):

To a solution of known intermediate 1 (727 mg, 2.37 mmol), (S)-3-((tert-butoxycarbonyl)amino)-2-(4-chlorophenyl)propanoic acid (711 mg, 2.37 mmol) and HATU (902 mg, 2.37 mmol) in DMF (12 mL) was added DIEA (2.1 mL) and stirred for 1 hour at room temperature. The reaction mixture was diluted ethyl acetate (30 mL) and washed with water (2 x 15 mL) and brine (2 x 15 mL). The organic layer was dried over anhydrous sodium sulfate, filtered, and concentrated in vacuo to afford 2 as a yellow oil (1.22 g, 100% yield). The crude was used directly for the next reaction. LC-MS: m/z 516.27 [M+1].

(S)-3-amino-2-(4-chlorophenyl)-1-(4-((5R,7R)-7-hydroxy-5-methyl-6,7-dihydro-5H-cyclopenta[d]pyrimidin-4-yl)piperazin-1-yl)propan-1-one (3):

To a solution of intermediate 2 (1.22 g, 2.37 mmol) in dioxane (7 mL) was added 4 M HCl in dioxane (5 mL). The reaction was stirred at room temperature for 4 hours. The reaction mixture was concentrated in vacuo and purified by reverse-phase HPLC (95-35% methanol in water) to obtain 3 as a TFA salt. The resultant TFA salt was dissolved in a mixture of 4:1 chloroform: isopropanol (50 mL) and washed with sat. aq sodium bicarbonate (50 mL) to give 3 as a white foam (868 mg, 88% yield). LC-MS: m/z 416.25 [M+1]. ^{1}H NMR (500 MHz, DMSO-d6) δ 8.43 (s, 1H), 7.43 – 7.38 (m, 2H), 7.35 – 7.28 (m, 2H), 4.84 (t, J = 7.3, 6.2 Hz, 1H), 4.07 (dd, J = 8.3, 5.3 Hz, 1H), 3.73 – 3.66 (m, 1H), 3.64 – 3.56 (m, 3H), 3.52 – 3.35 (m, 4H), 3.22 – 3.16 (m, 1H), 3.09 (dd, J = 12.6, 8.3 Hz, 1H), 2.72 – 2.67 (m, 1H), 2.01 – 1.87 (m, 2H), 1.04 (dd, J = 6.5, 3.9 Hz, 3H).

Synthesis of INY-03-041 and INY-03-112

3-(4-(10-hydroxydec-1-yn-1-yl)-1-oxoisoindolin-2-yl)piperidine-2,6-dione (5a)

Known intermediate 4a (500 mg, 1.55 mmol), dec-9-yn-1-ol (478 mg, 3.10 mmol), $Pd(PPh_3)_2Cl_2$ (113 mg, 0.16 mmol) and CuI (61 mg, 0.32 mmol) were dissolved in TEA (4 mL) and DMF (8 mL). The reaction mixture was flushed with nitrogen (x3) and stirred at 70°C for 3 hours. The

reaction mixture was cooled to room temperature, diluted with ethyl acetate (50 mL) and filtered through celite. The organic layer was washed with brine (3 x 20 mL), dried over anhydrous sodium sulfate, filtered and concentrated in vacuo. The crude material was purified by column chromatography on silica gel (9:1 DCM:MeOH) to afford 5a as a pale yellow solid (503 mg, 82% yield). LC-MS: m/z 397.24 [M+1]. ^{1}H NMR (500 MHz, DMSO-d6) δ 11.00 (s, 1H), 7.71 (dd, J = 7.6, 1.0 Hz, 1H), 7.64 (dd, J = 7.7, 1.0 Hz, 1H), 7.52 (t, J = 7.6 Hz, 1H), 5.76 (s, 2H), 5.15 (dd, J = 13.3, 5.2 Hz, 1H), 4.45 (d, J = 17.6 Hz, 1H), 4.31 (d, J = 17.6 Hz, 1H), 3.37 (t, J = 6.5 Hz, 2H), 2.92 (ddd, J = 17.3, 13.6, 5.5 Hz, 1H), 2.64 – 2.57 (m, 1H), 2.50 – 2.40 (m, 2H), 2.06 – 1.99 (m, 1H), 1.62 – 1.54 (m, 2H), 1.47 – 1.37 (m, 3H), 1.36 – 1.23 (m, 5H), 1.18 (t, J = 7.3 Hz, 1H).

3-(4-(10-hydroxydecyl)-1-oxoisoindolin-2-yl)piperidine-2,6-dione (6a)

To a solution of intermediate 5a (100 mg, 0.25 mmol) in MeOH (10 mL) was added Pd/C (10 mg). H_2 (g) was introduced to the reaction mixture, and the reaction was stirred at room temperature for 4 hours. The reaction mixture was filtered over celite and concentrated in vacuo to afford 6a as a white solid (91 mg, 91% yield). LC-MS: m/z 401.30 [M+1]. ^{1}H NMR (500 MHz, DMSO-d6) δ 10.98 (s, 1H), 7.60 – 7.54 (m, 1H), 7.50 – 7.41 (m, 2H), 5.13 (dd, J = 13.3, 5.1 Hz, 1H), 4.45 (d, J = 17.2 Hz, 1H), 4.34 – 4.28 (m, 2H), 3.36 (td, J = 6.5, 4.9 Hz, 2H), 2.92 (ddd, J = 17.3, 13.7, 5.4 Hz, 1H), 2.66 – 2.58 (m, 3H), 2.43 (qd, J = 13.3, 4.5 Hz, 1H), 2.01 (dtd, J = 12.7, 5.2, 2.2 Hz, 1H), 1.66 – 1.54 (m, 2H), 1.43 – 1.35 (m, 2H), 1.33 – 1.21 (m, 12H).

3-(4-(10-(((S)-2-(4-chlorophenyl)-3-(4-((5R,7R)-7-hydroxy-5-methyl-6,7-dihydro-5H-cyclopenta[d]pyrimidin-4-yl)piperazin-1-yl)-3-oxopropyl)amino)decyl)-1-oxoisoindolin-2-yl)piperidine-2,6-dione (INY-03-41)

To a solution of intermediate 6a (83 mg, 0.21 mmol) in DCM (4 mL) was added DMP (132 mg, 0.31 mmol). The reaction was stirred at room temperature for 2 hours. The reaction mixture was

filtered and concentrated in vacuo to obtain 10-(2-(2,6-dioxopiperidin-3-yl)-1-oxoisoindolin-4-yl)decanal (84 mg, quantitative yield). LC-MS: m/z 399.27 [M+1]. The crude material was then dissolved in DCE (2 mL), followed by addition of intermediate 3 (131 mg, 0.31 mmol). The reaction was stirred at r.t. for 30 minutes, after which STAB (89 mg, 0.42 mmol) was added. The reaction mixture was stirred for an additional 1 hour. The reaction was quenched by sat. aq sodium bicarbonate (10 mL) and extracted with DCM (3 x 20 mL). The organic layers were combined, dried over anhydrous sodium sulfate, filtered and concentrated in vacuo. The crude residue was purified by reverse-phase HPLC (75-15% methanol in water) to obtain INY-03-041 (TFA salt). The resultant TFA salt was dissolved in 4:1 chloroform:isopropanol (10 mL) and washed with sat. aq sodium bicarbonate. The organic layer was dried over anhydrous sodium sulfate, filtered and concentrated in vacuo to afford title compound as an off-white solid (42 mg, 25% yield). LC-MS: m/z 798.42 [M+1]. ^{1}H NMR (500 MHz, DMSO-d6) δ 8.43 (s, 1H), 7.56 (dd, J = 5.4, 3.2 Hz, 1H), 7.45 – 7.43 (m, 2H), 7.41 (d, J = 8.2 Hz, 2H), 7.34 (d, J = 8.2 Hz, 2H), 5.38 (d, 1H), 5.13 (dd, J = 13.3, 5.1 Hz, 1H), 4.87 – 4.80 (m, 1H), 4.45 (d, J = 17.1 Hz, 1H), 4.29 (dd, J = 15.4, 7.6 Hz, 2H), 3.70 – 3.56 (m, 5H), 3.51 – 3.42 (m, 3H), 3.41 – 3.36 (m, 1H), 3.24 – 3.16 (m, 2H), 2.92 (ddd, J = 17.9, 13.8, 5.4 Hz, 1H), 2.77 – 2.71 (m, 1H), 2.63 (t, J = 7.5 Hz, 3H), 2.60 – 2.55 (m, 2H), 2.42 (tt, J = 13.3, 6.6 Hz, 1H), 2.04 – 1.93 (m, 2H), 1.93 – 1.87 (m, 1H), 1.62 – 1.55 (m, 2H), 1.41 – 1.35 (m, 2H), 1.32 – 1.26 (m, 4H), 1.22 (s, 8H), 1.03 (d, J = 6.8 Hz, 3H).

3-(4-(10-hydroxydec-1-yn-1-yl)-1-oxoisoindolin-2-yl)-1-methylpiperidine-2,6-dione (5b)

5b was synthesized with similar procedures as 5a using intermediate 4b (90 mg, 0.27 mmol) as the starting material. 5b was obtained as a light orange solid (49 mg, 44% yield). LC-MS: m/z 411.51 [M+1]. ^{1}H NMR (500 MHz, DMSO-d6) δ 7.71 (dd, J = 7.6, 1.0 Hz, 1H), 7.63 (dd, J = 6.8, 1.2 Hz, 1H), 7.52 (t, J = 7.6 Hz, 1H), 5.21 (dd, J = 13.5, 5.1 Hz, 1H), 4.44 (d, J = 17.6 Hz, 1H), 4.30 (d, J = 17.6 Hz, 1H), 3.36 (t, J = 6.5 Hz, 2H), 3.04 – 2.95 (m, 4H), 2.79 – 2.72 (m, 1H), 2.47

(t, J = 7.1 Hz, 2H), 2.45 – 2.39 (m, 1H), 2.03 (dtd, J = 12.7, 5.2, 2.2 Hz, 1H), 1.61 – 1.52 (m, 2H), 1.47 – 1.34 (m, 4H), 1.34 – 1.24 (m, 6H).

3-(4-(10-hydroxydecyl)-1-oxoisoindolin-2-yl)-1-methylpiperidine-2,6-dione (6b)

6b was synthesized with similar procedures as 6a using intermediate 5b (42 mg, 0.1 mmol) as the starting material. 6b was obtained as an off-white solid (33 mg, 79% yield). LC-MS: m/z 415.57 [M+1]. ^{1}H NMR (500 MHz, DMSO-d6) δ 7.60 – 7.53 (m, 1H), 7.49 – 7.43 (m, 2H), 5.20 (dd, J = 13.4, 5.1 Hz, 1H), 4.45 (d, J = 17.1 Hz, 1H), 4.32 – 4.27 (m, 2H), 3.36 (td, J = 6.6, 5.1 Hz, 2H), 3.01 (s, 3H), 3.00 – 2.95 (m, 1H), 2.79 – 2.74 (m, 1H), 2.66 – 2.61 (m, 2H), 2.48 – 2.39 (m, 1H), 2.08 – 1.98 (m, 1H), 1.63 – 1.56 (m, 2H), 1.43 – 1.34 (m, 2H), 1.32 – 1.22 (m, 12H).

3-(4-(10-(((S)-2-(4-chlorophenyl)-3-(4-((5R,7R)-7-hydroxy-5-methyl-6,7-dihydro-5H-cyclopenta[d]pyrimidin-4-yl)piperazin-1-yl)-3-oxopropyl)amino)decyl)-1-oxoisoindolin-2-yl)-1-methylpiperidine-2,6-dione (INY-03-112)

INY-03-112 was synthesized with similar procedures as INY-03-041 using intermediate 6b (27 mg, 0.07 mmol) as the starting material. INY-03-112 was obtained as an off-white solid (9 mg, 16% yield). LC-MS: m/z 812.47 [M+1]. ^{1}H NMR (500 MHz, DMSO-d6) δ 8.43 (s, 1H), 7.57 (dd, J = 5.8, 2.8 Hz, 1H), 7.49 – 7.43 (m, 4H), 7.37 – 7.32 (m, 2H), 5.40 (d, J = 5.5 Hz, 1H), 5.21 (dd, J = 13.4, 5.1 Hz, 1H), 4.83 (q, J = 6.3 Hz, 1H), 4.45 (d, J = 17.1 Hz, 1H), 4.38 (dd, J = 8.9, 5.1 Hz, 1H), 4.29 (d, J = 17.1 Hz, 1H), 3.76 – 3.41 (m, 8H), 3.41 – 3.34 (m, 3H), 3.10 (t, J = 10.0 Hz, 1H), 3.01 (s, 3H), 2.99 – 2.95 (m, 1H), 2.83 – 2.73 (m, 3H), 2.63 (t, J = 7.7 Hz, 2H), 2.43 (qd, J = 13.2, 4.5 Hz, 1H), 2.05 – 1.87 (m, 3H), 1.59 (t, J = 7.5 Hz, 2H), 1.50 (s, 2H), 1.33 – 1.27 (m, 4H), 1.23 (s, 8H), 1.02 (d, J = 6.9 Hz, 3H).

QUANTIFICATION AND STATISTICAL ANALYSIS

Anti-proliferation Assay

Growth rate inhibition values were determined as described previously using python 3.7.3. Data was visualized using a non-linear regression curve fit in GraphPad Prism 8. N=3 biological replicates were used for each treatment condition and each data point represents the mean +/- SEM, as also indicated by the figure legend.

LC-MS Data Analysis

Reporter ion intensities were normalized and scaled using in house scripts and the R framework. Statistical analysis was carried out using a moderated t-test in the limma package within the R framework.

DATA AND SOFTWARE AVAILABILITY

The accession number for the proteomic data reported in this paper is Pride: PXD015207

2.6 Acknowledgements

We would like to thank Eric Wang and Milka Kostic for helpful comments on the manuscript. We would also like to thank Caitlin Mills and Kartik Subramanian (Laboratory for Systems Pharmacology at Harvard Medical School) for their help with proliferation data collection and analysis. This work was supported by the Training Grant in Chemical Biology (NIH 7 T32 GM095450-07, I.Y.), the Training Grant in Pharmacological Sciences (NIH 1 T32 GM132089-01, I.Y.), the National Science Foundation Graduate Research Fellowship Program (DGE1745303, E.C.E.), the NIH 1R01 CA218278-01A1 (E.S.F., N.S.G.) and the Ludwig Center at Harvard (E.C.E., A.T.).

CHAPTER 3

MULTI-OMICS APPROACH REVEALS AKT DEGRADATION SPECIFICALLY ALTERS NUCLEOTIDE METABOLISM AND STESS KINASE SIGNALING

Author Contributions

Alex Toker and Nathanael Gray conceived the study. Inchul You designed and synthesized the compounds. Emily C. Erickson and Inchul You designed and conducted the biological profiling of the degraders. Katherine Donovan performed mass spectrometry. Emily C. Erickson performed all omics profiling experiments and analysis was performed was Emily C. Erickson and Ralitsa R. Madsen. COSMOS analysis was performed by Ralitsa R. Madsen. Support was derived in part by funding from an F31 predoctoral fellowship (5F31CA254000-02) held by Emily C. Erickson.

3.1 Abstract

The serine/threonine kinase AKT, a well-characterized node in the PI3K signaling network, is a critical mediator of cell proliferation, survival, metabolism, and apoptosis. Over 50% of human tumors display AKT hyperactivation, but AKT inhibitors under clinical investigation lack therapeutic efficacy at tolerable doses and display significant on-target toxicities. To address the need for new strategies to target AKT, small molecule degraders targeting AKT have been developed and characterized. To assess rapid changes after AKT depletion, we characterized a second-generation AKT degrader INY-05-040. INY-05-040 induced long-lasting AKT degradation and more robust inhibition of downstream signaling and cell proliferation than catalytic inhibitors. We used a multi-omics approach to investigate the consequence of AKT degradation on metabolism and gene transcription, revealing a potent transcriptional response and degradation-specific increase in nucleosides. We applied an integrated network analysis approach to extract mechanistic insights from metabolomics and RNA-seq datasets and identified stress kinase signaling as a signature unique to AKT degradation. In cell-based studies, AKT degradation activated the stress kinases JNK and p38α leading to induction of apoptotic cell death which could be rescued by the JNK inhibitor JNK-IN-8. These results emphasize the utility of targeted protein degradation as a tool to decode the mechanisms governing AKT signaling in human cancer, and its potential as a cancer therapeutic.

3.2 Introduction

The phosphoinositide 3-kinase (PI3K)/AKT and RAS/MAPK pathways are key cellular networks that integrate extracellular stimuli and promote downstream signaling cascades to regulate proliferation, survival, and metabolism[1]. Aberrant activation of these pathways disrupts normal regulation of proliferation and survival, resulting in tumorigenesis[84,85,140,223,256]. Numerous therapies targeting PI3K/AKT and RAS/MAPK pathway components have been developed and evaluated for their potential as cancer therapeutics and some have been clinically approved[119]. Because of its central role in mediating PI3K signaling and frequent hyperactivation across cancer types, the serine/threonine protein kinase AKT has become an attractive therapeutic target[106,257,258]. Several drugs targeting AKT have been developed and evaluated in clinical trials, including ATP-competitive, allosteric, and covalent pan-AKT inhibitors[227,228,232,259,260]. No AKT inhibitors have to date been approved by regulatory agencies for the treatment of cancer; thus, drug development in this area is focused on the identification of more selective compounds, effective combinations to limit toxicity, and improvements in patient selection[261].

Recently, targeted protein degradation using small molecule degraders, also called PROteolysis TArgeting Chimeras (PROTACs), has emerged as a novel therapeutic modality and as a tool for the chemical depletion of proteins of interest[193,262–264]. In many cases, PROTACs display increased selectivity over the inhibitors from which they are designed, which presents advantages in limiting off-target toxicities[199]. Targeted protein degradation can also be used as a tool to understand network rewiring dynamics in response to acute depletion of the protein of interest. Potent and selective AKT-targeting PROTACs have been developed with improved selectivity and potency over parental AKT inhibitors[214,215,239]. Despite recent improvements in selectivity and potency, a lack of efficacy due to the development of intrinsic or acquired resistance has further hindered the progress of many therapeutic agents.

The extensive crosstalk between PI3K/AKT and RAS/MAPK signaling and the ability of these pathways to cross-compensate has emerged as a mechanism of resistance to either PI3K or RAS pathway small molecule inhibitors. For example, PI3K pathway inhibition has been shown to activate ERK signaling, whereas inhibition of MEK increases AKT activity[73,265]. Interestingly, mutations in *KRAS* or *BRAF* confer resistance to the pan-AKT degrader MS21; however, resistance could be overcome by the combination treatment of MS21 with the MEK inhibitor trametinib[215], indicating that targeting compensatory MAPK pathway activation could improve therapeutic response to AKT inhibitors.

To gain a more comprehensive understanding of the pathway response to AKT inhibition and degradation, we pursued a network analysis approach. AKT has well-characterized functions in key metabolic and transcriptional processes, including glucose metabolism, macromolecular biosynthesis , and the transcriptional regulation of target genes to support proliferation and growth[1,75]. Techniques to measure cellular response to biological perturbation, such as metabolomics and RNA-seq, are useful for providing a global view of the data. However, they only span one level of biological information and are therefore limited in their ability to provide mechanistic insights. The Causal Oriented Search of Multi-Omics Space (COSMOS) method integrates multiple omics datasets with an extensive prior knowledge network to generate mechanistic hypotheses from primary data sets[266].

Here, we have used a second-generation AKT degrader INY-05-040 that selectively and rapidly degrades AKT isoforms and inhibits downstream signaling and proliferation. Using a multi-omics approach combined with a computational network analysis to integrate metabolomic and transcriptomics data, we uncovered a degrader-specific increase in nucleosides and the induction of stress kinase signaling. We validated our computationally inferred hypotheses across a panel of breast cancer cell lines, underscoring the functionality of this approach to develop useful models across multiple datasets. We extensively characterized INY-05-040 as both a potential therapeutic and as a biological tool to decode novel aspects of AKT biology.

3.3 Results

3.3.1 Biochemical and cellular characterization of pan-AKT degrader INY-05-040

We previously reported the development of the first AKT-targeting degrader INY-03-041, a heterobifunctional degrader consisting of the catalytic AKT inhibitor GDC-0068 chemically linked to the Cereblon (CRBN) recruiter lenalidomide[7]. Despite the potency and selectivity of INY-03-041, initial experiments revealed a lack *in vivo* efficacy (**Appendix I**) and relatively slow kinetics required to degrade AKT isoforms in cells (12 h). These features prompted a chemical biology effort to develop an AKT degrader compound with improved degradation kinetics. This second generation AKT degrader compound, INY-05-040, consists of the catalytic pan-AKT inhibitor GDC-0068 chemically conjugated to a Von Hippel-Lindau (VHL) ligand via a ten-hydrocarbon linker (**Figure 3-1A**). To create a matched negative control compound, we inverted the configuration of the hydroxyproline residue on the VHL ligand, resulting in a compound with reversed stereochemistry incapable of binding VHL, INY-05-040-Neg (**Figure 3-1A**)[267].

We evaluated the biochemical selectivity of INY-05-040 against a panel of 468 kinases in a KINOMEscan assay and observed a comparable selectivity profile to GDC-0068 (**Figure 3-2A**). To assess degrader selectivity in cells, we used unbiased multiplexed mass spectrometry to profile the proteome of MOLT4 cells after 4 h treatment with 250 nM INY-05-040 and observed significant and selective downregulation of AKT isoforms (**Figure 3-2B**).
We selected breast cancer cell lines to evaluate the effects of AKT degradation due to the high frequency of PI3K pathway activation. Lack of AKT degradation after treatment with negative control compound INY-05-040-Neg indicates that AKT degradation is dependent on VHL-binding and validated the use of this compound as a non-degrading control (**Figure 3-1B**).

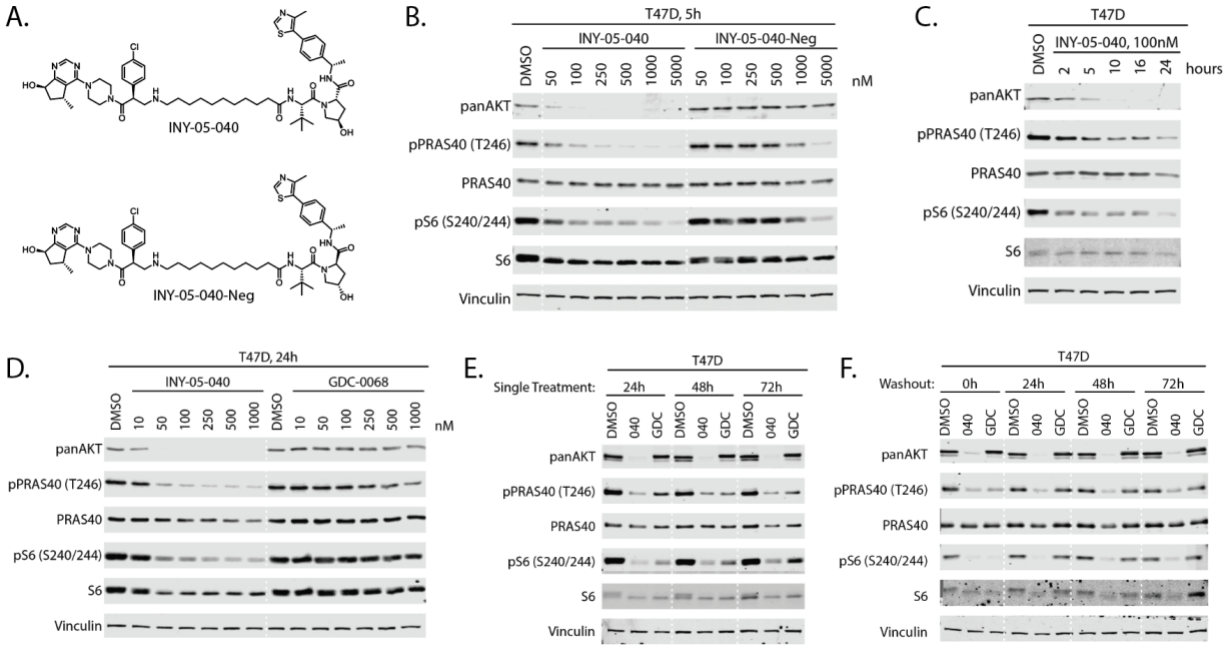

Figure 3-1. Design and characterization of INY-05-040. (**A**) Chemical structures of INY-05-040 and negative control INY-05-040-Neg. (**B**) Immunoblots for panAKT, phospho-PRAS40 (T246), total PRAS40, phospho-S6 (S240/244), total S6, and Vinculin after treatment of T47D cells treated for 5 h with INY-05-040 or INY-05-040-Neg at the concentrations listed (n = 2). (**C**) Immunoblots for panAKT, phospho-PRAS40 (T246), total PRAS40, phospho-S6 (S240/244), total S6, and Vinculin after treatment of T47D cells treated with DMSO or 100 nM INY-05-040 for the indicated times (n = 2). (**D**) Immunoblots for panAKT, phospho-PRAS40 (T246), total PRAS40, phospho-S6 (S240/244), total S6, and Vinculin after treatment of T47D cells treated for 24h with INY-05-040 or GDC-0068 at the concentrations listed (n = 2). (**E**) Immunoblots for panAKT, phospho-PRAS40 (T246), total PRAS40, phospho-S6 (S240/244), total S6, and Vinculin in T47D cells treated with 100 nM INY-05-040 or 100 nM GDC-0068 for the time indicated (n = 2). (**F**) Immunoblots for panAKT, phospho-PRAS40 (T246), total PRAS40, phospho-S6 (S240/244), total S6, and Vinculin in T47D cells treated with 100 nM INY-05-040 or 100 nM GDC-0068 for 5 h followed by washout for the indicated times (n = 2).

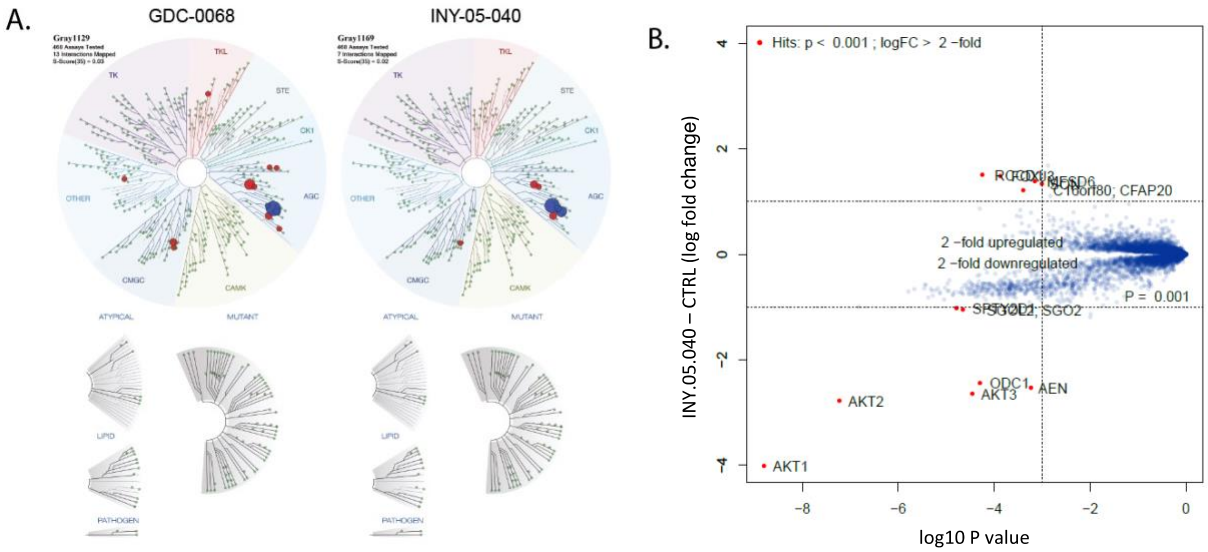

Figure 3-2. INY-05-040 biochemical selectivity and proteomics. (**A**) TREEspot visualization of the biochemical selectivity profile of GDC-0068 and INY-05-040 (1 μM). AKT isoforms are highlighted in blue, all other inhibited kinases are highlighted in red. (**B**) Scatterplot depicts the change in relative protein abundance of INY-05-040 (250nM, 4h)-treated MOLT4 cells compared with DMSO vehicle control treated cells. Protein abundance measurements were made using tandem mass tag quantitative mass spectrometry and significant changes were assessed with t test as implemented in the limma package. The $\log_2$ fold change (log2 FC) is shown on the y axis and negative $\log_{10}$p value ($-\log_{10}$ p value) on the x axis for one independent biological replicate for each treatment. See also **Appendix 2**.

Suppression of downstream signaling was observed at high concentrations of INY-05-040-Neg, as it comprises GDC-0068 which is still able to bind AKT and inhibit kinase activity (**Figure 3-1B**).

Abrogation of proteasome function or neddylation using specific inhibitors prevented AKT degradation by INY-05-040 in T47D and MDA-MB-468 cells (**Figure 3-3A**). We next evaluated degradation kinetics and effects on signaling in comparison to INY-03-041 and the parental inhibitor GDC-0068. INY-05-040 achieved half maximal degradation of AKT isoforms within 5 h of treatment in T47D and MDA-MB-468 cells, substantially more rapid than INY-03-041 (**Figures 3-1C** and **3-4A-B**). INY-05-040 was also more potent than INY-03-041, degrading AKT isoforms at 100nM after 5 h treatment and achieving a more complete degradation of AKT isoforms at later time points (**Figure 3-4**). We observed more potent inhibition of downstream AKT signaling with INY-05-040 than GDC-0068, as measured by the phosphorylation of the AKT substrate phospho-PRAS40 (T246), as well as phospho-S6 (S240/S244), a downstream readout of PI3K pathway activity, after 24 h treatment of T47D cells (**Figure 3-1D**).

We hypothesized that INY-05-040 may also mediate the same prolonged degradation of AKT and suppression of downstream signaling observed with INY-03-041. We observed prolonged destabilization of AKT after a single treatment with INY-05-040 or 5 h treatment followed by compound washout (**Figure 3-1E-F** and **Figure 3-5A-B**). Accordingly, we observed prolonged suppression of PRAS40 (T246) and S6 (S240/S244) phosphorylation, an effect that was more substantial with INY-05-040 treatment than with GDC-0068 treatment at doses that equivalently suppress PRAS40 phosphorylation at 5 h (**Figure 3-1E-F** and **Figure 3-5A-B**).

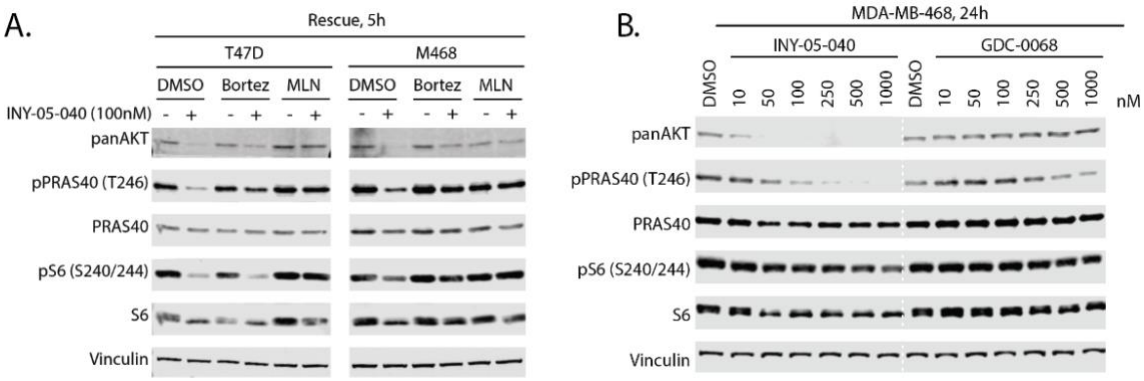

Figure 3-3. INY-05-040 degradation is dependent on neddylation and the proteasome and more potent than parental inhibitor GDC-0068. (**A** and **B**) Immunoblots for panAKT, phospho-PRAS40 (T246), total PRAS40, phospho-S6 (S240/244), total S6, and Vinculin after (**A**) 12-h co-treatment of T47D cells with DMSO, bortezomib (0.5μM), MLN-4924 (1 μM) and either INY-05-040 (100 nM) or DMSO (n = 2) or (**B**) after treatment of MDA-MB-468 cells treated for 24h with INY-05-040 or GDC-0068 at the concentrations listed (n = 2).

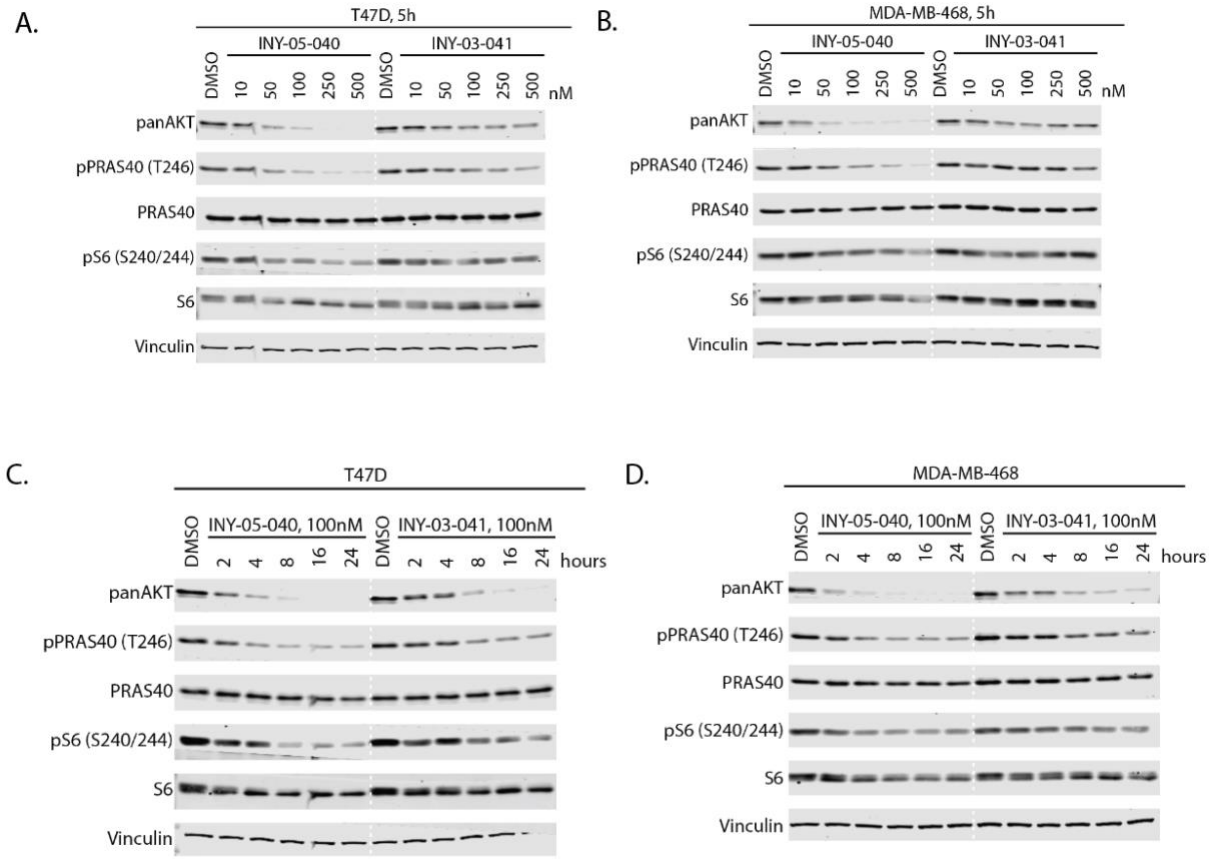

Figure 3-4. INY-05-040 degradation kinetics: dose curve and time course. (**A** and **B**) Immunoblots for panAKT, phospho-PRAS40 (T246), total PRAS40, phospho-S6 (S240/244), total S6, and Vinculin after 5 h treatment of (**A**) T47D or (**B**) MDA-MB-468 cells with INY-05-040 or INY-03-041 at the concentrations indicated (n = 2). (**C** and **D**) Immunoblots for panAKT, phospho-PRAS40 (T246), total PRAS40, phospho-S6 (S240/244), total S6, and Vinculin in (**C**) T47D or (**D**) MDA-MB-468 cells treated with 100 nM INY-05-040 or 100 nM INY-03-041 for the time indicated (n = 2).

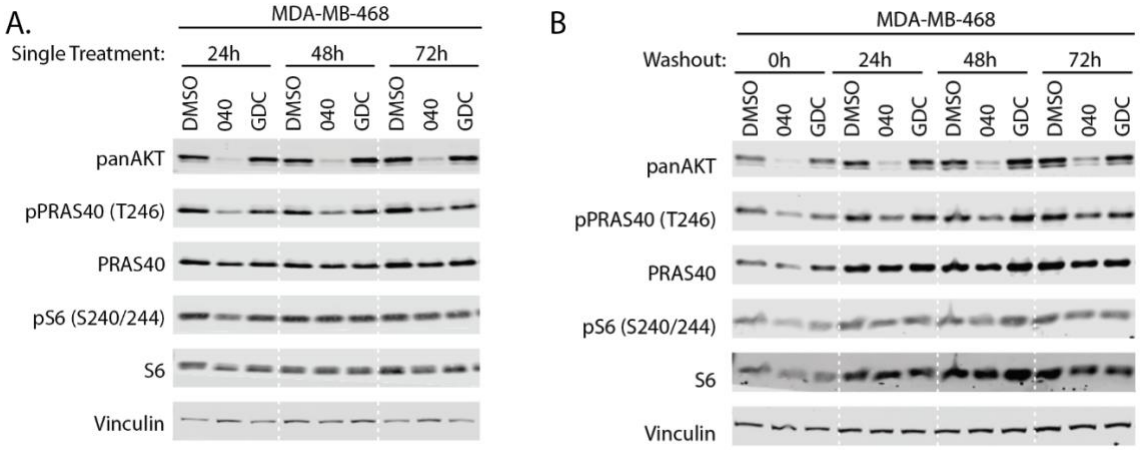

Figure 3-5. INY-05-040 single treatment and washout. (**A**) Immunoblots for panAKT, phospho-PRAS40 (T246), total PRAS40, phospho-S6 (S240/244), total S6, and Vinculin in MDA-MB-468 cells treated with 100 nM INY-05-040 or 750 nM GDC-0068 for the time indicated (n = 2). (**B**) Immunoblots for panAKT, phospho-PRAS40 (T246), total PRAS40, phospho-S6 (S240/244), total S6, and Vinculin in MDA-MB-468 cells treated with 100 nM INY-05-040 or 750 nM GDC-0068 for 5 h followed by washout for the indicated times (n = 2).

T47D, MCF7, MDA-MB-468, and BT474 cells were more sensitive to AKT degraders INY-05-040 and INY-03-041 than to catalytic AKT inhibitors GDC-0068 and AZD5363, or allosteric AKT inhibitors MK-2206 and ARQ 092 (**Figure 3-6**). The anti-proliferative effects of the negative control INY-05-040-Neg was intermediate between AKT inhibitors and degraders, potentially reflecting off-targets at high concentrations (**Figure 3-6**). By contrast the VHL ligand VH032 had little to no effect on cell proliferation, indicating that inhibition of proliferation by INY-05-040 is not attributable to VHL binding (**Figure 3-6**).

We next determined whether INY-05-040-mediated AKT degradation potentiates cell death. BT474 cells exhibited induction of cell death after 5 days treatment with AKT degrader (**Figure 3-7**). No cell death was observed after GDC-0068 treatment at a dose chosen to equivalently suppress PRAS40 (T246) phosphorylation (**Figure 3-7**).

3.3.2 Multi-omics profiling of the effects of INY-05-040-mediated AKT degradation

Next, we employed LC-MS/MS-based targeted metabolomics to evaluate differential alterations in metabolite levels in cells treated with degrader or catalytic inhibitor. We used drug concentrations that equivalently suppressed AKT signaling as measured by inhibition of PRAS40 phosphorylation (**Figure 3-8A**). We selected a 24-hour time point to capture robust metabolic changes. Analysis of three biological replicate metabolomics experiments in T47D cells revealed several consistent changes induced by both AKT degradation and inhibition and changes unique to AKT degradation. Specifically, we observed an increase in guanosine, inosine, and cytidine nucleosides with INY-05-040 treatment (**Figure 3-8B-D**). Interestingly, guanosine, inosine, and cytidine nucleosides were also increased in response to treatment with allosteric AKT inhibitor MK-2206, though not to the same magnitude as induced by INY-05-040 (**Figure 3-8B-C**).

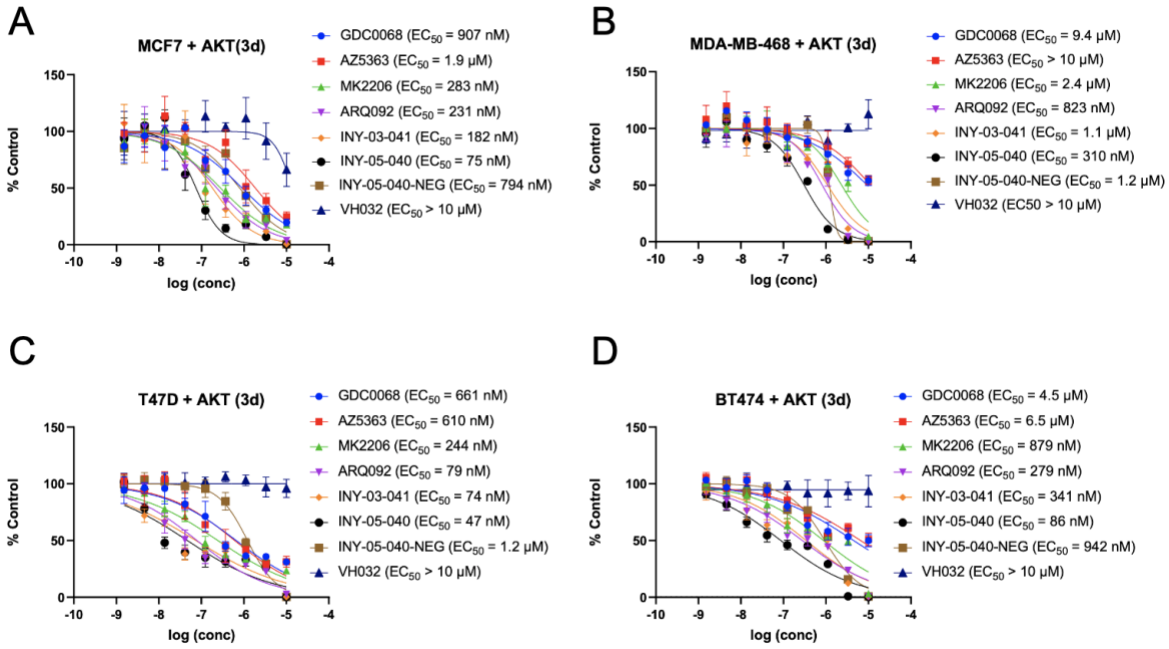

Figure 3-6. Anti-proliferative effects of AKT degradation or inhibition. CellTiterGlo anti-proliferation assay evaluating % inhibition in cell growth relative to DMSO treated control cells in (**A**) MCF7, (**B**) MDA-MB-468, (**C**) T47D, or (**D**) BT474 cells treated for 72h with GDC-0068 (blue), AZD5363 (red), MK2206 (green), ARQ 092 (purple), INY-03-041 (orange), INY-05-040 (black), INY-05-040-Neg (brown), and VH032 (dark blue) with and their EC50 concentrations in the figure legend. n=2.

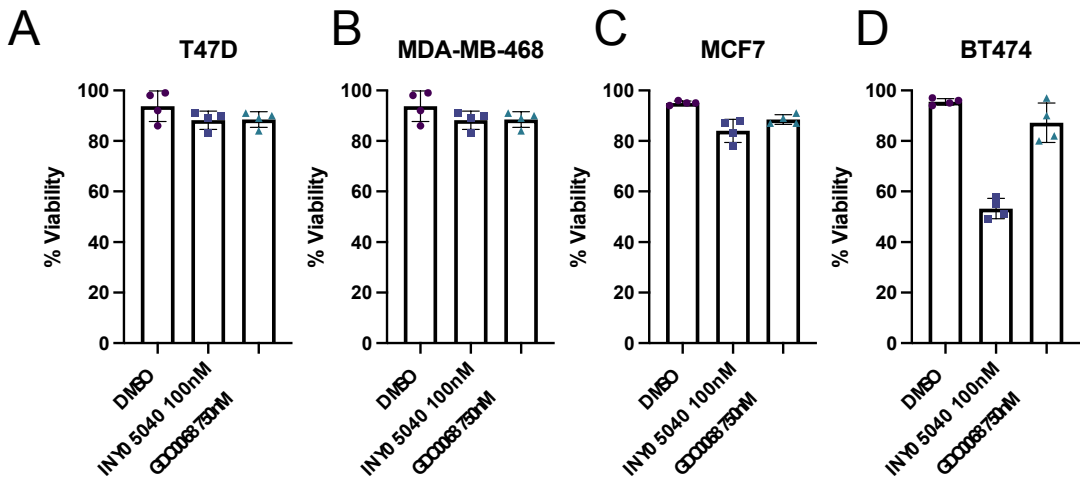

Figure 3-7. Degrader-specific induction of cell death in BT474 cells. Cell viability measured by Propidium Iodide assay to calculate % viability in (**A**) T47D, (**B**) MDA-MB-468 (**C**) MCF7, or (**D**) BT474 cells treated 120 h with DMSO, 100nM INY-05-040, 750nM GDC-0068. Data represent n=2 experiments comprised of two biological replicates. Error bars represent standard deviation.

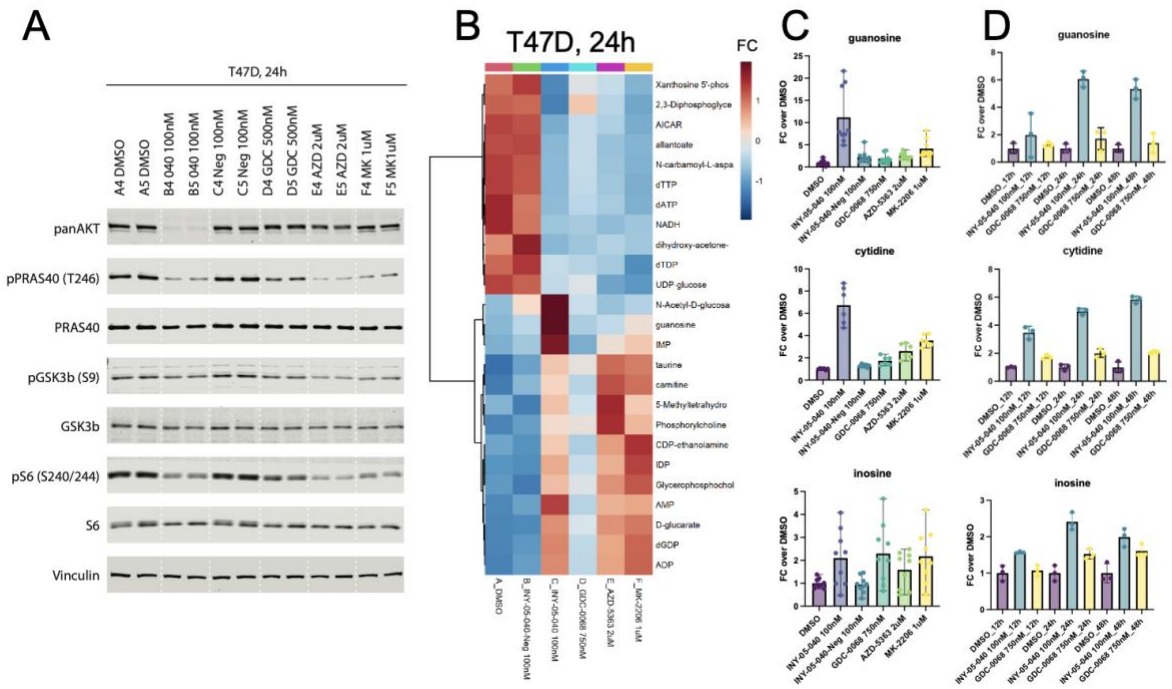

Figure 3-8. Metabolic profiling reveals increases in nucleoside species after INY-05-040 but not GDC-0068 treatment. (**A**) Immunoblots for panAKT, phospho-PRAS40 (T246), total PRAS40, phospho-GSK3β (S9), total GSK3β, phospho-S6 (S240/244), total S6, and Vinculin in T47D cells treated for 24h with DMSO, 100nM INY-05-040, 100nM INY-05-040-Neg, 500nM GDC-0068, 2μM AZD5363, or 1μM MK-2206. Samples were from one biological replicate of metabolomics experiments from cells treated in parallel to metabolite collection. (**B**) Heatmap of differentially regulated metabolites after treatment of T47D cells for 24h with the compounds listed above n=3 independent biological replicates. Heatmap represents fold change (FC) in metabolite abundance centered to row means. Heatmap generated in MetaboAnalyst 5.0 (**C**) Bar plots indicating the fold change increase in guanosine or cytidine nucleoside levels. Data representative of three independent metabolomics experiments (except for cytidine which was not detected in one experiment) where fold change calculated over respective experimental DMSO conditions. (**D**) Bar graphs indicating fold change of guanosine, inosine, or cytidine levels after metabolomics profiling of T47D cells after 12 h, 24 h, or 48 h treatment with 100nM INY-05-040, or 750nM GDC-0068. Data normalized to respective DMSO timepoint samples.

To determine whether alterations in metabolite levels are attributable to differential kinetics of pathway inhibition following degrader or inhibitor treatment, targeted metabolomics following 12 h, 24 h, or 48 h treatment of T47D cells with INY-05-040 and a concentration of GDC-0068 that equivalently suppressed downstream signaling was performed (**Figure 3-8D**). Increased guanosine, inosine, and cytidine nucleoside levels were detected at 12 h and further increased at later times (**Figure 3-8D**). Interestingly, even at later time points significant changes in nucleoside levels in GDC-0068-treated cells were detected (**Figure 3-8D**).

Next, we performed RNA sequencing (RNA-seq) to identify degrader-specific effects on transcription. T47D cells were treated for 5 h or 10 h with INY-05-040, negative control INY-05-040-Neg, or parental AKT inhibitor GDC-0068 in growth factor-replete conditions (**Figure 3-9A**). Under these conditions, equivalent suppression of the AKT substrates GSK3β (S9) and TSC2 (T1462) was observed at both 5 h and 10 h (**Figure 3-9A**).

Transcriptional changes were more pronounced at the 10 h than the 5 h for both AKT degrader and inhibitor treatment conditions, as expected given the kinetics required for transcriptional reprogramming (**Figure 3-9B**). Although the direction of most changes compared to control were similar in AKT degrader- and inhibitor-treated samples, the magnitude was significantly more pronounced in AKT degrader-treated cells, indicative of a more robust cellular response (**Figure 3-9C**).

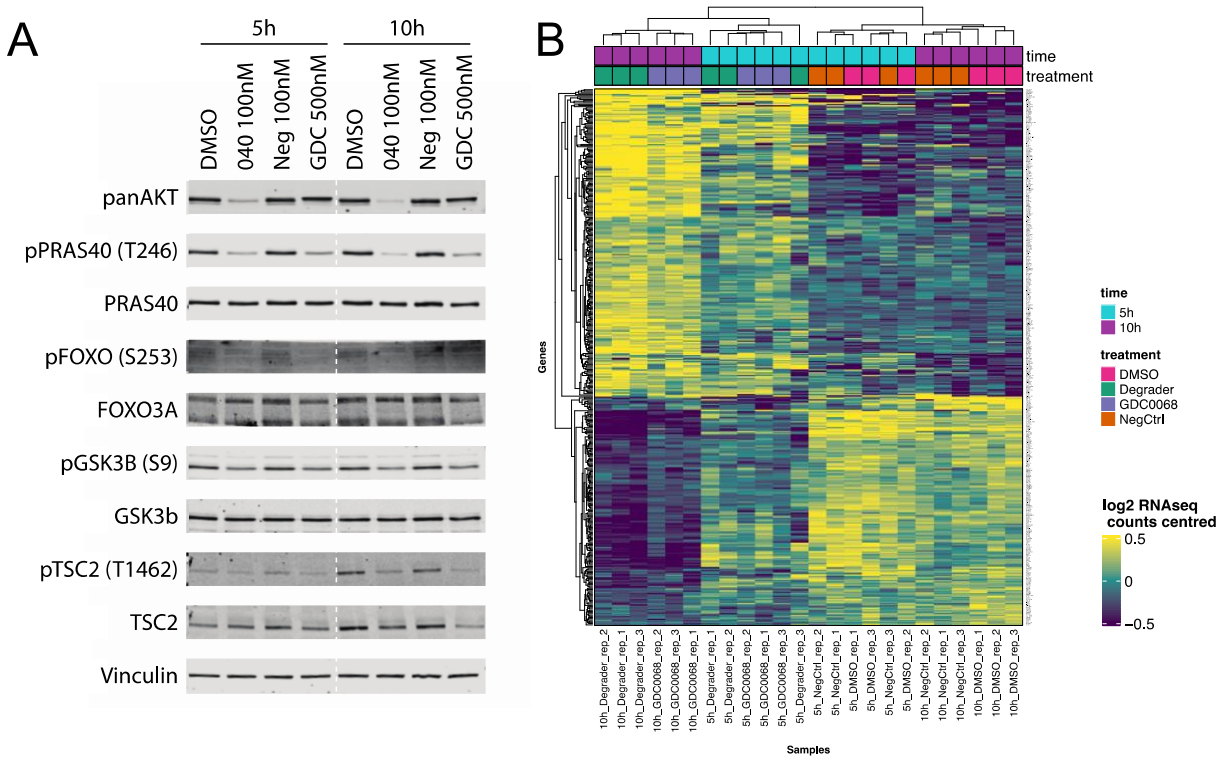

Figure 3-9. RNA-seq differential expression analysis. (**A**) Immunoblots for panAKT, phospho-PRAS40 (T246), total PRAS40, phospho-FOXO3A (S253), total FOXO3A, phosphor-GSK3β (S9) and total GSK3β, phospho-TSC2 (T1462), total TSC2, and Vinculin in T47D cells treated in parallel to RNA-seq samples with DMSO, 100 nM INY-05-040, 100 nM INY-05-040-Neg, or 500 nM GDC-0068 for 5 h or 10 h. (**B**) Heatmap of RNA-seq displaying mean centered log2 fold change intensity of differentially expressed genes in all conditions at all time points.

Analysis of gene set enrichment analysis (GSEA) normalized enrichment scores (NES) and PROGENy estimated pathway activation values revealed AKT degrader- and inhibitor-treated cells exhibited expected downregulation of hallmark signatures related to PI3K/AKT/mTOR signaling, mTORC1 signaling and glycolysis (**Figure 3-10A-B**). GSEA NES values at 10 h indicated differences between degrader and inhibitor effects on cholesterol homeostasis, androgen response, xenobiotic metabolism, and interferon alpha response signatures (**Figure 3-10A-B**).

Taken together, these data demonstrate that AKT degradation induced by INY-05-040 results in alterations in metabolic and transcriptional processes known to be modulated downstream of AKT, some exhibiting greater potency when compared to AKT inhibition. Additionally, nucleoside abundance was differentially affected by AKT degradation compared to either catalytic or allosteric AKT inhibitors, indicating that AKT may have a kinase-independent functions in regulating nucleoside abundance.

3.3.3 COSMOS network analysis

We used a network analysis approach to integrate metabolomics and transcriptomics datasets. We hypothesized that a network analysis would yield comprehensive insights into the increased and sustained potency of INY-05-040 over GDC-0068. The COSMOS (Causal Oriented Search of Multi-Omics Space) tool was used to integrate metabolomics and RNA-seq datasets and generate testable mechanistic hypotheses to explain alterations observed across multiple omics datasets (**Figure 3-11**)[266]. Metabolomics data and RNA-seq data were processed using the limma-voom framework to generate metabolite t-values, transcription factor enrichment estimations, as well as RNA-seq t-values as input data for COSMOS analysis.

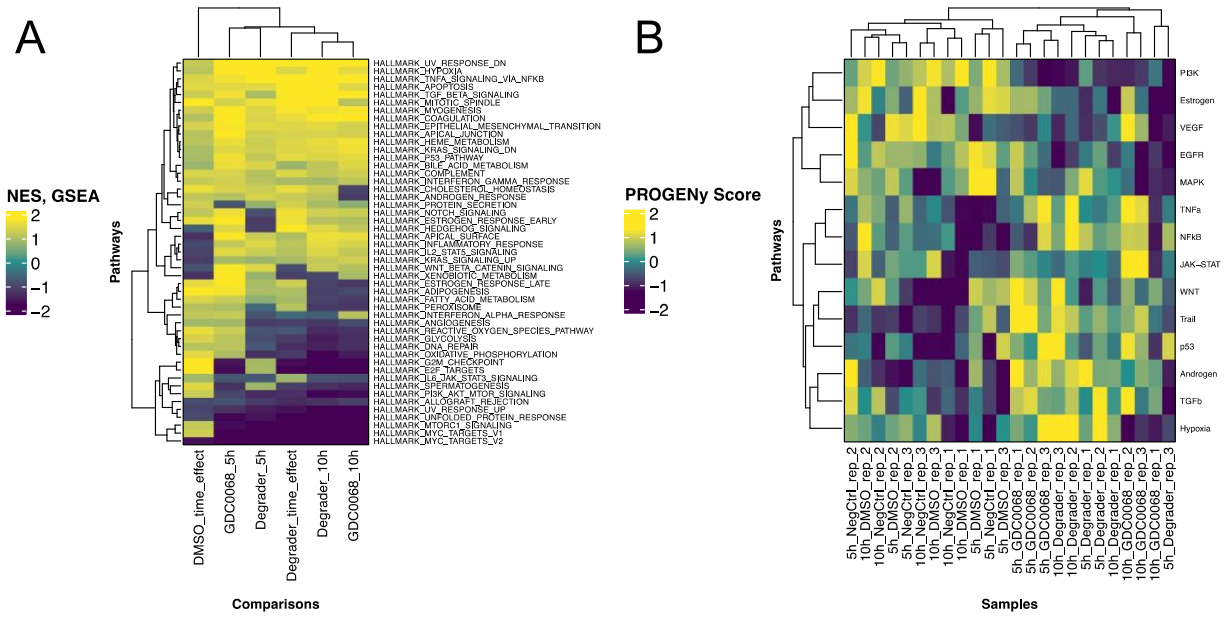

Figure 3-10. Gene set enrichment analysis of RNA-seq analysis. (**A**) GSEA NES Heatmap calculated from t-values indicates differences in hallmark signatures at different time points. (**B**) PROGENy heatmap of estimated pathway activity calculated from differential expression analysis t-values for comparisons of interest.

A

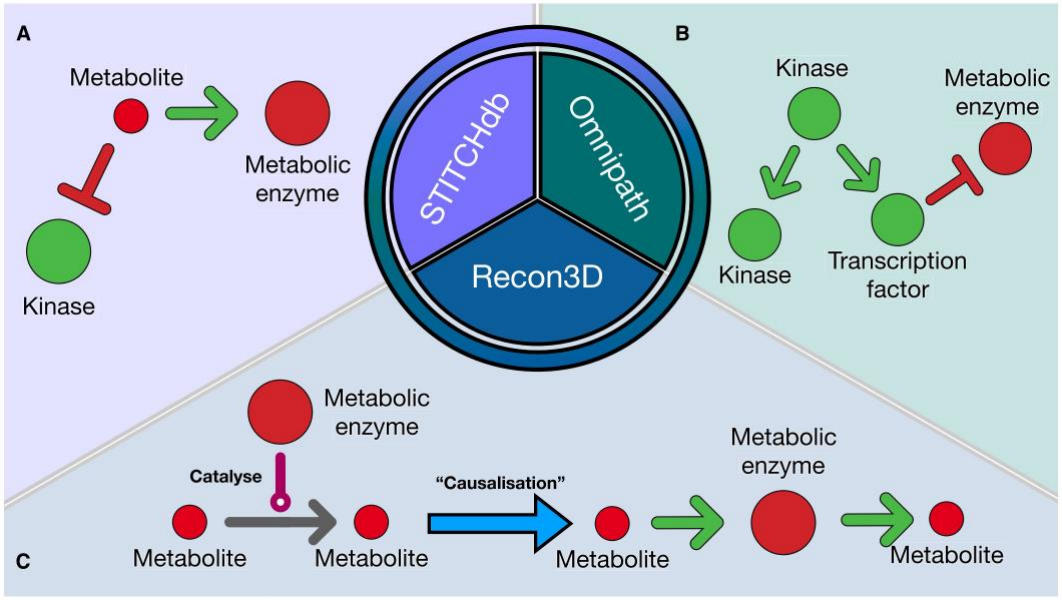

B

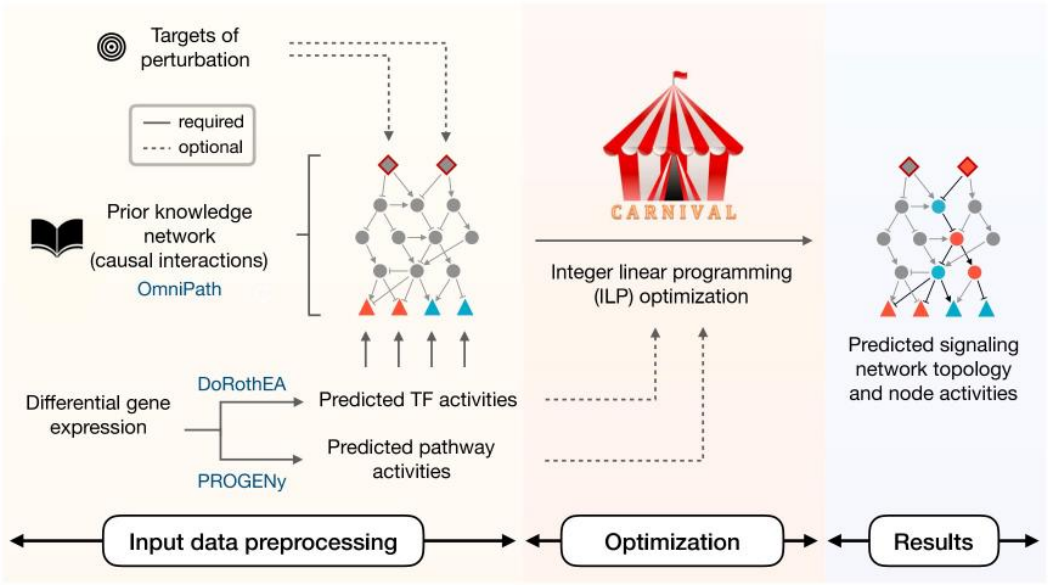

Figure 3-11. Graphical summary of COSMOS platform. (A) Schematic of meta PKN compiled by combining STITCH, OmniPath, and Recon3D. STITCH provides information about enzyme activities mediated by metabolites. OmniPath provies information about enzyme activities mediated by other enzymes. Recon3D provides information on metabolic enzyme reactants and products. Adapted from Dougourd, A. *et al*. *Mol Sys Bio.*2021. (**B**) The CARNIVAL pipeline requires prior knowledge network and differential gene expression analysis as input. Transcription factor activities are inferred using DoRothEA from differential gene expression analysis. CARNIVAL derives networks to explain the inferred transcription factor activities. Adapted from Liu, A. *et al. Systems Biology and Applications.* 2019.

COSMOS was iteratively performed using either AKT degrader or inhibitor input data to create forward and backward interaction networks, then combined into a single consensus network. Input data were shuffled through different starting points to exclude potential bias. The resulting networks display plausible ways in which known interactions in the prior knowledge network can explain the transcription factor and metabolite changes observed (**Figure 3-12**).

COSMOS networks consistently identified *MAPK1* (ERK2) and *MAPK3* (ERK1) as top degree nodes in both INY-05-040 and GDC-0068 networks, consistent with their role in compensatory pathway signaling in response to PI3K pathway inhibition (**Figure 3-13**). Other nodes consistently identified in both INY-05-040 and GDC-0068 networks were *CDKN1A* and *CDK1*, *TP53*, *MYC*, and *NFKB1* (**Figure 3-12 and Appendix 2**). *GSK3B* and *PAK1* were identified more frequently as top nodes in GDC0068 networks, both of which have known associations with AKT (**Figure 3-12 and Appendix 2**)[1,268]. By contrast, COSMOS identified the stress kinases JNK1 (*MAPK8*) and p38a (*MAPK14*) as top two degree nodes in the AKT degrader network (**Figure 3-13A**), indicative of how many edges they are attached to, or their "degree"[269].

3.3.4 COSMOS validation of degrader-specific stress kinase signaling

JNK and p38 kinases are activated in response to a variety of cellular stressors, including hypoxia, inflammation, and metabolic stresses to modulate cellular response to stress[270]. AKT is known to regulate stress kinase signaling via multiple mechanisms; for example, through the inhibitory phosphorylation of JNK regulators MKK4 and MKK7[271]. AKT is also known to regulate ASK1 (MEKK5), a MAP3K upstream of both p38 and JNK[272,273].

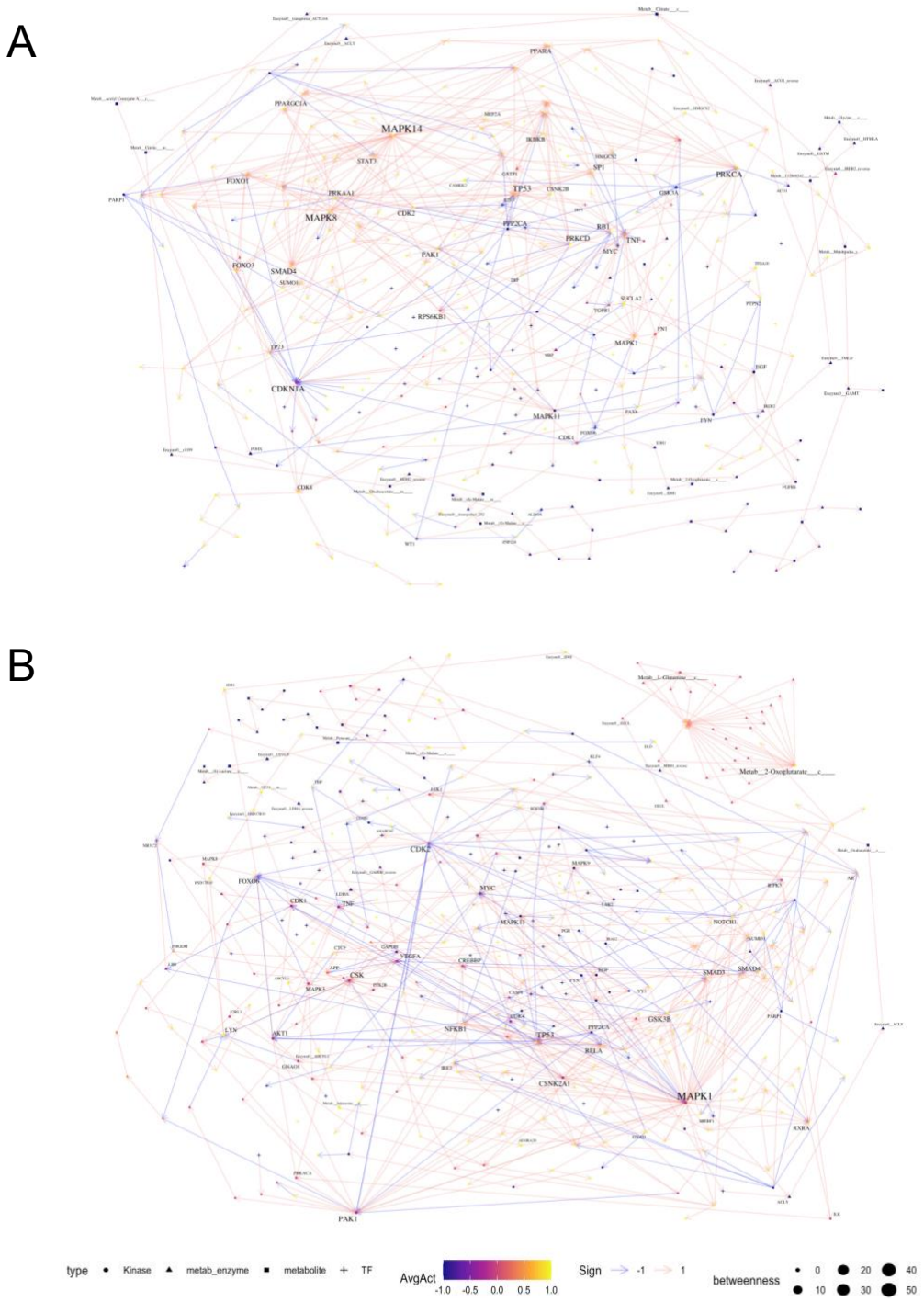

Figure 3-12. COSMOS networks. (**A**) Example network generated with INY-05-040 vs. DMSO input data. (**B**) Example networks generated with GDC-0068 vs. DMSO input data.

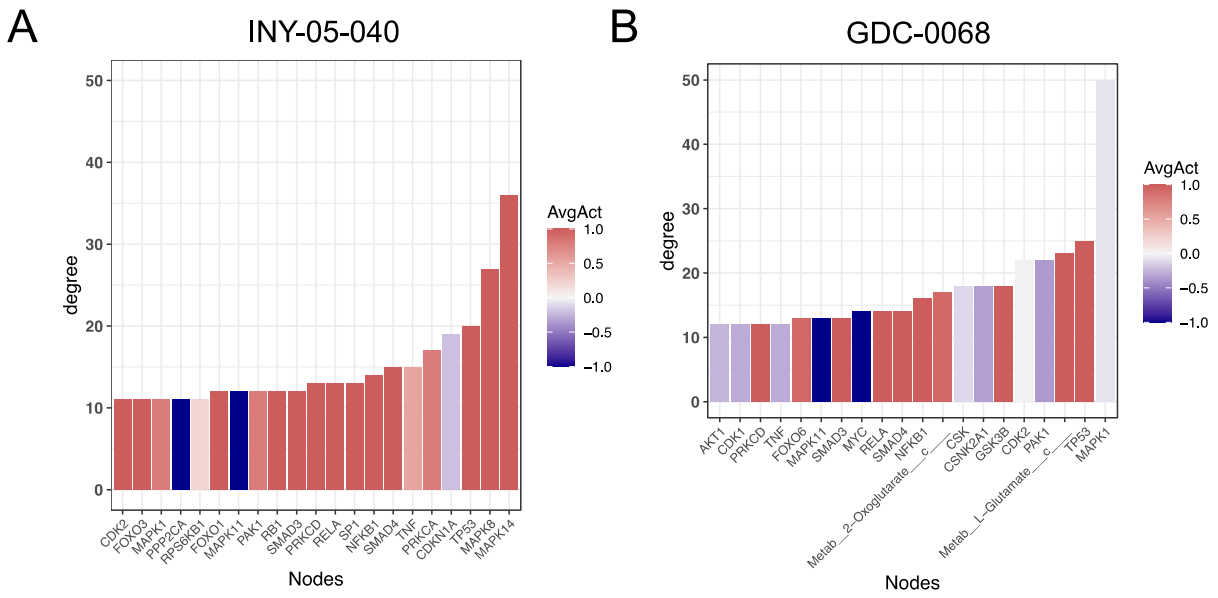

Figure 3-13. Top degrader and inhibitor degree nodes. Examples of top 20 degree nodes identified by COSMOS in **(A)** INY-05-040 and **(B)** GDC-0068 networks. Legends indicate inferred activity of each node.

We next determined the kinetics of JNK and p38α signaling over a time course in a panel of breast cancer cell lines to validate the predictions of the COSMOS analysis. We observed potent AKT degrader-specific induction of p38α phosphorylation (T180/Y182) and the JNK target p-c-Jun (S73), as well as increased total c-Jun protein levels (**Figure 3-14**). Distinct magnitude and kinetics of JNK and p38α signaling were observed in response to AKT degrader and inhibitor, but the response to INY-05-040 was consistently more robust than inhibitor under conditions of equivalent inhibition of PRAS40 phosphorylation (**Figure 3-14**). INY-05-040 treatment also increased phosphorylation of ERK1/2 (T202/204) in MCF7 and BT474 cells more potently than GDC-0068 (**Figure 3-14 and Appendix 2**). Interestingly, the opposite trend was observed in T47D cells, where INY-05-040 reduced ERK phosphorylation (**Appendix 2**), potentially reflecting distinct differences between cell lines in network rewiring.

The dynamics of inputs to JNK and p38α contribute to either cell survival or death, depending on the context[271]. JNK mediates apoptotic cell death in response to a variety of physiological stress signals[274]. Prolonged treatment of BT474 cells with INY-05-040 induced robust JNK signaling as measured by both expression and phosphorylation of its target gene c-Jun (**Figure 3-15A**). Pre-treatment of BT474 cells with the covalent JNK1/2/3 inhibitor JNK-IN-8 rescued cell death induced by INY-05-040 treatment (**Figure 3-15A**). By contrast, GDC-0068 did not induce significant cell death in BT474 cells, and pre-treatment with JNK-IN-8 had no effect (**Figure 3-15B**).

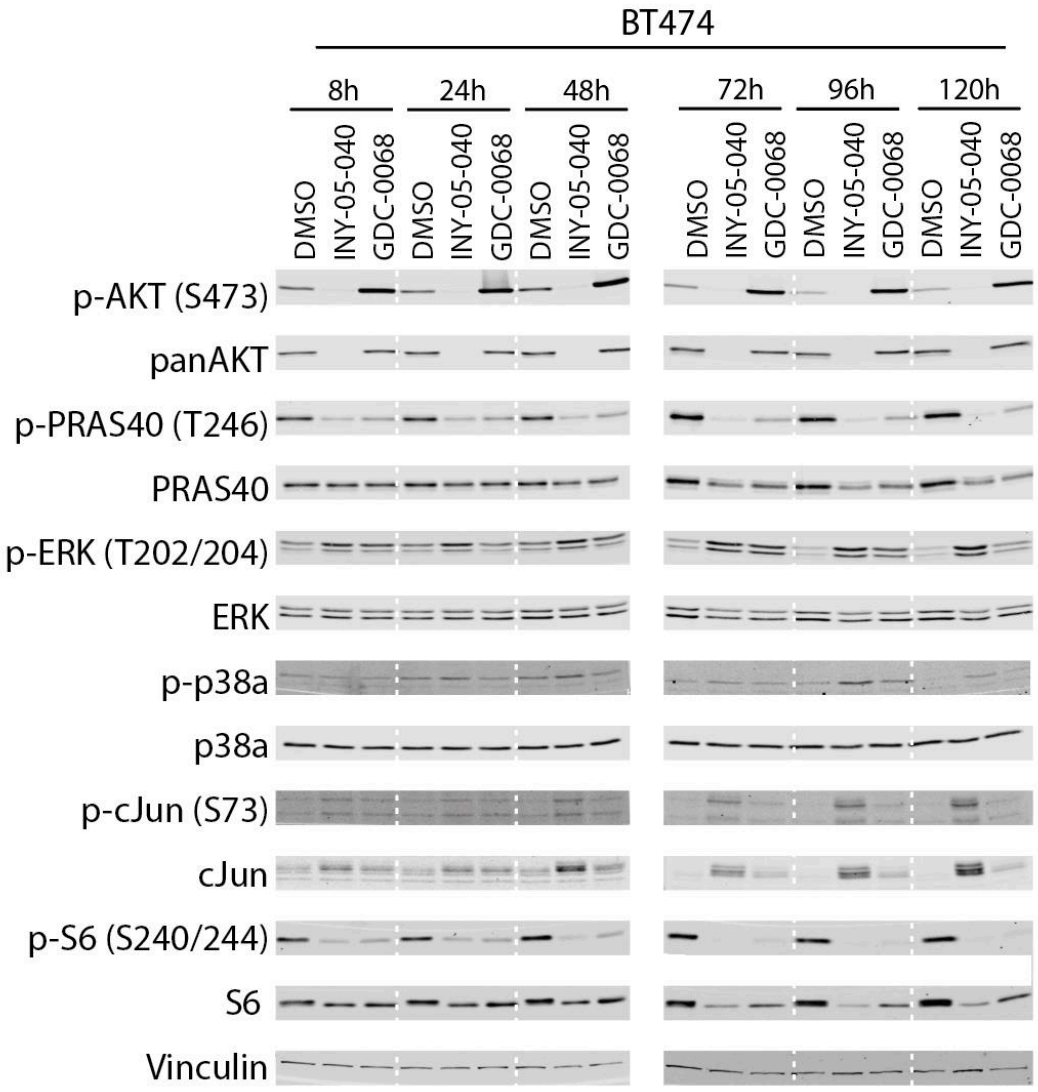

Figure 3-14. COSMOS validation of induction of stress kinase signaling. Immunoblots of phospho-AKT (S473), total pan-AKT, phospho-PRAS40 (T246), total PRAS40, phospho-ERK (T202/204), total ERK, phospho-p38α (T180/182), total p38α, phospho-cJun (S73), total cJun, phospho-S6 (S240/244), total S6, and Vinculin in BT474 cells treated with DMSO, 100nM INY-05-040, or 750nM GDC-0068 for the times indicated. White vertical bar indicates samples were run on separate gels.

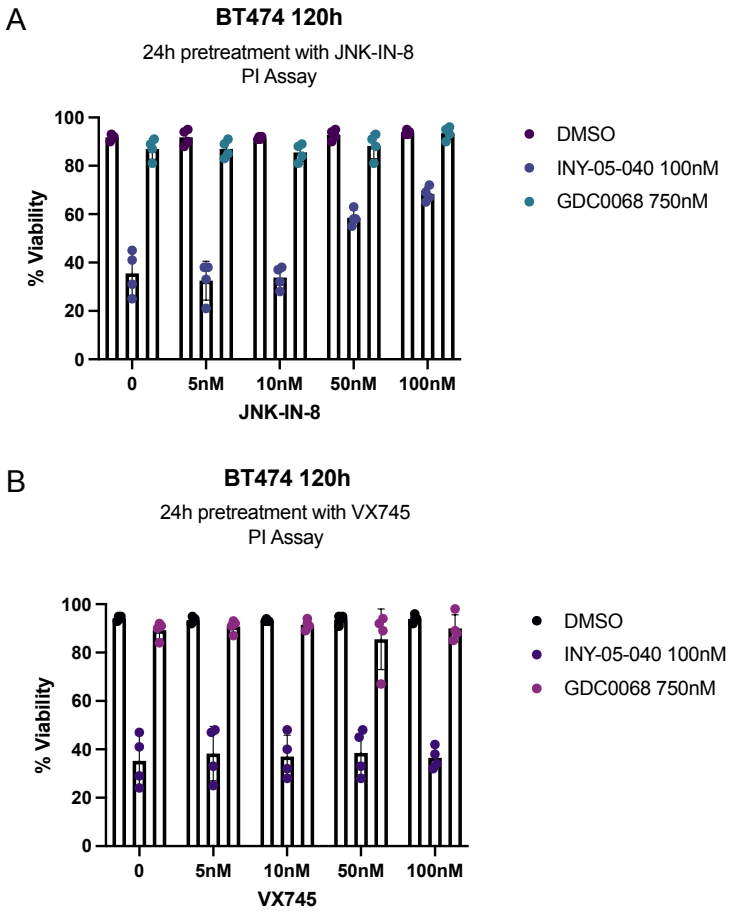

Figure 3-15. JNK inhibition rescues cell death of BT474 cells. (A) Propidium iodide cell viability assays of BT474 cells pre-treated for 24h with JNK1/2/3 inhibitor JNK-IN-8 at the concentrations listed below, followed by treatment with DMSO, 100nM INY-05-040, or 750nM GDC-0068 for 120h. **(B)** Propidium iodide cell viability assays of BT474 cells pre-treated for 24h with p38α inhibitor VX745 at the concentrations listed below, followed by treatment with DMSO, 100nM INY-05-040, or 750nM GDC-0068 for 120h. Data representative of n=2 experiments each with biological replicates.

Unlike JNK-IN-8, pre-treatment of BT474 cells with the p38α inhibitor VX745 did not result in a significant rescue of cell death in cells treated with INY-05-040 (**Figure 3-15B**). These data suggest that JNK activation mediates INY-05-040 induced cell death, at least in part, and this effect is independent of p38α.

3.4 Discussion

The continuing search for targeted agents to treat patients with PI3K pathway hyperactivation has focused on the identification of more selective compounds, effective combinations to limit toxicity, and improvements in patient selection[261]. Recent efforts have led to the development of the PI3Kα-selective inhibitor alpelisib, approved for the treatment of hormone receptor-positive, HER2-negative metastatic breast cancer in patients harboring the oncogenic H1047R *PIK3CA* mutation[119]. Targeted protein degradation has emerged as a novel therapeutic strategy to improve the selectivity of multi-targeted inhibitors, and in some cases yield prolonged degradation of target proteins and inhibition of downstream signaling[239,275]. Rapid and selective degradation of target proteins can also be used to investigate the cellular consequences and network rewiring that occurs as a result of acute protein depletion.

Here we have extensively characterized a second-generation VHL- and GDC-0068-based AKT degrader, INY-05-040, with long-lasting degradation kinetics, selectivity, and anti-proliferative effects compared to the parent inhibitor GDC-0068 and also compared to our first-generation AKT degrader INY-03-041[213]. Interestingly, INY-05-040 suppressed proliferation in MDA-MB-468 cells that are relatively insensitive to AKT inhibitors[246], which may indicate an AKT kinase-independent mechanism supporting cellular survival that can be uniquely targeted by degradation (**Figure 3-6B**). The ability of degraders to abrogate protein kinase-independent functions may expand their clinical utility. The enhanced selectivity of INY-05-040 may also improve off-target dose-limiting toxicities; however, increased potency may also increase on-target toxicities associated with inhibition of the PI3K pathway, including hyperglycemia,

hyperinsulinemia[276,277], rash and other dermatological toxicities[278,279], hepatic toxicity[279,280], and others[281]. The amenability of PROTACs in tissue- or tumor-targeting strategies using ligands to recruit tissue-specific E3 ligases, or through PROTAC-drug conjugates, may result in advancements in reducing on-target toxicities[282,283]. Although isoform-selective PROTACs for CDK6 and SGK3 have been reported and represent a strategy to mitigate on-target toxicities, this degree of selectivity has not yet been achieved with AKT-targeting degraders[214,215,241,284,285].

Beyond their potential use in the clinic, small molecule degraders offer the unique advantage of inducing acute protein loss before cells can reprogram signaling pathways and gene transcription to compensate for target loss. For example, degraders have proven useful in elucidating kinase-independent effects (e.g., BCR-ABL[286], FLT-3[184]), scaffolding roles (e.g., FAK[209]), and the function of complex components (e.g., TRIM24[208]). This enables investigation of protein function after rapid depletion and in the absence of secondary proteome and genome-wide alterations.

AKT has well-characterized roles in the regulation of metabolic pathways and gene transcription that contribute to cell proliferation and survival. AKT regulates metabolism directly by phosphorylating metabolic enzymes (e.g., ACLY), through transcription factors that mediate expression of metabolic genes (e.g., *FOXO*, *HIF1*, *SREBP*), and through downstream effectors (e.g., mTORC1). AKT degradation with INY-05-4040 resulted in extended depletion of AKT and suppression of downstream signaling, and in turn significant differences in the metabolic and transcriptional profiles when compared to conventional kinase inhibition. We observed a consistent increase of guanosine, cytidine, and inosine nucleosides specifically in response to AKT degradation. Although steady-state metabolomics does not allow for the analysis of pathway flux, we speculate that the increase of nucleosides and NMPs in response to AKT degradation occurs through induction of nucleolar stress and ribosome degradation, either through an mTORC1-dependent mechanism or directly by AKT[287,288]. Additional studies are required to explore this potential mechanism.

We used COSMOS network analysis to integrate metabolomics and RNA-seq datasets to provide a global view of our omics datasets and to generate mechanistic hypotheses [266]. This analysis identified JNK1 (*MAPK8*) and p38α (*MAPK14*), key components of the cellular stress response, as top degree nodes in degrader networks. Although JNK1 and p38α were consistently identified as top degree nodes throughout iterative COSMOS runs, the predicted activity of the nodes was not always consistent between runs. This may be due to computational inference of node activity that was not measured directly in input data. Alternatively, the inconsistencies observed in directionality of predicted activity may represent a gap in the prior knowledge network. This also emphasizes the role of network analyses as hypothesis generating tools that require robust experimental validation.

Although stress kinase nodes were identified consistently between multiple runs, we tested the fidelity of this tool by modeling the COSMOS predictions in cell lines. We monitored the specific induction of stress kinase signaling in a panel of breast cancer cell lines and observed cell-type specific induction of cell death and the magnitude of stress kinase activation. The regulation of stress responsive kinase signaling is complex and context-dependent given their broad roles in a cellular physiology[289]. Additionally, JNK activation mediates distinct cellular outcomes, either apoptosis or survival depending on the dynamics of pathway activation[271]. This is consistent with our observation that INY-05-040 induced the most robust and rapid activation of JNK and p38α signaling in BT474 cells which exhibited significant sensitivity to degrader-induced cell death.

Previous work has demonstrated that “switch-like” or ultrasensitive JNK induction is necessary for cell death, whereas gradual JNK induction is insufficient[271]. Phospho-protein profiling could identify cells that harbor ultrasensitive stress kinase signaling[271], and therefore exhibit a cytotoxic response to AKT degradation. Alternatively, induction of physiological or pharmacological stress kinase signaling may potentiate cell death in combination with AKT degraders in cells without ultrasensitive JNK signaling dynamics. The dynamics of JNK pathway

activity have been suggested to contain prognostically-relevant information, which suggests that network analysis approaches have broad potential for the development of more dynamic biomarkers[271]. We have yet to characterize the mechanism by which AKT degradation with INY-04-040 elicits specific activation of JNK and its subsequent role in cell death. Based on COSMOS network analysis, we can speculate that AKT degrader-mediated induction of metabolic or nucleolar stress could contribute to the activation of JNK and p38α. To extend this notion, AKT degradation may activate JNK signaling either through relief of inhibition of the JNK activators MKK4 and MKK7, or indirectly through the induction of cellular and metabolic stress. Relief of AKT inhibition of FOXO transcription factors may also contribute in part to induction of apoptosis, mitophagy, and autophagy[271].

Targeted protein degradation has emerged as both a novel therapeutic modality and also as a powerful tool to evaluate the effects of acute protein depletion on cellular networks. We have used a pan-AKT degrader INY-05-040 as a tool to uncover novel aspects of AKT biology, including the metabolic, transcriptional, and network rewiring events that occur in response to AKT degradation versus classical catalytic kinase inhibition. We have identified an increase in nucleosides and induction of stress kinases specifically in response to AKT degradation. Our results support the use of protein degraders as a strategy to better undercover novel biology underlying the pleiotropic effects of AKT inhibition.

Significance

The limited success to date of AKT inhibitors in the clinic due to lack of efficacy, development of resistance, and on-target toxicity has prompted the search for alternative therapeutic modalities of targeting AKT. Development of effective cancer therapeutics also requires a more thorough understanding of cellular response to these agents underlying their efficacy, as well as factors that affect the development of resistance. The use of PROTACs to selectively degrade AKT offers a unique window into understanding the biological effects of

acute AKT depletion. We identified a novel, potentially kinase-independent role for AKT in the regulation of nucleosides and underscore the importance of stress kinase signaling in mediating AKT degrader-induced cytotoxicity. Our work emphasizes the still incomplete and context-dependent understanding of AKT signaling, and supports the use of AKT degraders as more specific and potent compounds than existing inhibitors for therapeutic interventions.

3.5 Materials and Methods

Cell Culture

MOLT4, T47D, MCF-7, and MDA-MB-468 cells were obtained from ATCC and cultured in RPMI media (Wisent Bioproducts, Cat #350000CL) supplemented with 10% heat inactivated fetal bovine serum (Thermo Fisher Scientific) at 37°C in the presence of 5% CO_2.

Drug Treatment Experiments

Cells were plated in RPMI media with 10% serum at 2 mL per well in 6-well treated tissue culture plates (Greiner, Cat # TCG-657160) or in 3 mL per plate in 60 mm treated tissue culture plates (Corning, Cat # 430166) and incubated overnight. The next day, cells were treated with the indicated compounds at the appropriate concentration and protein lysates were harvested at the times specified.

Propidium Iodide Cell Death Assay

Cell viability was assayed with a propidium iodide assay, as previously described[290]. Briefly, cells in 96-well plates were treated with a final concentration of 30 mM propidium iodide (Cayman Chemical) for 20 min at 37°C. The initial fluorescence intensity was measured in a GENios FL (Tecan) at 560nm excitation/635nm emission. Digitonin (Millipore) was then added to each well at a final concentration of 600 mM. After incubating for 20 min at 37°C, the final

fluorescence intensity was measured. The fraction of dead cells was calculated by dividing the background-corrected initial fluorescence intensity by the final fluorescence intensity. Viability was calculated by (1 – fraction of dead cells).

Immunoblotting

Cells were washed once in 1x PBS then lysed in RIPA buffer (150 mM Tris-HCl, 150 mM NaCl, 0.5% (w/v) sodium deoxycholate, 1% (v/v) NP-40, pH 7.5) containing 0.1% (w/v) sodium dodecyl sulfate, 1 mM sodium pyrophosphate, 20 mM sodium fluoride, 50 nM calyculin, and 0.5% (v/v) protease inhibitor cocktail (Sigma-Aldrich) for 15 minutes. Cell extracts were precleared by centrifugation at 14,000 rpm for 10 minutes at 4°C. The Bio-Rad DC protein assay was used to assess protein concentration, and sample concentration was normalized using SDS sample buffer. Lysates were resolved on acrylamide gels by SDS-polyacrylamide gel electrophoresis and electrophoretically transferred to nitrocellulose membrane (BioRad) at 100 volts for 90 minutes. Membranes were blocked in 5% (w/v) nonfat dry milk or 5% (w/v) bovine serum albumin (Boston Bioproducts P-753) in tris-buffered saline (TBS) buffer for 1 hour then incubated with specific primary antibodies diluted in 5% (w/v) bovine serum albumin in TBS-T (TBS with 0.05% Tween-20) at 4°C overnight, shaking. The next day, membranes were washed with TBS-T then incubated for 1 hour at room temperature with fluorophore-conjugated secondary antibodies (LI-COR Biosciences). The membrane was washed again with TBS-T then imaged with a LI-COR Odyssey CLx Imaging System (LI-COR Biosciences).

Proliferation Assays

T47D, MDA-MB-468, MCF-7 or BT474 cells were plated in 96-well plates. After 24 h, cells were treated with GDC-0068, AZD5363, MK-2206, ARQ-092, INY-03-041, INY-05-040, INY-05-040-Neg, or VH032 compounds at concentrations indicated for 72 h. The anti-

proliferative effects of these compounds were assessed using the Cell Titer Glo assay kit (Promega). EC_{50} values were determined using GraphPad Prism using nonlinear regression curve fitting.

TMT LC-MS Sample Preparation

MOLT4 cells were treated with DMSO or 250 nM INY-03-041-01 for 4 hours in biological singlicate. Cells were harvested by centrifugation. Lysis buffer (8 M Urea, 50 mM NaCl, 50 mM 4-(2hydroxyethyl)-1-piperazineethanesulfonic acid (EPPS) pH 8.5), 1x Roche protease inhibitor and 1x Roche PhosphoStop was added to the cell pellets and cells were homogenized by 20 passes through a 21-gauge (1.25 in. long) needle to achieve a cell lysate with a protein concentration between 0.5-4 mg/mL. The homogenized sample was clarified by centrifugation at 20,000 x g for 10 minutes at 4°C. A Bradford assay was used to determine the final protein concentration in the cell lysate. 200 µg protein for each sample were reduced and alkylated as previously described (An *et al*., 2017). Proteins were precipitated using methanol/chloroform. In brief, four volumes of methanol were added to the cell lysate, followed by one volume of chloroform, and finally three volumes of water. The mixture was vortexed and centrifuged at 14,000 x g for 5 minutes to separate the chloroform phase from the aqueous phase. The precipitated protein was washed with three volumes of methanol, centrifuged at 14,000 x g for 5 min, and the resulting washed precipitated protein was allowed to air dry. Precipitated protein was resuspended in 4 M Urea, 50 mM HEPES pH 7.4, followed by dilution to 1 M urea with the addition of 200 mM EPPS pH 8 for digestion with LysC (1:50; enzyme:protein) for 12 hours at RT. The LysC digestion was diluted to 0.5 M Urea, 200 mM EPPS pH 8 and then digested with trypsin (1:50; enzyme:protein) for 6 hours at 37°C. Tandem mass tag (TMT) reagents (Thermo Fisher Scientific) were dissolved in anhydrous acetonitrile (ACN) according to manufacturer's instructions. Anhydrous ACN was added to each peptide sample to a final concentration of 30% v/v, and labeling was induced with the addition of TMT reagent to each sample at a ratio of 1:4

peptide:TMT label. The 11-plex labeling reactions were performed for 1.5 hours at RT and the reaction quenched by the addition of 0.3% hydroxylamine for 15 minutes at RT. The sample channels were combined at a 1:1:1:1:1:1:1:1:1:1:1 ratio, desalted using C18 solid phase extraction cartridges (Waters) and analyzed by LC-MS for channel ratio comparison. Samples were then combined using the adjusted volumes determined in the channel ratio analysis and dried down in a speed vacuum. The combined sample was then resuspended in 1% formic acid and acidified (pH 2-3) before being subjected to desalting with C18 SPE (Sep-Pak, Waters). Samples were then offline fractionated into 96 fractions by high pH reverse-phase HPLC (Agilent LC1260) through an Aeris peptide XB-C18 column (phenomenex) with mobile phase A containing 5% acetonitrile and 10 mM NH4HCO3 in LC-MS grade H_2O, and mobile phase B containing 90% acetonitrile and 10 mM NH4HCO3 in LC-MS grade H_2O (both pH 8.0). The 96 resulting fractions were then pooled in a non-continuous manner into 24 fractions and every fraction was used for subsequent mass spectrometry analysis.

Data were collected using an Orbitrap Fusion Lumos mass spectrometer (Thermo Fisher Scientific, San Jose, CA, USA) coupled with a Proxeon EASY-nLC 1200 LC pump (Thermo Fisher Scientific). Peptides were separated on a 50 cm and 75 μm inner diameter Easyspray column (ES803a, Thermo Fisher Scientific). Peptides were separated using a 190 minute gradient of 6 – 27% acetonitrile in 1.0% formic acid with a flow rate of 300 nL/min. Each analysis used an MS3-based TMT method as described previously (McAlister *et al.*, 2014). The data were acquired using a mass range of m/z 340 – 1350, resolution 120,000, AGC target 5 x 105, maximum injection time 100 ms, dynamic exclusion of 120 seconds for the peptide measurements in the Orbitrap. Data dependent MS2 spectra were acquired in the ion trap with a normalized collision energy (NCE) set at 35%, AGC target set to 1.8 x 104 and a maximum injection time of 120 ms. MS3 scans were acquired in the Orbitrap with a HCD collision energy set to 55%, AGC target set to 2 x 105, maximum injection time of 150 ms, resolution at 50,000 and with a maximum synchronous precursor selection (SPS) precursors set to 10.

LC-MS Data Analysis

Proteome Discoverer 2.2 (Thermo Fisher) was used for .RAW file processing and controlling peptide and protein level false discovery rates, assembling proteins from peptides, and protein quantification from peptides. MS/MS spectra were searched against a Uniprot human database (September 2016) with both the forward and reverse sequences. Database search criteria are as follows: tryptic with two missed cleavages, a precursor mass tolerance of 10 ppm, fragment ion mass tolerance of 0.6 Da, static alkylation of cysteine (57.02146 Da), static TMT labeling of lysine residues and N-termini of peptides (229.16293 Da), variable phosphorylation of serine, threonine and tyrosine (79.966 Da), and variable oxidation of methionine (15.99491 Da). TMT reporter ion intensities were measured using a 0.003 Da window around the theoretical *m/z* for each reporter ion in the MS3 scan. Peptide spectral matches with poor quality MS3 spectra were excluded from quantitation (summed signal-to-noise across 10 channels < 200 and precursor isolation specificity < 0.5). Only proteins containing at least two unique peptides identified in the experiment were included in final quantitation.

Statistics and Reproducibility

Sample sizes and statistical tests for each figure are noted in the figure legends. Replicates are biological unless otherwise noted. Error bars represent S.E. unless otherwise noted.

Synthesis of INY-05-040 and INY-05-040-Neg

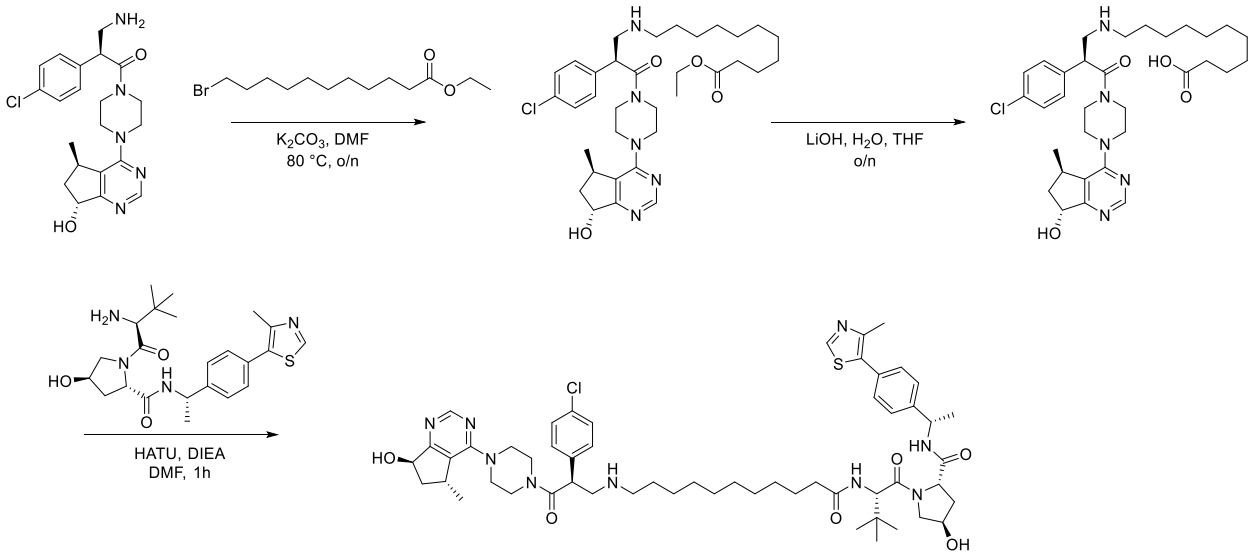

Synthesis of ethyl 11-(((S)-2-(4-chlorophenyl)-3-(4-((5R,7R)-7-hydroxy-5-methyl-6,7-dihydro-5H-cyclopenta[d]pyrimidin-4-yl)piperazin-1-yl)-3-oxopropyl)amino)undecanoate: (S)-3-amino-2-(4-chlorophenyl)-1-(4-((5R,7R)-7-hydroxy-5-methyl-6,7-dihydro-5H-cyclopenta[d]pyrimidin-4-yl)piperazin-1-yl)propan-1-one (150 mg, 0.36 mmol) was dissolved in DMF (2 mL). Potassium carbonate (150 mg, 1.08 mmol) was added to the reaction mixture, followed by dropwise addition of ethyl 11-bromoundecanoate (96 mg, 0.32 mmol). The reaction was stirred at 80 °C overnight. Next day, reaction mixture was filtered and purified by reverse phase HPLC (75% to 15% water in methanol) to obtain title compound as a yellow oil (133 mg, 56% yield). LC-MS: m/z 628.4 [M+1].

Synthesis of 11-(((S)-2-(4-chlorophenyl)-3-(4-((5R,7R)-7-hydroxy-5-methyl-6,7-dihydro-5H-cyclopenta[d]pyrimidin-4-yl)piperazin-1-yl)-3-oxopropyl)amino)undecanoic acid: To ethyl 11-(((S)-2-(4-chlorophenyl)-3-(4-((5R,7R)-7-hydroxy-5-methyl-6,7-dihydro-5H-cyclopenta[d]pyrimidin-4-yl)piperazin-1-yl)-3-oxopropyl)amino)undecanoate (133 mg, 0.18 mmol) was added 6N LiOH (1 mL) and THF (1 mL). The reaction mixture was stirred overnight.

Next day, 1N HCl was added to pH ~3, and the solid was filtered and collected to obtain the title compound (128 mg, 99% yield). LC-MS: m/z 600.42 [M+1].

Synthesis of (2S,4R)-1-((S)-2-(11-(((S)-2-(4-chlorophenyl)-3-(4-((5R,7R)-7-hydroxy-5-methyl-6,7-dihydro-5H-cyclopenta[d]pyrimidin-4-yl)piperazin-1-yl)-3-oxopropyl)amino)undecanamido)-3,3-dimethylbutanoyl)-4-hydroxy-N-((S)-1-(4-(4-methylthiazol-5-yl)phenyl)ethyl)pyrrolidine-2-carboxamide (**INY-05-040**): To of 11-(((S)-2-(4-chlorophenyl)-3-(4-((5R,7R)-7-hydroxy-5-methyl-6,7-dihydro-5H-cyclopenta[d]pyrimidin-4-yl)piperazin-1-yl)-3-oxopropyl)amino)undecanoic acid (120 mg, 0.17 mmol) was added (2S,4R)-1-((S)-2-amino-3,3-dimethylbutanoyl)-4-hydroxy-N-((S)-1-(4-(4-methylthiazol-5-yl)phenyl)ethyl)pyrrolidine-2-carboxamide (81 mg, 0.17 mmol), HATU (64 mg, 0.17 mmol), DIEA (200 µL, 1.18 mmol), and DMF (1 mL). The reaction was stirred for 1 hour, after which the reaction was purified by reverse phase HPLC (80% to 20% water in methanol) to obtain title compound (40 mg, 22% yield). LC-MS: m/z 1026.6 [M+1].

Synthesis of (2R,4S)-1-((S)-2-(11-(((S)-2-(4-chlorophenyl)-3-(4-((5R,7R)-7-hydroxy-5-methyl-6,7-dihydro-5H-cyclopenta[d]pyrimidin-4-yl)piperazin-1-yl)-3-oxopropyl)amino)undecanamido)-3,3-dimethylbutanoyl)-4-hydroxy-N-((S)-1-(4-(4-methylthiazol-5-yl)phenyl)ethyl)pyrrolidine-2-carboxamide (**INY-05-040-NEG)**: Similar protocol as above was carried out using (2R,4S)-1-((S)-2-(11-(((S)-2-(4-chlorophenyl)-3-(4-((5R,7R)-7-hydroxy-5-methyl-6,7-dihydro-5H-cyclopenta[d]pyrimidin-4-yl)piperazin-1-yl)-3-oxopropyl)amino)undecanamido)-3,3-dimethylbutanoyl)-4-hydroxy-N-((S)-1-(4-(4-methylthiazol-5-yl)phenyl)ethyl)pyrrolidine-2-carboxamide as the starting material. LC-MS: m/z 1026.57 [M+1].

LC/MS-MS Metabolomic Profiling

Cells were plated at 0.5, 0.75, or 1 x 10^6 cells per 60 mm treated tissue culture plates (Corning, Cat # 430166) and incubated overnight. Cells were maintained in RPMI (Wisent) + 10% FBS (Thermo Fisher Scientific), and fresh medium was added at the time of treatment. For

metabolite extraction, media was aspirated and cells were washed once with ice-cold phosphate-buffered saline (PBS). Ice cold 80% (v/v) mass spec-grade methanol was added, the plate was transferred to dry ice and scraped, and the resulting solution was collected. Insoluble material was pelleted by centrifugation at 20,000 x g for 5 minutes, and the resulting supernatant was evaporated under nitrogen gas. Samples were resuspended in 20 ml HPLC-grade water for MS analysis. For polar metabolite profiling, five microliters from each sample were injected and analyzed using a 5500 QTRAP hybrid triple quadrupole mass spectrometer (AB/SCIEX) coupled to a Prominence UFLC HPLC system (Shimadzu) with HILIC chromatography (Waters Amide XBridge) via selected reaction monitoring (SRM) with polarity switching. A total of 295 endogenous water-soluble metabolites were targeted for steady-state analyses. Electrospray source voltage was +4950 V in positive ion mode and −4500 V in negative ion mode. The dwell time was 3 ms per SRM transition 32. Peak areas from the total ion current for each metabolite were integrated using MultiQuant v2.1.1 software (AB/SCIEX). Nonhierarchical clustering was performed by MetaboAnalyst 5.0 using a Euclidean distance measure and Ward's clustering algorithm[291].

Metabolomic processing for COSMOS input

Metabolomics data normalized to matched protein samples from three independent experiments were combined into one dataset. Metabolites with missing values were removed, and the resulting data processed for differential expression using the limma-voom method with quantile normalization due to significant heteroscedascity. Subsequent linear modelling and computation of moderated *t*-statistics was performed with *lmFit()* and *eBayes()* as for the RNA-seq data, including experimental replicate as blocking factor due to a noticeable batch effect. For each drug treatment, metabolite *t*-values were exported as input for COSMOS if their unadjusted p-value $\leq$ 0.5, resulting in 58 metabolites for GDC-0068 and 77 metabolites for INY-

05-040. Scripts for metabolomics data processing and the resulting input files used for COSMOS can be found in **Appendix 2**.

RNA Isolation

Snap-frozen cells were thawed on ice and RNA was extracted with Takara's Nucleospin RNA Plus kit (cat # 740984.50) according to the manufacturer's instructions. RNA integrity was assessed for quantity and purity (Nanodrop 1000). Samples were submitted to Novogene for integrity assessment (Agilent 2100 analysis), mRNA library preparation (unstranded), and paired-end sequencing on a NovaSeqS4 lane.

RNA-seq processing for COSMOS input

The Nextflow (version 20.07.1) nf-core RNAseq pipeline (version 1.4.2) was used to perform raw read processing[292]. Spliced Transcript Alignment to a reference (STAR)[293] was used for read alignment to the human genome (Homo_sapiens.GRCh38.96.gtf) and featureCounts[294] for counting of mapped reads, where multimapped reads were discarded. Data analysis from this point forward was performed in R using the limma-voom method[295]. The cpm() function in the *edgeR* package[296] was used to convert raw counts to counts per million. Lowly expressed genes were filtered using the *TCGAbiolinks* package with quantile values of 0.75 (chosen empirically based on the observed count distribution). The trimmed mean of M (TMM) method was used to perform raw read count normalization[297]. The mean-variance relationship was modeled with voom(), followed by linear modeling and computation of moderated t-statistics using the lmFit() and eBayes() functions of the *limma* package[295].

Next, the voom-normalized counts were used to predict transcription factor activities with DoRothEA[298], choosing regulons within confidence groups "A", "B" and "C" (lower confidence regulons in groups "D" and "E" were not considered). The predicted transcription factor activity values were used as "signaling" input for COSMOS. The limma-based t-statistics

for all expressed genes were also provided as additional constraints on the linear solver. Detailed scripts for RNA-seq data processing scripts and the resulting input files used for COSMOS can be found in **Appendix 2**.

Gene set enrichment analysis

GSEA was performed in R on the list of genes ranked according to the t-statistic for each comparison of interest. Normalized enrichment values and associated p-values were calculated using fgsea. The normalized enrichment score computed by fgsea corresponds to the enrichment score normalized to mean enrichment of random samples, using the same gene set size.

COSMOS Analysis

COSMOS network analysis was performed according to the developer's instructions[266]. Briefly, the goal of this approach is to leverage prior signaling/metabolic reaction knowledge and causal integration of multi-omic datasets to generate the smallest possible coherent network that causally connects as many deregulated signaling components and metabolites as possible. Computationally, the algorithm relies on CARNIVAL's Integer Linear Programming (ILP) optimization, which was rerun multiple times for each dataset in order to determine the most consistent network predictions.

A "forward" optimization run to connect deregulated transcription factors ("signaling" input) as starting points to metabolites was performed first, followed by a "backward" optimization run connecting metabolites to signaling components. Time limits for solving were set empirically, ensuring that the gap values of the resulting networks were $\leq$ 5% (indicative of a good fit). In total, 15 combined networks were generated for INY-05-040 vs. DMSO and 8 combined networks were generated for GDC-0068 vs. DMSO. To exclude potential bias, the position of RNA-set *t*-values were shuffled in each run, thus artificially forcing the solver to

initiate the optimization from different starting points. Given our prior knowledge of AKT1 and AKT2 (the two isoforms for which we detected expression at the mRNA level) inhibition, several COSMOS runs also included specifying the inhibition of these two signaling nodes *a priori*, as indicated in the final figures.

Subsequent network analysis and visualization was performed in R, using the rCy3[299] package to interface with Cytoscape[300]. For the final visualization, a filter was applied such that text was only displayed for nodes with betweenness values of >0.05, the size of the text is indicative of the degree, and the color of the node indicative of its COSMOS-derived activation value. The names of nodes are shown only if betweenness >0.05 and degree >15.

KEY RESOURCES TABLES

Antibodies

Antibody	Mol. Weight (kDa)	Lot #	Vendor	Cat. #
pan-AKT	60	20	Cell Signaling Technology	4691
p-PRAS40 (T246)	40	12	Cell Signaling Technology	2997
Total PRAS40	40	11	Cell Signaling Technology	2691
p-GSK3**b (S9)**	46	13	Cell Signaling Technology	9336
GSK3**b**	46	14	Cell Signaling Technology	9315
p-FOXO3A (S253)	97	2	Cell Signaling Technology	9466
FOXO3A	82-97	6	Cell Signaling Technology	2497
p-TSC2 (T1462)	200	7	Cell Signaling Technology	3617
TSC2	200	2	Cell Signaling Technology	3990
Vinculin	124	6	Cell Signaling Technology	13901
p-p44/42 (ERK1/2) (T204/202)	42, 44	12	Cell Signaling Technology	9101
ERK1/2	42, 44	21	Cell Signaling Technology	4695
4EBP	15-20	10	Cell Signaling Technology	9452
p-S6 (S240/244)	32	7	Cell Signaling Technology	5364
S6	32	9	Cell Signaling Technology	2217
p-p38 MAPK (T180/Y182)	43	10	Cell Signaling Technology	4511
p38 MAPK	40	9	Cell Signaling Technology	8690
p-c-Jun (S73)	48	5	Cell Signaling Technology	3270
c-Jun	48	13	Cell Signaling Technology	9165
p-AKT (S473)	60	24	Cell Signaling Technology	4060
pAKT (T308)	80	18	Cell Signaling Technology	2965

2’ Antibody	Vendor	Lot #	Cat. #	Dilution
IRDye 800CW Goat anti-Rabbit IgG (H + L)	LI-COR	D00825-14	926–32211	1:20,000

Chemicals & Reagents

Reagent	Source	Identifier
DMSO	Fisher	Cat# BP231-100
Bortezomib (PS-241)	Cayman Chemical	Cat# 10008822
Pevonedistat (MLN4924)	Selleckchem	Cat# S7109
GDC-0068	Selleckchem	Cat# S2808
RPMI Medium	Wisent Bioproducts	Cat# 350000CL
JNK-IN-8	MedChemExpress	HY-13319
VX-745	Torcis	3915
ARQ 092	Cayman Chemical	21388
MK-2206	Cayman Chemical	11593
Borussertib	Selleckchem	S8839
VH032	MedChemExpress	HY-120217
AZD5363	Cayman Chemical	15406
CellTox Green Cytotoxicity Assay	Promega	G8743

Cell Lines

Reagent	Source	Identifier
T47D	ATCC	HTB-133
MCF7	ATCC	HTB-22
MDA-MB-468	ATCC	HTB-132
MOLT4	ATCC	CRL-1582
BT474	ATCC	HTB-20

Software & Algorithms

Reagent	Source	Identifier
GraphPad Prism	GraphPad Software, Inc.	www.graphpad.com/
Adobe Illustrator	Adobe Creative Cloud	www.adobe.com/creativecloud.html
R framework	Team RCR: A language and Environment for Statistical Computing	www.R-project.org/

CHAPTER 4

DISCUSSION

4.1 Summary of Thesis

Recently, advances in chemical biology and drug development have expanded our molecular toolbox to enable selective targeting of proteins by proteasomal degradation[264,301–304]. The overall aims of the studies outlined in this thesis are to advance our understanding of the role of AKT in the PI3K signaling pathway using degrader compounds and to evaluate these drugs as potential therapeutics for cancers with hyperactivated AKT. Small molecule PI3K pathway inhibitors as monotherapies have been largely unsuccessful in the clinic, due to systemic toxicities and lack of efficacy[5,83,259,305,306]. This thesis aimed to address these two therapeutic shortfalls by evaluating AKT-targeting PROTACs as an alternative approach to targeting AKT.

Chapter 2 demonstrated that AKT-targeting degraders selectively and rapidly degrade AKT isoforms in cultured cancer cells. Our first-generation AKT degrader INY-03-041 comprises the AKT-recruiting ligand GDC-0068 (ipatasertib) and the IMiD lenalidomide for recruitment of the E3 ubiquitin ligase CRBN. INY-03-041-mediated AKT degradation was dependent on the proteasome, neddylation, and binding to both AKT and CRBN. INY-03-041 suppressed proliferation and downstream PI3K pathway signaling more efficiently than the parental inhibitor GDC-0068 at doses that equivalently suppressed PRAS40 phosphorylation. Unexpectedly, we discovered prolonged AKT degradation concomitant with potent inhibition of downstream signaling, either after a single treatment of INY-03-041 or prolonged compound washout. This highlights one of the unique features of AKT degradation and underscores its potential advantages as a therapeutic.

Chapter 3 focused on the characterization of a second-generation AKT degrader, INY-05-040, composed of the catalytic AKT inhibitor GDC-0068 and a ligand targeting the E3 ubiquitin ligase, VHL. Compared to the first-generation AKT degrader INY-03-041, INY-05-040 exhibited more rapid degradation kinetics and increased selectivity. We hypothesized these features would increase therapeutic tractability and allow for the assessment of the biological

consequences of rapid AKT degradation. This chapter aimed to characterize the potency and selectivity of INY-05-040 and increase our understanding of the effects of acute AKT depletion on cellular metabolism and transcription. Steady-state polar metabolite profiling was used to assess changes to in metabolites after 24 hours of treatment with INY-05-040 compared to catalytic or allosteric AKT inhibitors. We identified a significant upregulation of nucleosides in degrader treated cells. RNA-seq analysis of samples treated with either catalytic AKT inhibitor or degrader were used to assess transcriptional changes unique to AKT degradation. Most transcriptional changes overlapped between degrader and inhibitor, but the magnitude of these changes was more pronounced with degrader than inhibitor. We used a multi-omics network analysis integration approach, COSMOS, to generate mechanistic hypotheses to explain changes observed in our omics datasets. Key components of the integrated stress response, JNK1 (*MAPK8*) and p38α (*MAPK14*), were consistently identified as top degree nodes in the degrader networks, suggesting that activation of stress kinase signaling may be an AKT degrader-specific response. We validated the specific upregulation of these stress-responsive kinases in a panel of breast cancer cell lines following INY-05-040 exposure. Lastly, we were able to rescue degrader-induced cell death with JNK inhibition, but not p38α inhibition, indicating that INY-05-040-specific induction of JNK signaling may underlie the increased efficacy of these compounds.

In summary, this thesis showcases the development and characterization of two potent and selective AKT-targeting degraders, including their extensive characterization. This novel approach to targeting AKT may have therapeutic potential and has extended our knowledge of AKT signaling by demonstrating the contribution of stress kinase signaling to AKT degrader-induced cell death.

4.2 Discussion

4.2.1 Advantages and Challenges of Targeting AKT using PROTACs

Given its role in promoting tumor initiation and progression, the PI3K pathway has been extensively targeted for anti-cancer therapies[85,261,307]. Many of these strategies have been hampered by on-target-off-tumor and off-target toxicities that restrict the use and efficacy of these inhibitors in the clinic. Targeted therapies directed at PI3K pathway components have largely been limited to protein and lipid kinase inhibitors, where achieving selectivity has been a challenge. The identification of novel targeting strategies, especially those that improve drug selectivity, may more effectively restrict PI3K pathway-driven cancer growth with fewer dose-limiting toxicities. Targeted protein degradation has recently been identified as a novel therapeutic strategy that offers several advantages over traditional small molecule protein kinase inhibitors, such as improved selectivity, potency, and reduced toxicity.

We considered the amenability of targeting AKT using PROTACs. AKT is a well-studied protein kinase with partial crystal structures available[308,309]. Several catalytic and allosteric AKT inhibitors have been developed, providing a selection of AKT-targeting ligands from which to design PROTAC compounds[140]. We and others have synthesized AKT degraders based on the catalytic AKT inhibitors GDC-0068, AZD5363, or GSK690693 and the E3 ubiquitin ligases CRBN or VHL[214,215,239]. Interestingly, our initial efforts aimed at designing AKT degraders using the allosteric AKT inhibitors ARQ 092 and MK-2206 were unsuccessful, and no AKT degraders based on allosteric AKT inhibitors have yet been reported in the literature. We hypothesize that this lack of success may be due to the inability of an E3 ligase and AKT to form a productive ternary complex in the orientation fostered by compound design with an allosteric AKT ligand.

We observed enhanced selectivity of AKT degraders over the parental catalytic pan-AKT inhibitor GDC-0068, in agreement with previous reports of PROTACs enhancing the selectivity of the kinase inhibitors from which they were designed[199]. The degradation profile of a PROTAC relies on the recruited E3 ligase and ligand recruiting the protein of interest, and is dependent

upon efficient ternary complex formation to induce target protein ubiquitination and subsequent proteasomal degradation[186,310]. Both CRBN- (INY-03-041) and VHL-targeting (INY-05-040) AKT degraders resulted in productive degradation, indicating that both CRBN and VHL E3 ligases can produce productive ternary complexes with AKT isoforms to enhance the selectivity of GDC-0068. VHL and CRBN both possess highly selective small molecule ligands, and are broadly expressed across tissues, which made them rational E3 choices for PROTAC design.

Our initial rationale for pursuing AKT targeting degraders was to harness the increased selectivity often observed with targeted protein degradation to develop isoform-selective compounds[241,284,285]. However, our efforts aimed at achieving AKT isoform selectivity have thus far been unsuccessful, consistent with published reports of other AKT degraders[214,215]. Ternary complex formation mediated by interactions between E3 ligase and target protein, and through stabilizing interactions with the PROTAC linker, are essential for target protein degradation[205,211]. AKT isoforms are structurally similar, particularly in the catalytic kinase core[30]. The use of catalytic AKT inhibitors may restrict the orientation of the ternary complex to interactions with regions of high similarity between AKT isoforms, resulting in pan-AKT degradation. A more extensive medicinal chemistry campaign using existing AKT inhibitors may improve isoform selectivity by differentially affecting the stability of ternary complex formation between isoforms. Alternatively, the identification of novel AKT-targeting ligands may open the door to compounds that facilitate PROTAC-mediated AKT ubiquitination to a region of lower homology between AKT isoforms, such as the linker or hydrophobic motifs.

Molecular and physiological effects of AKT degradation

Other groups have also used AKT degraders to uncover novel aspects of AKT biology. Xu *et al.* reported that AKT degradation by the AKT PROTAC MS21 promoted Aurora B destabilization by decreasing AKT phosphorylation of Aurora B (T73), which usually prevents its proteasomal degradation. MS21 suppressed xenograft tumor growth through Aurora B

inhibition, and the efficacy of this compound was found to be greater in PI3K/PTEN pathway mutant cancers with WT *KRAS* and *BRAF*[311]. More recently, Yu *et al.* published a structure-activity relationship study of multiple AKT PROTACs with various linker lengths and compositions, E3 ligands, and AKT inhibitors[214]. These authors also characterized two AKT degraders designed from GDC-0068 and ligands targeting either VHL or CRBN[214]. Although these groups explored the chemical and functional properties of these degraders, to date there has been no effort to systematically profile the metabolic and transcriptional consequences to AKT degradation.

In my studies I observed prolonged degradation of AKT and inhibition of downstream signaling after INY-03-041 or INY-05-040-mediated AKT degradation, highlighting a novel aspect of AKT degrader pharmacology[239]. Interestingly, prolonged AKT destabilization appears to be a common feature amongst AKT PROTACs. A preliminary experiment showed that INY-03-041 stability in RPMI medium at 37°C was < 40 h (data not shown). Because the stability of chemically labile PROTACs in cell culture media is generally poor, several possibilities may explain the prolonged destabilization of AKT. First, the deregulation of specific or general protein synthesis, or gene expression, downstream of the AKT/mTORC1 axis may blunt the resynthesis of AKT itself. AKT has a long reported half-life of approximately 36 hours, which may indicate low basal resynthesis rates[238,312]. Another related possibility is that potent suppression of AKT-dependent regulation of ribosome biogenesis through mTORC1 may prevent global protein resynthesis[69,313,314]. Lastly, it is possible that PROTACs may retain their chemical stability for long periods of time in an intracellular environment, allowing even a few molecules of compound to catalyze multiple rounds of degradation to maintain long-lasting degradation of AKT.

We observed enhanced anti-proliferative effects of AKT degraders over catalytic inhibitors. This may relate to the increased potency of degraders that act catalytically to induce multiple rounds of degradation, lowering the dose required for effect. Degraders targeting other

protein kinases have been reported to exhibit equivalent[221] or enhanced[218] anti-proliferative effects over their parent compounds. Enhanced anti-proliferative effects may also relate to the prolonged degradation of AKT, sustained inhibition of downstream signaling, and lack of PI3K pathway re-activation.

PI3K pathway signaling is intrinsically regulated by feedback inhibition[158,315]. Relief of feedback inhibition has been hypothesized as an escape mechanism for cancer cells that in turn reduces the efficacy of targeted therapies[160,316,317]. Feedback inhibition resulting from AKT inhibition has been demonstrated through both the mTORC1 axis, and through FOXO-mediated transcriptional induction of receptor tyrosine kinase expression[157]. We observed robust and expected increases in RTK expression and phosphorylation upon prolonged AKT degrader treatment (**Appendix 2**). However, prolonged treatment with either AKT inhibitor or degrader did not indicate a strong rebound in the phosphorylation of PRAS40 or S6 under either condition. We also observed robust upregulation of ERK phosphorylation upon INY-05-040 treatment in BT474 and MCF7 cells, especially at long timepoints, though this response was not consistent across cell lines (**Figure 3-15 and Appendix 2**). This is consistent with the idea that compensatory increases in RTKs drive signaling through parallel growth-promoting pathways. Xu *et al.* observed that co-targeting AKT and the MAPK pathway may be an attractive therapeutic combinaton[215]. Although we have extensively evaluated pathway rewiring in response to degrader vs inhibitor treatment, prolonged AKT destabilization may not be permissive to reactivation of PI3K signaling, though this does not exclude the possibility of compensatory upregulation of signaling through parallel pathways. Resistance to AKT inhibitors can arise in some cases due to upregulation of AKT3[118]. Because degraders have been shown to overcome inhibitor-induced compensatory upregulation of target proteins[318], targeting AKT with degraders may represent a more potent and sustained method of inhibiting pathway output.

Therapeutic potential of AKT degraders

Unlike small molecule inhibitors, PROTACs' relatively larger size makes them vulnerable to metabolic modifications and may hinder their bioavailability[319]. Nevertheless, there have been reports of successful *in vivo* protein degradation using PROTACs[218]. We hypothesized that the relatively long times required for degradation of AKT isoforms in cells with INY-03-041 (~12 h) combined with the short half-life of the compound observed in pharmacokinetics experiments would not allow for efficient degradation of AKT isoforms *in vivo,* since degrader could be cleared from tissues before AKT degradation can occur. Initially, we did not observe degradation of AKT isoforms in xenograft tumors or mouse tissues using INY-03-041. However, we did observe AKT degradation with INY-03-041 at higher doses and longer time points, suggesting this degrader is effective *in vivo* (**Appendix 1**). By contrast, INY-05-040 degraded AKT on a much faster timescale *in vitro* (half-maximal degradation at 5 h), suggesting its amenability to *in vivo* degradation. We observed successful degradation of AKT isoforms in xenograft tumors, liver, and kidney tissues using INY-05-040 (**Appendix 1**). Ongoing studies are investigating the formulation of these compounds and assessing their potential to degrade AKT isoforms *in vivo.*

The clinical progression of AKT inhibitors as therapeutic agents has been limited by concerns about safety and tolerability[320]. The increased selectivity of AKT degraders may enhance their efficacy and limit off-target toxicities compared to multi-targeted kinase inhibitors. However, increased potency may also represent a liability of degrader compounds due to greater on-target adverse events associated with inhibiting the PI3K pathway, including hyperglycemia and hyperinsulinemia[276,277], dermatological toxicities[278,279], and hepatic toxicity[279,280], among others[281]. The recent success of the PI3Kα inhibitor alpelisib has demonstrated the benefits of isoform-selective inhibition[119]. While AKT degraders offer enhanced selectivity over catalytic AKT inhibitors, AKT isoform-selective compounds have yet to

be developed or evaluated in clinical trials. To evaluate their therapeutic potential, an initial goal of this work was to validate PROTAC-mediated AKT degradation *in vivo.*

Given the prolonged degradation of AKT after single compound administration *in vitro,* we hypothesize that infrequent compound administration may effectively reduce AKT protein levels and inhibit downstream signaling for long periods of time *in vivo,* independently of compound stability. The limiting factor in this scenario is the time required for degrader to reach its target in the tumor to catalyze AKT degradation before the drug is metabolized or eliminated by other means. The same is true for irreversible covalent AKT inhibitors, such as borussertib, whose mechanism of action may prove more advantageous for *in vivo* targeting compared to reversible inhibitors[89]. Advances in compound formulation and dosing schedules, especially given the prolonged degradation of AKT observed after compound washout, may be able to mitigate on-target toxicities and provide a window of opportunity to improve the therapeutic efficacy of degraders.

Although this work has focused on targeting AKT in cancer, AKT-targeting degrader compounds may hold promise for the treatment rare diseases caused by germline or mosaic mutations in the PI3K pathway, such as PTEN hamartomas, *PIK3CA*-related overgrowth spectrum (PROS), and Proteus syndrome, among others[321]. These diseases are often associated with benign tumors or overgrowth of organs, though the severity of the disease is variable and dependent on the mutation and degree of mosaicism[322]. PI3K pathway inhibitors, notably AKT inhibitor ARQ 092, are being evaluated for their potential to treat these diseases, suggesting AKT degraders may be valuable in the rare disease setting[323–325].

4.2.2 PROTACs as tool compounds to study AKT function

While AKT is one of the most actively studied protein kinases, several aspects of AKT function remain to be explored in both normal physiology and disease. Many of these limitations stem from insufficient tools to 1) address the contribution of each AKT isoform specifically; 2)

evaluate the acute effects of protein depletion without genetic perturbation; 3) understand kinase-independent contributions to downstream signaling; and 4) deconvolute pathway feedback. Using AKT degraders, we were able to investigate three of these four aspects: acute effects, kinase-independent roles, and pathway networks altered by AKT degradation.

Cellular dynamics altered by acute, prolonged AKT degradation

Inducible small hairpin RNAs, transient transfection and CRISPR-mediated knockdown or knockout require long incubation periods, thus preventing the assessment of acute changes due to protein loss while also allowing cellular reprogramming and compensation by other cellular network dynamics. Herein we validate that AKT degraders rapidly, potently, and specifically deplete AKT isoforms. Thus, AKT degraders were used to assess the broad signaling consequences of acute AKT depletion. Because AKT has well-studied roles in metabolism and transcription, we performed steady-state metabolomics after 24 h treatment and RNA-seq after 5 hours or 10 hours treatment with INY-05-040 or GDC-0068 at concentrations that equivalently suppress PRAS40 phosphorylation to control for the degree of pathway inhibition.

Interestingly, the metabolomics and transcriptomics analyses identified similar changes, but of different magnitudes, between AKT degradation and inhibition, indicating that the potency of AKT inhibition was particularly important for the strength of cellular responses, including the more dramatic inhibition of proliferation and induction of cell death. Importantly, the omics data were collected under conditions where AKT degradation and inhibition equivalently suppressed substrate phosphorylation. However, the measurement of PRAS40 phosphorylation as a readout of the strength of AKT inhibition does not necessarily equate to equal inhibition of other AKT substrates, which may rely on other contextual features of AKT such as conformation or localization. For example, at concentrations where PRAS40 phosphorylation was equivalently suppressed, inhibition of S6 phosphorylation was markedly reduced in degrader treated

conditions compared to GDC-0068. One explanation is that AKT could play a scaffolding role in a complex to promote downstream signaling independently of PRAS40, which would more efficiently inhibit S6 phosphorylation. Alternatively, degradation of AKT could prevent rebound signaling through AKT at later timepoints that would be susceptible to pathway reactivation with inhibition, but not degradation.

Degrader-specific effects on processes moderated by AKT signaling

Degraders can be used as biological tools to shed light on kinase-independent functions of AKT by inducing acute protein depletion and may illuminate the limitations of existing catalytic, allosteric, or covalent AKT inhibitors. Kinase-independent or conformation-specific functions of AKT that promote cell survival and endocytic recycling have recently been described[146,326,327]. PROTACs may have a therapeutic advantage over inhibitors due to their reported ability to abrogate kinase-independent functions[209].

We used degraders to probe novel aspects of the role of AKT in PI3K signaling and uncovered that the dynamics and potency of AKT inhibition are important for inducing cytotoxic responses. Catalytic and allosteric AKT inhibitors have previously been used to identify a conformation-specific role of AKT in promoting survival[146]. We observed dramatic differences in nucleoside levels between AKT degrader and inhibitor-treated cells. Interestingly, the metabolic profile of cells treated with allosteric AKT inhibitors more closely resembled AKT degrader than catalytic AKT inhibitors, which may indicate a kinase-independent or conformation-specific role of AKT in metabolism. The open conformation induced by catalytic AKT inhibitors may also affect the pool of AKT regulators (such as PDK1, PHLPP, or PIP3) that target the open conformation, whereas AKT degraders or allosteric inhibitors that either deplete total AKT levels or constrain AKT to a closed conformation would differentially affect this pool of regulators.

We also saw more similar induction of the stress kinase response with allosteric and covalent AKT inhibitors than with catalytic inhibitors, indicating that the potency and

maintenance of AKT inhibition will be crucial factors in understanding the clinical value of these compounds. Understanding the signaling dynamics after treatment of cells with catalytic, allosteric, covalent AKT inhibitors or AKT degraders may increase our ability to design combination therapies that rationally exploit vulnerabilities generated by different classes of AKT inhibitors. It also underscores the potential advantage of covalent AKT inhibitors and AKT degraders over both catalytic and potentially allosteric inhibitors because of their ability to suppress scaffolding or kinase-independent roles. Interestingly, the conformation of AKT bound by MK-2206 is distinct from the autoinhibited conformation of AKT, indicating that scaffolding roles of allosteric inhibitor bound AKT may be different from baseline autoinhibited AKT[328].

A limitation that has only been partially addressed by this work is whether targeting the E3 VHL contributes to the phenotypes attributed to AKT degradation. We have used ligands targeting VHL (VH032) and CRBN (lenalidomide) as controls for engagement of E3s. We have tested E3 targeting compounds VH032 and lenalidomide in proliferation assays. Future experiments will include VH032 to validate stress kinase signaling, as VHL inactivation has been shown to activate the cellular stress response.

AKT degradation uniquely induces stress kinase signaling

The use of a multi-omics integration approach provided a global view of the data and allowed us to uncover insights into cellular processes spanning multiple levels of biological information[266]. We used COSMOS to integrate RNA-seq and metabolomics datasets to generate mechanistic hypotheses for our experimental observations. The ability of COSMOS to correctly identify the stress kinase response as a degrader-specific response showcases the value of this approach to extract mechanistic hypotheses from the integration of multiple omics datasets using a prior knowledge network. Additionally, validation of COSMOS predictions supports the widespread use of this hypothesis-generating tool. The use of network analyses also has broad potential for biomarker identification and can further our understanding of

biological networks. This knowledge can then be exploited for the identification of therapeutic targets.

The use of a network analysis approach does have limitations. First, it relies extensively on the connections and regulatory relationships between transcription factors, kinases, phosphatases, and metabolites in the prior knowledge network – only a fraction of which have been functionally characterized. Second, only a few of all potential interactions in experimental samples can be sampled at one time using omics approaches, which leaves large sections of the prior knowledge network unused. COSMOS may generate hypotheses that do not explain the true biological mechanism given limitations in prior knowledge network composition and input omics data. In summary, understanding that COSMOS is a predictive, hypothesis-generating tool whose results must be explored and validated experimentally lends strength to this approach to interpret complex multi-omics datasets.

COSMOS identified JNK1 (*MAPK8*) and p38α (*MAPK14*) as top degree nodes in degrader networks, which we validated as a degrader-specific response in a panel of cell lines. The functions of stress-activated protein kinase pathways are complex and context-dependent due to their broad roles in a range of cellular responses[289]. Furthermore, JNK activation may mediate distinct cellular outcomes, either apoptosis or survival, depending on the dynamics of pathway activation[271]. We identified BT474 cells as ultrasensitive to AKT degradation and subsequent activation of JNK signaling. We showed that AKT-mediated cell death could be rescued by a JNK1/2/3 inhibitor, indicating that JNK activation contributes to degrader-induced cell death, at least in part. The lack of cell death seen in other cell lines may be due to differences in the dynamics of JNK activation, with a more transient and graded JNK response potentiating cell survival[271]. AKT directly regulates JNK signaling by inhibitory phosphorylation of the JNK activators MKK4 at S80 and MKK7 at T385[271]. However, whether AKT degrader is regulating JNK activators MKK4/MKK7, directly regulating JNK, or indirectly regulating JNK through induction of metabolic or cellular stress or the production of cytokines remains to be

determined, and additional experiments are required to test these possibilities (**Figure 4-1**). The increase in nucleosides observed in AKT degrader-treated cells may suggest induction of nucleolar stress and ribophagy that contribute to stress kinase activation, although we have not yet measured nucleolar stress directly (**Figure 4-2**). Exploring the crosstalk between AKT inhibition and stress kinase signaling is an interesting area for future investigation.

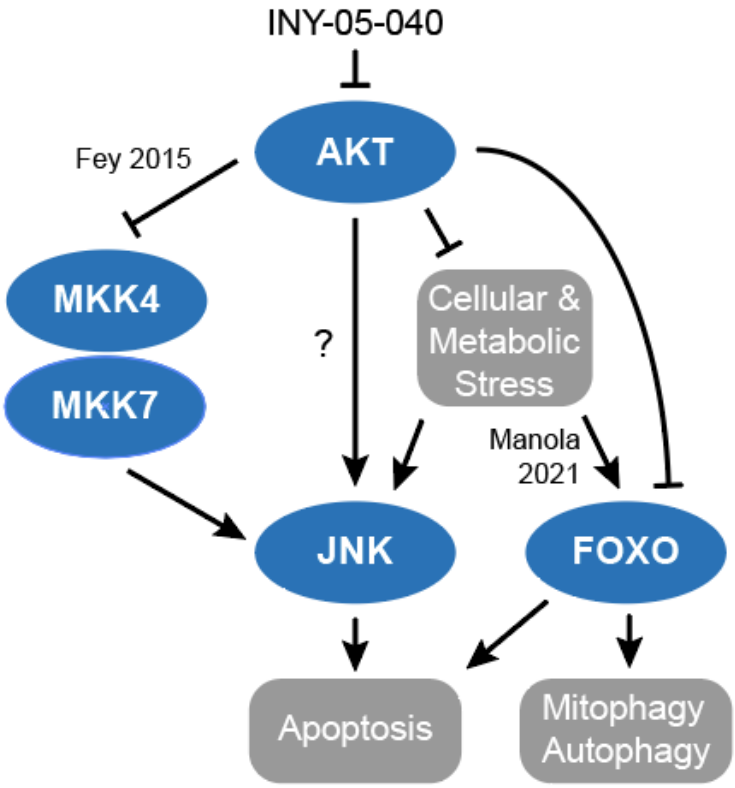

Figure 4-1. Model of JNK activation after degradation of AKT. We hypothesize that AKT degradation may activate JNK signaling either through relief of inhibition of JNK activators MKK4 and MKK7, directly through an unknown mechanism, or indirectly through the induction of cellular and metabolic stress. Relief of AKT inhibition of FOXO, either directly or through the induction of stress, may partially contribute to induction of apoptosis, mitophagy, and autophagy.

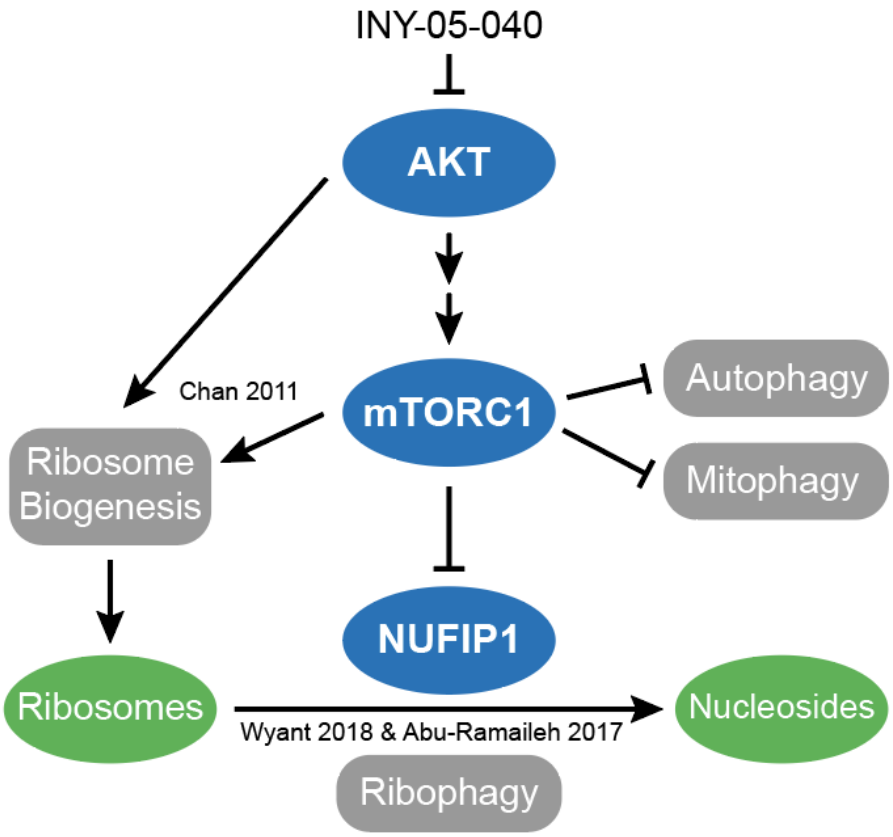

Figure 4-2. Model of AKT degrader-dependent increase in nucleoside levels. We hypothesize that the increase in nucleoside levels seen in metabolomics experiments specifically after AKT degradation, not inhibition may be due to an increase in ribophagy and suppression of ribosome biogenesis because of more complete inhibition of AKT and mTORC1.

4.3 Future Directions

This thesis characterized two small molecule AKT degraders for their potential to selectively degrade AKT *in vitro* and *in vivo*. Additionally, it highlighted the use of targeted protein degradation as a strategy to uncover novel aspects of AKT biology, including the metabolic, transcriptional, and network rewiring events that occur in response to potent and prolonged AKT degradation. Beyond the future directions that have been discussed in Chapters 2 and 3, several questions remain to be addressed, whose investigation would expand on the findings of this thesis.

Therapeutic efficacy of AKT degraders

Although we and others have demonstrated effective AKT degradation *in vivo*, further optimization of compound formulation and chemistry will be required to optimize the *in vivo* efficacy of AKT degraders (**Appendix 1**)[214,215]. Pharmacokinetics and pharmacodynamics profiling experiments to determine tolerable doses and optimal dosing schedules will be necessary to inhibit tumor growth without adverse systemic toxicities. Preliminary pharmacodynamics experiments have revealed differences in AKT degradation between organs, which may reflect differences in the systemic metabolism or distribution of these compounds (**Appendix 1**). Understanding the pharmacokinetics, metabolism, and secretion of AKT degraders will be important for achieving and maintaining concentrations of drug to exert desired effects on tumor metabolism and for managing toxicities.

It would also be informative to assess glucose tolerance in response to AKT degradation. Hyperglycemia is a major and potentially dose-limiting adverse event observed upon treatment with PI3K or AKT inhibitors, affecting patient quality of life as well as treatment efficacy[119,168,329]. Activation of AKT promotes translocation of glucose transporters to the plasma membrane to stimulate glucose uptake in response to insulin[330]. Inhibition of PI3K or AKT impairs glucose uptake, which promotes insulin secretion and can reactivate PI3K signaling,

reducing the efficacy of PI3K pathway inhibition and inducing systemic toxicities resembling a diabetes phenotype[276]. Because we observed AKT degradation in liver, we would expect AKT degradation to produce a similar or more severe elevation of blood glucose and insulin along with increased compound potency (**Appendix 1**). High insulin levels have been shown to partially reactivate PI3K signaling, even in the continued presence of PI3K inhibitors[126]. Complete degradation of AKT may prevent pathway reactivation downstream of AKT which may underscore an advantage of AKT degraders in preventing pathway reactivation in response to high insulin. However, this does not exclude the reactivation of parallel pathways that limit the efficacy of these inhibitors, nor the toxicities associated with systemic hyperglycemia and hyperinsulinemia. Future studies could also explore combination of AKT degradation with several strategies that have been proposed to better detect, prevent, and treat PI3K pathway inhibitor-induced hyperglycemia. These strategies include management by medications such as potassium channel inhibitors to prevent pancreatic insulin release, SGLT2 inhibitors which clear blood glucose by blocking renal reabsorption, diverting glucose to urine[331,332], dietary interventions including ketogenic diets[126,333], or modifications in treatment intervals[276].

The use of tissue- or tumor-specific E3 ligases could potentially be used to further enhance selectivity and reduce systemic toxicities, such as hyperglycemia[283]. Progress on this front has been limited by the lack of small-molecule ligands to recruit diverse E3 ligases. Though not unique to degraders, an alternate strategy to achieve tissue- or tumor-selectivity is the use of an antibody-PROTAC conjugate, recently described in a proof-of-concept paper[282]. This would enable tissue- or tumor-specific targeted protein degradation and combine the potency advantage of degradation with the specificity afforded by antibody targeting. Lastly, one could explore whether long-lasting degradation of AKT *in vitro* translates to prolonged degradation *in vivo,* and if intermittent dosing could mitigate off-target effects while still inhibiting tumor growth.

Another consideration when measuring the therapeutic efficacy of AKT degraders *in vivo* is the role of the immune system. Our lab has developed an immune-competent *INPP4B*$^{-/-}$ genetically engineered mouse model which closely recapitulates human TNBC, a population of breast cancer patients for whom chemotherapy is the standard of care and prognosis is generally poor[11,12]. PI3K pathway inhibition has been shown to increase immune infiltration through transcriptional regulation of chemokines and genes involved in immune cell recruitment[334], so we expect AKT degrader-treated tumors to show an increase in CD45+ lymphocytes, increased expression of immune cell recruiting cytokines such as CCL2, and downregulation of ITGB3, which suppresses immune cell invasion in breast cancer[335]. If increased tumor immune infiltrate is observed subsequent to AKT degradation, it would be interesting to investigate immune checkpoint therapies in combination with AKT degradation. To complement our previous multi-omics analyses, RNA-seq or metabolomics on these tumors could be used to assess immune-related gene transcription, and whether degrader-mediated changes in metabolism or transcription are recapitulated *in vivo*.

Metabolic and transcriptional consequences of AKT degradation

AKT degradation resulted in a striking increase in guanine, cytosine, and inosine nucleosides that was not observed in response to AKT inhibition. Because downstream pathway signaling, measured by phosphorylation of PRAS40 and S6 was inhibited equivalently, this may indicate a non-kinase-dependent AKT regulation of nucleoside metabolism. Because we observed a specific increase in nucleosides and some NMPs, we hypothesize that AKT degradation specifically inhibits ribosome biogenesis and nucleolar stress, both through mTORC1-dependent and independent mechanisms (**Figure 4-1**)[287,288]. To determine if more potent inhibition of mTORC1 downstream of AKT degradation is contributing to the increase in nucleosides, one could co-treat cells with GDC-0068 and a selective inhibitor of mTORC1, followed by a measurement of nucleoside levels by metabolomics[316], where one would expect to

see an increase in nucleosides, given the more complete inhibition of mTORC1 in addition to inhibition of AKT. Organelle-specific enrichment (i.e. LysoIP) followed by metabolomics may be used to determine if increased lysosomal degradation of ribosomes is due to degrader-specific inhibition of mTORC1[287]. It would also be interesting to assess changes in ribosome biogenesis or nucleolar stress in response to AKT degradation or inhibition.

Alternatively, metabolomics profiling of cells expressing kinase-inactive AKT, CRISPR-mediated AKT knockout, or siRNA/shRNA-mediated AKT knockdown could be used to assess whether nucleoside accumulation is dependent on AKT kinase activity or a scaffolding effect. Although these strategies may suffer from limitations including non-specific knockdown, compensatory pathway rewiring, and effects from transfection reagents, this could be a means of confirming kinase-independent effects.

We identified activation of stress kinase signaling as a cellular response specific to AKT degradation. However, it is unclear whether this response is mediated by an intrinsic or a non-cell-autonomous mechanism. We observed enrichment of a TNFα transcriptional signature in RNA-seq data in response to AKT degradation, indicating that induction of cytokine signaling could be a mechanism of stress kinase activation (**Figure 4-2**). This hypothesis could be investigated by incubating naïve cells with conditioned media generated by treatment of cells with AKT degrader. An increase in the phosphorylation of stress kinase markers p38α (T180/Y182), JNK (T183/Y185), JNK target p-cJun (S73), and total cJun abundance would suggest that a non-autonomous mechanism, such as the production of cytokines, is responsible for the activation of stress kinases. Importantly, cells treated with conditioned media should be evaluated for AKT degradation to ensure there is no active compound remaining in cells. Conversely, monitoring the phosphorylation of MKK4 and MKK7 at AKT-regulated sites could inform the direct contribution of AKT degradation to JNK signaling.

It will also be critical to address the contribution of degrader-mediated JNK activation to cell death in a larger panel of cell lines. The role of JNK in promoting apoptotic cell death in

response to physiological stress or therapeutic agents is well-characterized[336]. However, the complex network dynamics of JNK activation may mediate either apoptosis or survival in a context-dependent manner[271]. A computational modeling approach using information extracted from JNK signaling pathway dynamics has been used to develop prognostically useful models to stratify patients into responders and non-responders[271]. A similar modeling approach could be used to determine if there is a correlation between JNK activation and sensitivity to AKT degradation. We could use cell line profiling data to identify cell lines that are sensitive to AKT degrader, then profile these cell lines to determine if switch-like activation of JNK mediates apoptosis in cell lines sensitive to AKT degrader versus inhibitor treatment, which may help explain differential sensitivity.

4.4 Summary

In conclusion, the data described herein have expanded the repertoire of small molecule agents able to modulate AKT signaling. This thesis reports the extensive characterization of two AKT-targeting degraders, INY-03-041 and INY-05-040, and supports further investigation into their use as anti-tumor therapeutics. It also highlights the use of AKT degraders as tool compounds to explore novel aspects of AKT biology previously inaccessible using existing technologies whose long incubation times or lack of selectivity preclude the accurate assessment of acute perturbations of the system. A unique feature of AKT degrader pharmacology is the prolonged degradation and suppression of pathway signaling after a single treatment, providing a window into understanding the dynamics of pathway response in the absence of AKT protein. Together, this thesis characterizes new AKT degrader compounds *in vitro* and *in vivo* and addresses gaps in our understanding of canonical AKT signaling by uncovering a role of AKT in the activation of the stress kinase response and provides insight into the basic pathway regulation that can inform current and future PI3K-AKT pathway inhibition strategies.

Appendix 1

IN VIVO EFFICACY OF AKT DEGRADERS INY-03-041 AND INY-05-040

This section contains data covered by a confidentiality agreement.
Please do not share or reproduce.

Introduction

An important consideration in this project was the tractability of AKT degraders as therapeutic agents. Because targeted protein degradation is a relatively new therapeutic modality, relatively little is known about the pharmacokinetic properties of these small molecule degraders. However, there have been examples of degraders that work successfully *in vivo*[218]. Important questions that we aimed to address in these studies were 1) is measurable AKT degradation achievable *in vivo*; 2) are AKT degraders tolerated; and 3) what are the effects of AKT degradation on tumor and non-tumor tissues.

We evaluated the pharmacodynamics and pharmacokinetics of INY-03-041- and INY-05-040-mediated AKT degradation in breast cancer xenograft models in nude mice, and in mice bearing no tumors. The long degradation times required by INY-03-041, and potentially the formulation, hindered our ability to observe *in vivo* degradation with this compound. However, *in vivo* degradation was later confirmed at higher doses and longer treatment times. INY-05-040-mediated AKT degradation *in vivo* was readily apparent in a T47D xenograft mouse model, and in mice bearing no tumors, which may reflect the improved kinetic properties of second-generation INY-05-040 relative to first-generation AKT inhibitor INY-03-041, or the use of a ligand targeting VHL instead of CRBN. The ability of AKT degraders to functionally deplete AKT isoforms in mouse models highlights their potential as therapeutic agents in the clinic.

Results

Evaluating AKT degradation after INY-03-041 treatment in MDA-MB-468 xenografts

Because CRBN is a ubiquitously expressed E3 ubiquitin ligase, we anticipated the possibility that INY-03-041 could degrade AKT across nearly all tissues *in vivo*, though degraders have not been reported to cross the blood-brain barrier[337]. Sequence variations reported between mouse and human CRBN are not likely to affect degrader function in mouse models, though we decided to examine INY-03-041-mediated AKT degradation in mice bearing

MDA-MB-468 human breast cancer cell line xenografts to ensure any possible degradation would be apparent[338].

We analyzed the pharmacokinetics and pharmacodynamics of INY-03-041, which revealed a relatively short half-life of only 3.32 hours INY-03-041 in the blood (**Figure S1-1**). We were concerned that the short half-life of compound in the blood would not permit degradation of AKT given the relatively long times (~12 h) required for AKT degradation needed in cell culture. We examined the effects of daily intraperitoneal (IP) injections of 10mg/kg INY-03-041 treatment on MDA-MB-468 xenograft tumors, as well as liver, heart, and kidney in nude mice (**Figure S1-1B**). Unfortunately, we did not observe significant degradation of AKT in either xenograft tumors or the tissues after 3 days treatment with 10mg/kg INY-03-041. We did not observe significant weight loss in mice upon treatment with INY-03-041, though this may have been due to lack of target engagement (**Figure S1-1C**). Interestingly, INY-03-041 treatment seemed to maintain tumor volume whereas control tumors increased in size over the three-day treatment period (**Figure S1-1C**). However, the small sample size and short treatment times may indicate that experimental noise could account for these changes.

Evaluating AKT degradation after INY-05-040 treatment in T47D xenografts

We hypothesized that the development of second-generation AKT degrader INY-05-040 with faster degradation kinetics would improve *in vivo* degradation of AKT. Once again, we evaluated the pharmacokinetics and pharmacodynamics of INY-05-040. The half-life of INY-05-040 in the blood, ~ 2 hours, was even shorter than the half-life of first-generation AKT degrader INY-03-041 (**Figure S2-2A**). However, with more rapid degradation of AKT observed in cell culture studies in response to INY-05-040, we hypothesized that this AKT degrader still may function *in vivo*.

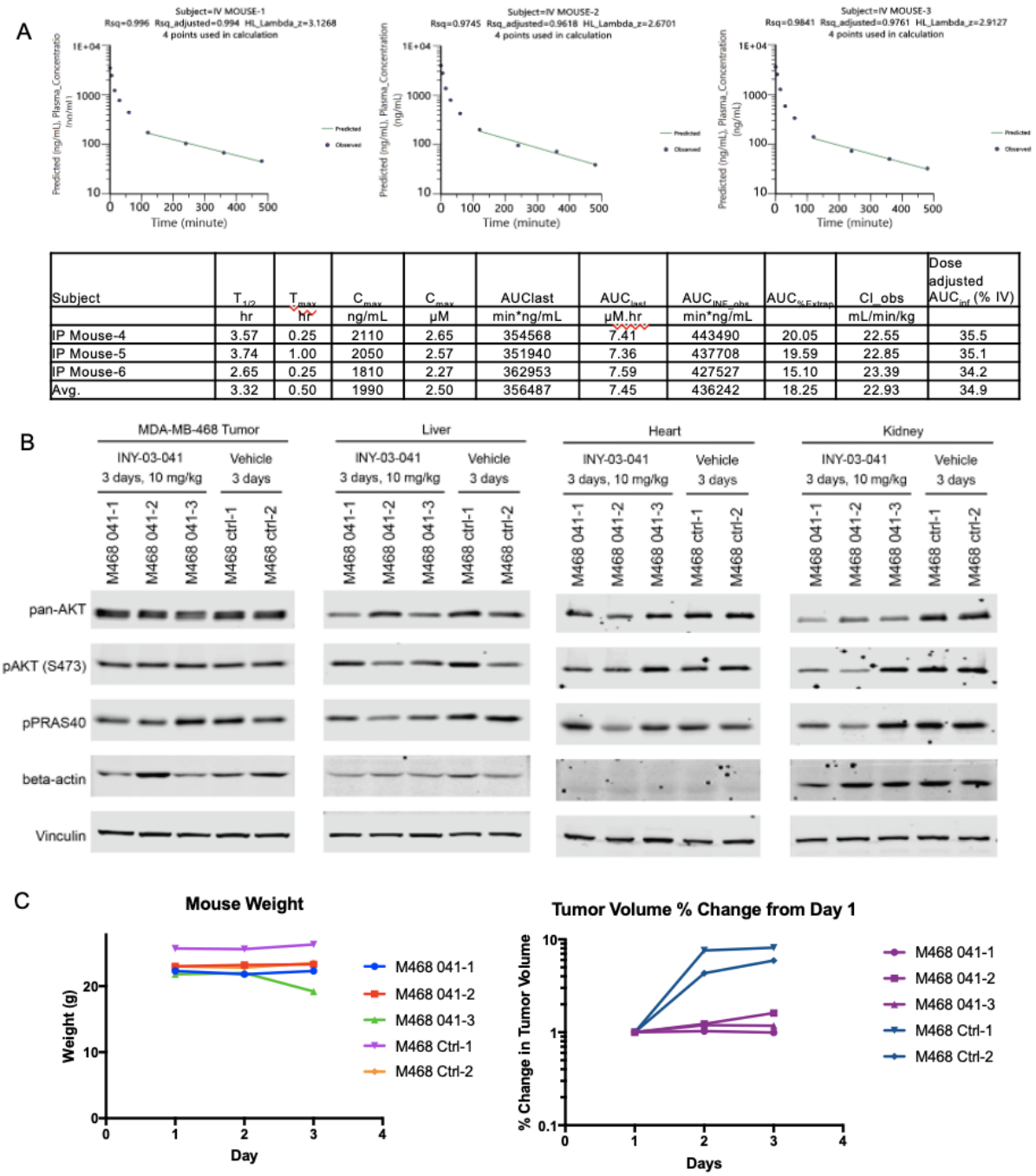

Subject	$T_{1/2}$	T_{max}	C_{max}	C_{max}	AUClast	AUC_{last}	AUC_{INF_obs}	$AUC_{\%Extrap}$	Cl_obs	Dose adjusted AUC_{inf} (% IV)
	hr	hr	ng/mL	µM	min*ng/mL	µM.hr	min*ng/mL		mL/min/kg	
IP Mouse-4	3.57	0.25	2110	2.65	354568	7.41	443490	20.05	22.55	35.5
IP Mouse-5	3.74	1.00	2050	2.57	351940	7.36	437708	19.59	22.85	35.1
IP Mouse-6	2.65	0.25	1810	2.27	362953	7.59	427527	15.10	23.39	34.2
Avg.	3.32	0.50	1990	2.50	356487	7.45	436242	18.25	22.93	34.9

Figure S1-1: Pharmacokinetics and pharmacodynamics of INY-03-041. (A) PK after a single administration of 10mg/kg IP INY-03-041 (B) PD of MDA-MB-468 xenograft tumor after IP treatment QD for 3 days with 10mg/kg INY-03-041. (C) Mouse body weight and tumor size after administration of 10mg/kg IP INY-03-041.

A

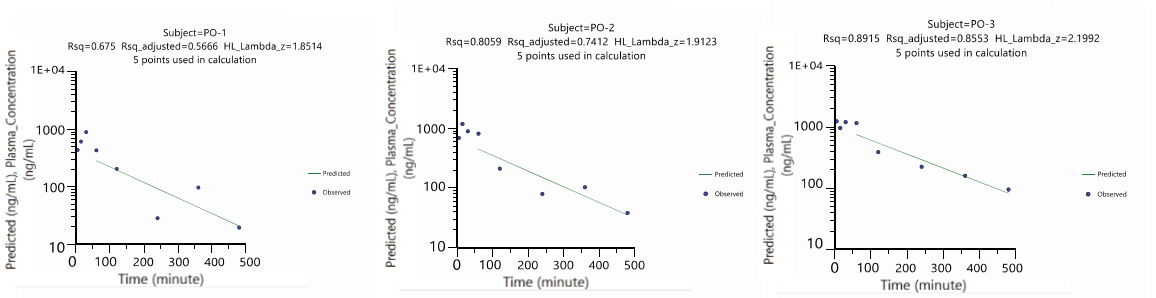

Subject	$T_{1/2}$	T_{max}	C_{max}	C_{max}	AUClast	AUC_{last}	AUC_{INF_obs}	$AUC_{\%Extrap}$	Cl_obs
	hr	hr	ng/mL	µM	min*ng/mL	µM.hr	min*ng/mL		mL/min/kg
IP Mouse-4	1.85	0.50	894	0.87	84918	1.38	88027	3.53	113.60
IP Mouse-5	1.91	0.25	1180	1.15	119615	1.94	125955	5.03	79.39
IP Mouse-6	2.20	0.08	1240	1.21	187321	3.04	205425	8.81	48.68
Avg.	1.99	0.28	1105	1.08	130618	2.12	139802	5.79	80.56

B

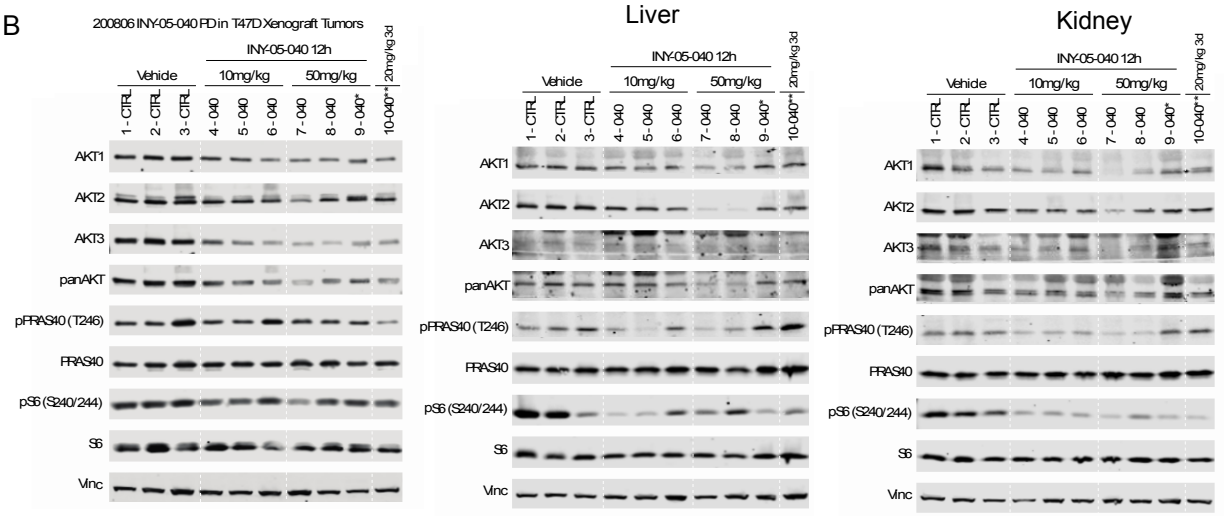

C

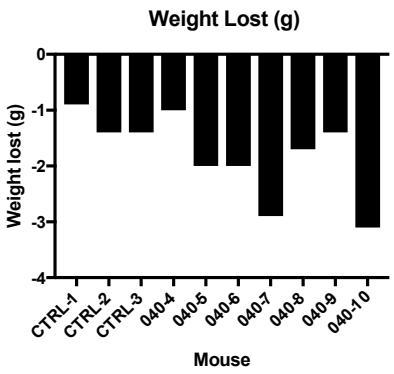

Figure S1-2. Pharmacokinetics and pharmacodynamics of INY-05-040. (A) PK after a single administration of 10mg/kg IP INY-05-040 (B) PD of T47D xenograft tumor after IP treatment for 12 h with 10mg/kg (samples 4-6) or 50mg/kg INY-05-040 (samples 7-8) or for 24 h with 50mg/kg INY-05-040 (sample 9) or 20 mg/kg (sample 10). (C) Change in mouse body weight from start of treatment to endpoint and tumor volume upon harvest after treatment.

We examined the effects of either 10mg/kg or 50 mg/kg INY-05-040 treatment via IP injections for 12 h or 3 days on mice bearing T47D xenograft tumors (**Figure S2-2B**). We observed degradation of AKT isoforms, especially AKT3 in xenograft tumors, AKT2 in the liver, and AKT1 in the kidney (**Figure S2-2B**). While only modest inhibition of downstream signaling was observed in xenograft tumors, phosphorylation of PRAS40 (T246) and S6 (S240/244) were decreased in liver and kidney tissues after AKT degrader treatment (**Figure S2-2B**). We did observe significant weight loss upon treatment with INY-05-040, even after treatment for 12 h, indicating potential toxicity (**Figure S2-2C**).

Evaluating AKT degradation after INY-03-041 or INY-05-040 treatment

Our collaborators evaluated the ability of INY-03-41 or INY-05-040 to degrade AKT isoforms after 4 days of IP treatment at 25 mg/kg. Pharmacokinetics measurements after the third 25mg/kg IP dose of either INY-03-041 or INY-05-040 showed greater area under the curve (AUC) for INY-03-041, indicating the potential for greater drug exposure than INY-05-040 (**Figure S1-3A**). Surprisingly, we observed better degradation of AKT isoforms with INY-03-041 than INY-05-040 in liver, spleen, kidney, and lungs in this study (**Figure S1-3B**). The discrepancy between this study and the initial study where no *in vivo* efficacy was observed may be explained by the increased dosage of 25 mg/kg rather than 10 mg/kg and potentially the longer treatment time of 4 days over 3 days. Both INY-05-040 and INY-03-041 treatment decreased mouse body weight over the course of the study (**Figure S1-3C**). Intriguingly, blood glucose concentrations after third dose of either degrader were stable, though this should be investigated more rigorously before drawing conclusions about AKT degrader effects on blood glucose (**Figure S1-3D**).

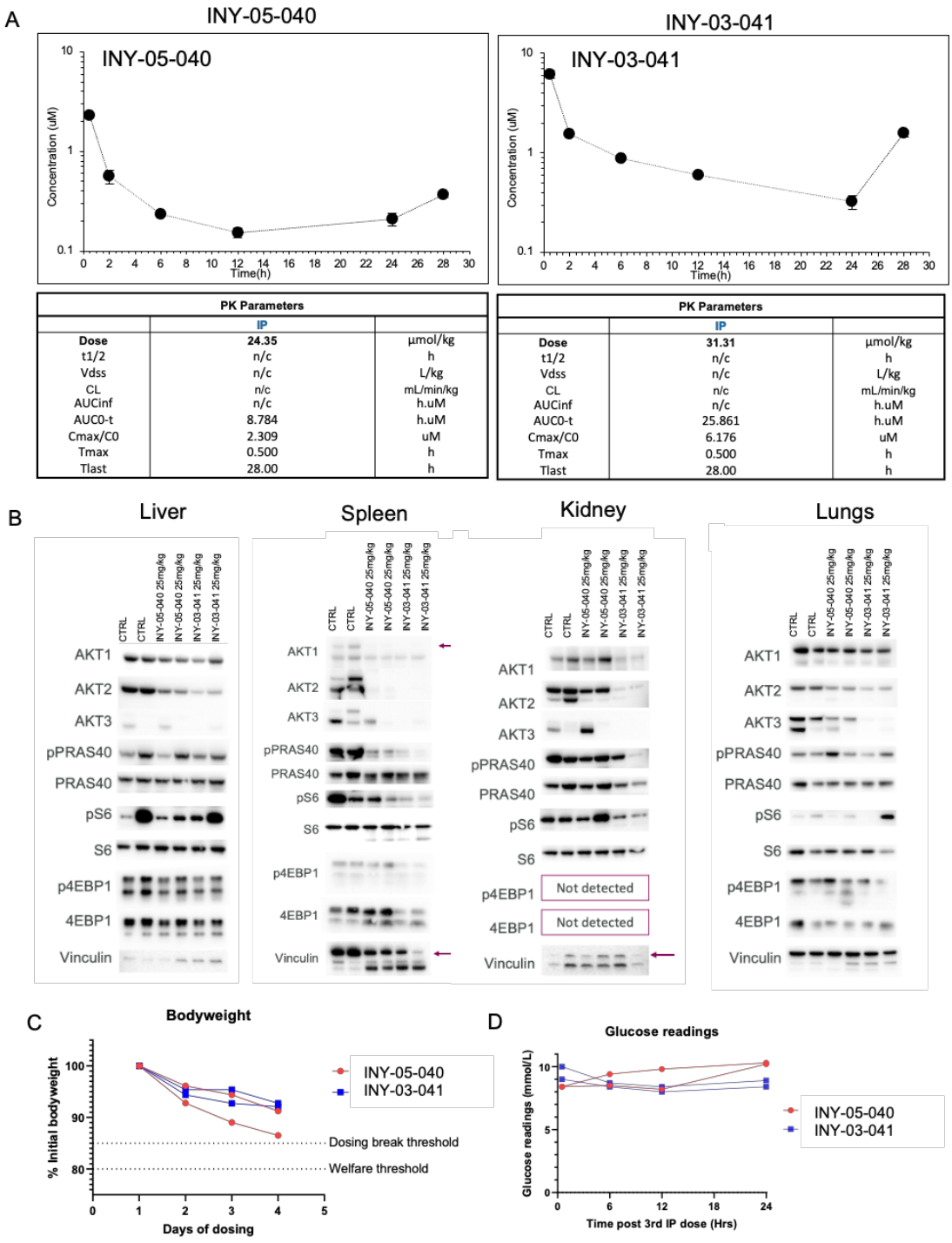

PK Parameters		
	IP	
Dose	24.35	µmol/kg
t1/2	n/c	h
Vdss	n/c	L/kg
CL	n/c	mL/min/kg
AUCinf	n/c	h.uM
AUC0-t	8.784	h.uM
Cmax/C0	2.309	uM
Tmax	0.500	h
Tlast	28.00	h

PK Parameters		
	IP	
Dose	31.31	µmol/kg
t1/2	n/c	h
Vdss	n/c	L/kg
CL	n/c	mL/min/kg
AUCinf	n/c	h.uM
AUC0-t	25.861	h.uM
Cmax/C0	6.176	uM
Tmax	0.500	h
Tlast	28.00	h

Figure S1-3: Pharmacokinetics and pharmacodynamics of INY-05-040 and INY-03-041. (A) PK after day 3 of daily administration of 25mg/kg IP INY-05-040 or INY-03-041 (B) PD of liver, spleen, kidney, or lungs after 4 days IP 25mg/kg INY-05-040 or INY-03-041. (C) Change in mouse body weight from start of treatment to endpoint and glucose readings measured as time post 3rd IP dose.

Discussion

A major goal of this work was to validate the ability of AKT degraders INY-03-041 and INY-05-040 to degrade AKT isoforms *in vivo*. Here, through initial pharmacokinetics and pharmacodynamics studies, we have shown that both AKT degraders can deplete AKT in an *in vivo* setting. We observed differences in the extent of AKT degradation between different tissues, which may reflect the metabolism or distribution of the drug after IP injection. For example, we observed robust AKT degradation in the liver, spleen, and kidneys of mice treated with AKT degraders (**Figure 3-2B and Figure 3-3B**). The decreases in body weight observed in response to AKT degraders may indicate on-target toxicity due to the potent degradation of AKT in normal tissues as discussed above. Alterations in dosing schedule, dose, formulation, may improve the tolerability of AKT degraders. Other strategies such as the use of antibody conjugates or tissue-specific E3 ligases are explored further in the discussion section.

Materials and Methods

Xenograft Studies: INY-03-041

Female nude mice (6 weeks old) were purchased from Taconic and maintained under pathogen-free conditions. Described procedures were approved by the Institutional Care and Use Committee at Beth Israel Deaconess Medical Center (BIDMC). The sample size was not predetermined using statistical methods for these preliminary pharmacodynamics experiments. Mice were injected with 2x10^6 MDA-MB-468 cells (n=10 mice) in 50% Matrigel 50% PBS into the mammary fat pad. Tumor formation was examined every 2-3 days. After tumors reached 6-7cm in diameter, mice were randomly divided into vehicle and treatment groups. Mice were treated via IP injection with INY-03-041 at 10mg/ml concentration. Tumor volume was calculated using the formula = (W^2 x L)/2; W = width, L = length[339].

Xenograft Studies: INY-05-040

Female nude mice (6 weeks old) were purchased from Taconic and maintained under pathogen-free conditions. Described procedures were approved by the Institutional Care and Use Committee at Beth Israel Deaconess Medical Center (BIDMC). The sample size was not predetermined using statistical methods for these preliminary pharmacodynamics experiments. Mice were injected with 2x10^6 T47D cells (n=10 mice) in 50% Matrigel 50% PBS into the mammary fat pad. Mice bearing T47D xenograft tumors were implanted with 17β-estradiol tablets at the time of cell injection. Tumor formation was examined every 2-3 days. After tumors reached 6-7cm in diameter, mice were randomly divided into vehicle and treatment groups. Mice were treated via IP injection with INY-05-040 at 10mg/ml concentration. Tumor volume was calculated using the formula = (W^2 x L)/2; W = width, L = length[339].

Tissue Homogenization

Tissues and tumors were flash frozen on dry ice immediately after harvest, and frozen at -80°C until further processing. Tissues and tumors were homogenized into powder form on mortar and pestles chilled on dry ice.

Immunoblotting

Homogenized tumor was lysed in RIPA buffer (150 mM Tris-HCl, 150 mM NaCl, 0.5% (w/v) sodium deoxycholate, 1% (v/v) NP-40, pH 7.5) containing 0.1% (w/v) sodium dodecyl sulfate, 1 mM sodium pyrophosphate, 20 mM sodium fluoride, 50 nM calyculin, and 0.5% (v/v) protease inhibitor cocktail (Sigma-Aldrich®) for 15 minutes. Tumor extracts were precleared by centrifugation at 14,000 rpm for 10 minutes at 4°C. Supernatants were recovered and extracts were cleared again by centrifugation at 14,000 rpm for 10 minutes at 4°C. The Bio-Rad DC protein assay was used to assess protein concentration, and sample concentration was normalized using SDS sample buffer. Lysates were resolved on acrylamide gels by SDS-polyacrylamide gel electrophoresis and electrophoretically transferred to nitrocellulose

membrane (BioRad) at 100 volts for 90 minutes. Membranes were blocked in 5% (w/v) nonfat dry milk in tris-buffered saline (TBS) buffer for 1 hour then incubated with specific primary antibodies diluted in 5% (w/v) nonfat dry milk in TBS-T (TBS with 0.05% Tween-20) at 4°C overnight, shaking. The next day, membranes were washed with TBS-T then incubated for 1 hour at room temperature with fluorophore-conjugated secondary antibodies (LI-COR Biosciences). The membrane was washed again with TBS-T then imaged with a LI-COR Odyssey CLx Imaging System (LI-COR Biosciences).

Appendix 2

SUPPLEMENTAL DATA FOR CHAPTERS 2 AND 3

Data listed below available at this link:

https://osf.io/j8ed2/?view_only=27cc1de53c904931a456f48fa77ae4c3

Chapter 2 Supplemental Data:

Table S2-1. **Biochemical IC50 (nM) of INY-03-041 and INY-03-112 and KINOMEscan hits.**

Table S2-2. **Proteomics Output**. From limma processing of MOLT4 cells treated for 4 hr with INY-03-041 vs DMSO control.csv

Chapter 3 Supplemental Data:

Metabolomics Analysis

03_Metabolomics_processing_norm_prot.nb.html *Metabolomics processing code.*

201117_Trial1_Metabolomics_NormProt_withKEGG.csv *Metabolomics raw data T47D 24h Trial 1.*

201202_Trial2_Metabolomics_NormProt_withKEGG.csv *Metabolomics raw data T47D 24h Trial 2.*

201202_Trial3_Metabolomics_NormProt_withKEGG.csv *Metabolomics raw data T47D 24h Trial 3.*

RNA-seq Analysis

00_Setup_and_preprocessing.nb.html *RNA-seq processing code.*

01_Differential_gene_expression_analysis.nb.html *RNA-seq processing code.*

02_GSEA_pathway_analyses.nb.html *RNA-seq processing code.*

Merged_gene_counts.txt *RNA-seq raw data.*

Metadata_EE.csv Metadata for *RNA-seq raw data.*

COSMOS_input

2021-06-02_COSMOS_metabo_t_Degrader_24h.csv *INY-05-040 metabolomics t-values for COSMOS input.*

2021-06-02_COSMOS_metabo_t_Degrader_24h.RData *INY-05-040 metabolomics t-values for COSMOS input.*

2021-06-02_COSMOS_metabo_t_GDC0068_24h.csv *GDC0068 metabolomics t-values for COSMOS input.*

2021-06-02_COSMOS_metabo_t_GDC0068_24h.RData *GDC0068 metabolomics t-values for COSMOS input.*

2021-06-07_COSMOS_TF_t_Degrader_10h.csv *INY-05-040 RNA-seq TF enrichment values for COSMOS input.*

2021-06-07_COSMOS_TF_t_GDC0068_10h.csv *GDC0068 RNA-seq TF enrichment values for COSMOS input.*

2021-06-09_COSMOS_RNA_t_Degrader_10h.csv *INY-05-040 RNA-seq t-values for COSMOS input.*

2021-06-09_COSMOS_RNA_t_Degrader_10h.RData *INY-05-040 RNA-seq t-values for COSMOS input.*

2021-06-09_COSMOS_RNA_t_GDC0068_10h.csv *GDC0068 RNA-seq t-values for COSMOS input.*

2021-06-09_COSMOS_RNA_t_GDC0068_10h.RData *GDC0068 RNA-seq t-values for COSMOS input.*

cosmos_PKN.csv *Prior Knowledge Network.*

COSMOS_scripts

04_Post_COSMOS_processing_DEGRADER.nb.html *Code for INY-05-040 COSMOS processing.*

04_Post_COSMOS_processing_GDC0068.nb.html *Code for GDC0068 COSMOS processing.*

04a_Post_COSMOS_processing_enrichment.nb.html *Code for INY-05-040 COSMOS processing.*

COSMOS_example_2021-07-26_out_degrader.txt *Example code for INY-05-040 COSMOS run.*

COSMOS_example_2021-07-26_out_GDC0068.txt *Example code for GDC0068 COSMOS run.*

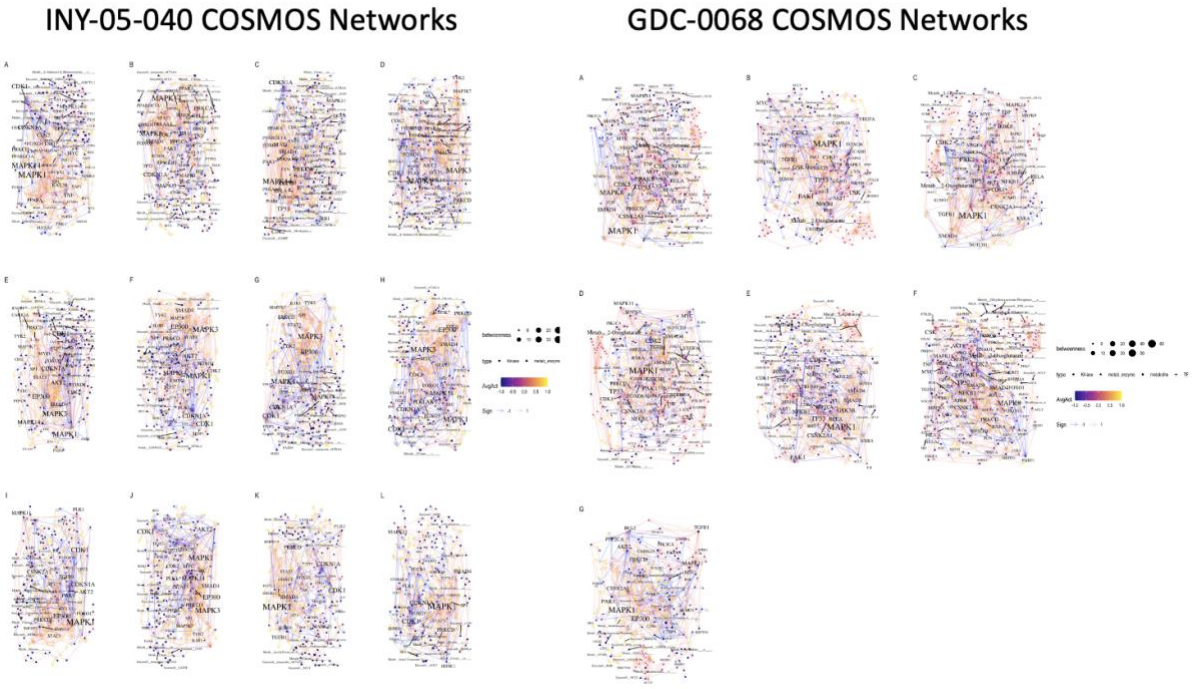

Figure S2-1: COSMOS Networks. (**A**) Networks generated with INY-05-040 vs. DMSO input data. In networks D-J, AKT was specified as inhibited. In Networks K and L AKT was removed as upstream input from prior knowledge networks. (**B**) Networks generated for GDC-0068. In network G, AKT was explicitly specified as inhibited.

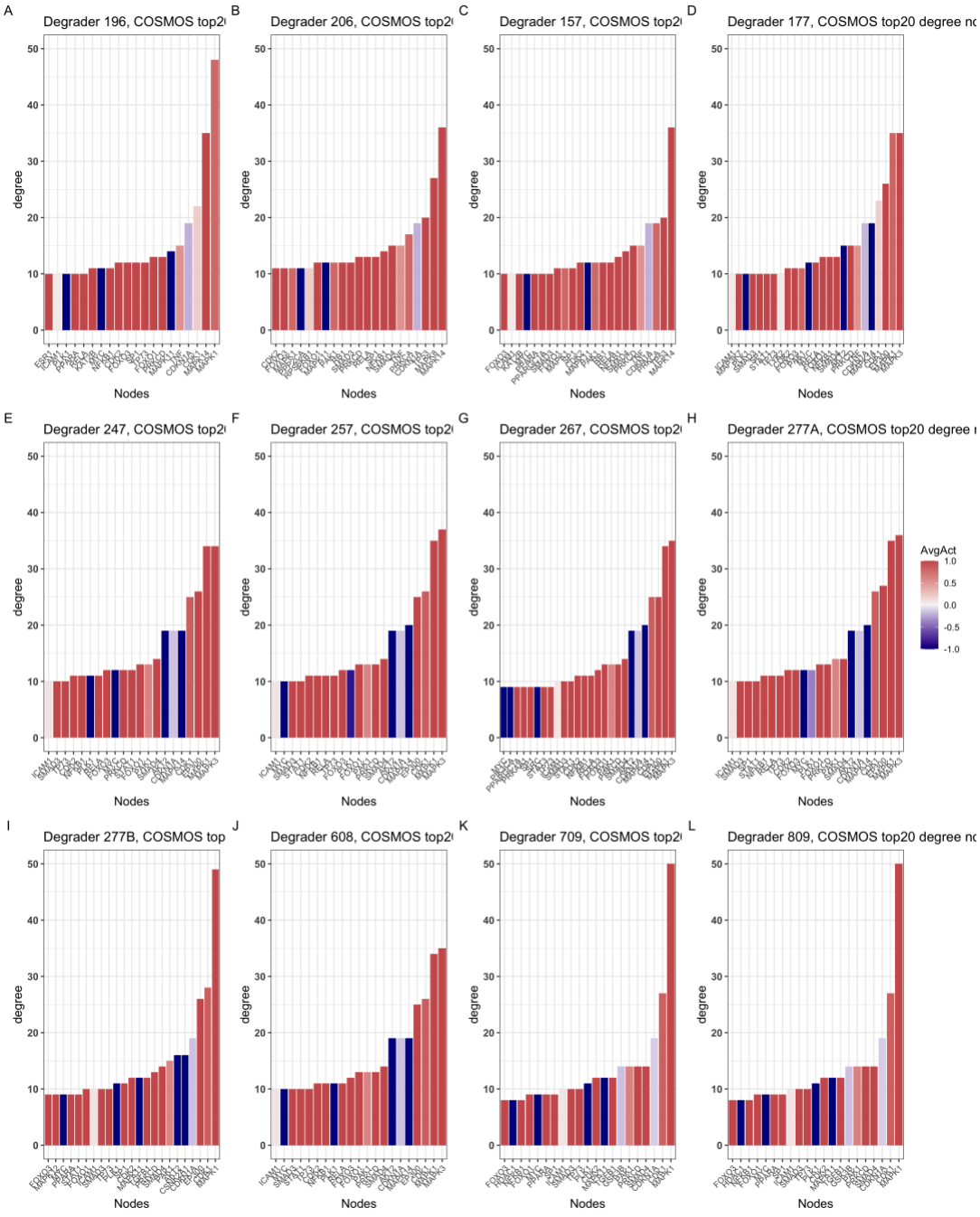

Figure S2-2: Top Degree Nodes from COSMOS Analysis: All COSMOS networks generated for INY-05-040.

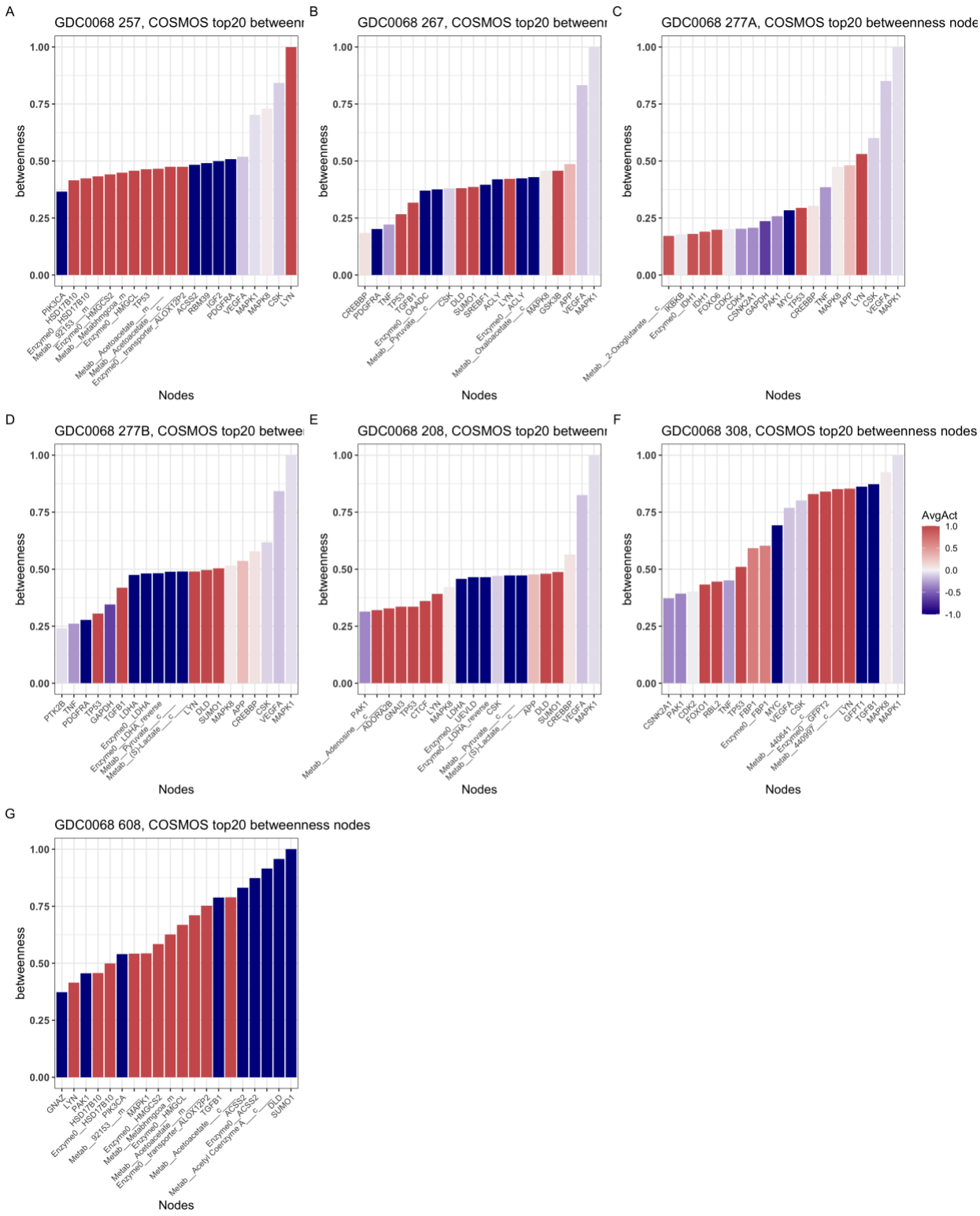

Figure S2-3: Top Degree Nodes from COSMOS Analysis: All COSMOS networks generated for GDC-0068.

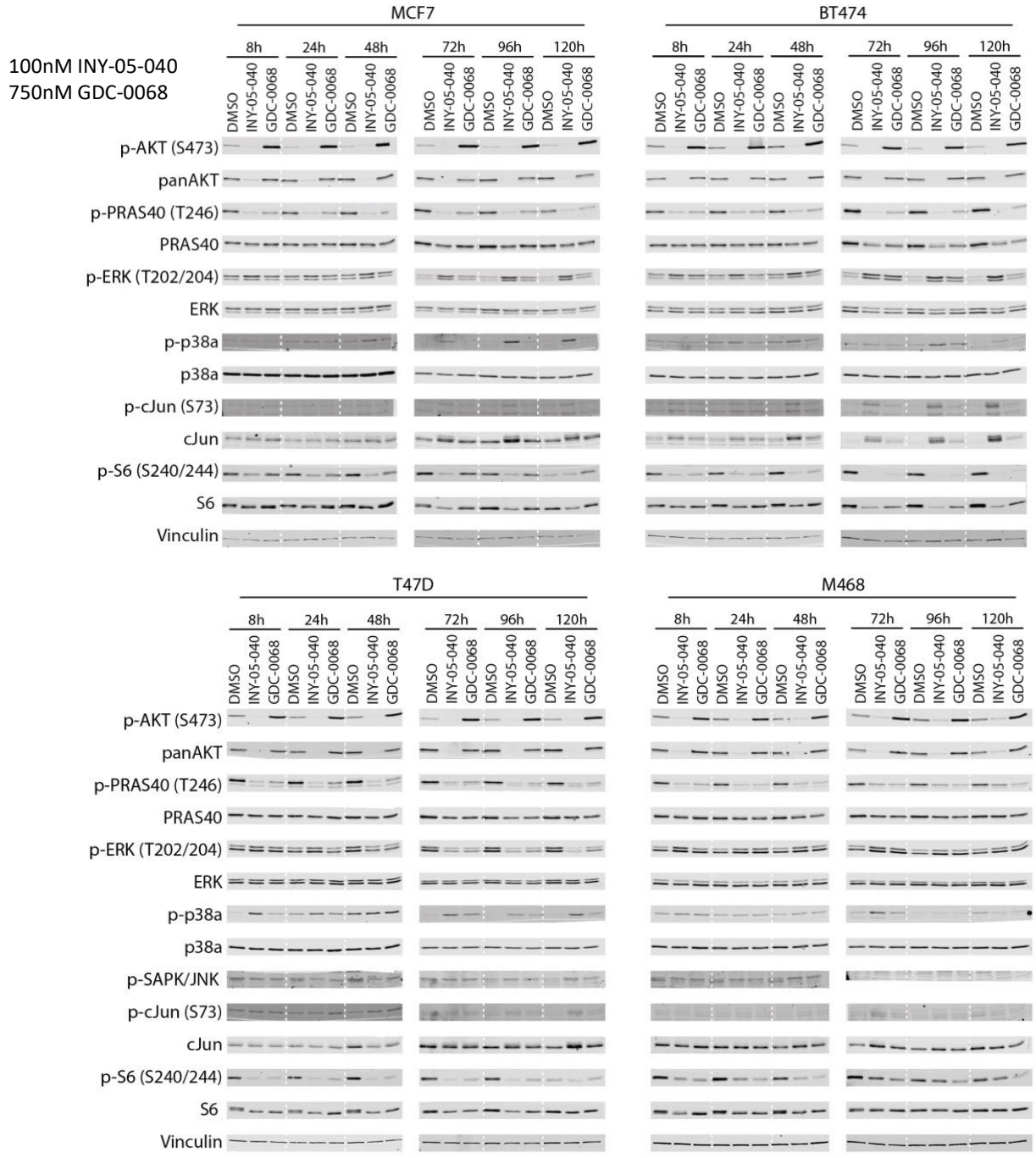

Figure S2-4: Stress Kinase Signaling Validation. Immunoblots of (**A**) MCF7 (B) BT474 (C) T47D (D) MDA-MB-468 cells treated with DMSO, 100nM INY-05-040, or 750nM GDC-0068 for the times indicated.

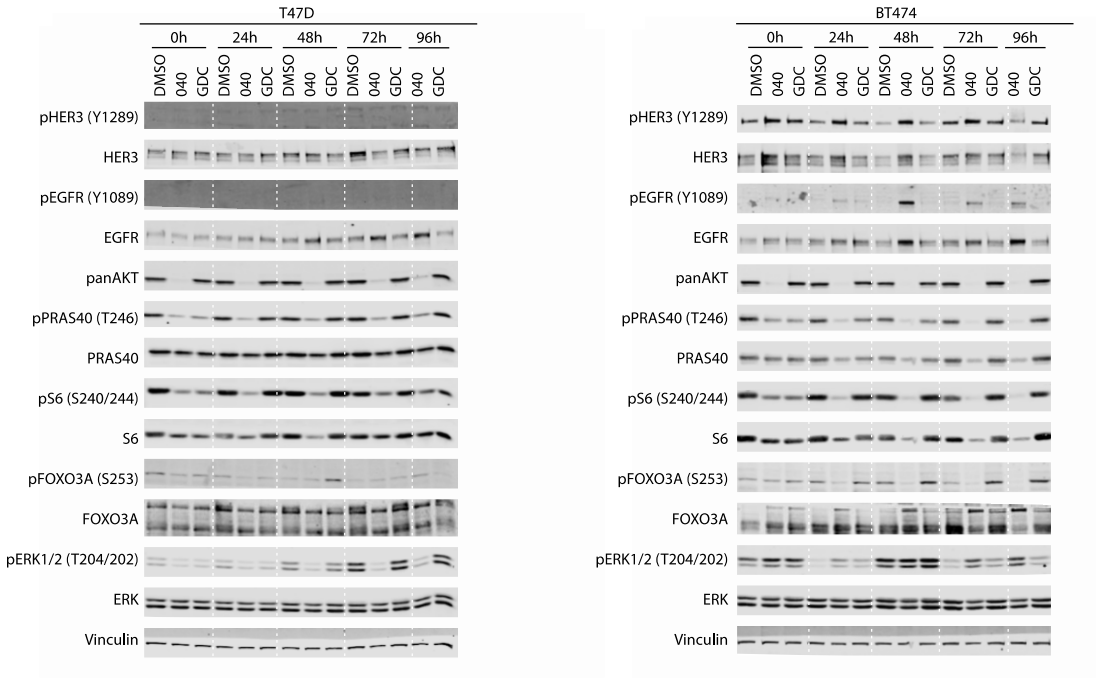

Figure S2-5: RTK induction after INY-05-040 or GDC-0068 treatment. Immunoblots of phospho-HER3 (Y1298), total HER3, phospho-EGFR (Y1098), total EGFR, panAKT, phospho-PRAS40 (T246), total PRAS40, phospho-S6 (S240/244), total S6, phospho-FOXO3A (S253), total FOXO3A, phospho-ERK1/2 (T204/202), total ERK, and Vinculin in (**A**) T47D or (**B**) BT474 cells treated with DMSO, 100nM INY-05-040, or 750nM GDC-0068 for the times indicated.

BIBLIOGRAPHY

1. Manning, B. D. & Toker, A. AKT/PKB Signaling: Navigating the Network. *Cell* **169**, 381–405 (2017).
2. Fruman, D. A. *et al.* The PI3K pathway in human disease Introduction and Historical Context. *Cell* **170**, 605–635 (2017).
3. Sanchez-Vega, F. *et al.* Oncogenic Signaling Pathways in The Cancer Genome Atlas. *Cell* **173**, 321-337.e10 (2018).
4. Yuan, T. L. & Cantley, L. C. PI3K pathway alterations in cancer: Variations on a theme. *Oncogene* **27**, 5497–5510 (2008).
5. Fruman, D. A. *et al.* The PI3K Pathway in Human Disease. *Cell* **170**, 605–635 (2017).
6. Engelman, J. A. Targeting PI3K signalling in cancer: Opportunities, challenges and limitations. *Nature Reviews Cancer* **9**, 550–562 (2009).
7. Engelman, J. A., Luo, J. & Cantley, L. C. The evolution of phosphatidylinositol 3-kinases as regulators of growth and metabolism. **7**, 606–619 (2006).
8. Vanhaesebroeck, B., Stephens, L. & Hawkins, P. PI3K signalling: The path to discovery and understanding. *Nat. Rev. Mol. Cell Biol.* **13**, 195–203 (2012).
9. Fruman, D. A. *et al.* The PI3K Pathway in Human Disease. *Cell* **170**, 605–635 (2017).
10. Cantley, L. C. *et al. The phosphoinositide 3-kinase pathway*. *Science* **296**, 1655–1657 (American Association for the Advancement of Science, 2002).
11. Kofuji, S. *et al.* INPP4B is a Ptdins(3,4,5)P3 phosphatase that can act as a tumor suppressor. *Cancer Discov.* **5**, 730–739 (2015).
12. Liu, H. *et al.* The INPP4B Tumor Suppressor Modulates EGFR Trafficking and Promotes Triple-Negative Breast Cancer. *Cancer Discov.* **10**, 1226–1239 (2020).
13. Czech, M. P. PIP2 and PIP3: complex roles at the cell surface. *Cell* **100**, 603–606 (2000).
14. Lemmon, M. A. Pleckstrin homology (PH) domains and phosphoinositides. *Biochem. Soc. Symp.* **74**, 81–93 (2007).
15. Tessier, M. & Woodgett, J. R. Role of the Phox homology domain and phosphorylation in activation of serum and glucocorticoid-regulated kinase-3. *J. Biol. Chem.* **281**, 23978–23989 (2006).
16. Lien, E. C., Dibble, C. C. & Toker, A. PI3K signaling in cancer: beyond AKT. *Curr. Opin. Cell Biol.* **45**, 62–71 (2017).
17. Wisniewski, D. *et al.* A Novel SH2-Containing Phosphatidylinositol 3,4,5-Trisphosphate 5-Phosphatase (SHIP2) Is Constitutively Tyrosine Phosphorylated and Associated With src Homologous and Collagen Gene (SHC) in Chronic Myelogenous Leukemia Progenitor Cells. *Blood* **93**, 2707–2720 (1999).
18. Gasser, J. A. *et al.* SGK3 Mediates INPP4B-Dependent PI3K Signaling in Breast Cancer. *Mol. Cell* **56**, 595–607 (2014).
19. Castel, P. *et al.* PDK1-SGK1 Signaling Sustains AKT-Independent mTORC1 Activation and Confers Resistance to PI3Kα Inhibition. *Cancer Cell* **30**, 229–242 (2016).
20. Wertheimer, E. *et al.* Rac signaling in breast cancer: A tale of GEFs and GAPs. *Cellular Signalling* **24**, 353–362 (2012).
21. Ebi, H. *et al.* PI3K regulates MEK/ERK signaling in breast cancer via the Rac-GEF, P-Rex1. *Proc. Natl. Acad. Sci.* **110**, 21124–21129 (2013).
22. Sosa, M. S. *et al.* Identification of the Rac-GEF P-Rex1 as an Essential Mediator of ErbB Signaling in Breast Cancer. *Mol. Cell* **40**, 877–892 (2010).
23. Hu, H. *et al.* Phosphoinositide 3-Kinase Regulates Glycolysis through Mobilization of Aldolase from the Actin Cytoskeleton. *Cell* **164**, 433–446 (2016).
24. Horwood, N. J., Urbaniak, A. M. & Danks, L. Tec family kinases in inflammation and disease. *International Reviews of Immunology* **31**, 87–103 (2012).
25. Bradshaw, J. M. The Src, Syk, and Tec family kinases: Distinct types of molecular

switches. *Cellular Signalling* **22**, 1175–1184 (2010).
26. Manning, B. D. & Cantley, L. C. AKT/PKB Signaling: Navigating Downstream. *Cell* **129**, 1261–1274 (2007).
27. Clark, A. R. R. & Toker, A. Signalling specificity in the Akt pathway in breast cancer. *Biochem. Soc. Trans.* **42**, 1349–1355 (2014).
28. Risso, G., Blaustein, M., Pozzi, B., Mammi, P. & Srebrow, A. Akt/PKB: one kinase, many modifications. *Biochem. J.* **468**, 203–214 (2015).
29. Matheny, R. W. & Adamo, M. L. Current Perspectives on Akt Akt-ivation and Akt-ions. *Exp. Biol. Med.* **234**, 1264–1270 (2009).
30. Fortier, A. M., Asselin, E. & Cadrin, M. Functional specificity of Akt isoforms in cancer progression. *Biomol. Concepts* **2**, 1–11 (2011).
31. Pearce, L. R., Komander, D. & Alessi, D. R. The nuts and bolts of AGC protein kinases. *Nat. Rev. Mol. Cell Biol.* **11**, 9–22 (2010).
32. Baffi, T. R. *et al.* TORC2 controls the activity of PKC and Akt by phosphorylating a conserved TOR interaction motif. *Sci. Signal.* **14**, 1–20 (2021).
33. Liu, P. *et al.* Cell-cycle-regulated activation of Akt kinase by phosphorylation at its carboxyl terminus. *Nature* **508**, 541–545 (2014).
34. Sundaresan, N. R. *et al.* The deacetylase SIRT1 promotes membrane localization and activation of Akt and PDK1 during tumorigenesis and cardiac hypertrophy. **4**, (2011).
35. Wang, S. *et al.* Extensive crosstalk between O-GlcNAcylation and phosphorylation regulates Akt signaling. *PLoS One* **7**, e37427 (2012).
36. Guo, J. *et al.* pVHL suppresses kinase activity of Akt in a proline-hydroxylation-dependent manner. *Science (80-.).* **353**, 929–932 (2016).
37. Chan, C.-H. *et al.* Posttranslational regulation of Akt in human cancer. *Cell Biosci.* **4**, 59 (2014).
38. Li, R. *et al.* Akt SUMOylation regulates cell proliferation and tumorigenesis. *Cancer Res.* **73**, 5742–5753 (2013).
39. Ebner, M. *et al.* PI(3,4,5)P3Engagement Restricts Akt Activity to Cellular Membranes. *Mol. Cell* **65**, 416-431.e6 (2017).
40. Chu, N. *et al.* Akt Kinase Activation Mechanisms Revealed Using Protein Semisynthesis. *Cell* **174**, 897-907.e14 (2018).
41. Dummler, B. & Hemmings, B. a. Physiological roles of PKB/Akt isoforms in development and disease. *Biochem. Soc. Trans.* **35**, 231–235 (2007).
42. Fayard, E., Tintignac, L. A., Baudry, A. & Hemmings, B. A. Protein kinase B/Akt at a glance. *J. Cell Sci.* **118**, 5675–5678 (2005).
43. Gonzalez, E. & Mcgraw, T. E. The Akt kinases: Isoform specificity in metabolism and cancer. *Cell Cycle* **8**, 2502–2508 (2009).
44. Yang, Z.-Z. *et al.* Protein Kinase Bα/Akt1 Regulates Placental Development and Fetal Growth. *J. Biol. Chem.* **278**, 32124–32131 (2003).
45. Cho, H. *et al.* Insulin resistance and a diabetes mellitus-like syndrome in mice lacking the protein kinase Akt2 (PKB beta). *Science* **292**, 1728–1731 (2001).
46. Easton, R. M. *et al.* Role for Akt3/Protein Kinase B in Attainment of Normal Brain Size. *Mol. Cell. Biol.* **25**, 1869–1878 (2005).
47. Tschopp, O. *et al.* Essential role of protein kinase Bγ (PKBγ/Akt3) in postnatal brain development but not in glucose homeostasis. *Development* **132**, 2943–2954 (2005).
48. Santi, S. A. & Lee, H. The Akt isoforms are present at distinct subcellular locations. *Am. J. Physiol. Physiol.* **298**, C580–C591 (2010).
49. Gonzalez, E. & Mcgraw, T. E. Insulin-modulated Akt subcellular localization determines Akt isoform-specific signaling. **2009**, (2009).
50. Gonzalez, E. & McGraw, T. E. Insulin-modulated Akt subcellular localization determines Akt isoform-specific signaling. *Proc. Natl. Acad. Sci.* **106**, 7004–7009 (2009).

51. Chin, Y. R. & Toker, A. The Actin-Bundling Protein Palladin Is an Akt1-Specific Substrate that Regulates Breast Cancer Cell Migration. *Mol. Cell* **38**, 333–344 (2010).
52. Wani, R., Tsang, A. W. & Furdui, C. M. Oxidation of Akt2 kinase promotes cell migration and regulates G 1-S transition in the cell cycle. *Cell Cycle* **10**, 3263–3268 (2011).
53. Wani, R. *et al.* Isoform-specific regulation of Akt by PDGF-induced reactive oxygen species. *Proc. Natl. Acad. Sci. U. S. A.* **108**, 10550–10555 (2011).
54. Lee, M. Y. *et al.* Endothelial Akt1 mediates angiogenesis by phosphorylating multiple angiogenic substrates. *Proc. Natl. Acad. Sci.* **111**, 12865–12870 (2014).
55. Gao, D. *et al.* Phosphorylation by Akt1 promotes cytoplasmic localization of Skp2 and impairs APCCdh1-mediated Skp2 destruction. *Nat. Cell Biol. 2009 114* **11**, 397–408 (2009).
56. Lin, H. K. *et al.* Phosphorylation-dependent regulation of cytosolic localization and oncogenic function of Skp2 by Akt/PKB. *Nat. Cell Biol.* **11**, 420–432 (2009).
57. Rössig, L. *et al.* Akt-Dependent Phosphorylation of p21 Cip1 Regulates PCNA Binding and Proliferation of Endothelial Cells. *Mol. Cell. Biol.* **21**, 5644–5657 (2001).
58. Héron-Milhavet, L. *et al.* Only Akt1 Is Required for Proliferation, while Akt2 Promotes Cell Cycle Exit through p21 Binding. *Mol. Cell. Biol.* **26**, 8267–8280 (2006).
59. Ng, Y., Ramm, G., Lopez, J. A. & James, D. E. Rapid Activation of Akt2 Is Sufficient to Stimulate GLUT4 Translocation in 3T3-L1 Adipocytes. *Cell Metab.* **7**, 348–356 (2008).
60. Brognard, J., Sierecki, E., Gao, T. & Newton, A. C. PHLPP and a second isoform, PHLPP2, differentially attenuate the amplitude of Akt signaling by regulating distinct Akt isoforms. *Mol. Cell* **25**, 917–31 (2007).
61. Yoshizaki, T. *et al.* Myosin 5a Is an Insulin-Stimulated Akt2 (Protein Kinase Bβ) Substrate Modulating GLUT4 Vesicle Translocation. *Mol. Cell. Biol.* **27**, 5172–5183 (2007).
62. Cenni, V. *et al.* Ankrd2/ARPP is a novel Akt2 specific substrate and regulates myogenic differentiation upon cellular exposure to H2O2. *Mol. Biol. Cell* **22**, 2946–2956 (2011).
63. Peres, J., Mowla, S. & Prince, S. The T-box transcription factor , TBX3 , is a key substrate of AKT3 in melanomagenesis. **6**, (2014).
64. Irie, H. Y. *et al.* Distinct roles of Akt1 and Akt2 in regulating cell migration and epithelial-mesenchymal transition. *J. Cell Biol.* **171**, 1023–1034 (2005).
65. Chin, Y. R. & Toker, A. Function of Akt/PKB signaling to cell motility, invasion and the tumor stroma in cancer. *Cell. Signal.* **21**, 470–476 (2009).
66. Chin, Y. R. *et al.* Targeting Akt3 signaling in triple-negative breast cancer. *Cancer Res.* **74**, 964–973 (2014).
67. Ackah, E. *et al.* Akt1/protein kinase Bα is critical for ischemic and VEGF-mediated angiogenesis. *J. Clin. Invest.* **115**, 2119–2127 (2005).
68. Yoeli-Lerner, M. & Toker, A. Akt/PKB signaling in cancer: A function in cell motility and invasion. *Cell Cycle* **5**, 603–605 (2006).
69. Saxton, R. A. & Sabatini, D. M. mTOR Signaling in Growth, Metabolism, and Disease. *Cell* **168**, 960–976 (2017).
70. Magnuson, B., Ekim, B. & Fingar, D. C. Regulation and function of ribosomal protein S6 kinase (S6K) within mTOR signalling networks. *Biochem. J* **441**, 1–21 (2012).
71. Dibble, C. C. & Cantley, L. C. Regulation of mTORC1 by PI3K signaling. *Trends Cell Biol.* **25**, 545–555 (2015).
72. Ben-Sahra, I., Hoxhaj, G., Ricoult, S. J. H., Asara, J. M. & Manning, B. D. mTORC1 induces purine synthesis through control of the mitochondrial tetrahydrofolate cycle. *Science (80-.).* **351**, 728–733 (2016).
73. Carracedo, A. *et al.* Inhibition of mTORC1 leads to MAPK pathway activation through a PI3K-dependent feedback loop in human cancer. *J. Clin. Invest.* **118**, 3065–3074 (2008).
74. Huang, S. & Czech, M. P. The GLUT4 Glucose Transporter. *Cell Metabolism* **5**, 237–252 (2007).

75. Hoxhaj, G. & Manning, B. D. The PI3K–AKT network at the interface of oncogenic signalling and cancer metabolism. *Nature Reviews Cancer* **20**, 74–88 (2020).
76. Semenza, G. L. Targeting HIF-1 for cancer therapy. *Nature Reviews Cancer* **3**, 721–732 (2003).
77. Waldhart, A. N. *et al.* Phosphorylation of TXNIP by AKT Mediates Acute Influx of Glucose in Response to Insulin. *Cell Rep.* **19**, 2005–2013 (2017).
78. Roberts, D. J., Tan-Sah, V. P., Ding, E. Y., Smith, J. M. & Miyamoto, S. Hexokinase-II Positively Regulates Glucose Starvation-Induced Autophagy through TORC1 Inhibition. *Mol. Cell* **53**, 521–533 (2014).
79. Düvel, K. *et al.* Activation of a metabolic gene regulatory network downstream of mTOR complex 1. *Mol. Cell* **39**, 171–183 (2010).
80. Porstmann, T. *et al.* SREBP Activity Is Regulated by mTORC1 and Contributes to Akt-Dependent Cell Growth. *Cell Metab.* **8**, 224–236 (2008).
81. Ben-Sahra, I. & Manning, B. D. mTORC1 signaling and the metabolic control of cell growth. *Current Opinion in Cell Biology* **45**, 72–82 (2017).
82. Valvezan, A. J. *et al.* mTORC1 Couples Nucleotide Synthesis to Nucleotide Demand Resulting in a Targetable Metabolic Vulnerability. *Cancer Cell* **32**, 1–15 (2017).
83. Janku, F., Yap, T. A. & Meric-Bernstam, F. *Targeting the PI3K pathway in cancer: Are we making headway? Nature Reviews Clinical Oncology* **15**, 273–291 (Nature Publishing Group, 2018).
84. Mayer, I. A. & Arteaga, C. L. The PI3K/AKT Pathway as a Target for Cancer Treatment. *Annu. Rev. Med.* **67**, 11–28 (2016).
85. Engelman, J. A. Targeting PI3K signalling in cancer: opportunities, challenges and limitations. *Nat. Rev. Cancer* **9**, 550–62 (2009).
86. Lawrence, M. S. *et al.* Discovery and saturation analysis of cancer genes across 21 tumour types. *Nat. 2014 5057484* **505**, 495–501 (2014).
87. Gonzalez-Angulo, A. M. & Blumenschein, G. R. Defining biomarkers to predict sensitivity to PI3K/Akt/mTOR pathway inhibitors in breast cancer. (2012). doi:10.1016/j.ctrv.2012.11.002
88. Lin, J. *et al.* Targeting activated Akt with GDC-0068, a novel selective Akt inhibitor that is efficacious in multiple tumor models. *Clin. Cancer Res.* **19**, 1760–1772 (2013).
89. Weisner, J. *et al.* Preclinical efficacy of covalent-allosteric AKT inhibitor borussertib in combination with trametinib in KRAS-mutant pancreatic and colorectal cancer. *Cancer Res.* **79**, 2367–2378 (2019).
90. Davies, B. R. *et al.* Preclinical pharmacology of AZD5363, an inhibitor of AKT: Pharmacodynamics, antitumor activity, and correlation of monotherapy activity with genetic background. *Mol. Cancer Ther.* **11**, 873–887 (2012).
91. Burke, J. E. Structural Basis for Regulation of Phosphoinositide Kinases and Their Involvement in Human Disease. *Molecular Cell* **71**, 653–673 (2018).
92. Vallejo-Díaz, J., Chagoyen, M., Olazabal-Morán, M., González-García, A. & Carrera, A. C. The Opposing Roles of PIK3R1/p85α and PIK3R2/p85β in Cancer. *Trends in Cancer* **5**, 233–244 (2019).
93. Lindhurst, M. J. *et al.* Mosaic overgrowth with fibroadipose hyperplasia is caused by somatic activating mutations in PIK3CA. *Nat. Genet.* **44**, 928–933 (2012).
94. Podsypanina, K. *et al.* Mutation of Pten/Mmac1 in mice causes neoplasia in multiple organ systems. *Proc. Natl. Acad. Sci. U. S. A.* **96**, 1563–1568 (1999).
95. Trotman, L. C. *et al.* Pten dose dictates cancer progression in the prostate. *PLoS Biol.* **1**, e59 (2003).
96. Wang, S. *et al.* Prostate-specific deletion of the murine Pten tumor suppressor gene leads to metastatic prostate cancer. *Cancer Cell* **4**, 209–221 (2003).
97. Bertucci, M. C. & Mitchell, C. A. Phosphoinositide 3-kinase and INPP4B in human breast

cancer. *Ann. N. Y. Acad. Sci.* **1280**, 1–5 (2013).
98. Grabiner, B. C. *et al.* A diverse array of cancer-associated MTOR mutations are hyperactivating and can predict rapamycin sensitivity. *Cancer Discov.* **4**, 554–563 (2014).
99. Murugan, A. K. mTOR: Role in cancer, metastasis and drug resistance. *Seminars in Cancer Biology* **59**, 92–111 (2019).
100. Wagle, N. *et al.* Activating mTOR mutations in a patient with an extraordinary response on a phase I trial of everolimus and pazopanib. *Cancer Discov.* **4**, 546–553 (2014).
101. Gagliardi, P. A., Puliafito, A. & Primo, L. PDK1: At the crossroad of cancer signaling pathways. *Semin. Cancer Biol.* **48**, 27–35 (2018).
102. Maurer, M. *et al.* 3-Phosphoinositide-dependent kinase 1 potentiates upstream lesions on the phosphatidylinositol 3-kinase pathway in breast carcinoma. *Cancer Res.* **69**, 6299–6306 (2009).
103. Revathidevi, S. & Munirajan, A. K. Akt in cancer: Mediator and more. *Seminars in Cancer Biology* **59**, 80–91 (2019).
104. Kim, M. S., Jeong, E. G., Yoo, N. J. & Lee, S. H. Mutational analysis of oncogenic AKT E17K mutation in common solid cancers and acute leukaemias. *Br. J. Cancer* **98**, 1533–1535 (2008).
105. Lien, E. C. *et al.* Glutathione biosynthesis is a metabolic vulnerability in PI(3)K/Akt-driven breast cancer. *Nat. Cell Biol.* **18**, 572–8 (2016).
106. Davies, M. A. *et al.* A novel AKT3 mutation in melanoma tumours and cell lines. *Br. J. Cancer* **99**, 1265–1268 (2008).
107. Malanga, D. *et al.* Activating E17K mutation in the gene encoding the protein kinase AKT1 in a subset of squamous cell carcinoma of the lung. *Cell Cycle* **7**, 665–669 (2008).
108. Parsons, D. W. *et al.* Colorectal cancer: Mutations in a signalling pathway. *Nature* **436**, 792 (2005).
109. Askham, J. M. *et al.* AKT1 mutations in bladder cancer: Identification of a novel oncogenic mutation that can co-operate with E17K. *Oncogene* **29**, 150–155 (2010).
110. Parikh, C. *et al.* Disruption of PH-kinase domain interactions leads to oncogenic activation of AKT in human cancers. *Proc. Natl. Acad. Sci. U. S. A.* **109**, 19368–19373 (2012).
111. Mundi, P. S., Sachdev, J., McCourt, C. & Kalinsky, K. *AKT in cancer: new molecular insights and advances in drug development*. *British Journal of Clinical Pharmacology* **82**, 943–956 (Blackwell Publishing Ltd, 2016).
112. Altomare, D. A. & Testa, J. R. Perturbations of the AKT signaling pathway in human cancer. *Oncogene* **24**, 7455–7464 (2005).
113. Nakatani, K. *et al.* Up-regulation of Akt3 in estrogen receptor-deficient breast cancers and androgen-independent prostate cancer lines. *J. Biol. Chem.* **274**, 21528–21532 (1999).
114. Turner, K. M. *et al.* Genomically amplified Akt3 activates DNA repair pathway and promotes glioma progression. *Proc. Natl. Acad. Sci.* **112**, 3421–3426 (2015).
115. Rychahou, P. G. *et al.* Akt2 overexpression plays a critical role in the establishment of colorectal cancer metastasis. *Proc. Natl. Acad. Sci. U. S. A.* **105**, 20315–20320 (2008).
116. Hinz, N. & Jücker, M. Distinct functions of AKT isoforms in breast cancer: a comprehensive review. *Cell Commun. Signal.* **17**, 1–29 (2019).
117. Maroulakou, I. G., Oemler, W., Naber, S. P. & Tsichlis, P. N. Akt1 ablation inhibits, whereas Akt2 ablation accelerates, the development of mammary adenocarcinomas in mouse mammary tumor virus (MMTV)-ErbB2/Neu and MMTV-polyoma middle T transgenic mice. *Cancer Res.* **67**, 167–177 (2007).
118. Stottrup, C., Tsang, T. & Chin, Y. R. Upregulation of AKT3 Confers Resistance to the AKT Inhibitor MK2206 in Breast Cancer. *Mol. Cancer Ther.* **15**, 1964–1974 (2016).
119. Castel, P., Toska, E., Engelman, J. A. & Scaltriti, M. The present and future of PI3K inhibitors for cancer therapy. *Nature Cancer* **2**, 587–597 (2021).

120. Rodon, J., Dienstmann, R., Serra, V. & Tabernero, J. Development of PI3K inhibitors: Lessons learned from early clinical trials. *Nature Reviews Clinical Oncology* **10**, 143–153 (2013).
121. Erickson, E. C. & Toker, A. Can Improved Use of Biomarkers Alter the Fate of PI3K Pathway Inhibitors in the Clinic ? *Cancer Res.* 1–5 (2021). doi:10.1158/0008-5472.CAN-21-2035
122. Okkenhaug, K., Graupera, M. & Vanhaesebroeck, B. Targeting PI3K in cancer: Impact on tumor cells, their protective stroma, angiogenesis, and immunotherapy. *Cancer Discov.* **6**, 1090–1105 (2016).
123. Hanker, A. B., Kaklamani, V. & Arteaga, C. L. Challenges for the clinical development of PI3K inhibitors: Strategies to improve their impact in solid tumors. *Cancer Discov.* **9**, 482–491 (2019).
124. Costa, C. *et al.* Measurement of PIP3 levels reveals an unexpected role for p110β in Early adaptive responses to p110α-Specific inhibitors in luminal breast cancer. *Cancer Cell* **27**, 97–108 (2015).
125. Schwartz, S. *et al.* Feedback suppression of PI3Kα signaling in PTEN-mutated tumors is relieved by selective inhibition of PI3Kβ. *Cancer Cell* **27**, 109–122 (2015).
126. Hopkins, B. D. *et al.* Suppression of insulin feedback enhances the efficacy of PI3K inhibitors. *Nature* **560**, 499–503 (2018).
127. Soler, A. *et al.* Inhibition of the p110α isoform of PI 3-kinase stimulates nonfunctional tumor angiogenesis. *J. Exp. Med.* **210**, 1937–1945 (2013).
128. Soler, A., Angulo-Urarte, A. & Graupera, M. PI3K at the crossroads of tumor angiogenesis signaling pathways. *Molecular and Cellular Oncology* **2**, (2015).
129. Kaneda, M. M. *et al.* PI3Kγ is a molecular switch that controls immune suppression. **539**, 437–442 (2016).
130. Davis, R. J. *et al.* Anti-PD-L1 efficacy can be enhanced by inhibition of myeloid-derived suppressor cells with a selective inhibitor of PI3Kd/g. *Cancer Res.* **77**, 2607–2619 (2017).
131. Matasar, M. J. *et al.* Copanlisib plus rituximab versus placebo plus rituximab in patients with relapsed indolent non-Hodgkin lymphoma (CHRONOS-3): a double-blind, randomised, placebo-controlled, phase 3 trial. *Lancet Oncol.* **22**, 678–689 (2021).
132. Baselga, J. *et al.* Phase III study of taselisib (GDC-0032) + fulvestrant (FULV) v FULV in patients (pts) with estrogen receptor (ER)-positive, PIK3CA -mutant (MUT), locally advanced or metastatic breast cancer (MBC): Primary analysis from SANDPIPER. *J. Clin. Oncol.* **36**, LBA1006–LBA1006 (2018).
133. Juric, D. *et al.* Phase I dose-escalation study of taselisib, an oral PI3K inhibitor, in patients with advanced solid tumors. *Cancer Discov.* **7**, 704–715 (2017).
134. Edgar, K. A. *et al.* Isoform-specific phosphoinositide 3-kinase inhibitors exert distinct effects in solid tumors. *Cancer Res.* **70**, 1164–1172 (2010).
135. Jia, S. *et al.* Essential roles of PI(3)K-p110β in cell growth, metabolism and tumorigenesis. *Nature* **454**, 776–779 (2008).
136. Wee, S. *et al.* PTEN-deficient cancers depend on PIK3CB. *Proc. Natl. Acad. Sci. U. S. A.* **105**, 13057–13062 (2008).
137. André, F. *et al.* Alpelisib plus fulvestrant for PIK3CA-mutated, hormone receptor-positive, human epidermal growth factor receptor-2–negative advanced breast cancer: final overall survival results from SOLAR-1. *Ann. Oncol.* **32**, 208–217 (2021).
138. Vanhaesebroeck, B., Perry, M. W. D., Brown, J. R., André, F. & Okkenhaug, K. PI3K inhibitors are finally coming of age. *Nat. Rev. Drug Discov.* **20**, 741–769 (2021).
139. Ellis, H. & Ma, C. X. *PI3K Inhibitors in Breast Cancer Therapy*. *Current Oncology Reports* **21**, 1–9 (Springer, 2019).
140. Song, M., Bode, A. M., Dong, Z. & Lee, M.-H. H. AKt as a therapeutic target for cancer. *Cancer Res.* **79**, 1019–1031 (2019).

141. Shi, Z. *et al.* Functional Mapping of AKT Signaling and Biomarkers of Response From the FAIRLANE Trial of Neoadjuvant Ipatasertib Plus Paclitaxel for Triple-Negative Breast Cancer. *Clin. Cancer Res.* clincanres.2498.2021 (2021). doi:10.1158/1078-0432.ccr-21-2498
142. Arencibia, J. M., Pastor-Flores, D., Bauer, A. F., Schulze, J. O. & Biondi, R. M. *AGC protein kinases: From structural mechanism of regulation to allosteric drug development for the treatment of human diseases*. *Biochimica et Biophysica Acta - Proteins and Proteomics* **1834**, 1302–1321 (Elsevier, 2013).
143. N. Turner1, R. Dent2, J. O'Shaughnessy3, S. Kim4, S. Isakoff5, C.H. Barrios6, S. Saji7, I. Bondarenko8, Z. Nowecki9, Q. Lian10, S. Reilly11, H. Hinton12, M. Wongchenko13, A. Mani14, M. Oliveira15N. Turner1, R. Dent2, J. O'Shaughnessy3, S. Kim4, S. Isakoff, M. O. Ipatasertib (IPAT) + paclitaxel (PAC) for PIK3CA/AKT1/PTEN-altered hormone receptor-positive (HR+) HER2-negative advanced breast cancer (aBC): Prim... | OncologyPRO. *Annals of Oncology (2020) 31 (suppl_4): S348-S395. 10.1016/annonc/annonc268* Available at: https://oncologypro.esmo.org/meeting-resources/esmo-virtual-congress-2020/ipatasertib-ipat-paclitaxel-pac-for-pik3ca-akt1-pten-altered-hormone-receptor-positive-hr-her2-negative-advanced-breast-cancer-abc-prim. (Accessed: 14th January 2022)
144. Jones, R. H. *et al.* Fulvestrant plus capivasertib versus placebo after relapse or progression on an aromatase inhibitor in metastatic, oestrogen receptor-positive breast cancer (FAKTION): a multicentre, randomised, controlled, phase 2 trial. *Lancet Oncol.* **21**, 345–357 (2020).
145. Schmid, P. *et al.* AZD5363 plus paclitaxel versus placebo plus paclitaxel as first-line therapy for metastatic triple-negative breast cancer (PAKT): A randomised, double-blind, placebo-controlled, phase II trial. *J. Clin. Oncol.* **36**, 1007–1007 (2018).
146. Vivanco, I. *et al.* A kinase-independent function of AKT promotes cancer cell survival. *Elife* **3**, (2014).
147. Wu, W.-I. I. *et al.* Crystal structure of human AKT1 with an allosteric inhibitor reveals a new mode of kinase inhibition. *PLoS One* **5**, e12913 (2010).
148. Yap, T. A. *et al.* First-in-man clinical trial of the oral pan-AKT inhibitor MK-206 in patients with advanced solid tumors. *J. Clin. Oncol.* **29**, 4688–4695 (2011).
149. Yu, Y. *et al.* Targeting AKT1-E17K and the PI3K/AKT Pathway with an Allosteric AKT Inhibitor, ARQ 092. *PLoS One* **10**, e0140479 (2015).
150. Quambusch, L. *et al.* Covalent-Allosteric Inhibitors to Achieve Akt Isoform-Selectivity. *Angew. Chemie - Int. Ed.* **58**, 18823–18829 (2019).
151. Hudes, G. *et al.* Temsirolimus, Interferon Alfa, or Both for Advanced Renal-Cell Carcinoma. *N. Engl. J. Med.* **356**, 2271–2281 (2007).
152. Motzer, R. J. *et al.* Efficacy of everolimus in advanced renal cell carcinoma: a double-blind, randomised, placebo-controlled phase III trial. *Lancet* **372**, 449–456 (2008).
153. Ilagan, E. & Manning, B. D. Emerging Role of mTOR in the Response to Cancer Therapeutics. *Trends in Cancer* **2**, 241–251 (2016).
154. Janku, F. Phosphoinositide 3-kinase (PI3K) pathway inhibitors in solid tumors: From laboratory to patients. *Cancer Treatment Reviews* (2017). doi:10.1016/j.ctrv.2017.07.005
155. Barile, E., De, S. K. & Pellecchia, M. PDK1 inhibitors. *Pharmaceutical patent analyst* **1**, 145–163 (2012).
156. Yang, C. *et al.* PDK1 inhibitor GSK2334470 exerts antitumor activity in multiple myeloma and forms a novel multitargeted combination with dual mTORC1/C2 inhibitor PP242. *Oncotarget* **8**, 39185–39197 (2017).
157. Chandarlapaty, S. *et al.* AKT inhibition relieves feedback suppression of receptor tyrosine kinase expression and activity. *Cancer Cell* **19**, 58–71 (2011).
158. Chandarlapaty, S. *et al.* AKT inhibition relieves feedback suppression of receptor tyrosine

kinase expression and activity. *Cancer Cell* **19**, 58–71 (2011).
159. Muranen, T. *et al.* Inhibition of PI3K/mTOR Leads to Adaptive Resistance in Matrix-Attached Cancer Cells. *Cancer Cell* **21**, 227–239 (2012).
160. Chakrabarty, A., Sánchez, V., Kuba, M. G., Rinehart, C. & Arteaga, C. L. Feedback upregulation of HER3 (ErbB3) expression and activity attenuates antitumor effect of PI3K inhibitors. *Proc. Natl. Acad. Sci. U. S. A.* **109**, 2718–2723 (2012).
161. O'Reilly, K. E. *et al.* mTOR inhibition induces upstream receptor tyrosine kinase signaling and activates Akt. *Cancer Res.* **66**, 1500–1508 (2006).
162. Elkabets, M. *et al.* MTORC1 inhibition is required for sensitivity to PI3K p110α inhibitors in PIK3CA-mutant breast cancer. *Sci. Transl. Med.* **5**, (2013).
163. Le, X. *et al.* Systematic functional characterization of resistance to PI3K inhibition in breast cancer. *Cancer Discov.* **6**, 1134–1147 (2016).
164. Stretton, C. *et al.* GSK3-mediated raptor phosphorylation supports amino-acid-dependent mTORC1-directed signalling. *Biochem. J.* **470**, 207–221 (2015).
165. Evangelisti, C., Chiarini, F., Paganelli, F., Marmiroli, S. & Martelli, A. M. Crosstalks of GSK3 signaling with the mTOR network and effects on targeted therapy of cancer. *Biochimica et Biophysica Acta - Molecular Cell Research* **1867**, 118635 (2020).
166. Ilic, N., Utermark, T., Widlund, H. R. & Roberts, T. M. PI3K-targeted therapy can be evaded by gene amplification along the MYC-eukaryotic translation initiation factor 4E (eIF4E) axis. *Proc. Natl. Acad. Sci. U. S. A.* **108**, (2011).
167. Chang, D. Y., Ma, W. L. & Lu, Y. S. Role of alpelisib in the treatment of pik3ca-mutated breast cancer: Patient selection and clinical perspectives. *Ther. Clin. Risk Manag.* **17**, 193–207 (2021).
168. Brandão, M., Caparica, R., Eiger, D. & de Azambuja, E. Biomarkers of response and resistance to PI3K inhibitors in estrogen receptor-positive breast cancer patients and combination therapies involving PI3K inhibitors. *Ann. Oncol. Off. J. Eur. Soc. Med. Oncol.* **30**, x27–x42 (2019).
169. LoRusso, P. M. Inhibition of the PI3K/AKT/mTOR pathway in solid tumors. *J. Clin. Oncol.* **34**, 3803–3815 (2016).
170. Mayer, I. A. *et al.* Stand up to cancer phase Ib study of pan-phosphoinositide-3-kinase inhibitor buparlisib with letrozole in estrogen receptor-positive/human epidermal growth factor receptor 2-negative metastatic breast cancer. *J. Clin. Oncol.* **32**, 1202–1209 (2014).
171. Ros, S. *et al.* Metabolic Imaging Detects Resistance to PI3Kα Inhibition Mediated by Persistent FOXM1 Expression in ER+ Breast Cancer. *Cancer Cell* **38**, 516-533.e9 (2020).
172. Josephs, D. H. & Sarker, D. Pharmacodynamic biomarker development for PI3K pathway therapeutics. *Transl. Oncogenomics* **7**, 33–49 (2016).
173. Guillou, H., Stephens, L. R. & Hawkins, P. T. Quantitative Measurement of Phosphatidylinositol 3,4,5-trisphosphate. *Methods in Enzymology* **434**, 117–130 (2007).
174. Josephs, D. H. & Sarker, D. Pharmacodynamic biomarker development for PI3K pathway therapeutics. *Translational Oncogenomics* **7**, 33–49 (2016).
175. Li, A. *et al.* Characterizing advanced breast cancer heterogeneity and treatment resistance through serial biopsies and comprehensive analytics. *npj Precis. Oncol.* **5**, 1–12 (2021).
176. An, S. & Fu, L. Small-molecule PROTACs: An emerging and promising approach for the development of targeted therapy drugs. *EBioMedicine* **36**, 553–562 (2018).
177. Fauvel, B. & Yasri, A. Antibodies directed against receptor tyrosine kinases: Current and future strategies to fight cancer. *mAbs* **6**, 838–851 (2014).
178. McDonnell, D. P., Wardell, S. E. & Norris, J. D. Oral Selective Estrogen Receptor Downregulators (SERDs), a Breakthrough Endocrine Therapy for Breast Cancer. *Journal of Medicinal Chemistry* **58**, 4883–4887 (2015).

179. Sakamoto, K. M. *et al.* Protacs: Chimeric molecules that target proteins to the Skp1-Cullin-F box complex for ubiquitination and degradation. *Proc. Natl. Acad. Sci. U. S. A.* **98**, 8554–8559 (2001).
180. Wu, T. *et al.* Targeted protein degradation as a powerful research tool in basic biology and drug target discovery. *Nat. Struct. Mol. Biol.* **27**, 605–614 (2020).
181. Clift, D. *et al.* A Method for the Acute and Rapid Degradation of Endogenous Proteins. *Cell* **171**, 1692-1706.e18 (2017).
182. Burslem, G. M. *et al.* The Advantages of Targeted Protein Degradation Over Inhibition: An RTK Case Study. *Cell Chem. Biol.* **25**, 67–77 (2018).
183. Li, W. *et al.* Phthalimide conjugations for the degradation of oncogenic PI3K. *Eur. J. Med. Chem.* **151**, 237–247 (2018).
184. Burslem, G. M., Song, J., Chen, X., Hines, J. & Crews, C. M. Enhancing Antiproliferative Activity and Selectivity of a FLT-3 Inhibitor by Proteolysis Targeting Chimera Conversion. *J. Am. Chem. Soc.* **140**, 16428–16432 (2018).
185. Salami, J. *et al.* Androgen receptor degradation by the proteolysis-targeting chimera ARCC-4 outperforms enzalutamide in cellular models of prostate cancer drug resistance. *Commun. Biol.* **1**, 1–9 (2018).
186. Bondeson, D. P. *et al.* Catalytic in vivo protein knockdown by small-molecule PROTACs. *Nat. Chem. Biol.* **11**, 611–617 (2015).
187. Krönke, J. *et al.* Lenalidomide induces ubiquitination and degradation of CK1α in del(5q) MDS HHS Public Access. *Nature* **523**, 183–188 (2015).
188. Yang, K. *et al.* Development of the first small molecule histone deacetylase 6 (HDAC6) degraders. *Bioorganic Med. Chem. Lett.* **28**, 2493–2497 (2018).
189. Bassi, Z. I. *et al.* Modulating PCAF/GCN5 Immune Cell Function through a PROTAC Approach. *ACS Chem. Biol.* **13**, 2862–2867 (2018).
190. Komander, D. & Rape, M. The ubiquitin code. *Annu. Rev. Biochem.* **81**, 203–229 (2012).
191. Toma-Fukai, S. & Shimizu, T. Structural Diversity of Ubiquitin E3 Ligase. *Molecules* **26**, 6682 (2021).
192. Deshaies, R. J. & Joazeiro, C. A. P. RING domain E3 ubiquitin ligases. *Annual Review of Biochemistry* **78**, 399–434 (2009).
193. Burslem, G. M. & Crews, C. M. Proteolysis-Targeting Chimeras as Therapeutics and Tools for Biological Discovery. *Cell* **181**, 102–114 (2020).
194. Wang, Y., Jiang, X., Feng, F., Liu, W. & Sun, H. Degradation of proteins by PROTACs and other strategies. *Acta Pharm. Sin. B* **10**, 207–238 (2020).
195. Winter, G. E. *et al.* Phthalimide conjugation as a strategy for in vivo target protein degradation. *Science (80-.).* **348**, 1376–1381 (2015).
196. Olson, C. M. *et al.* Pharmacological perturbation of CDK9 using selective CDK9 inhibition or degradation. *Nat. Chem. Biol.* **14**, 163–170 (2018).
197. Noblejas-López, M. D. M. *et al.* Activity of BET-proteolysis targeting chimeric (PROTAC) compounds in triple negative breast cancer. *J. Exp. Clin. Cancer Res.* **38**, 1–9 (2019).
198. Burslem, G. M., Song, J., Chen, X., Hines, J. & Crews, C. M. Enhancing Antiproliferative Activity and Selectivity of a FLT-3 Inhibitor by Proteolysis Targeting Chimera Conversion. *J. Am. Chem. Soc.* **140**, 16428–16432 (2018).
199. Huang, H.-T. T. *et al.* A Chemoproteomic Approach to Query the Degradable Kinome Using a Multi-kinase Degrader. *Cell Chem. Biol.* **25**, 88-99.e6 (2018).
200. Zhang, C. *et al.* Proteolysis Targeting Chimeras (PROTACs) of Anaplastic Lymphoma Kinase (ALK). *Eur. J. Med. Chem.* **151**, 304–314 (2018).
201. Chen, H., Chen, F., Liu, N., Wang, X. & Gou, S. Chemically induced degradation of CK2 by proteolysis targeting chimeras based on a ubiquitin–proteasome pathway. *Bioorg. Chem.* **81**, 536–544 (2018).
202. McCoull, W. *et al.* Development of a Novel B-Cell Lymphoma 6 (BCL6) PROTAC to

Provide Insight into Small Molecule Targeting of BCL6. *ACS Chem. Biol.* **13**, 3131–3141 (2018).
203. Li, Y. *et al.* Discovery of MD-224 as a First-in-Class, Highly Potent, and Efficacious Proteolysis Targeting Chimera Murine Double Minute 2 Degrader Capable of Achieving Complete and Durable Tumor Regression. *J. Med. Chem.* **62**, 448–466 (2019).
204. Zengerle, M., Chan, K. H. & Ciulli, A. Selective Small Molecule Induced Degradation of the BET Bromodomain Protein BRD4. *ACS Chem. Biol.* **10**, 1770–1777 (2015).
205. Gadd, M. S. *et al.* Structural basis of PROTAC cooperative recognition for selective protein degradation. *Nat. Chem. Biol.* **13**, 514–521 (2017).
206. Lai, A. C. *et al.* Modular PROTAC Design for the Degradation of Oncogenic BCR-ABL. *Angew. Chem. Int. Ed. Engl.* **55**, 807–10 (2016).
207. Burslem, G. M. *et al.* The Advantages of Targeted Protein Degradation Over Inhibition: An RTK Case Study (with supplementery information). *Cell Chem. Biol.* **25**, 67-77.e3 (2018).
208. Gechijian, L. N. *et al.* Functional TRIM24 degrader via conjugation of ineffectual bromodomain and VHL ligands article. *Nat. Chem. Biol.* **14**, 405–412 (2018).
209. Cromm, P. M., Samarasinghe, K. T. G., Hines, J. & Crews, C. M. Addressing Kinase-Independent Functions of Fak via PROTAC-Mediated Degradation. *J. Am. Chem. Soc.* **140**, 17019–17026 (2018).
210. Smith, B. E. *et al.* Differential PROTAC substrate specificity dictated by orientation of recruited E3 ligase. *Nat. Commun.* **10**, 1–13 (2019).
211. Schapira, M., Calabrese, M. F., Bullock, A. N. & Crews, C. M. Targeted protein degradation: expanding the toolbox. *Nat. Rev. Drug Discov.* **18**, 949–963 (2019).
212. Paiva, S.-L. L. & Crews, C. M. Targeted protein degradation: elements of PROTAC design. *Curr. Opin. Chem. Biol.* **50**, 111–119 (2019).
213. You, I. *et al.* Discovery of an AKT Degrader with Prolonged Inhibition of Downstream Signaling Cell Chemical Biology Brief Communication Discovery of an AKT Degrader with Prolonged Inhibition of Downstream Signaling. *Cell Chem. Biol.* **27**, 1–8 (2020).
214. Yu, X. *et al.* Design, Synthesis, and Evaluation of Potent, Selective, and Bioavailable AKT Kinase Degraders. *J. Med. Chem.* **64**, 18054–18081 (2021).
215. Xu, J. *et al.* AKT degradation selectively inhibits the growth of PI3K/PTEN pathway mutant cancers with wild-type KRAS and BRAF by destabilizing Aurora kinase B. *Cancer Discov.* candisc.0815.2020 (2021). doi:10.1158/2159-8290.cd-20-0815
216. Zhang, X., Crowley, V. M., Wucherpfennig, T. G., Dix, M. M. & Cravatt, B. F. Electrophilic PROTACs that degrade nuclear proteins by engaging DCAF16. *Nat. Chem. Biol.* **15**, 737–746 (2019).
217. Bondeson, D. P. *et al.* Catalytic in vivo protein knockdown by small-molecule PROTACs. *Nat. Chem. Biol.* **11**, 611–617 (2015).
218. Dobrovolsky, D. *et al.* Bruton tyrosine kinase degradation as a therapeutic strategy for cancer. *Blood* **133**, 952–961 (2018).
219. Krönke, J. *et al.* Lenalidomide causes selective degradation of IKZF1 and IKZF3 in multiple myeloma cells. *Science (80-.).* **343**, 301–305 (2014).
220. Popow, J. *et al.* Highly Selective PTK2 Proteolysis Targeting Chimeras to Probe Focal Adhesion Kinase Scaffolding Functions. *J. Med. Chem.* **62**, 2508–2520 (2019).
221. Powell, C. E. *et al.* Chemically Induced Degradation of Anaplastic Lymphoma Kinase (ALK). *J. Med. Chem.* **61**, 4249–4255 (2018).
222. Toker, A. Achieving specificity in Akt signaling in cancer. *Advances in Biological Regulation* **52**, 78–87 (2012).
223. Hennessy, B. T., Smith, D. L., Ram, P. T., Lu, Y. & Mills, G. B. Exploiting the PI3K/AKT pathway for cancer drug discovery. *Nat Rev Drug Discov* **4**, 988–1004 (2005).
224. Cantley, L. C. & Neel, B. G. *New insights into tumor suppression: PTEN suppresses*

tumor formation by restraining the phosphoinositide 3-kinase/AKT pathway. *Proceedings of the National Academy of Sciences of the United States of America* **96**, 4240–4245 (1999).
225. Shayesteh, L. *et al. PIK3CA is implicated as an oncogene in ovarian cancer*. (1999).
226. Brown, J. S. & Banerji, U. Maximising the potential of AKT inhibitors as anti-cancer treatments. *Pharmacol. Ther.* **172**, 101–115 (2017).
227. Oliveira, M. *et al.* FAIRLANE, a double-blind placebo-controlled randomized phase II trial of neoadjuvant ipatasertib plus paclitaxel for early triple-negative breast cancer. *Ann. Oncol.* **30**, 1289–1297 (2019).
228. Turner, N. C. *et al.* BEECH: a dose-finding run-in followed by a randomised phase II study assessing the efficacy of AKT inhibitor capivasertib (AZD5363) combined with paclitaxel in patients with estrogen receptor-positive advanced or metastatic breast cancer, and in a PIK3CA . *Ann. Oncol. Off. J. Eur. Soc. Med. Oncol.* **30**, 774–780 (2019).
229. Lin, A. *et al.* Off-target toxicity is a common mechanism of action of cancer drugs undergoing clinical trials. *Sci. Transl. Med.* **11**, 8412 (2019).
230. Do, K. *et al.* Biomarker-driven phase 2 study of MK-2206 and selumetinib (AZD6244, ARRY-142886) in patients with colorectal cancer. *Invest. New Drugs* **33**, 720–728 (2015).
231. Keppler-Noreuil, K. M. *et al.* Pharmacodynamic Study of Miransertib in Individuals with Proteus Syndrome. *Am. J. Hum. Genet.* **104**, 484–491 (2019).
232. Uhlenbrock, N. *et al.* Structural and chemical insights into the covalent-allosteric inhibition of the protein kinase Akt †. (2019). doi:10.1039/c8sc05212c
233. Brown, K. K. & Toker, A. The phosphoinositide 3-kinase pathway and therapy resistance in cancer. *F1000Prime Rep.* **7**, (2015).
234. Yang, J. *et al.* Targeting PI3K in cancer: Mechanisms and advances in clinical trials 06 Biological Sciences 0601 Biochemistry and Cell Biology. *Molecular Cancer* **18**, (2019).
235. Park, S., Kim, Y. S., Kim, D. Y., So, I. & Jeon, J. H. PI3K pathway in prostate cancer: All resistant roads lead to PI3K. *Biochimica et Biophysica Acta - Reviews on Cancer* **1870**, 198–206 (2018).
236. Chamberlain, P. P. & Hamann, L. G. Development of targeted protein degradation therapeutics. *Nat. Chem. Biol.* **15**, 937–944 (2019).
237. Churcher, I. Protac-Induced Protein Degradation in Drug Discovery: Breaking the Rules or Just Making New Ones? *J. Med. Chem.* **61**, 444–452 (2018).
238. Basso, A. D. *et al.* Akt forms an intracellular complex with heat shock protein 90 (Hsp90) and Cdc37 and is destabilized by inhibitors of Hsp90 function. *J. Biol. Chem.* **277**, 39858–39866 (2002).
239. You, I. *et al.* Discovery of an AKT Degrader with Prolonged Inhibition of Downstream Signaling. *Cell Chem. Biol.* **27**, 66-73.e7 (2020).
240. Blake, J. F. *et al.* Discovery and preclinical pharmacology of a selective ATP-competitive Akt inhibitor (GDC-0068) for the treatment of human tumors. *J. Med. Chem.* **55**, 8110–8127 (2012).
241. Brand, M. *et al.* Homolog-Selective Degradation as a Strategy to Probe the Function of CDK6 in AML. *Cell Chem. Biol.* **26**, 300-306.e9 (2018).
242. Soucy, T. A., Smith, P. G. & Rolfe, M. Targeting NEDD8-activated cullin-RING ligases for the treatment of cancer. *Clinical Cancer Research* **15**, 3912–3916 (2009).
243. Hafner, M. *et al.* Quantification of sensitivity and resistance of breast cancer cell lines to anti-cancer drugs using GR metrics. *Sci. Data* **4**, 1–9 (2017).
244. Cross, D. A. E., Alessi, D. R., Cohen, P., Andjelkovich, M. & Hemmings, B. A. Inhibition of glycogen synthase kinase-3 by insulin mediated by protein kinase B. *Nature* **378**, 785–789 (1995).
245. Wang, H. *et al.* Proline-rich Akt substrate of 40kDa (PRAS40): A novel downstream target of PI3k/Akt signaling pathway. *Cellular Signalling* **24**, 17–24 (2012).

246. Lin, J. *et al.* Targeting activated Akt with GDC-0068, a novel selective Akt inhibitor that is efficacious in multiple tumor models. *Clin. Cancer Res.* **19**, 1760–1772 (2013).
247. Farnaby, W. *et al.* BAF complex vulnerabilities in cancer demonstrated via structure-based PROTAC design. *Nat. Chem. Biol.* **15**, 672–680 (2019).
248. Silva, M. C. *et al.* Targeted degradation of aberrant tau in frontotemporal dementia patient-derived neuronal cell models. *Elife* **8**, (2019).
249. Nowak, R. P. *et al.* Plasticity in binding confers selectivity in ligand-induced protein degradation article. *Nat. Chem. Biol.* **14**, 706–714 (2018).
250. Jansen, V. M., Mayer, I. A. & Arteaga, C. L. Is There a Future for AKT Inhibitors in the Treatment of Cancer? *Clin. Cancer Res.* **22**, 2599–601 (2016).
251. Stottrup, C., Tsang, T. & Chin, Y. R. Upregulation of AKT3 Confers Resistance to the AKT Inhibitor MK2206 in Breast Cancer. *Mol. Cancer Ther.* **15**, 1964–1974 (2016).
252. Cai, J., Cai, L. Q., Hong, Y. & Zhu, Y. S. Functional characterisation of a natural androgen receptor missense mutation (N771H) causing human androgen insensitivity syndrome. *Andrologia* **44**, 523–529 (2012).
253. Han, X. *et al.* Discovery of ARD-69 as a Highly Potent Proteolysis Targeting Chimera (PROTAC) Degrader of Androgen Receptor (AR) for the Treatment of Prostate Cancer. *J. Med. Chem.* **62**, 941–964 (2019).
254. Degtyarev, M. *et al.* Akt inhibition promotes autophagy and sensitizes PTEN-null tumors to lysosomotropic agents. *J. Cell Biol.* **183**, 101–116 (2008).
255. Koseoglu, S., Lu, Z., Kumar, C., Kirschmeier, P. & Zou, J. AKT1, AKT2 and AKT3-dependent cell survival is cell line-specific and knockdown of all three isoforms selectively induces apoptosis in 20 human tumor cell lines. *Cancer Biol. Ther.* **6**, 755–762 (2007).
256. Guerrero-Zotano, A., Mayer, I. A. & Arteaga, C. L. PI3K/AKT/mTOR: role in breast cancer progression, drug resistance, and treatment. *Cancer Metastasis Rev.* **35**, 515–524 (2016).
257. Turner, K. M. *et al.* Genomically amplified Akt3 activates DNA repair pathway and promotes glioma progression. *Proc. Natl. Acad. Sci.* **112**, 3421–3426 (2015).
258. Hyman, D. M. *et al.* AKT inhibition in solid tumors with AKT1 mutations. *J. Clin. Oncol.* **35**, 2251–2259 (2017).
259. Nitulescu, G. M. *et al.* Akt inhibitors in cancer treatment: The long journey from drug discovery to clinical use (Review). *Int. J. Oncol.* **48**, 869–885 (2016).
260. Huck, B. R. & Mochalkin, I. Recent progress towards clinically relevant ATP-competitive Akt inhibitors. *Bioorganic and Medicinal Chemistry Letters* **27**, 2838–2848 (2017).
261. Jansen, V. M., Mayer, I. A. & Arteaga, C. L. Is there a future for AKT inhibitors in the treatment of cancer? *Clin. Cancer Res.* **22**, 2599–2601 (2016).
262. Nalawansha, D. A. & Crews, C. M. PROTACs: An Emerging Therapeutic Modality in Precision Medicine. *Cell Chem. Biol.* **27**, 998–1014 (2020).
263. Konstantinidou, M. *et al.* PROTACs– a game-changing technology. *Expert Opin. Drug Discov.* **14**, 1–14 (2019).
264. Cromm, P. M. & Crews, C. M. Targeted Protein Degradation: from Chemical Biology to Drug Discovery. *Cell Chem. Biol.* **24**, 1181–1190 (2017).
265. Zmajkovicova, K. *et al.* MEK1 Is Required for PTEN Membrane Recruitment, AKT Regulation, and the Maintenance of Peripheral Tolerance. *Mol. Cell* **50**, 43–55 (2013).
266. Dugourd, A. *et al.* Causal integration of multi-omics data with prior knowledge to generate mechanistic hypotheses. *Mol. Syst. Biol.* **17**, 1–17 (2021).
267. Bricelj, A., Steinebach, C., Kuchta, R., Gütschow, M. & Sosič, I. E3 Ligase Ligands in Successful PROTACs: An Overview of Syntheses and Linker Attachment Points. *Front. Chem.* **9**, 1–46 (2021).
268. Higuchi, M., Onishi, K., Kikuchi, C. & Gotoh, Y. Scaffolding function of PAK in the PDK1-Akt pathway. *Nat. Cell Biol.* **10**, 1356–1364 (2008).

269. Rocca, A. & Kholodenko, B. N. Can Systems Biology Advance Clinical Precision Oncology ? *Cancers (Basel).* **13**, 1–26 (2021).
270. Dhillon, A. S., Hagan, S., Rath, O. & Kolch, W. MAP kinase signalling pathways in cancer. *Oncogene* **26**, 3279–3290 (2007).
271. Fey, D. *et al.* Signaling pathway models as biomarkers: Patient-specific simulations of JNK activity predict the survival of neuroblastoma patients. *Sci. Signal.* **8**, 1–16 (2015).
272. Widenmaier, S. B., Ao, Z., Kim, S. J., Warnock, G. & McIntosh, C. H. S. Suppression of p38 MAPK and JNK via Akt-mediated inhibition of apoptosis signal-regulating kinase 1 constitutes a core component of the β-cell pro-survival effects of glucose-dependent insulinotropic polypeptide. *J. Biol. Chem.* **284**, 30372–30382 (2009).
273. Zhao, H. F., Wang, J. & To, S. S. T. The phosphatidylinositol 3-kinase/Akt and c-Jun N-terminal kinase signaling in cancer: Alliance or contradiction? (Review). *Int. J. Oncol.* **47**, 429–436 (2015).
274. Waetzig, V. *et al.* Concurrent protective and destructive signaling of JNK2 in neuroblastoma cells. *Cell. Signal.* **21**, 873–880 (2009).
275. Wang, Y., Jiang, X., Feng, F., Liu, W. & Sun, H. Degradation of proteins by PROTACs and other strategies. *Acta Pharm. Sin. B* **10**, 207–238 (2020).
276. Nunnery, S. E. & Mayer, I. A. *Management of toxicity to isoform α-specific PI3K inhibitors*. *Annals of oncology : official journal of the European Society for Medical Oncology* **30**, x21–x26 (Oxford University Press, 2019).
277. Esposito, A., Viale, G. & Curigliano, G. Safety, Tolerability, and Management of Toxic Effects of Phosphatidylinositol 3-Kinase Inhibitor Treatment in Patients with Cancer: A Review. *JAMA Oncology* **5**, 1347–1354 (2019).
278. Calautti, E., Li, J., Saoncella, S., Brissette, J. L. & Goetinck, P. F. Phosphoinositide 3-kinase signaling to Akt promotes keratinocyte differentiation versus death. *J. Biol. Chem.* **280**, 32856–32865 (2005).
279. Hudis, C. *et al.* A phase 1 study evaluating the combination of an allosteric AKT inhibitor (MK-2206) and trastuzumab in patients with HER2-positive solid tumors. *Breast Cancer Res.* **15**, 1–10 (2013).
280. Saura, C. *et al.* A first-in-human phase I study of the ATP-competitive AKT inhibitor Ipatasertib demonstrates Robust and safe targeting of AKT in patients with solid tumors. *Cancer Discov.* **7**, 102–113 (2017).
281. Martorana, F. *et al.* AKT Inhibitors: New Weapons in the Fight Against Breast Cancer? *Frontiers in Pharmacology* **12**, 546 (2021).
282. Maneiro, M. M. *et al.* Antibody-PROTAC Conjugates Enable HER2-Dependent Targeted Protein Degradation of BRD4. *ACS Chem. Biol.* **15**, 1306–1312 (2020).
283. Pettersson, M. & Crews, C. M. PROteolysis TArgeting Chimeras (PROTACs) — Past, present and future. *Drug Discov. Today Technol.* **31**, 15–27 (2019).
284. Tovell, H. *et al.* Design and Characterization of SGK3-PROTAC1, an Isoform Specific SGK3 Kinase PROTAC Degrader. *ACS Chem. Biol.* **14**, 2024–2034 (2019).
285. Rana, S. *et al.* Selective degradation of CDK6 by a palbociclib based PROTAC. *Bioorganic Med. Chem. Lett.* **29**, 1375–1379 (2019).
286. Burslem, G. M. *et al.* Targeting BCR-ABL1 in chronic myeloid leukemia by PROTAC-mediated targeted protein degradation. *Cancer Res.* **79**, 4744–4753 (2019).
287. Wyant, G. A. *et al.* Nufip1 is a ribosome receptor for starvation-induced ribophagy. *Science (80-.).* **360**, 751–758 (2018).
288. Abu-Remaileh, M. *et al.* Lysosomal metabolomics reveals V-ATPase- and mTOR-dependent regulation of amino acid efflux from lysosomes. *Science (80-.).* **358**, 807–813 (2017).
289. Wagner, E. F. & Nebreda, Á. R. Signal integration by JNK and p38 MAPK pathways in cancer development. *Nat. Rev. Cancer 2009 98* **9**, 537–549 (2009).

290. Zhang, L. *et al.* Quantitative determination of apoptotic death in cultured human pancreatic cancer cells by propidium iodide and digitonin. *Cancer Lett.* **142**, 129–137 (1999).
291. Pang, Z. *et al.* MetaboAnalyst 5.0: Narrowing the gap between raw spectra and functional insights. *Nucleic Acids Res.* **49**, W388–W396 (2021).
292. Ewels, P. A. *et al.* The nf-core framework for community-curated bioinformatics pipelines. *Nat. Biotechnol. 2020 383* **38**, 276–278 (2020).
293. Dobin, A. *et al.* STAR: Ultrafast universal RNA-seq aligner. *Bioinformatics* **29**, 15–21 (2013).
294. Liao, Y., Smyth, G. K. & Shi, W. FeatureCounts: An efficient general purpose program for assigning sequence reads to genomic features. *Bioinformatics* **30**, 923–930 (2014).
295. Ritchie, M. E. *et al.* limma powers differential expression analyses for RNA-sequencing and microarray studies. *Nucleic Acids Res.* **43**, e47–e47 (2015).
296. Robinson, M. D., McCarthy, D. J. & Smyth, G. K. edgeR: A Bioconductor package for differential expression analysis of digital gene expression data. *Bioinformatics* **26**, 139–140 (2009).
297. Robinson, M. D. & Oshlack, A. A scaling normalization method for differential expression analysis of RNA-seq data. *Genome Biol.* **11**, 1–9 (2010).
298. Garcia-Alonso, L. *et al.* Transcription factor activities enhance markers of drug sensitivity in cancer. *Cancer Res.* **78**, 769–780 (2018).
299. Gustavsen, J. A., Pai, S., Isserlin, R., Demchak, B. & Pico, A. R. RCy3: Network biology using Cytoscape from within R. *F1000Research* **8**, 1774 (2019).
300. Cline, M. S. *et al.* Integration of biological networks and gene expression data using cytoscape. *Nat. Protoc.* **2**, 2366–2382 (2007).
301. Lai, A. C. & Crews, C. M. Induced protein degradation: An emerging drug discovery paradigm. *Nat. Rev. Drug Discov.* **16**, 101–114 (2017).
302. Toure, M. & Crews, C. M. Small-molecule PROTACS: New approaches to protein degradation. *Angew. Chemie - Int. Ed.* **55**, 1966–1973 (2016).
303. Neklesa, T. K., Winkler, J. D. & Crews, C. M. Targeted protein degradation by PROTACs. *Pharmacol. Ther.* **174**, 138–144 (2017).
304. Hanzl, A. & Winter, G. E. Targeted protein degradation: current and future challenges. *Current Opinion in Chemical Biology* **56**, 35–41 (2020).
305. Landel, I., Quambusch, L., Depta, L. & Rauh, D. Spotlight on AKT: Current Therapeutic Challenges. *ACS Med. Chem. Lett.* **11**, 225–227 (2020).
306. Kim, S. B. *et al.* Ipatasertib plus paclitaxel versus placebo plus paclitaxel as first-line therapy for metastatic triple-negative breast cancer (LOTUS): a multicentre, randomised, double-blind, placebo-controlled, phase 2 trial. *Lancet Oncol.* **18**, 1360–1372 (2017).
307. Fruman, D. A. & Rommel, C. PI3K and cancer: lessons, challenges and opportunities. *Nat. Rev. Drug Discov.* **13**, 140–56 (2014).
308. Wu, W.-I. *et al.* Crystal Structure of Human AKT1 with an Allosteric Inhibitor Reveals a New Mode of Kinase Inhibition. *PLoS One* **5**, e12913 (2010).
309. Yang, J. *et al.* Crystal structure of an activated Akt/Protein Kinase B ternary complex with GSK3-peptide and AMP-PNP. *Nat. Struct. Biol.* **9**, 940–944 (2002).
310. Lai, A. C. *et al.* Modular PROTAC Design for the Degradation of Oncogenic BCR-ABL. *Angew. Chemie - Int. Ed.* **55**, 807–810 (2016).
311. Xu, J. *et al.* AKT Degradation Selectively Inhibits the Growth of PI3K/PTEN Pathway–Mutant Cancers with Wild-Type KRAS and BRAF by Destabilizing Aurora Kinase B. *Cancer Discov.* **11**, 3064–3089 (2021).
312. Gu, S., Cui, D., Chen, X., Xiong, X. & Zhao, Y. PROTACs: An Emerging Targeting Technique for Protein Degradation in Drug Discovery. *BioEssays* **40**, (2018).
313. Chan, J. C. *et al.* AKT promotes rRNA synthesis and cooperates with c-MYC to stimulate

ribosome biogenesis in cancer. *Sci. Signal.* **4**, 1–11 (2011).
314. Zhang, Y. *et al.* Coordinated regulation of protein synthesis and degradation by mTORC1. *Nature* **513**, 440–443 (2014).
315. Garrett, M. First-in-Man Clinical Trial of the Oral Pan-AKT Inhibitor MK-2206 in Patients With Advanced Solid Tumors. *J. Clin. Oncol.* (2011). doi:10.1200/JCO.2011.37.4751
316. Lee, B. J. *et al.* Selective inhibitors of mTORC1 activate 4EBP1 and suppress tumor growth. *Nat. Chem. Biol.* **17**, 1065–1074 (2021).
317. Pratilas, C. A. & Solit, D. B. Targeting the mitogen-activated protein kinase pathway: Physiological feedback and drug response. *Clin. Cancer Res.* **16**, 3329–3334 (2010).
318. Han, X. *et al.* Discovery of ARD-69 as a Highly Potent Proteolysis Targeting Chimera (PROTAC) Degrader of Androgen Receptor (AR) for the Treatment of Prostate Cancer. *J. Med. Chem.* **62**, 941–964 (2019).
319. Lipinski, C. A., Lombardo, F., Dominy, B. W. & Feeney, P. J. Experimental and computational approaches to estimate solubility and permeability in drug discovery and development settings. *Advanced Drug Delivery Reviews* **64**, 4–17 (2012).
320. Jansen, V. M., Mayer, I. A. & Arteaga, C. L. Is there a future for AKT inhibitors in the treatment of cancer? *Clin. Cancer Res.* **22**, 2599–2601 (2016).
321. Hillmann, P. & Fabbro, D. PI3K/mTOR pathway inhibition: Opportunities in oncology and rare genetic diseases. *International Journal of Molecular Sciences* **20**, (2019).
322. Madsen, R. R., Vanhaesebroeck, B. & Semple, R. K. *Cancer-Associated PIK3CA Mutations in Overgrowth Disorders*. *Trends in Molecular Medicine* **24**, 856–870 (Trends Mol Med, 2018).
323. Munoz, J. & Kurzrock, R. Targeted therapy in rare cancers-adopting the orphans. *Nature Reviews Clinical Oncology* **9**, 631–642 (2012).
324. Venot, Q. *et al.* Targeted therapy in patients with PIK3CA-related overgrowth syndrome. *Nature* **558**, 540–546 (2018).
325. Leoni, C. *et al.* First evidence of a therapeutic effect of miransertib in a teenager with Proteus syndrome and ovarian carcinoma. *Am. J. Med. Genet. Part A* **179**, 1319–1324 (2019).
326. Hsu, J. W. *et al.* The protein kinase Akt acts as a coat adaptor in endocytic recycling. *Nat. Cell Biol.* **22**, 927–933 (2020).
327. Remy, I., Montmarquette, A. & Michnick, S. W. PKB/Akt modulates TGF-β signalling through a direct interaction with Smad3. *Nat. Cell Biol.* **6**, 358–365 (2004).
328. Chu, N. *et al.* The structural determinants of ph domain-mediated regulation of akt revealed by segmental labeling. *Elife* **9**, 1–23 (2020).
329. Xing, Y. *et al.* Phase II trial of AKT inhibitor MK-2206 in patients with advanced breast cancer who have tumors with PIK3CA or AKT mutations, and/or PTEN loss/PTEN mutation. *Breast Cancer Res.* **21**, 1–12 (2019).
330. Świderska, E. *et al.* Role of PI3K/AKT Pathway in Insulin-Mediated Glucose Uptake. in *Blood Glucose Levels* (IntechOpen, 2020). doi:10.5772/intechopen.80402
331. Hopkins, B. D., Goncalves, M. D. & Cantley, L. C. Insulin–PI3K signalling: an evolutionarily insulated metabolic driver of cancer. *Nature Reviews Endocrinology* **16**, 276–283 (2020).
332. Nasiri, A. R., Rodrigues, M. R., Li, Z., Leitner, B. P. & Perry, R. J. SGLT2 inhibition slows tumor growth in mice by reversing hyperinsulinemia. *Cancer Metab.* **7**, 1–13 (2019).
333. Rugo, H. S. *et al.* Time course and management of key adverse events during the randomized phase III SOLAR-1 study of PI3K inhibitor alpelisib plus fulvestrant in patients with HR-positive advanced breast cancer. *Ann. Oncol.* **31**, 1001–1010 (2020).
334. Borcoman, E. *et al.* Inhibition of PI3K pathway increases immune infiltrate in muscle-invasive bladder cancer. (2019). doi:10.1080/2162402X.2019.1581556
335. Su, X. *et al.* Antagonizing integrin β3 increases immunosuppression in cancer. *Cancer*

Res. **76**, 3484–3495 (2016).
336. Davis, R. J. Signal transduction by the JNK group of MAP kinases. *Cell* **103**, 239–252 (2000).
337. Chamberlain, P. P. & Hamann, L. G. Development of targeted protein degradation therapeutics. *Nat. Chem. Biol.* **15**, 937–944 (2019).
338. Akuffo, A. A. *et al.* Ligand-mediated protein degradation reveals functional conservation among sequence variants of the CUL4-type E3 ligase substrate receptor cereblon. *J. Biol. Chem.* **293**, 6187–6200 (2018).
339. Faustino-Rocha, A. *et al.* Estimation of rat mammary tumor volume using caliper and ultrasonography measurements. *Lab Anim. (NY).* **42**, 217–224 (2013).